

**ISTANBUL TECHNICAL UNIVERSITY ★ INSTITUTE OF SCIENCE AND TECHNOLOGY**

**A RESERVOIR ENGINEERING STUDY FOR FIELD DEVELOPMENT - AN  
APPLICATION TO REAL FIELD DATA**

**M.Sc. THESIS**

**Harun KIRMACI**

**Department of Petroleum and Natural Gas Engineering**

**Petroleum and Natural Gas Engineering Programme**

**OCT 2014**



**ISTANBUL TECHNICAL UNIVERSITY ★ INSTITUTE OF SCIENCE AND TECHNOLOGY**

**A RESERVOIR ENGINEERING STUDY FOR FIELD DEVELOPMENT - AN  
APPLICATION TO REAL FIELD DATA**

**M.Sc. THESIS**

**Harun KIRMACI  
(505081507)**

**Department of Petroleum and Natural Gas Engineering  
Petroleum and Natural Gas Engineering Programme**

**Thesis Advisor: Prof. Dr. Mustafa ONUR**

**OCT 2014**



**İSTANBUL TEKNİK ÜNİVERSİTESİ ★ FEN BİLİMLERİ ENSTİTÜSÜ**

**SAHA GELİŞTİRMEDE BİR REZERVUAR MÜHENDİSLİĞİ ÇALIŞMASI –  
GERÇEK SAHA VERİLERİ İLE UYGULAMA**

**YÜKSEK LİSANS TEZİ**

**Harun KIRMACI  
(505081507)**

**Petrol ve Doğal Gaz Mühendisliği Anabilim Dalı**

**Petrol ve Doğal Gaz Mühendisliği Programı**

**Tez Danışmanı: Prof. Dr. Mustafa ONUR**

**EKİM 2014**



**Harun KIRMACI**, an M.Sc. student of ITU **Institute of Science** student ID 505081507, successfully defended the thesis “**A RESERVOIR ENGINEERING STUDY FOR FIELD DEVELOPMENT – AN APPLICATION TO REAL FIELD DATA**”, which he prepared after fulfilling the requirements specified in the associated legislations, before the jury whose signatures are below.

**Thesis Advisor:**      **Prof. Dr. Mustafa ONUR**      .....

**Istanbul Technical University**

**Jury Members:**      **Prof. Dr. Emin Demirbağ**      .....

**Istanbul Technical University**

**Assoc. Prof. Dr. Murat Çınar**      .....

**Istanbul Technical University**

**Date of Submission:**    **13 Oct 2014**

**Date of Defence:**      **22 Oct 2014**





## FOREWORD

In this thesis, a reservoir engineering study for determining an optimum field development strategy considering both the contractual and technical constraints with application to real field data obtained from gas condensate reservoir was presented. In the study, the most commonly accepted reservoir engineering tools and software in petroleum industry; PETREL for 3D geological modeling, ECLIPSE for dynamic reservoir simulation, and SAPHIR for interpretation of well-test data, were used. Data sets taken from a variety of different sources were analyzed and interpreted for construction of static and dynamic reservoir modeling activities and then converted to compatible input format for the used software in the study. After building static and dynamic reservoir models and characterizing the formation, an optimum field development strategy was suggested by honoring the contractual and technical constraints. In summary, the study not only shows the basic steps to be followed when conducting a reservoir engineering study for an optimum field development, but also proves useful for those integrating a variety of different sources of data for building static and dynamic reservoir modeling with the use of modern reservoir engineering software aforementioned above.

This study would not have been possible without the support of many people: First of all, I would like to express my sincere gratitude and appreciation to Prof. Dr. Mustafa Onur, who read my numerous revisions, chaired my advisory committee, for his valuable guidance, support, and patience in helping me bring this study to completion. I will forever be thankful to my advisor, Prof. Dr. Mustafa Onur who has been helpful in providing advice many times during my undergraduate, graduate school career, and my professional work career. He was and remains my best model for a scientist, mentor, engineer, and teacher. His enthusiasm, love for continuous learning, love for teaching and love for achieving are contagious.

Secondly, I greatly thank to my thesis jury members Prof. Dr. Emin Demirbağ and Assoc. Prof. Dr. Murat Çınar for their contribution to my thesis.

Thirdly, I would like to thank to Assoc. Prof. Dr. Ömer İnanç Türeyen, for supporting me during the past three years throughout my graduate school career. During these three years, I gained much vital theoretical background from him that I am applying for my daily professional works.

I also greatly thank to my wife Ayşe and my children Elif Ela and Ömer Emre for allowing time to me for the whole course of this study by restricting their personnel needs.

Oct 2014

Harun KIRMACI

(Petroleum and Natural Gas Engineer)



## TABLE OF CONTENTS

<b>FOREWORD</b> .....	<b>vii</b>
<b>TABLE OF CONTENTS</b> .....	<b>ix</b>
<b>ABBREVIATIONS</b> .....	<b>xi</b>
<b>LIST OF TABLES</b> .....	<b>xiii</b>
<b>LIST OF FIGURES</b> .....	<b>xv</b>
<b>SUMMARY</b> .....	<b>xix</b>
<b>ÖZET</b> .....	<b>xxi</b>
<b>1. INTRODUCTION</b> .....	<b>1</b>
1.2 Statement of Problem .....	3
1.3 Scope of Study.....	4
<b>2. TECHNICAL AND CONTRACTUAL CONSTRAINTS</b> .....	<b>5</b>
<b>3. ANALYSIS OF AVAILABLE DATA</b> .....	<b>9</b>
3.1 Geophysical Data .....	10
3.2 Well Logs .....	13
3.2.1 Well X-1 logs.....	14
3.2.2 Well X-2 logs.....	15
3.2.3 Well X-3 logs.....	16
3.2.4 Well X-4 logs.....	17
3.3 Cores.....	18
3.3.1 Well X-1 core data.....	22
3.3.2 Well X-2 core data.....	23
3.3.3 Well X-3 core data.....	24
3.3.4 Well X-4 core data.....	25
3.4 PVT .....	26
3.5 Well Test .....	30
3.5.1 Well X-1 well tests .....	30
3.5.2 Well X-2 well tests .....	31
3.5.2.1 Well X-2 open-hole test (1306-1340 mss).....	31
3.5.2.2 Well X-2 open-hole test (1365-1381 mss).....	34
3.5.2.3 Well X-2 cased hole test – after first acid (1325-1335 mss).....	36
3.5.2.4 Well X-2 cased-hole test – after second acid (1325-1335 mss).....	38
3.5.2.5 Well X-4 open hole test (1498-1554 mss) .....	42
3.6 Gas-Water Contact (GWC) .....	44
<b>4. 3D GEOLOGICAL MODELING</b> .....	<b>49</b>
4.1 Structural Modeling.....	50
4.2 Well Logs and Well Tops.....	52
4.3 3D Grid Generation .....	56
4.3.1 Horizons.....	57
4.3.2 Zones – layering.....	58
4.3.3 Fluid contacts .....	62
4.4 Property Modeling.....	62
4.4.1 Scaling up well-logs.....	67
4.4.2 Petrophysical modeling .....	69

4.4.2.1 Porosity distribution .....	72
4.4.2.2 Water saturation distribution .....	75
4.4.2.3 Permeability distribution .....	79
4.4.2.4 Net to gross.....	84
4.5 Volume Calculation & GIIP .....	85
4.6 Uncertainty Analysis .....	86
<b>5. SIMULATION MODEL .....</b>	<b>89</b>
5.1. Upscaling Fine Scale Geological Model .....	90
5.1.1. Quality check of up scaled model .....	101
5.2. Fluid Model .....	103
5.3. Rock Physics Function .....	109
5.4. Well Modeling .....	117
5.4.1. Location and number of wells – base case.....	120
5.4.2. Well completions – base case .....	124
5.5. Development Strategy – Base Case.....	124
5.6. Definition of Simulation Case – Base Case.....	125
<b>6. APPLICATIONS .....</b>	<b>133</b>
6.1. Analysis of Base Case .....	133
6.2. Well Locations.....	136
6.3. Optimization of Well Completion .....	138
<b>7. CONCLUSIONS .....</b>	<b>141</b>
7.1 Concluding Remarks .....	141
7.3 Recommendation for Future Works .....	144
<b>REFERENCES .....</b>	<b>147</b>
<b>APPENDICES .....</b>	<b>151</b>
APPENDIX-A PVTi Fluid Model.....	151
<b>CIRRICULUM VITAE .....</b>	<b>167</b>

## ABBREVIATIONS

<b>B<sub>o</sub></b>	: Oil Formation Volume Factor at p, rb/STB
<b>B<sub>g</sub></b>	: Gas Formation Volume Factor, rb/scf
<b>B<sub>w</sub></b>	: Water Formation Volume Factor at p, rb/STB
<b>C</b>	: Wellbore Storage Coefficient, bbl/psi
<b>BHP</b>	: Bottom Hole Pressure
<b>c<sub>w</sub></b>	: Water Compressibility, psia <sup>-1</sup>
<b>c<sub>f</sub></b>	: Formation (rock) Compressibility, psia <sup>-1</sup>
<b>CCE</b>	: Constant Composition Expansion
<b>CGR</b>	: Condensate to Gas Ratio, bbl/MMscf
<b>CPI</b>	: Computer Processed Information Log
<b>CVD</b>	: Constant Volume Depletion
<b>GDT</b>	: Gas Down To
<b>GR</b>	: Gamma Ray
<b>GOC</b>	: Gas Oil Contact
<b>GWC</b>	: Gas Water Contact
<b>FWL</b>	: Free Water Level
<b>LLS</b>	: Laterolog Shallow Resistivity
<b>h</b>	: Thickness or Height, m
<b>HCPV</b>	: Hydrocarbon Poro Volume
<b>k</b>	: Permeability, md
<b>k<sub>rg</sub></b>	: Relative Permeability of Gas
<b>k<sub>ro</sub></b>	: Relative Permeability of Oil
<b>k<sub>rw</sub></b>	: Relative Permeability of Water
<b>k<sub>rg</sub> @ S<sub>org</sub></b>	: Relative Permeability of Gas at Residual Oil Saturation
<b>k<sub>rg</sub> @ S<sub>wmin</sub></b>	: Relative Permeability of Gas at Minimum Water Saturation
<b>k<sub>ro</sub> @ S<sub>omax</sub></b>	: Relative Permeability of Oil at Maximum Value of Oil Saturation
<b>k<sub>rw</sub> @ S<sub>orw</sub></b>	: Relative Permeability of Water at Residual Oil Saturation
<b>k<sub>rw</sub> @ S=1</b>	: Relative Permeability of Water at a Saturation Value of Unity +
<b>k<sub>rog</sub></b>	: The Oil Relative Permeability for a System with Oil, Gas and, Connate Water which is Tabulated as a Function of Oil Saturation
<b>k<sub>row</sub></b>	: The Oil Relative Permeability for a System with Oil and Water only
<b>mKB</b>	: Meter Kelly Bushing, m
<b>Mscf</b>	: Thousand Standard Cubic Foot
<b>Mss</b>	: Meter Sub Sea, m
<b>NTG</b>	: Net to Gross Ratio
<b>OIIP</b>	: Oil Initially in Place, rb
<b>GIIP</b>	: Gas Initially in Place, SCF
<b>OGIP</b>	: Original Gas in Place, STB
<b>OHIP</b>	: Original Hydrocarbon in Place, rb
<b>OOIP</b>	: Original Oil in Place, STB
<b>p</b>	: Average Reservoir Pressure at Time t, psia
<b>P<sub>c</sub></b>	: Capillary Pressure, psia
<b>p<sub>i</sub></b>	: Initial Reservoir Pressure, psia

<b><math>p_r</math></b>	: Average Reservoir Pressure, psia
<b><math>p_{wh}</math></b>	: Well Head Pressure, psia
<b>PBU</b>	: Pressure Build Up
<b>PTA</b>	: Pressure Transient Analysis
<b>PVT</b>	: Pressure Volume Temperature
<b>ppm</b>	: Parts per Million
<b><math>R_{inv}</math></b>	: Radius of Investigation, ft
<b>rb</b>	: Reservoir Barrels
<b>RF</b>	: Recovery Factor
<b><math>R_s</math></b>	: Dissolved Gas-Oil Ratio at p, scf/STB
<b><math>R_{si}</math></b>	: Initial Dissolved Gas-Oil Ratio, scf/STB
<b><math>R_p</math></b>	: Producing Gas-Oil Ratio, scf/STB
<b>s</b>	: Skin factor
<b>Sg</b>	: Gas Saturation
<b>Sgcr</b>	: Critical Gas Saturation
<b>So</b>	: Oil Saturation
<b>Sor</b>	: Residual Oil Saturation
<b>Sorg</b>	: Residual Oil Saturation to Gas
<b>Sorw</b>	: Residual Oil Saturation to Water
<b>Sw</b>	: Water Saturation
<b>Swc</b>	: Critical Water Saturation
<b>Swco</b>	: Connate Water Saturation
<b>Swcr</b>	: Critical Water Saturation
<b>Swmin</b>	: Minimum Water Saturation
<b>scf</b>	: Standard Cubic Feet
<b>SPE</b>	: Society of Petroleum Engineers
<b>STB</b>	: Stock Tank Barrel
<b><math>S_w</math></b>	: Water Saturation
<b>THP</b>	: Tubing Head Pressure
<b><math>W_p</math></b>	: Cumulative Water Produced, STB
<b><math>W_e</math></b>	: Cumulative Water Influx from Aquifer, rb
<b><math>W_{inj}</math></b>	: Cumulative Water Injected, STB
<b><math>W_D</math></b>	: Dimensionless water influx
<b>WHP</b>	: Well Head Pressure
<b>WUT</b>	: Water Up To, mss
<b><math>\Delta P</math></b>	: Initial Minus Prevailing Pressure ( $p_i-p$ ), psia
<b><math>\Delta V</math></b>	: Expansion of the Material due to Change in Pressure, unit of volume

## LIST OF TABLES

<b>Table 3.1:</b> Recovered cores porosity statistics of all wells. ....	21
<b>Table 3.2:</b> Recovered cores permeability statistics of all wells. ....	21
<b>Table 3.3:</b> Porosity permeability correlation coefficients. ....	21
<b>Table 3.4:</b> Well log – core porosity statistics comparison .....	22
<b>Table 3.5:</b> Recovered cores from well X-1. ....	22
<b>Table 3.6:</b> Recovered cores from well X-2. ....	23
<b>Table 3.7:</b> Recovered cores from well X-3. ....	24
<b>Table 3.8:</b> Recovered cores from well X-4. ....	25
<b>Table 3.9:</b> Compositional data - sampling conditions .....	27
<b>Table 3.10:</b> Compositional data – sampling conditions of well X-2 sample. ....	29
<b>Table 3.11:</b> Data for well X-1 open-hole and cased-hole tests. ....	31
<b>Table 3.12:</b> Data for well X-2 open-hole and cased-hole tests. ....	31
<b>Table 3.13:</b> PTA inputs for well X-2. ....	33
<b>Table 3.14:</b> Test analysis result summary (1306-1340 mss).....	34
<b>Table 3.15:</b> Summary of test analysis results (1365-1381 mss).....	36
<b>Table 3.16:</b> Summary of test analysis results after first acid (1325-1335 mss). ....	38
<b>Table 3.17:</b> Summary of test analysis results after second acid (1325-1335 mss)....	41
<b>Table 3.18:</b> PTA inputs for well X-4. ....	43
<b>Table 3.19:</b> Summary of the test analysis results for well X-4 test (1498-1554 mss). .....	44
<b>Table 3.20:</b> Pressure reading from the field. ....	45
<b>Table 4.1:</b> Formation tops – all wells. ....	61
<b>Table 4.2:</b> Zone thickness. ....	61
<b>Table 4.3:</b> Layer thickness. ....	61
<b>Table 4.4:</b> Statistics of core permeability.....	63
<b>Table 4.5:</b> Permeability-porosity correlation equations. ....	65
<b>Table 4.6:</b> Statistics of derived permeabilities based on log-porosity and core permeabilities. ....	65
<b>Table 4.7:</b> Statistical information of porosity distribution .....	74
<b>Table 4.8:</b> Statistical information of water saturation distribution.....	78
<b>Table 4.9:</b> Statistical information of permeability X, Y, and Z distribution. ....	83
<b>Table 4.10:</b> Volumetric report of base case. ....	86
<b>Table 4.11:</b> Uncertainty range of the reservoir parameters.....	87
<b>Table 4.12:</b> Probabilistic GIIP range.....	87
<b>Table 5.1:</b> Special core analysis data that used in normalization.....	110
<b>Table 5.2:</b> Comparison of GIIP calculations.....	114
<b>Table 6.1:</b> Base case - cumulative field productions.....	136
<b>Table 6.2:</b> Cumulative field productions after the replacement of P15 and P32. ...	138
<b>Table 6.3:</b> Cumulative field productions the case 40m perforation. ....	140





## LIST OF FIGURES

<b>Figure 1.1:</b> Integrated reservoir modeling workflow.....	2
<b>Figure 3.1:</b> 2D seismic lines.....	10
<b>Figure 3.2:</b> Top of formation X depth map - 2D view.....	11
<b>Figure 3.3:</b> Top of formation X depth map - 3D view.....	12
<b>Figure 3.4:</b> Main faults - 3D view.....	12
<b>Figure 3.5:</b> Well locations – cross section.....	13
<b>Figure 3.6:</b> Well X-1 logs.....	14
<b>Figure 3.7:</b> Well X-2 logs.....	15
<b>Figure 3.8:</b> Well X-3 logs.....	16
<b>Figure 3.9:</b> X4 well logs.....	18
<b>Figure 3.10:</b> Core porosity-permeability cross-plot of all wells.....	19
<b>Figure 3.11:</b> Core porosity histograms for each well.....	20
<b>Figure 3.12:</b> Core permeability histograms for each well.....	20
<b>Figure 3.13:</b> Core permeability (lnk) histograms for each well.....	21
<b>Figure 3.14:</b> Core porosity - permeability cross - plot of well X-1.....	23
<b>Figure 3.15:</b> Core porosity - permeability cross - plot of well X-2.....	24
<b>Figure 3.16:</b> Core porosity - permeability cross - plot of well X-3.....	25
<b>Figure 3.17:</b> Core porosity - permeability cross - plot of well X-4.....	26
<b>Figure 3.18:</b> Separator flow rate measurement – well X-2.....	28
<b>Figure 3.19:</b> Pressure and rate history plot for well X-2 test (1306-1340 mss).....	33
<b>Figure 3.20:</b> Log-log diagnostic plot (1306-1340 mss).....	33
<b>Figure 3.21:</b> Semi-log Horner plot of well X-2 (1306-1340 mss).....	34
<b>Figure 3.22:</b> Pressure and rate history plot for well X-2 (1365-1381 mss).....	35
<b>Figure 3.23:</b> Log-log diagnostic plot (1365-1381 mss).....	35
<b>Figure 3.24:</b> Semi-log Horner plot of well X-2 (1365-1381 mss).....	36
<b>Figure 3.25:</b> Pressure and rate history plot for well X-2-after first acid (1325-1335 mss).....	37
<b>Figure 3.26:</b> Log-log diagnostic plot after first acid (1325-1335 mss).....	37
<b>Figure 3.27:</b> Semi-log Horner plot of well X-2 - after first acid (1325-1335 mss).....	38
<b>Figure 3.28:</b> Pressure and rate history plot for well X-2 after second acid (1325-1335 mss).....	39
<b>Figure 3.29:</b> Log-log diagnostic plot after second acid (1325-1335 mss).....	40
<b>Figure 3.30:</b> Semi-log Horner plot after second acid (1325-1335 mss).....	40
<b>Figure 3.31:</b> Well X-2 tests comparison, log-log diagnostic plot.....	42
<b>Figure 3.32:</b> Pressure and rate history plot - well X-4 PBU test (1498-1554 mss).....	43
<b>Figure 3.33:</b> Log-log diagnostic plot for well X-4 (1498-1554 mss).....	43
<b>Figure 3.34:</b> Semi-log Horner plot of well X-4 (1498-1554 mss).....	44
<b>Figure 3.35:</b> Cross sectional view of GDT (1391mss) and WUP (1502mss).....	46
<b>Figure 3.36:</b> Pressure – depth & GWC.....	46
<b>Figure 3.37:</b> Water saturation vs. height.....	47
<b>Figure 4.1:</b> Formation structural top map & GWC.....	51
<b>Figure 4.2:</b> Formation structural base map & GWC.....	51

<b>Figure 4.3:</b> Fault pillars. ....	52
<b>Figure 4.4:</b> Well tops.....	53
<b>Figure 4.5:</b> Well logs – all wells. ....	54
<b>Figure 4.6:</b> Well log porosity histograms – all wells. ....	54
<b>Figure 4.7:</b> Core porosity histograms – all wells. ....	55
<b>Figure 4.8:</b> Water saturation histograms – all wells.....	55
<b>Figure 4.9:</b> 3D Grids (50m x 50m cell size).....	57
<b>Figure 4.10:</b> Horizon – 3D view. ....	58
<b>Figure 4.11:</b> Zones – 2D well log porosity all wells. ....	60
<b>Figure 4.12:</b> Each zone: number of sub-layers.....	60
<b>Figure 4.13:</b> Zones – 3D view.....	61
<b>Figure 4.14:</b> Gas water contact – 1460 mss. ....	62
<b>Figure 4.15:</b> Permeability-porosity cross plot for all zones. ....	64
<b>Figure 4.16:</b> Permeability vs porosity each zone & correlation equations. ....	64
<b>Figure 4.17:</b> Permeability logs – all wells.....	66
<b>Figure 4.18:</b> Up-scaled porosity for all wells.....	68
<b>Figure 4.19:</b> Up-scaled water saturation of X-1, X-2 and X-3.....	68
<b>Figure 4.20:</b> Up-scaled permeability for all wells.....	69
<b>Figure 4.21:</b> Orientation of the X-Field. ....	71
<b>Figure 4.22:</b> Variogram model for porosity – major direction.....	72
<b>Figure 4.23:</b> Variogram model for porosity – minor direction. ....	73
<b>Figure 4.24:</b> Variogram model for porosity – vertical direction. ....	73
<b>Figure 4.25:</b> Porosity distribution 3D- cross sectional view. ....	74
<b>Figure 4.26:</b> Porosity distribution histogram. ....	75
<b>Figure 4.27:</b> Variogram model for water saturation – major direction. ....	76
<b>Figure 4.28:</b> Variogram model for water saturation – minor direction. ....	76
<b>Figure 4.29:</b> Variogram model for water saturation – vertical direction. ....	77
<b>Figure 4.30:</b> Water saturation distribution 3D – cross sectional view. ....	78
<b>Figure 4.31:</b> Water saturation distribution histogram. ....	78
<b>Figure 4.32:</b> Variogram model for permeability – major direction. ....	80
<b>Figure 4.33:</b> Variogram model for permeability – minor direction. ....	80
<b>Figure 4.34:</b> Variogram model for permeability – minor direction. ....	81
<b>Figure 4.35:</b> Permeability-X distribution 3D – cross sectional view.....	82
<b>Figure 4.36:</b> Permeability-Y distribution 3D – cross sectional view.....	82
<b>Figure 4.37:</b> Permeability-Z distribution 3D – cross sectional view. ....	82
<b>Figure 4.38:</b> Permeability-X distribution histogram. ....	83
<b>Figure 4.39:</b> Permeability-Y distribution histogram. ....	83
<b>Figure 4.40:</b> Permeability-Z distribution histogram.....	84
<b>Figure 4.41:</b> NTG model, 3D and cross sectional view. ....	85
<b>Figure 4.42:</b> GIIP uncertainty. ....	87
<b>Figure 5.1:</b> 3D view of NTG - fine scaled model (top), up scaled model (bottom)..	91
<b>Figure 5.2:</b> Layers of up scaled model. ....	92
<b>Figure 5.3:</b> Original well-log porosity (black line) versus up scaled model porosity (colored bars).....	93
<b>Figure 5.4:</b> Original well-log water saturation (blue line) versus up scaled model water saturation (colored bars). ....	93
<b>Figure 5.5:</b> 3D and cross sectional view comparison of porosity distribution – fine scaled model (top) and up scaled model (bottom). ....	94
<b>Figure 5.6:</b> Porosity histogram – statistics comparison of fined scaled model (on the left) and up scaled model (on the right). ....	95

<b>Figure 5.7:</b> 3D and cross sectional view: comparison of water saturation distribution – fine scaled model (on the top) and up scaled model (on the bottom). .	96
<b>Figure 5.8:</b> Water saturation histogram – statistics comparison of fined scaled model (on the left) and up scaled model (on the right). .....	97
<b>Figure 5.9:</b> 3D and cross sectional view: comparison of permeability-X distribution – fine scaled model (on the top) and up scaled model (on the bottom). .	98
<b>Figure 5.10:</b> Permeability histogram – statistics comparison of fined scaled model (on the left) and up scaled model (on the right). .....	99
<b>Figure 5.11:</b> 3D View of the cells below GWC (fine scaled – up scaled). .....	100
<b>Figure 5.12:</b> Quality check of cell angle. ....	102
<b>Figure 5.13:</b> Quality check of cell inside out. ....	103
<b>Figure 5.14:</b> Phase envelope. ....	105
<b>Figure 5.15:</b> EoS model versus CCE observations – liquid saturation. ....	106
<b>Figure 5.16:</b> EoS model versus CCE observations – relative volume. ....	106
<b>Figure 5.17:</b> EoS model versus CCE observations – vapor Z-factor. ....	107
<b>Figure 5.18:</b> EoS model versus CVD observations – liquid saturation. ....	107
<b>Figure 5.19:</b> EoS model versus CVD observations – 2-phase Z-factor. ....	108
<b>Figure 5.20:</b> EoS model versus CVD observations – vapor Z-factor. ....	108
<b>Figure 5.21:</b> EoS model versus CVD observations – vapor viscosity. ....	108
<b>Figure 5.22:</b> Water-oil relative permeability laboratory measurements. ....	111
<b>Figure 5.23:</b> Gas-oil relative permeability laboratory measurements. ....	112
<b>Figure 5.24:</b> Corey model input parameters. ....	112
<b>Figure 5.25:</b> Oil-water relative permeability – Corey model. ....	114
<b>Figure 5.26:</b> Gas-oil relative permeability – Corey model. ....	114
<b>Figure 5.27:</b> Capillary pressure. ....	115
<b>Figure 5.28:</b> Rock compaction. ....	115
<b>Figure 5.29:</b> Three-Phase relative permeability model assumed by ECLIPSE (ECLIPSE Reference Manuel, 2011). .....	116
<b>Figure 5.30:</b> Single branch PIPESIM model. ....	118
<b>Figure 5.31:</b> IPR curve and well productivity index. ....	119
<b>Figure 5.32:</b> Tubing size sensitivity, inflow-outflow curves for different tubing sizes. ....	120
<b>Figure 5.33:</b> Proposed wells - 700m radius. ....	122
<b>Figure 5.34:</b> Proposed wells – 500 m radius. ....	123
<b>Figure 5.35:</b> Proposed wells – 400 m radius. ....	123
<b>Figure 5.36:</b> Well X-2 production test history match with simulation model. ....	128
<b>Figure 5.37:</b> Simulation result of the base case with 16 wells. ....	129
<b>Figure 5.38:</b> Simulation result of the base case with 22 wells. ....	130
<b>Figure 5.39:</b> Simulation result of the base case with 31 wells. ....	131
<b>Figure 5.40:</b> Simulation result of the base case with 31 wells – gas compressors installation at 2025 (BHP limit reduced to 600psi). ....	132
<b>Figure 6.1:</b> Height above GWC – base case well locations. ....	134
<b>Figure 6.2:</b> Gas productions rates of the wells. ....	135
<b>Figure 6.3:</b> Cumulative gas production of the wells. ....	135
<b>Figure 6.4:</b> Water production rates of the wells. ....	135
<b>Figure 6.5:</b> New locations of P15 and P32. ....	137
<b>Figure 6.6:</b> Simulation result of the base case after the replacement of P15 and P32. ....	137
<b>Figure 6.7:</b> Well completion of well P5. ....	139
<b>Figure 6.8:</b> Simulation result of the base case with 40m perforation. ....	140



## **A RESERVOIR ENGINEERING STUDY FOR FIELD DEVELOPMENT - AN APPLICATION TO REAL FIELD DATA**

### **SUMMARY**

Determination of technically and commercially viable development strategy is one of the main goals of the reservoir engineering studies. Although the goal is very clear, the task is not straight forward where the integration and analyses of dataset from different sources and scales are required. It is clear that this is not an easy target to achieve and requires massive works to be performed to find out technically and commercially viable development strategy. For instance, characterizing the complex heterogeneous geological structures and multi-phase fluid flow in porous media are the major steps that need to be overcome prior to predicting any of the reservoir system parameters and forecast reservoir performance based on the drawn development strategy. There are many practical difficulties associated with performing such a complex study such as data integration where the data collected from different sources and scales, limitations of the available data either in representation of the whole field or quantity of data itself, and solving flow equations in million cells models etc. Besides, contractual terms have to be taken into account while determining the appropriate development strategy in which the maximum achievable profit scenario should be another target. For this purpose, it is a common practice to construct a reservoir model that can handle vast amount data and use it as a tool to predict the result of the different scenarios for maximization of profit by honoring the technical, commercial and contractual constraints. In recent years, significant advances in technology and computer science were achieved: thus, the market was prompted to provide sophisticated tools for integration of vast amount data in a single platform and simulation of the behavior of hydrocarbon reservoirs accurately.

In this study, all the above mentioned reservoir engineering studies were conducted on a gas condensate carbonate reservoir. First of all, all the available data including but not limited to 2D-3D seismic, core, well-log, well-test, and PVT were reviewed carefully and used for reservoir characterization purposes. Secondly, analyzed dataset used for the construction of 3D static reservoir model (fine-scaled geo-cellular model) by the integration of the available dataset in PETREL. Possible gas initially in place (GIIP) calculations and uncertainty studies on the calculated GIIP values was performed in PETREL as well. Probabilistic P10, P50, and P90 GIIP values were calculated as 3.609 tcf, 2.937 tcf, and 2.369 tcf, respectively.

Since the reservoir fluid is a super critical gas condensate fluid in which the dew point pressure is very close to the reservoir pressure, compositional fluid model was constructed and tuned in PVTi for the characterization of the reservoir fluid.

Rock physics functions such as relative permeabilities, capillary pressure, and rock compaction were constructed in PETREL based on available core data and using industry widely accepted Corey and Newman correlations.

Single branch well model was constructed in PIPESIM to be able to determine the inflow performance of the wells that will be used in the simulation. Additionally, optimum tubing size was selected by performing Nodal Analysis in PIPESIM based on available production data from the field.

Numerical reservoir simulation model was constructed to simulate the dynamic behavior of reservoir and fluid flow in porous media. Since the reservoir fluid is gas condensate, constructing compositional simulation was preferred and ECLIPSE 300 compositional simulator was used for estimating system parameters, forecasting reservoir and well performance, deciding well spacing, determining reservoir management strategies, assessing and evaluating the results of different development scenarios that may be applied in the field, and making investment decisions etc.

In conclusion, approximately 78% recovery was achieved by drilling totally 31 wells in the field and installing gas compressors at the beginning of 2025.

## SAHA GELİŞTİRMEDE BİR REZERVUAR MÜHENDİSLİĞİ ÇALIŞMASI - GERÇEK SAHA VERİLERİ İLE UYGULAMA

### ÖZET

Rezervuar mühendisliği çalışmalarının en önemli hedeflerinden biri teknik ve ticari uygulanabilir bir saha geliştirme planı belirlemektir. Farklı kaynaklardan ve ölçeklerden verilerin analizini ve birleştirilmesini gerektiren bu görevde, amaç oldukça belirgin olsa da sonuca ulaşmak oldukça karmaşık ve zordur. Teknik ve ticari uygulanabilir bir saha geliştirme senaryosu bulmanın çok kolay ulaşılabilir bir hedef olmadığı ve bu hedefin çok geniş kapsamlı bir çalışma gerektirdiği açıktır. Örneğin, belirlenen geliştirme senaryona göre herhangi bir rezervuar sistemi parametresi ve rezervuarın performansını tahmin etmeden önce üstesinden gelinmesi gereken iki önemli basamak karmaşık ve heterojen jeolojik yapıların ve gözenekli ortamda çok fazlı akışkan akışının tanımlanması gerekmektedir. Böyle karmaşık bir çalışmanın sahadan toplanan farklı kaynaklardan ve ölçekten verilerin birleştirilmesi, toplanan verilerin sahanın tümünü temsil etmesi noktasında ve miktarının yetersizliği ve akış denklemlerinin milyon hücreli modellerde çözümlenmesi gibi pratik zorlukları vardır. Bununla birlikte maksimum elde edilebilir karı verecek saha geliştirme planı belirlenmeye çalışılırken, kontratın da dikte ettiği koşulları da göz önünde bulundurmamak diğer bir zorluktur. Bu nedenle çok geniş çaplı verilerin işlenebileceği ve teknik-ticari ve sözleşmeye ilişkin sınırları göz önünde bulundurarak karı maksimize edecek saha geliştirme planını belirlerken farklı geliştirme senaryolarının sonuçlarının tahmin edilebileceği bir araç olarak rezervuar modeli kurmak genel bir uygulamadır. Son yıllarda teknolojiye ve bilgisayar biliminde oldukça büyük ilerlemeler kaydedildi. Böylece petrol ve gaz endüstrisi marketinde çok fazla verinin tek bir platformda birleştirildiği ve hidrokarbon rezervuarlarının davranışlarının tahmin edilebildiği gelişmiş programlar piyasaya sürüldü.

Bu çalışmada, yukarıda sayılan bütün rezervuar çalışmaları gaz yoğunluk gerçek bir karbonat rezervuar için yapıldı. İlk olarak, var olan bütün veriler; 2B-3B sismik, kuyu logları, kayaç numuneleri, kuyu testleri ve PVT gibi, dikkatlice incelendi ve rezervuar modelleme çalışmalarında kullanıldı. İkinci olarak, analizi yapılan veriler üç boyutlu statik rezervuar modelini kurmak için PETREL'de birleştirildi. Sahadaki en büyük belirsizliklerden biri olan gaz – su kontağı, kuyu testlerinden elde edilen basınç verileri ve gaz ile su gradyanları kullanılarak yaklaşık 1460 mss olarak saptandı ve hacimsel yerinde hidrokarbon hesaplamalarında kullanıldı. Daha sonra, olası yerinde gaz miktarı ve üzerindeki belirsizlikler çalışıldı. Olası P10, P50 ve P90 yerinde gaz miktarı sırasıyla 3.609 tcf, 2.937 tcf ve 2.369 tcf olarak belirlendi.

Rezervuar akışkanı yoğunlaşma basıncının rezervuar basıncına çok yakın olan süper kritik bir gaz yoğunlaşması sebebiyle, bileşimsel akışkan modellemesi ve karşılaştırması PVTi'da yapıldı. Öncelikli olarak sahadan alınan akışkan numunesi üzerinde yapılan PVT testleri sonucunda elde edilen akışkan kompozisyonu PVTi

bileşimsel akışkan modelleme yazılımına yüklendi. Daha sonra laboratuarda yapılan sabit kompozisyon genişletme (CCE) deneyi, sabit hacim tüketim (CVD) deneyi ve seperatör testi deneyi verileri kullanılarak ve kurulan akışkan modeli parametreleri üzerinde regresyon yaparak deneysel veriler ile kurulan akışkan modeli karşılaştırmaları yapıldı. Sonuç olarak en iyi karşılaştırma elde edilen bileşimsel akışkan modeli simülasyon için gerekli olan PVT tablolarını elde etmekte kullanıldı.

Görelî geçirgenlik, kılcal basınç ve kayaç sıkıştırılabilirliği gibi kayaç özellikleri eldeki kayaç numuneleri verilerine ve endüstride kabul gören Corey ve Newman korelasyonlarına göre PETREL’de oluşturuldu. Bu alanda eldeki verilerin yetersizliği sebebiyle belirsizlerin oldukça fazla olduğu saptandı ve bu belirsizliklerin ancak sahadan alınacak ek veriler yardımıyla daha sonradan yapılacak çalışmalarda giderilebileceği belirlendi.

Simülasyonda kullanılacak kuyu performansı ve kuyu-içi akış performansı, PIPESIM’de kurulan tek kuyulu bir modelle belirlendi. Ayrıca en iyi üretim dizisi boyutu yine PIPESIM’de yapılan Düğüm (Nodal) Analizi çalışmaları ile belirlendi. Yapılan analizler sonucunda simülasyonda kullanılacak kuyu akış performansı 50 MMft<sup>3</sup>/gün ve en iyi üretim dizisi boyutu da 4.5 inç olarak saptandı.

Gözenekli ortamda dinamik akışkan akışı davranışını modellemek için numerik simülasyon modeli kuruldu. Rezervuar akışkanının gaz yoğunluk (kondensat) olması sebebiyle kompozisyonel (bileşimsel) simülasyon yöntemi tercih edildi ve sistem parametreleri tahmininde, rezervuar ve kuyu performansı tahmininde, uygun kuyu yerleşim planı belirlenirken, rezervuar yönetimi stratejisi belirlenirken, farklı geliştirme senaryolarının sonuçlarının analizinde ECLIPSE 300 bileşimsel simülatörü kullanıldı.

En iyi saha geliştirme senaryosu belirlenirken birçok teknik ve kontratla ilişkili sınır şartlar göz önünde bulunduruldu. Teknik ve kontratla ilişkili aşağıda sıralanan sınırlar temel saha geliştirme senaryosu oluşturulurken ve ana simülasyon modeli kurulurken göz önünde bulunduruldu:

- Kontrat başlangıç tarihi: 01.01.2013.
- Üretim başlangıç tarihi: 01.01.2016.
- Toplam kontrat süresi (üretim başlangıcından sonra): 20 yıl.
- İlk üretim gaz debisi hedefi: 150 MMft<sup>3</sup>/gün kuru gaz.
- İlk üretimde kalma süresi: 3 yıl.
- Pik üretim gaz debisi hedefi: 400 MMft<sup>3</sup>/gün kuru gaz.
- Pik üretimde kalma süresi: 10 yıl.
- Gaz işleme tesisi giriş basıncı: 1015 psia.
- Kuyuların minimum ekonomik gaz üretimi debisi: 1 MMft<sup>3</sup>/gün.
- Performans faktörü: Kontratta belirlenmiş gaz üretim debileri hedeflerinin altında bir debi ile üretim yapılması durumunda, hak edişler birden küçük ve yapılan gaz üretimi ile hedeflenen gaz üretiminin bölünmesi oranında bir katsayı ile çarpılacak.
- Açılacak kuyu tipi: Tüm kuyular rezervuarın yüksek basınçlı bir gaz rezervuarı olması sebebiyle düşey kuyu olacak.
- Gaz işleme tesisi ve kuyuların verimi: Gaz işleme tesisinde ve kuyularda olabilecek planlı ve plansız bakımlar ve arızalar sebebiyle yılın %10 ‘unda üretim yapılamayacağı göz önünde bulundurularak üretim hedefleri planlanmalı.



- Üretimde olacak fire faktörü: Kontratta tanımlanan ihraç gazı özelliklerini tutturabilmek için tasarlanan gaz işleme tesisinde gazın içindeki LPG'yi, asit gazları ve buharlaşmış suyu ayırmaktan dolayı kayıplar meydana gelecektir. Ayrıca gaz işleme tesisini ve kuyuları işletmek için belli bir miktar yakıt gazına ihtiyaç duyulmaktadır. Bu sebeple bütün bu kayıpları göz önünde bulundurmak için üretim hedefleri belirlenirken %14.05 üretim fire faktörü göz önünde bulundurulmalı.
- Malzeme seçimi: Kuyularda, gaz işleme tesisinde, saha içi boru hatlarında ve gaz ihraç boru hatlarında kullanılacak malzeme seçimi üretilecek gaz özelliklerine ve sahanın üretim ömrüne göre yapılacaktır.

Sonuç olarak, yukarıda sıralanan bütün teknik ve kontrata ilişkin sınırları göz önünde bulunduran rezervuar modeli ile sahada 31 kuyu açarak ve 2025 başlarında gaz kompresörleri devreye alarak yaklaşık %78 gaz kurtarımı başarıldı.

Daha sonra oluşturulan modelde ve temel senaryoda kuyu lokasyonu optimizasyonu ve kuyu tamamlama optimizasyonu gibi bazı uygulamalar yapıldı ve değerlendirildi.

Son olarak üzerinde çalışılan sahada ve üzerinde çalışma yapılan sahaya benzer sahalarda yapılması gereken ileri rezervuar çalışmaları ve sahadan alınması gereken ek veriler irdelendi ve önerildi.



## 1. INTRODUCTION

Reservoir management studies with high tech reservoir modeling and simulation software have taken a very important role in last twenty five years in the oil and gas industry with the increasing demand on non-renewable hydrocarbon (Mattax and Dalton 1990). Applying best reservoir management practices to exploit the limited natural sources as much as possible will only be possible by describing the complex reservoir structures and understanding fluid movement in the porous media as closer to reality as possible (Oliver et al. 2008; Caers 2005; Ertekin et al. 2001; Aziz and Settari 1979). Modern professional reservoir modeling software are taking the first place in the process of describing complex geological structures, understanding dynamic reservoir fluid behavior and predicting future performance of reservoirs. Typical reservoir studies can be very complex due to requirement of integration of several disciplines that those have different data sources in the different scale. Each of them has different perspective to look the problem and different tools to describe invisible underground structures; such as geophysicist has seismic data to model structures, geologist has logs to describe formation properties, reservoir engineer has well tests to predict reservoir parameters and reservoir performance.

On the other hand, the aim of reservoir simulation model is to construct a numerical model that is able to simulate the dynamic behavior of reservoir and fluid flow in porous media. Reservoir simulation is now widely used in petroleum industry for estimating system parameters, forecasting reservoir and well performance, deciding well spacing, determining reservoir management strategies, assessing and evaluating the results of different development scenarios that may be applied in field, and making investment decisions etc. 3D static reservoir model which the detailed geological description of reservoir is constructed generally with high resolution data from different sources and contains more than million cells, is the primary input of the reservoir simulators. The main components of the dynamic reservoir models are the 3D static geo-cellular model, fluid (Equation of State, EoS) model, rock-fluid

interaction model, well model, equilibration (i.e., initial conditions) model and if exist historical production data.

Figure 1.1 is a schematic view of the integrated reservoir modeling workflow from seismic to simulation. As can be seen from the Figure 1.1, first step is the collection of data from the field which is followed by analysis and integration of all the available dataset to describe the structure. Geological model construction is the next step followed by fluid and rock physical modeling. Final step is the construction of simulation model by properly integrating all the available information to predict the future performance of the reservoir under different development and production strategies. In this study given integrated reservoir modeling workflow in Fig. 1.1 is followed step by step and applied into real field dataset to determine the appropriate field development strategy for the field of interest in this study.

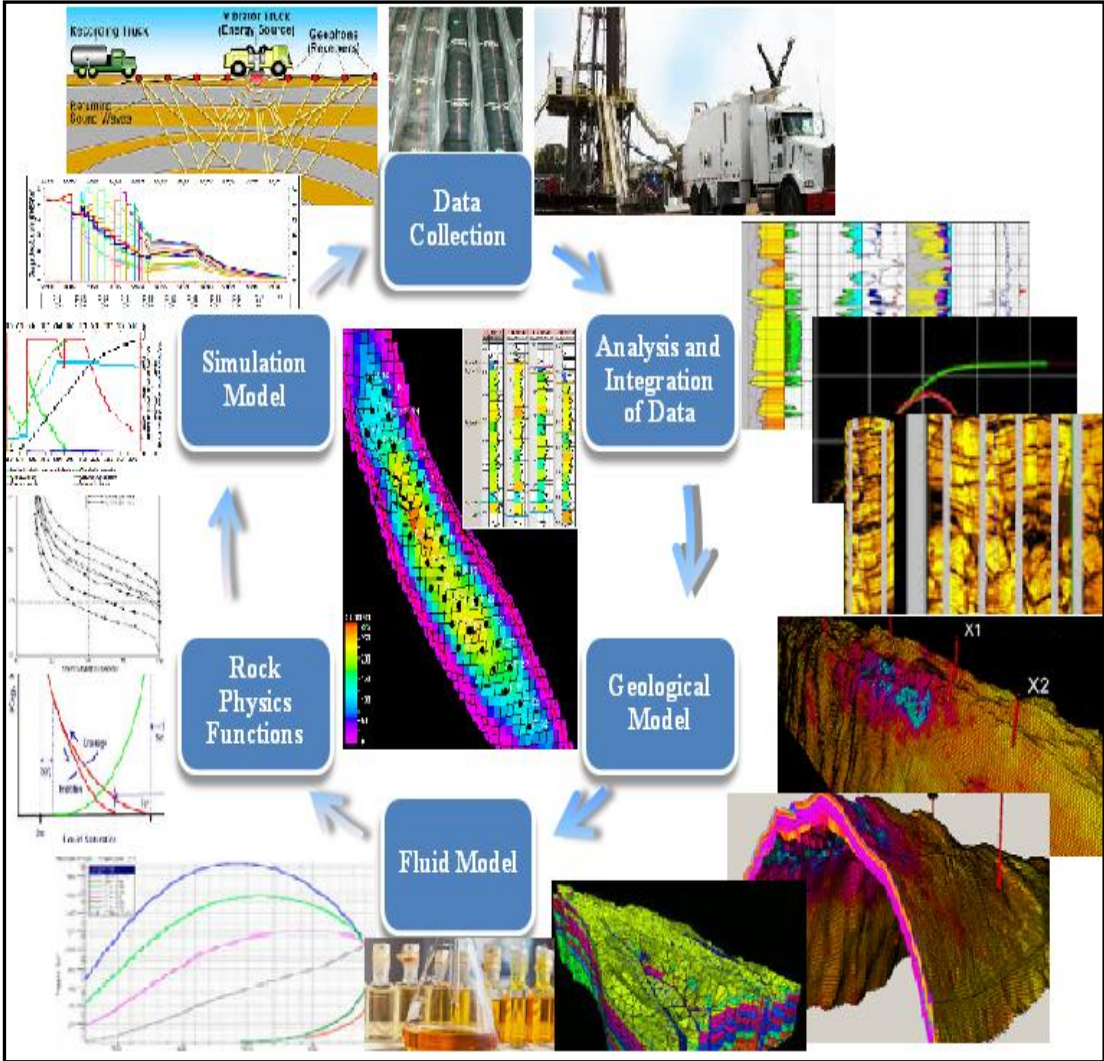


**Figure 1.1:** Integrated reservoir modeling workflow.

## **1.2 Statement of Problem**

In recent years, majority of oil and natural gas producing countries have shown great interest in signing service contract rather than production sharing agreements for developing their oil and gas projects and/or exploration projects. Production sharing agreements (PSA) is one of the main contract types that applied in oil and gas industry to arrange the relation between the host country and international oil companies (IOC). The IOCs bear responsibility for exploration and production in a condition that if the successful production is achieved; all the investment cost reimbursed by produced oil and remaining oil/gas production is identified as profit to share between IOC and hosting government. In this type of contract, the owner of the oilfield is the national oil company (NOC) of the hosting country although the hydrocarbon production can be owned by IOC. Besides, field is fully operated by IOC, and all the investments are made by IOC as well where the compensation of the IOC is made by a share from production. In PSA, development strategy of the field is fully determined by IOC according to the outputs of the profit maximization studies. On the other hand, a service contract is a long-term contractual framework that arranges the relation between the host country and IOC where the IOCs develop and explore the oil and gas fields of the hosting countries on behalf of them. The major difference between the PSA and service contract is the used compensation system of the IOC. In a service contract, hosting government is compensating all of the IOC expenditures as well as paying additionally pre-determined service fees. In this type of the contract, unlike the PSA, no sharing is applied on the production, and the field is not fully operated by IOC although all the pre-investments are undertaken by IOC. Therefore, unlike the PSA, development strategy of the field is not fully determined by IOC in a service contract. If the project is not an exploration project, pre-development plan is submitted by the IOC while signing the contract. For instance, early production rate duration, plateau production rate duration, and service fees are pre-determined contractual terms that the IOC has to develop the field accordingly. It is obvious that there are almost no advantages of service type of comparing the PSA for the IOC.

This study is prepared for the determination of reservoir development strategy of the Field-X based on a service contract terms agreed in between the IOC and hosting government. Since there is a confidentially agreement between the IOC and hosting

government, it is not allowed to disclose the name of the IOC, name of the hosting government, and name/location of the field. Additionally, signed service contract terms manipulated not to disclose the contractual terms as it is.

### **1.3 Scope of Study**

To be able to determine the development strategy of the field, contractual and technical constraints determined between the companies (IOC and hosting government) should be considered first. Then, all the available dataset is studied. Then, 3D static geological model is constructed based on available data. Once the static model completed, dynamic reservoir model is built based on 3D static geological model and available data. Then, required number of wells and their locations is determined in which the desired contractual terms is achieved and none of the constraints disregarded.

Therefore, the contractual and technical constrains are first to be stated and these are given in Chapter 2. The available dataset that were available are geophysical data, well-log, core, PVT, and well-tests. Such data sets are evaluated and presented in Chapter 3. 3D static geological model is constructed based on analyzed dataset which is presented in Chapter 4. Based on the constructed geological model, a dynamic simulation model was constructed and presented in Chapter 5. After completing all of these steps, base case development strategy, number of wells, and locations were determined based on constructed models by honoring the contractual and technical constraints. A few applications performed on the base case simulation model are given Chapter 6. Concluding remarks and recommendations for future works are given in Chapter 7.

## **2. TECHNICAL AND CONTRACTUAL CONSTRAINS**

As stated before, both contractual and technical constraints need to be considered first in a preparation of development strategy. Therefore, the main purpose of this study is to determine a development strategy of the Field-X by taking into consideration of the following technical and contractual constraints:

- **Commencement of the contract:** After the contract signature in between the IOC and hosting government, a contract effective date is determined by the ministry cabinet of the hosting government. The effective date of a service contract is assumed as a commencement date of the signed contract and the contractual obligations of the IOC are started with the effective date. In this study contract effective date is 01.01.2013. To be able to start production from the field, gas processing facility to handle the early production (150 MMscf/d) needs to be constructed and couple of well needs to be drilled. To achieve the early production target, four wells planned to be drilled and a gas processing facility with a 150 MMscf/d gas handling capacity is planned to be constructed. These activities will be completed before the end of 2016; therefore, simulation start date is determined as 01.01.2016.
- **Contract duration:** Contract duration is a pre-determined term that the IOC has the right to produce from the field and claim service fees within this duration. Count down on the contract duration starts with the first production date from the field and if the field is not completely depleted until contract end date, all the operations will be handed over to hosted government. In this study contract duration is 20 years which will be commenced with the first production from the field.
- **Early production target:** Achieving early production with a constant 150 MMscf/d gas rates is another contractual obligation of the IOC. If the average gas production rate from the field is 150 MMscf/d within a month, then the early production target will be achieved and the IOC will be able to claim service fees for this period. Otherwise, if the gas production from the field is

lower than the targeted early production, a performance factor will be applied to the service fees according to the production from the field which will reduce the earning of the IOC.

- Duration of the early production: 150 MMscf/d gas productions from the field has to be maintained at least three years until reaching the plateau production capacity.
- Plateau production target: Plateau production is an event that the hydrocarbon extraction from the field is reached its maximum level and tried to be maintained until the decline on the production starts. Achieving plateau production with a constant 400 MMscf/d gas rates is another contractual obligation of the IOC in this contract. If the average gas production rate from the field is 400 MMscf/d within a month, then the plateau production target is assumed to be achieved by IOC. To be able to handle 400 MMscf/d gas productions, an additional gas processing facility with a 250 MMscf/d handling capacity is required to be constructed. Therefore, IOC is obliged to construct gas processing facility with a 400 MMscf/d gas handling capacity prior to 2019 and obliged to reach plateau production on the first of Jan 2019.
- Duration of the plateau production: 400 MMscf/d plateau production from the field has to be maintained at least ten years: however, if the plateau production is achieved to be extended more than ten years, IOC will have the right to claim service fees for this period at the maximum level.
- Facility inlet pressure: According to the gas processing facility design and engineering studies, minimum inlet pressure of the facility is determined as 1015 psi. Therefore, minimum inlet pressure of the facility is another constraint to be considered in the simulation that determines the development strategy of the field.
- Economical minimum production rates of a well: Producing wells have some daily operational cost such as electricity for the control panels and injected chemicals to avoid corrosion. Therefore, gas production from a well need to greater than a certain amount that can meet the operational costs. In this field minimum economical gas production is determined as 1 MMscf/d according to associated operational expenses.



- Type of wells: According to the engineering studies, field is significantly over pressured and drilling of the vertical wells is the best option due to high pressure gas reservoir conditions. Therefore, all the proposed wells need to be vertical wells in the simulation model and development strategy need to be determined accordingly.
- Facility/wells downtime: There will be planned and unplanned shut downs on the wells and gas processing facility due to regular maintenance and unplanned failures of the system. In this study, planned and unplanned shut downs will be considered with 10% facility and wells efficiency factor.
- Performance factor: As mentioned previously, producing less than desired early and plateau production target rates will reduce service fees of the IOC's (Performance factor which is less than 1.0). Therefore, development strategy needs to be defined to make sure that desired production targets are achieved. This will only be possible to have some additional wells online in case of failure any of the wells and having some extra gas processing handling capacity to mitigate the downtimes by producing more than targeted amounts on the uptimes.
- Shrinkage factor: Another contractual obligation is to deliver the dry gas with the defined dry gas specs in the contract. Therefore, impurities (acid gas), LPG and evaporated water in the gases need to be separated from the produced gas. In addition, there will be fuel gas consumption to operate the gas processing facility and wells. Therefore, facility designed to meet the required export gas specs where there will be 3.94% loses from produced gas due to LPG recovery, 5.78% loses due to acid gas removal, 0.34% loses due to dehydration and 3.99% loses due to fuel gas consumption. As a result in order to meet the desired early production target and plateau production target, totally 14.05% production loses need to be considered in the simulation.
- Material selection: As previously, discussed contract duration is 20 years after production starts: therefore, material selection has to be made based on production life time of the project.



### 3. ANALYSIS OF AVAILABLE DATA

A variety of data is acquired from the Field – X to explore and appraise the field. At the beginning, 2D seismic campaign were conducted to delineate the field which was shot in two phases. First phase which comprises lines pik-01 to pik-29 as shown in Figure 3.1 were processed and interpreted. After five years, the second phase which comprises pik-101 to pik-122 as shown in Figure 3.1 was processed and interpreted. Based on both survey results, the first exploration well X-1 was drilled and tested gas and condensate. Then, three appraisal wells were drilled; well X-2; X-3 and X-4. The appraisal wells X-2 and X-3 tested gas and condensate as well; however, the appraisal well X-4 was a water-leg<sup>1</sup> well. From the drilled four wells, final well reports, conventional core analysis, logs, well test data and PVT data are available. Later on, 3D seismic data were acquired successfully, processed and interpreted to decrease the structural uncertainty. In addition to this, surface well-test operations were conducted on the existing well X-2 to obtain additional PVT data. There has not been any hydrocarbon production to date except the testing period. Therefore, there is no historical pressure and, flow rate measurements that can be used for history matching purposes.

In this section whole available data are introduced step by step. To achieve one of the main objectives of this study, which is constructing 3D static and dynamic reservoir models, all available data is prepared and cleaned up carefully. 3D static geological reservoir model is built in geological modeling software PETREL, and most of the input data is prepared in PETREL inputs format. On the other hand for the simulation study ECLIPSE E300 compositional simulator will be used. Therefore, while performing reservoir engineering input clean up and preparation, compatibility of the inputs format with ECLIPSE 300 is considered. On the other hand, fluid characterization is performed with PVTi.

---

<sup>1</sup> A water leg well is a well that is completed in a water zone.

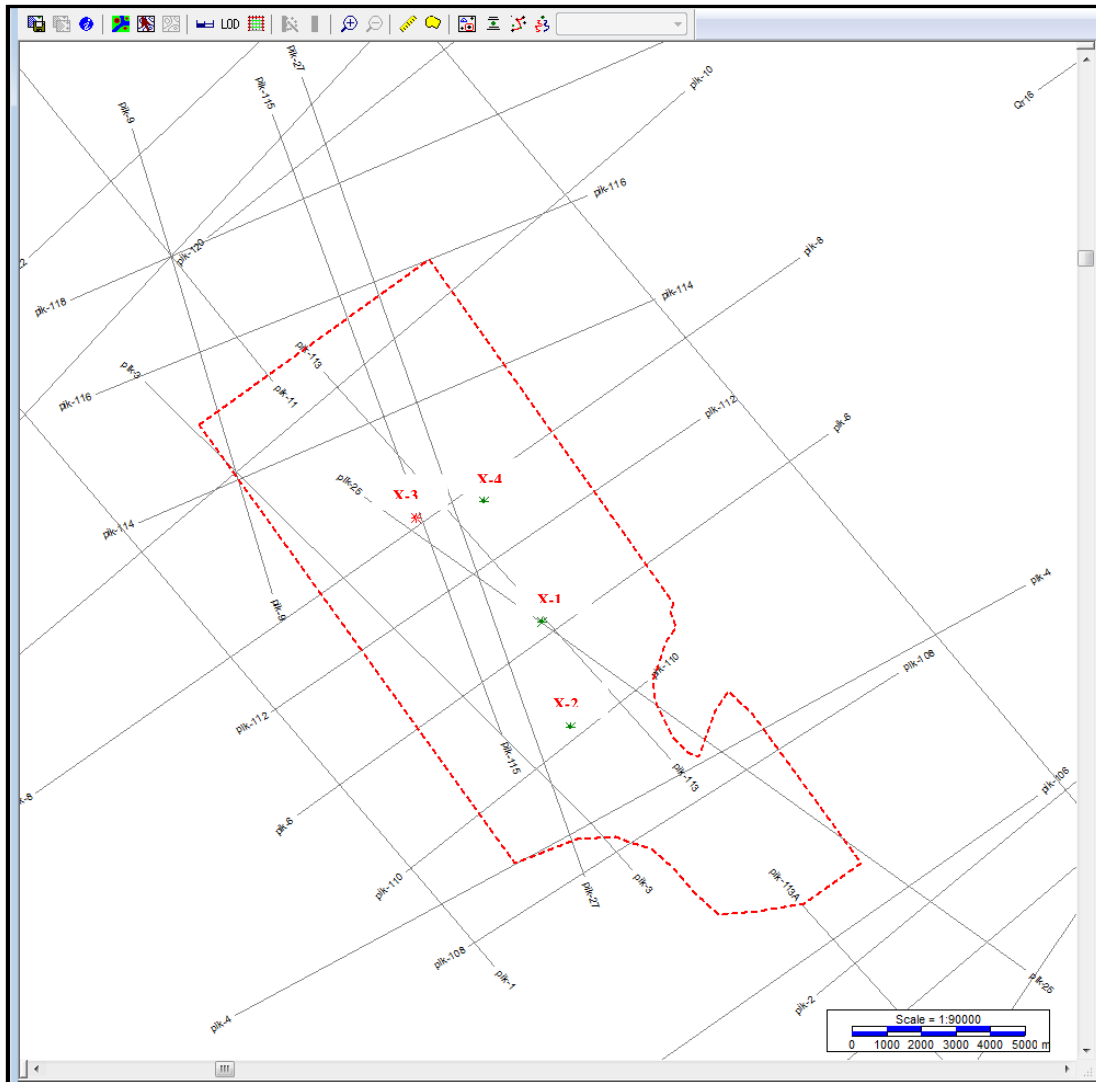


**Figure 3.1:** 2D seismic lines.

### 3.1 Geophysical Data

2D and 3D seismic data are available which were processed and interpreted. After processing 2D and 3D seismic both data packages were evaluated by geophysical team, and formation top and formation base time maps were constructed. All the constructed time maps were converted to depth maps by constructing velocity model for the field. Additionally, existing normal and reverse faults were identified by the geophysicists, and the fault sticks were prepared by them. In this study there will not be any further study on the evaluation of geophysical data. As main geophysical inputs, generated structural maps and fault sticks by geophysical team was used for constructing the 3D static model. On the other hand, all the surface modeling, well

tie in<sup>2</sup>, well tops matching and fault modeling for the geological model purposes are conducted in PETREL as part of this study. In Figure 3.2, formation X top map 2D view is shown where all the existing wells locations; faults and formation closure are marked on the map. Similarly, 3D view of structure is shown in Figure 3.3. Furthermore, the structure is bounded by three main faults systems which lie down in the SE-NW direction as demonstrated in the Figure 3.4.

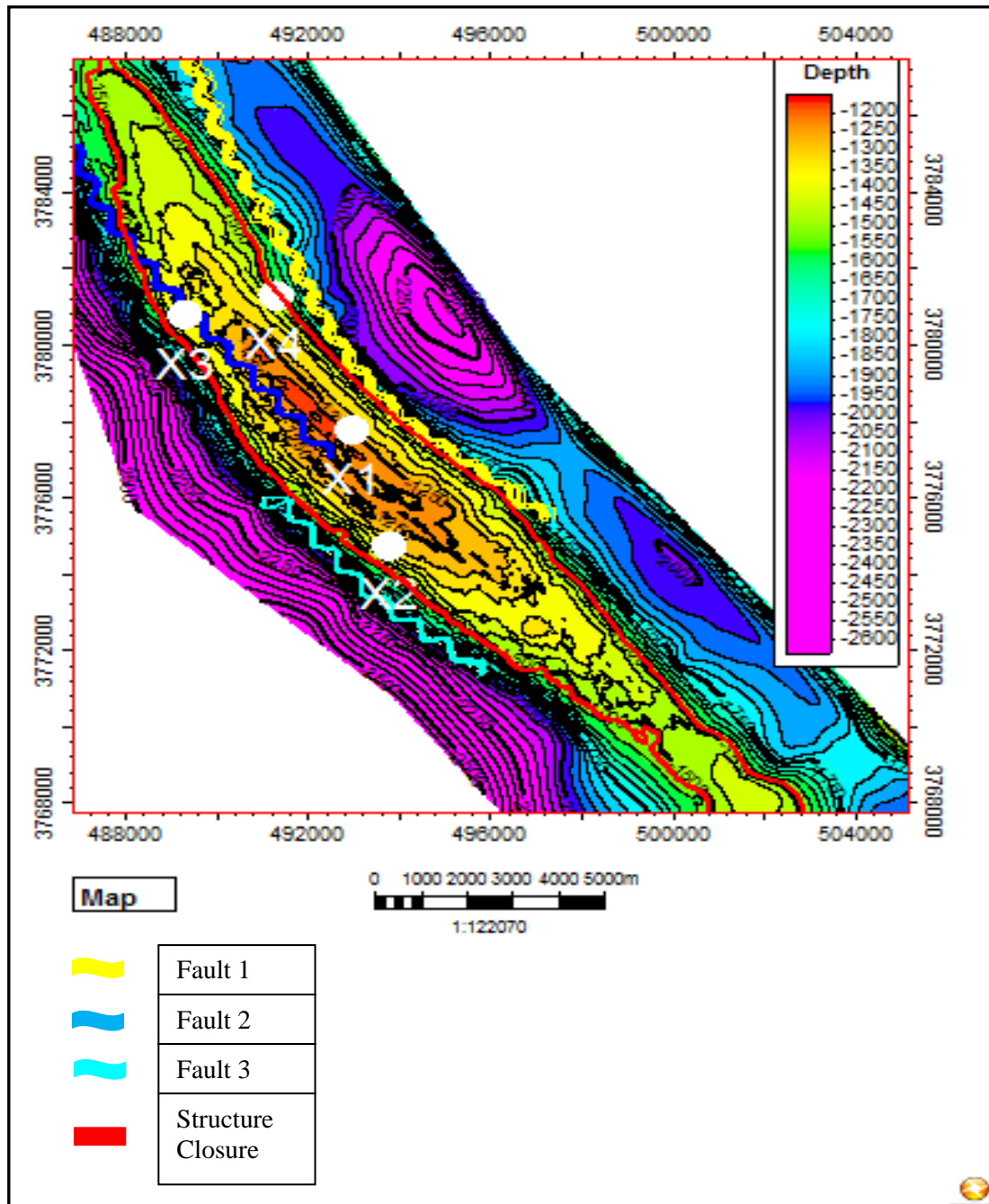


**Figure 3.2:** Top of formation X depth map - 2D view.

<sup>2</sup> A comparison or the location of a comparison, of well data. Properly processed and interpreted seismic lines can show good ties, or correlations, at intersection points.

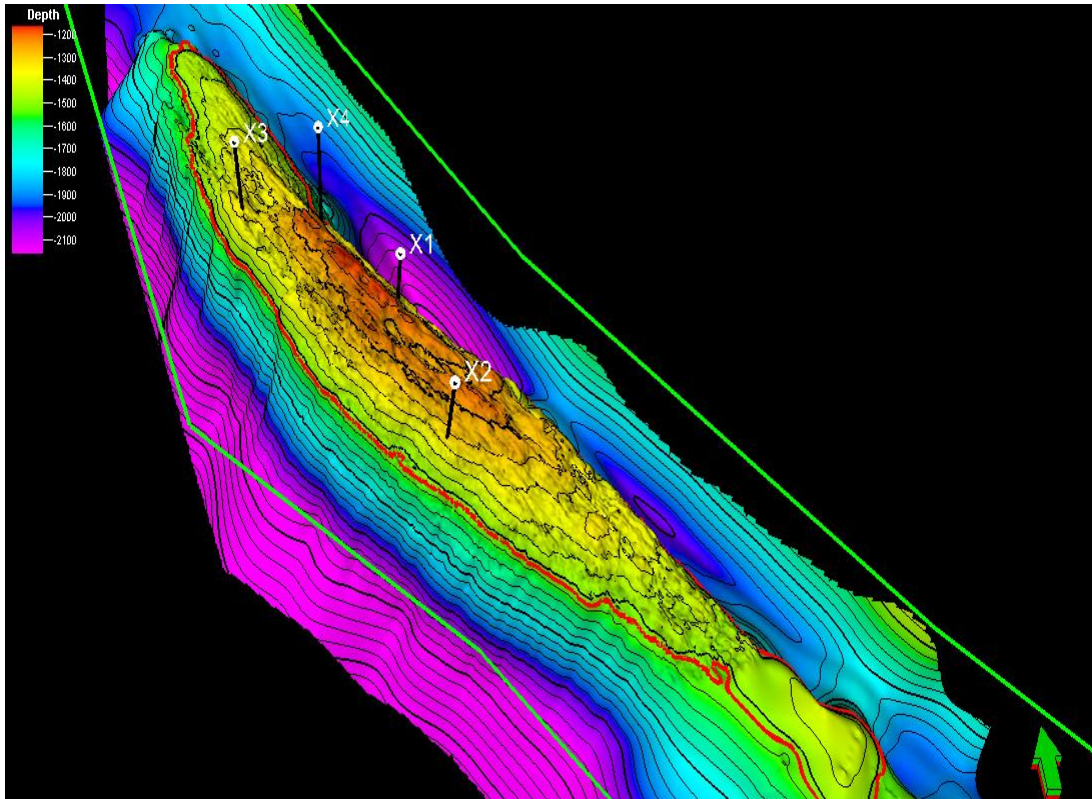


Figure 3.3: Top of formation X depth map - 3D view.

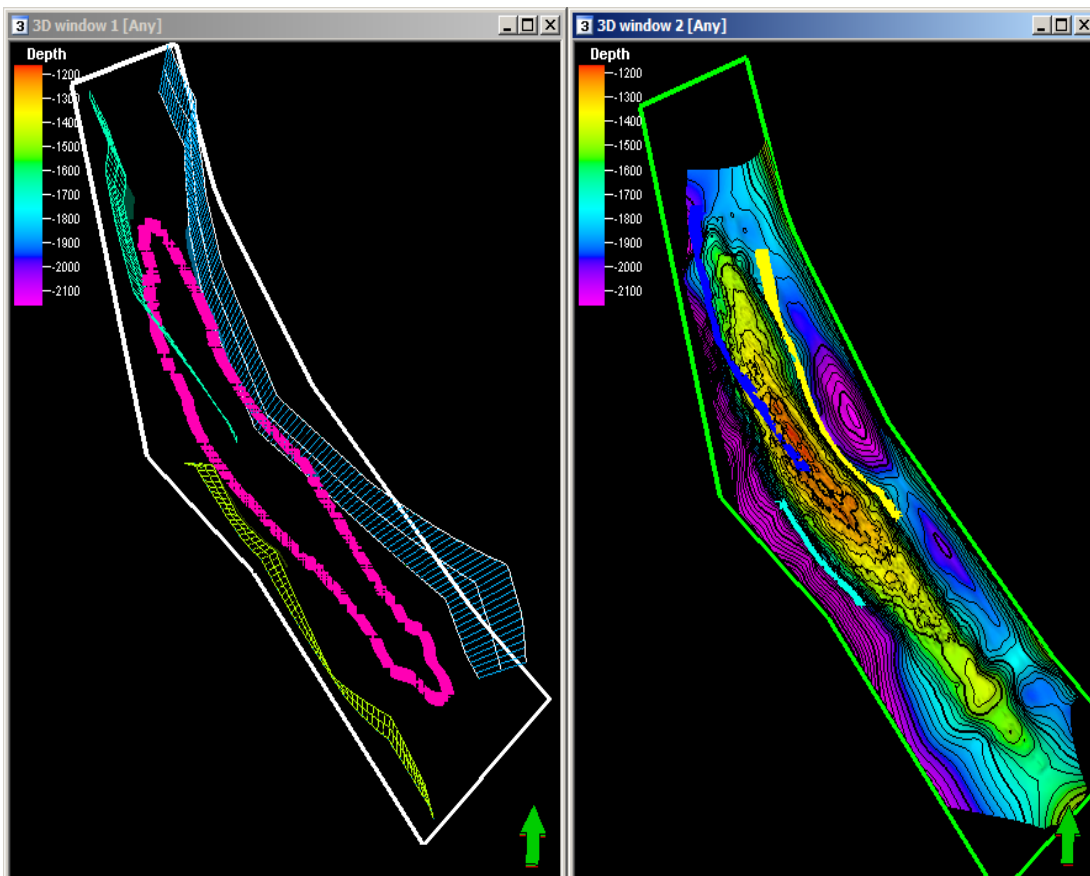
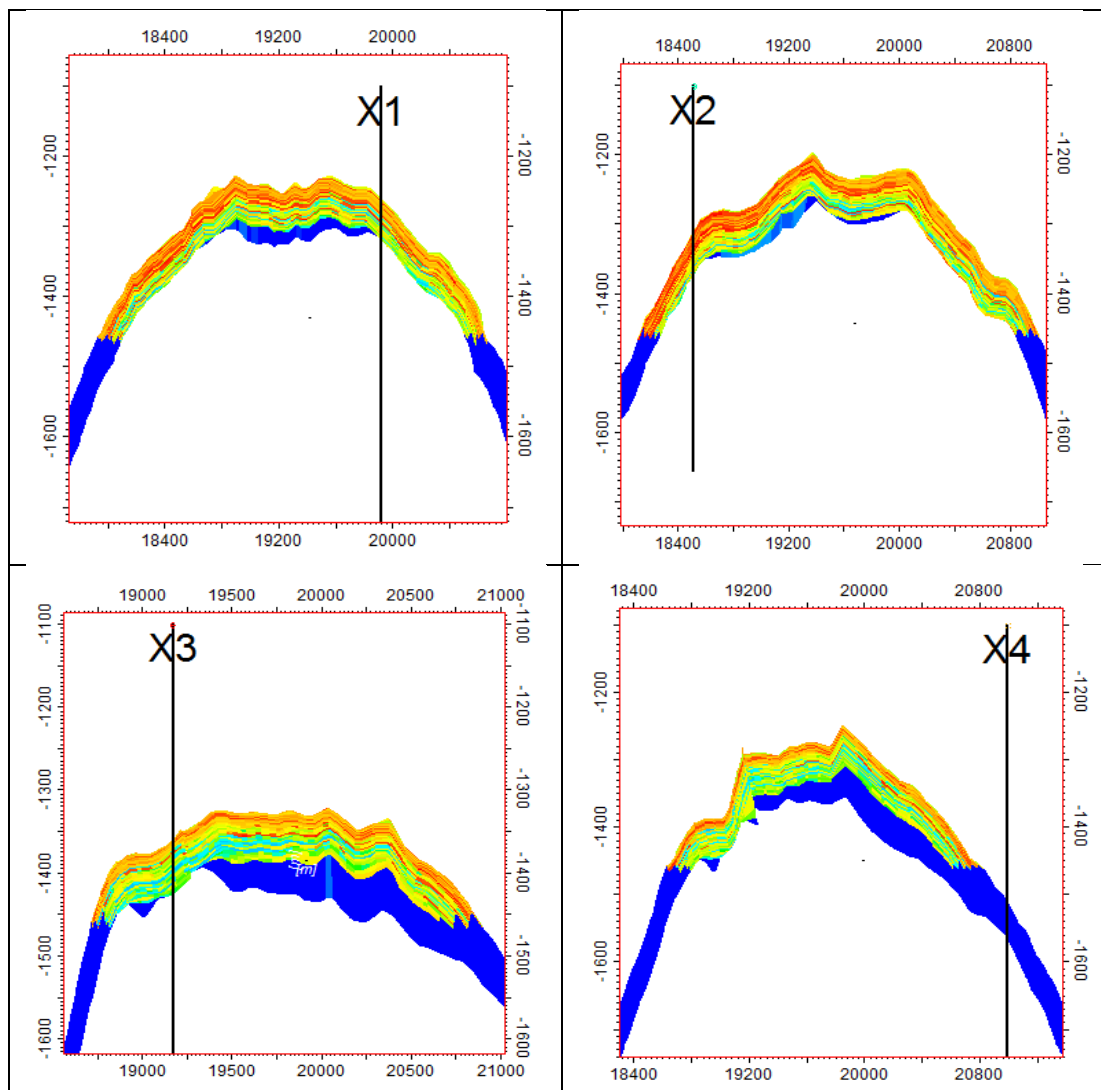


Figure 3.4: Main faults - 3D view.

### 3.2 Well Logs

Well logs are available from the four existing wells (Wells X-1: X-2: X-3 and X-4) in the field. In this study, log data will be analyzed and used as a geological input in the 3D static model. Especially, after comparing with the core data, porosity log and water saturation log will be used in the petrophysical modeling part of the static model. Porosity and water saturation logs from the existing wells will be distributed to whole field after variogram modeling (Journel, 1978). In addition, those inputs will be the basis of making reservoir zones and layers. Figure 3.5 shows the cross-sectional view of the water saturation maps and the location of the wells where the log data gathered from the formation. As it can be seen from the figure well X-1 located relatively more near to crest than the others (well X-2, X-3 and X-4). Additionally, it is obvious that well X-4 completed in water zone.



**Figure 3.5:** Well locations – cross section.

**3.2.1 Well X-1 logs**

Figure 3.6 shows the well X-1’s log porosity, water saturation, gamma ray, and laterolog shallow resistivity from the left to right. As can be seen from Figure 3.6, formation starts at approximately 1265 mss and ends at 1331 mss. So, the formation thickness at well X-1 is around 66 m. Porosity is almost constant in the whole formation where the average log porosity value is around 20 percent. It is also important to note that water saturation is very low in the upper section and it increases gradually through the lower parts. Gamma ray readings are almost constant and very low. This indicates that the formation is clean, and there is no shale barrier to identify. On the other hand, resistivity readings are higher in the upper section than the lower section and decrease gradually in through the lower section which is in line with the water saturation log. Water saturation is very low in the upper section of the formation; therefore, resistivity measurement is expectedly lower in those sections. All in all, all the log data will be analyzed and used as geological inputs of the 3D static reservoir model.

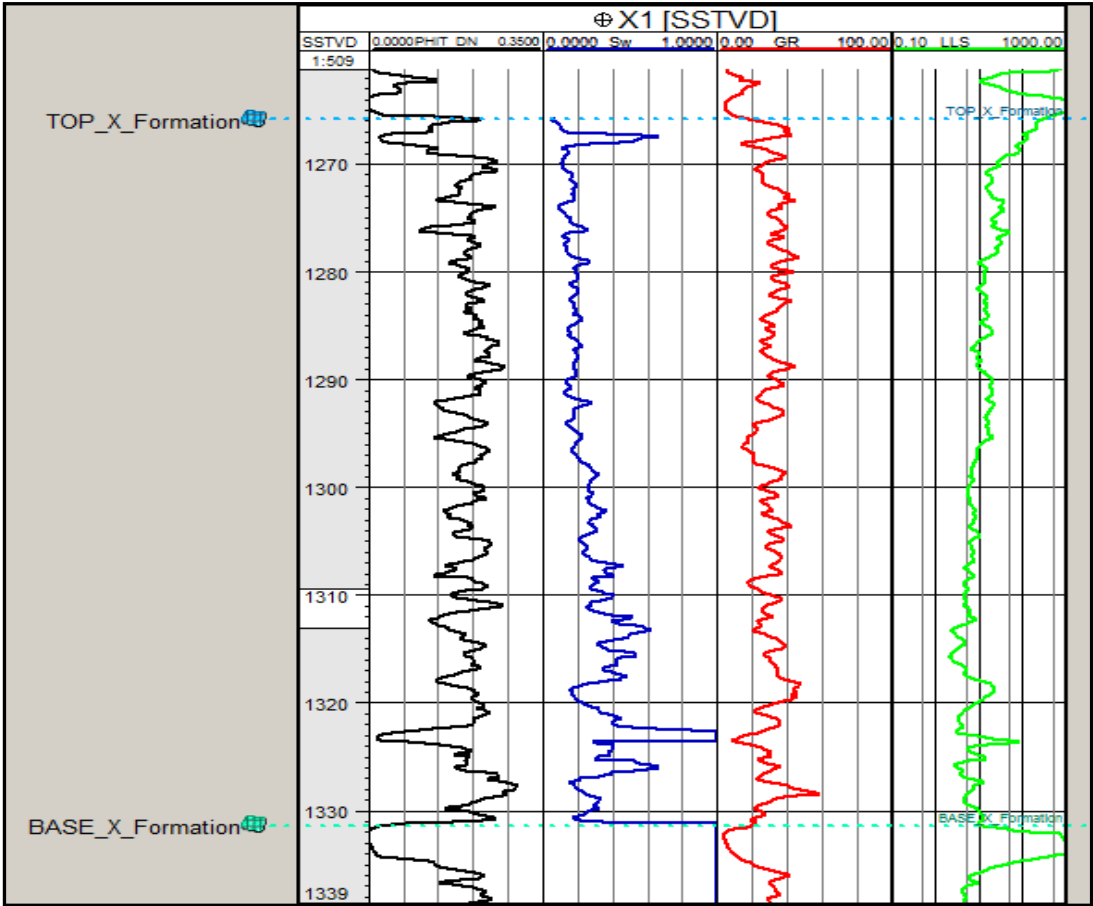


**Figure 3.6:** Well X-1 logs.



### 3.2.2 Well X-2 logs

Figure 3.7 shows the well X-2's log porosity, water saturation, laterolog shallow resistivity and gamma ray from the left to right. As can be seen from the Figure 3.7, the formation starts at approximately 1311 mss and ends at 1372 mss. So, the formation thickness at the well X-2 is around 61 m. Porosity is almost constant in the whole formation where the average log porosity value is around 20 percent. It is also important to note that water saturation is very low in the upper section and it increases gradually through the lower parts. However, this behavior is more distinct than the well X-1 log which can be indication of better petrophysical property in that area. Water saturation is almost zero in the upper part; on the contrary resistivity is very high in that part. It can be interpreted as high permeability and porosity is the reason of very low formation water in the upper sections. Gamma ray readings are almost constant and very low. So, the formation is clean and there is no shale barrier to identify.

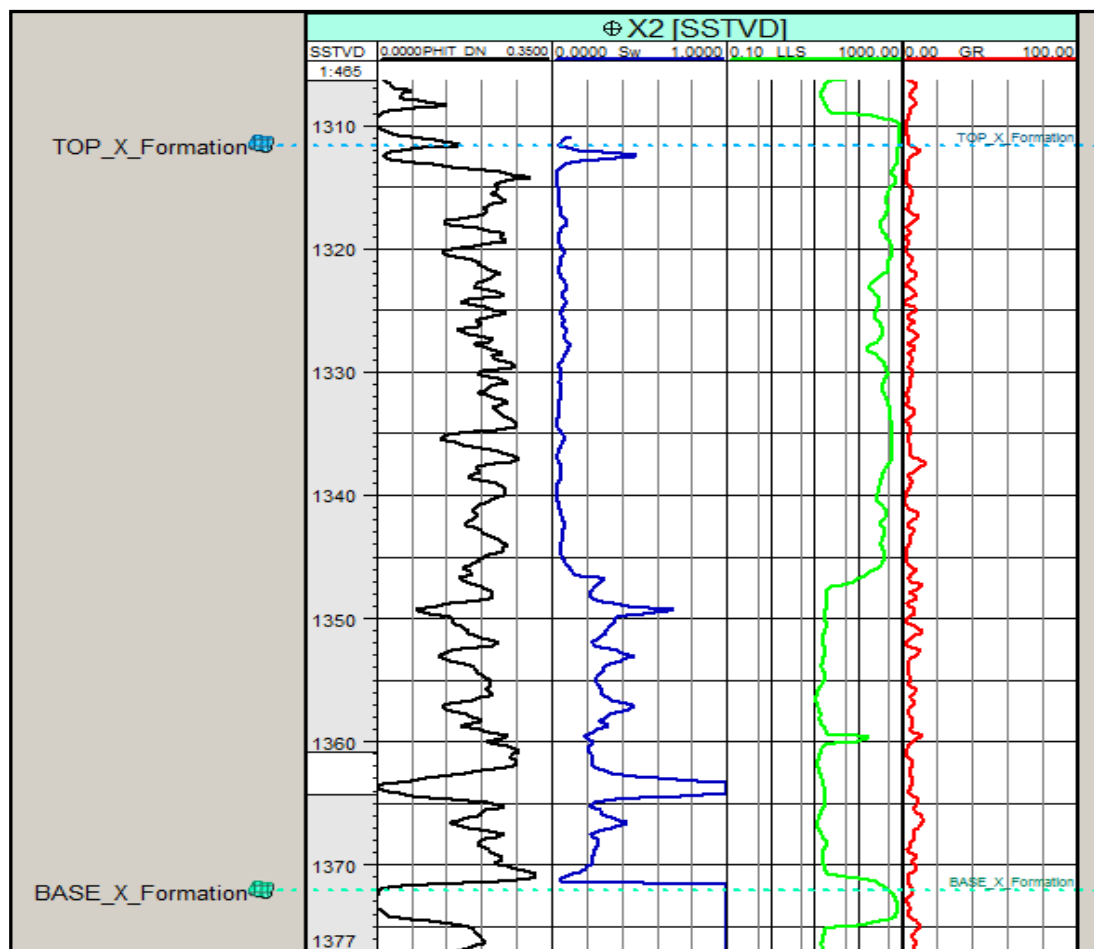


Figure 3.7: Well X-2 logs.

### 3.2.3 Well X-3 logs

Figure 3.8 shows the well X-3 log porosity, water saturation, gamma ray and laterolog shallow resistivity from the left to right. From Figure 3.8, it can be seen that the formation starts at approximately 1330 mss and ends at 1392 mss. Hence, its thickness is around 62 m. Porosity is almost constant in the whole formation where the average log porosity value is around 19 percent. Also note that water saturation is very low in the upper section and it increases gradually through the lower parts. However, this behavior is less distinct than the well X-2 log and more distinct than well X-1 which can be an indication of better petrophysical properties existence in that region than those of well X-1's area. Besides, this region has purer petrophysical properties than the region of well X-2. Water saturation is almost zero in the upper part; on the contrary resistivity is very high in that part. It can be interpreted as the region of high permeability and porosity is the reason of very low formation water in the upper sections. Gamma ray readings are almost constant and very low. This shows that the formation is clean in that region as well and there is no shale barrier to identify.

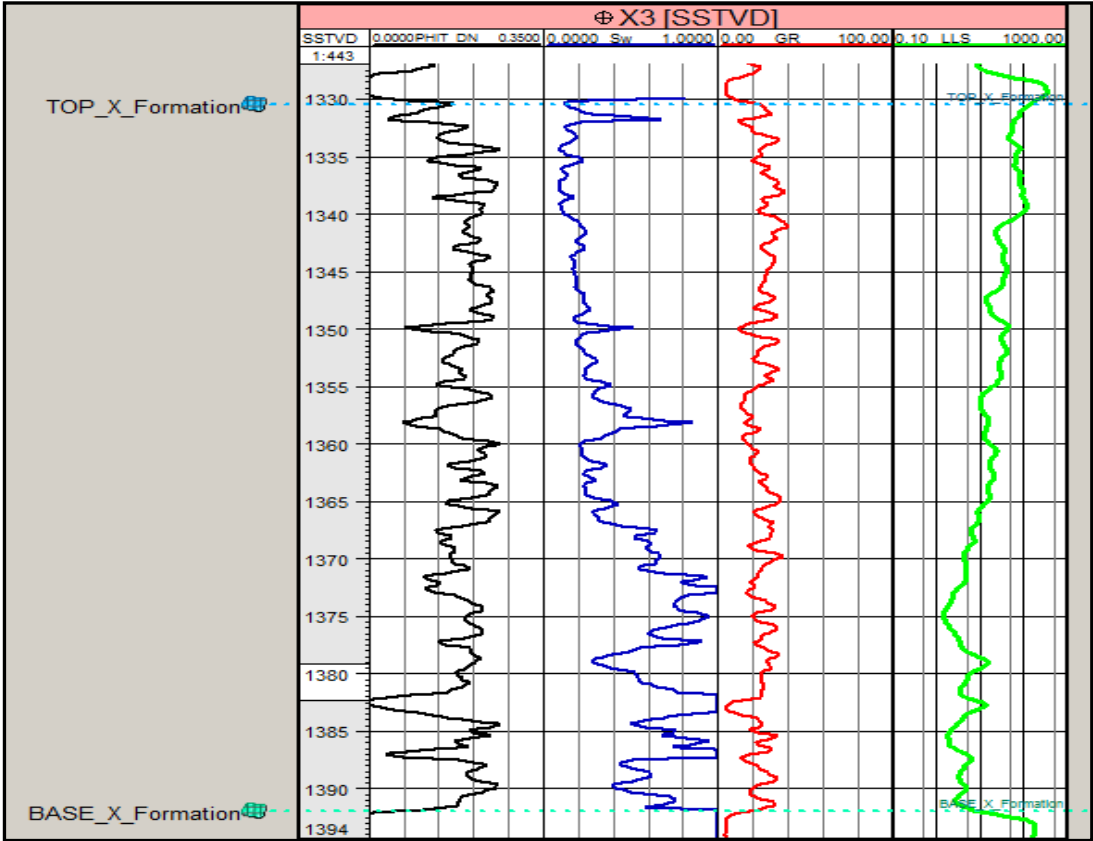
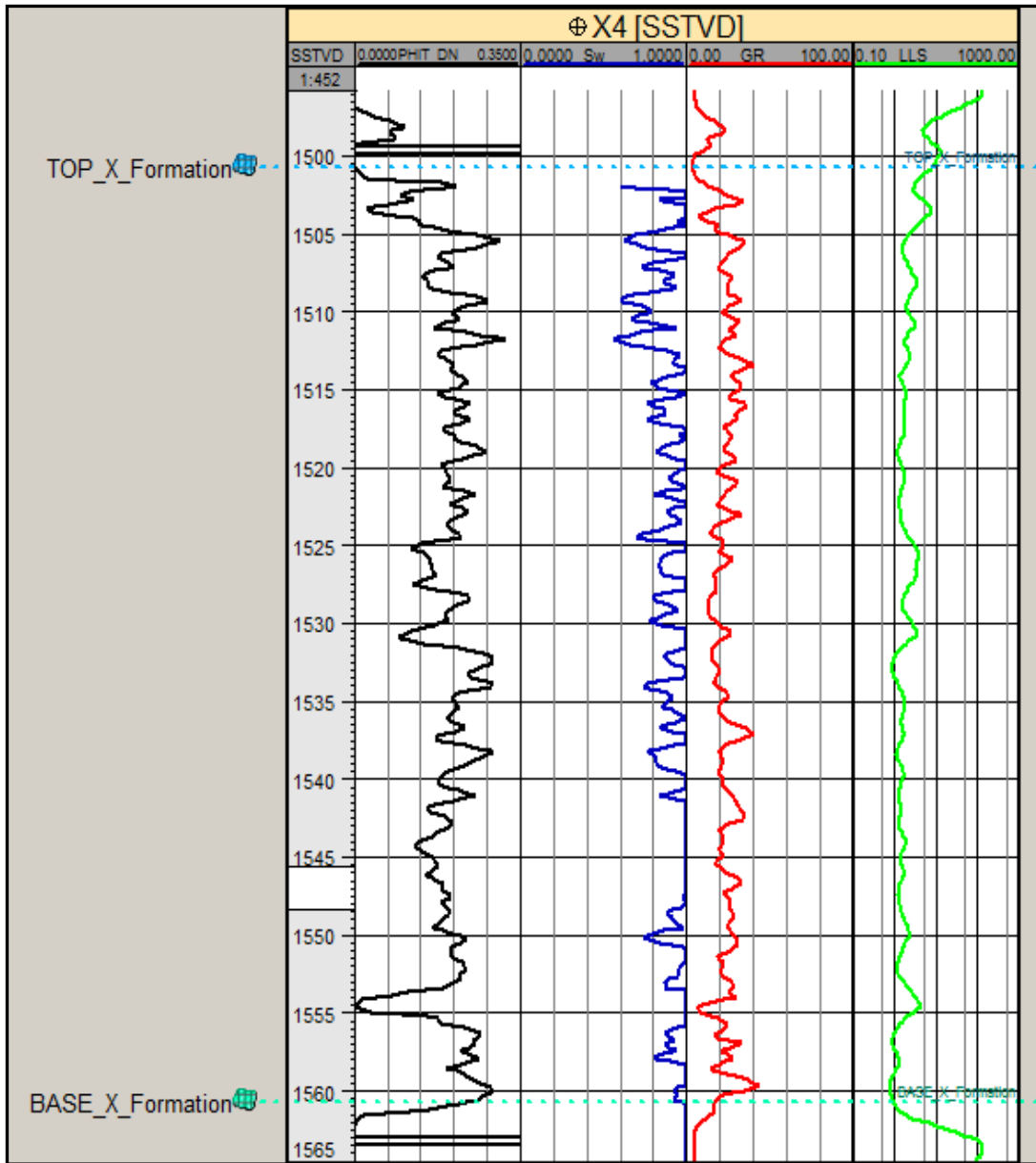


Figure 3.8: Well X-3 logs.

### 3.2.4 Well X-4 logs

Figure 3.9 shows the well X-4's log porosity, water saturation, gamma ray and laterolog shallow resistivity from the left to right. From Figure 3.9, it can be seen that formation starts at approximately 1501 mss and ends at 1561 mss. So, its thickness is around 60 m. Porosity is almost constant in the whole formation where the average log porosity value is around 20 percent. Also note that well X-4 is a water leg well and tested water only. Therefore, water saturation is almost unity (i.e., 100%) in the whole formation. Since the whole formation is fully filled with water, the resistivity measurements are very low as expected. Gamma ray readings are almost constant and very low. Like in the other wells, this indicates that the formation is clean and there is no shale barrier to identify. It is needless to say that while performing petrophysical modeling study, some of the log data of well X-4 will not be used. For instance, water saturation will not be used due to location of the well in the field. On the other hand, while distributing porosity, well X-4's log porosity will be used. Formation starts at approximately 1501 mss in the well X-4 and the GWC is shallower than this depth. If the water saturation log of the well X-4 is used in the petrophysical modeling, it will increase the mean value of the water saturation of the field and therefore, it will mislead the distribution which will be made by SGS. Besides, the cells below GWC will be fully filled with water and well X-4 provides the water saturation information below GWC which is not inside the zone of interest in terms of water saturation distribution. On the contrary, formation porosity and permeability are not varying materially with the formation depth. Therefore, there is no restriction to use well log information of the well X-4, while performing porosity permeability distribution through the field. Additionally, if any need arises to connect aquifer to the formation in the simulation, modeling the porosity and permeability below GWC will be necessary. Considering the above mentioned reasons, water saturation log of the well X-4 will not be used while modeling water saturation of the field. However, rest of the well log information from the well X-4 will be very beneficial and used for geological property modeling.

In conclusion, since the well X-4 was completed in water zone, log information except water saturation used as a geological input on the 3D static reservoir modeling activities.



**Figure 3.9:** X4 well logs.

### 3.3 Cores

There are core data that recovered from all the existing four wells in the field. The detail information about the recovered cores from each of the existing wells are given in the below section 3.3.1 to 3.3.4. In this study core data was analyzed and used as a geological input in the 3D static model. First of all, a comparison of log and core data was conducted before starting 3D static reservoir model. Especially, core data was used as quality check information to the well logs. Before making any property distribution in the field consistency check of the property is made by core and log data. Furthermore, those inputs are the basis of making reservoir zones and layers

together with log data. Additionally, due to limited well-test information (to be discussed later), core data was used for permeability modeling. Figure 3.10 shows the porosity – permeability cross plot of all wells core data. Additionally, core porosity, permeability and log permeability histograms are given in Figures 3.11 to 3.13 respectively. After analyzing well logs and cores, reservoir was divided to sub-zones and layers according to the similarity of the property that seen in any of the specific section & interval. Once the zones and layers are obtained, permeability and porosity of the each zone is drawn and those relationships are combined with well log data to obtain the permeability models for each zone. Moreover, well-test data is analyzed and compared with the obtained permeability model. If there is any discrepancy between the cores derived permeability and well-test derived permeability, the model will be modified according to the well-test derived results. In addition, core porosity and permeability statistics from all wells are given in Tables 3.1 and 3.2, respectively. Besides, correlation coefficient between log porosity and permeability are tabulated in Table 3.3.

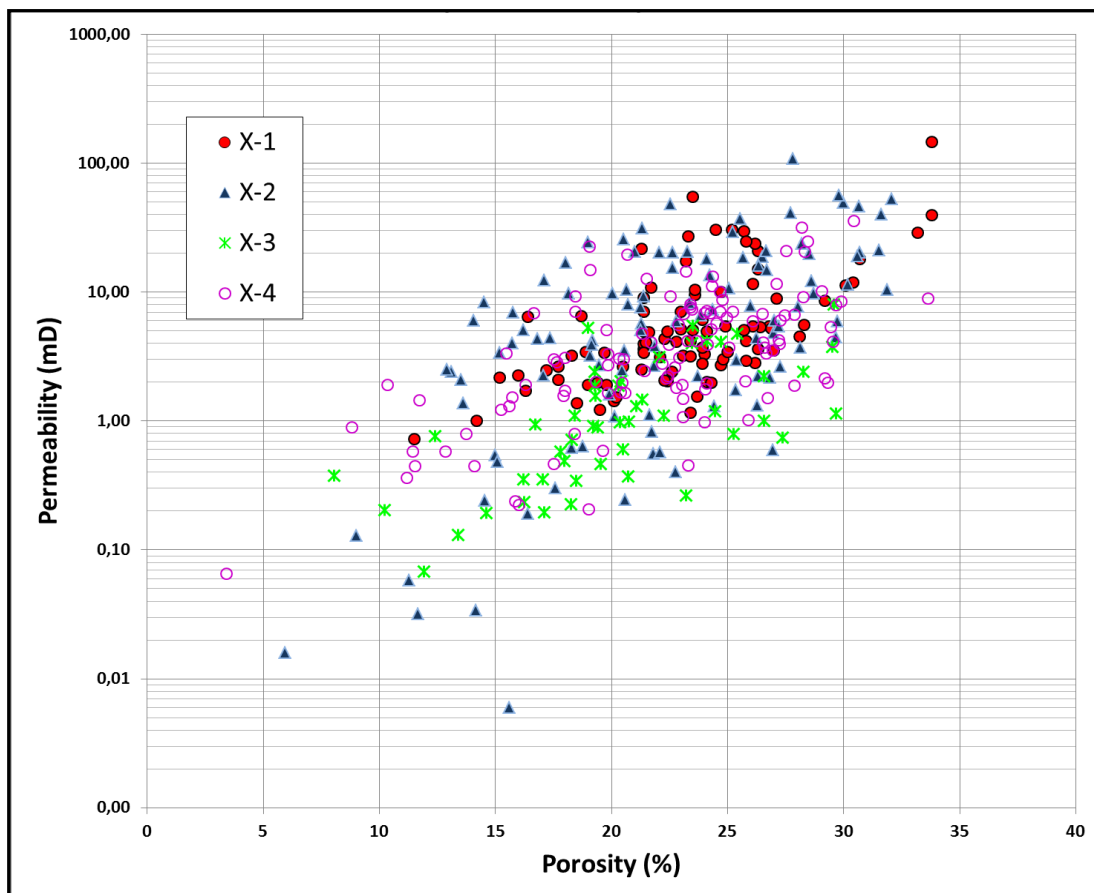


**Figure 3.10:** Core porosity-permeability cross-plot of all wells.

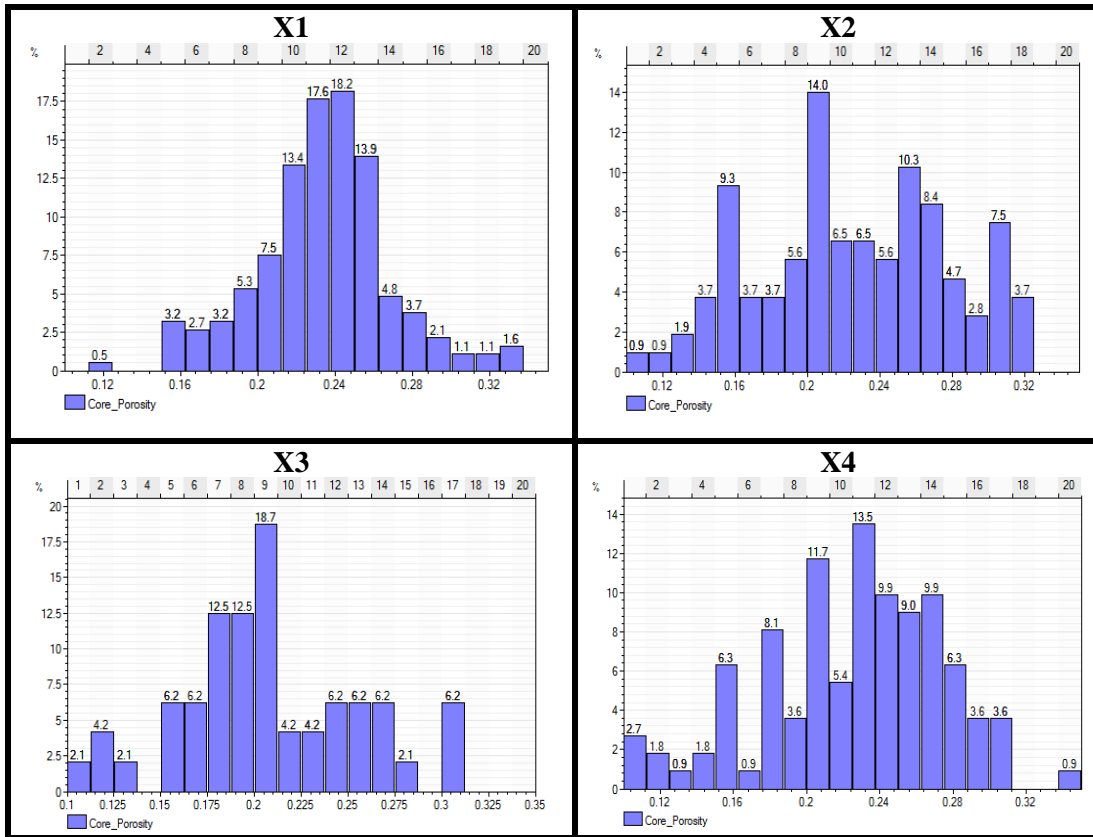


Figure 3.11: Core porosity histograms for each well.

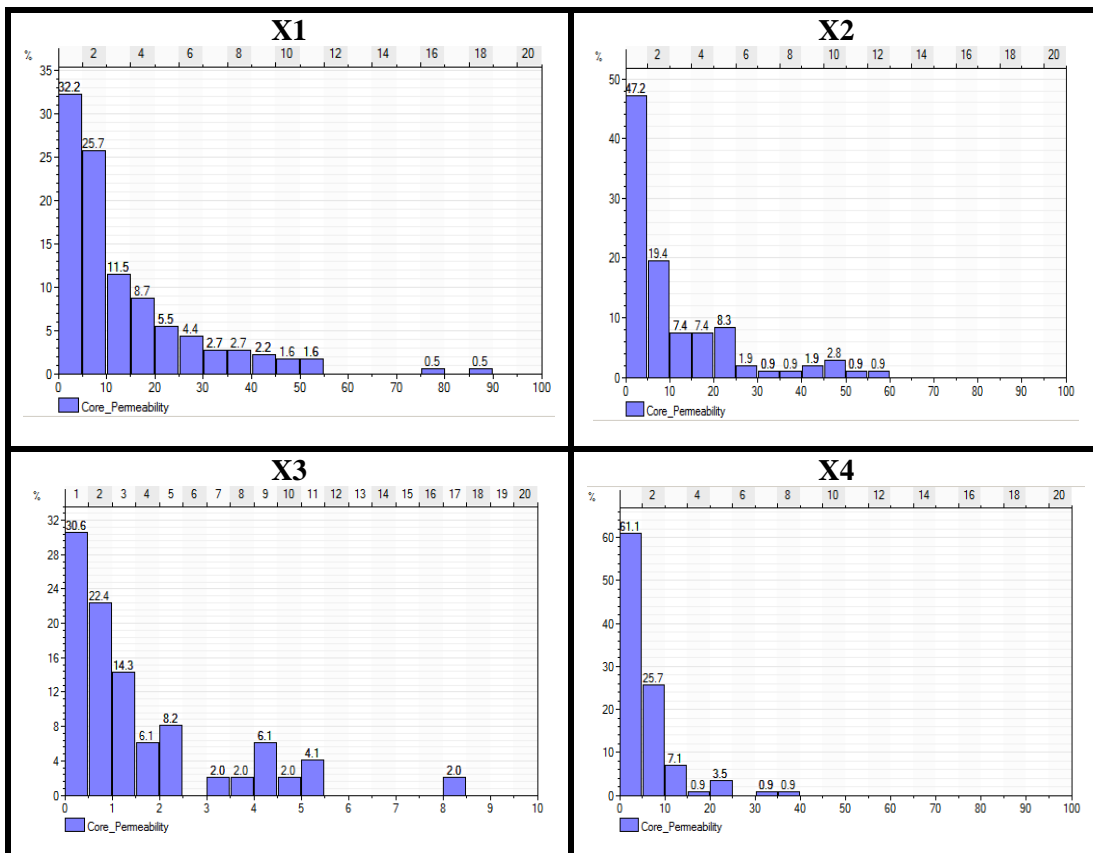
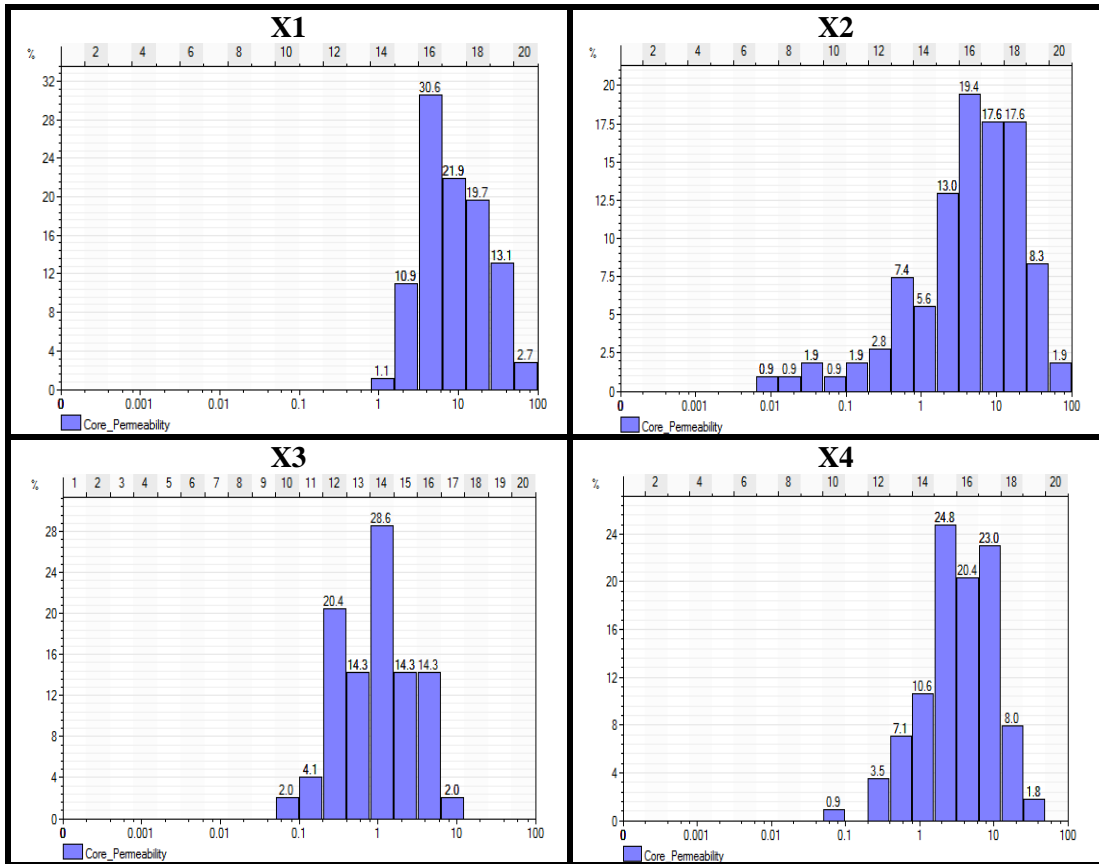


Figure 3.12: Core permeability histograms for each well.



**Figure 3.13:** Core permeability (lnk) histograms for each well.

**Table 3.1:** Recovered cores porosity (%) statistics of all wells.

Well	Min	Mean	Max
X - 1	11.50	23.09	33.80
X - 2	9.00	22.71	32.08
X - 3	8.05	20.01	29.67
X - 4	3.40	21.86	33.63

**Table 3.2:** Recovered cores permeability (md) statistics of all wells.

Well	Min	Mean	Max
X - 1	1	15	140
X - 2	0	11	109
X - 3	0	2	8
X - 4	0	6	35

**Table 3.3:** Porosity permeability correlation coefficients.

Well	Correlation Coefficient
X - 1	0.2155
X - 2	0.3811
X - 3	0.4369
X - 4	0.3900

Table 3.4 presents a comparison of the log and core derived porosity values. As it can be seen from the table, although there is a good agreement between the mean values of core and log porosities of wells, core measured porosities are slightly higher than log measured porosities. In this study log-porosity data was used for petrophysical modeling due to two main reasons: Firstly, a conservative approximation is always preferred for field development planning. Secondly, core data are not covering the whole formation whereas log data cover whole formation.

**Table 3.4:** Well log – core porosity statistics comparison

Well	Source	Min	Mean	Max
X - 1	Core	11.50	23.09	33.80
	Log	2.00	19.47	30.00
X - 2	Core	9.00	22.71	32.08
	Log	0.00	19.51	32.00
X - 3	Core	8.05	20.01	29.67
	Log	0.00	18.36	26.00
X - 4	Core	3.40	21.86	33.63
	Log	0.00	19.69	32.00

### 3.3.1 Well X-1 core data

Well X-1's core data approximately cover the upper 40 m of the formation. Except core 3 and core 5, almost 100% recoveries were achieved from the well as can be seen in Table 3.5 which shows the interval of the recovered cores from the existing well X-1. It is needless to say that reservoir rock type is carbonate; therefore, core recoveries percentage from the formation is high. However, cores have not been taken from the full formation and it is limited to some intervals as summarized in Table 3.5. Note that difference between mKB to mss for well X-1 is 81.4 m (mKB = mss + 81.4). Figure 3.14 shows the porosity – permeability cross - plot of well X-1 that obtained from the well X-1's core data.

**Table 3.5:** Recovered cores from well X-1.

No	Interval (mKB)	Meter	Recovery (%)
1	1350.00 - 1356.75	6.21	92
2	1356.75 - 1365.75	9.00	100
3	1365.75 - 1370.75	2.00	40
4	1370.75 – 1389.00	18.25	100
5	1389.00 – 1401.00	0.48	4



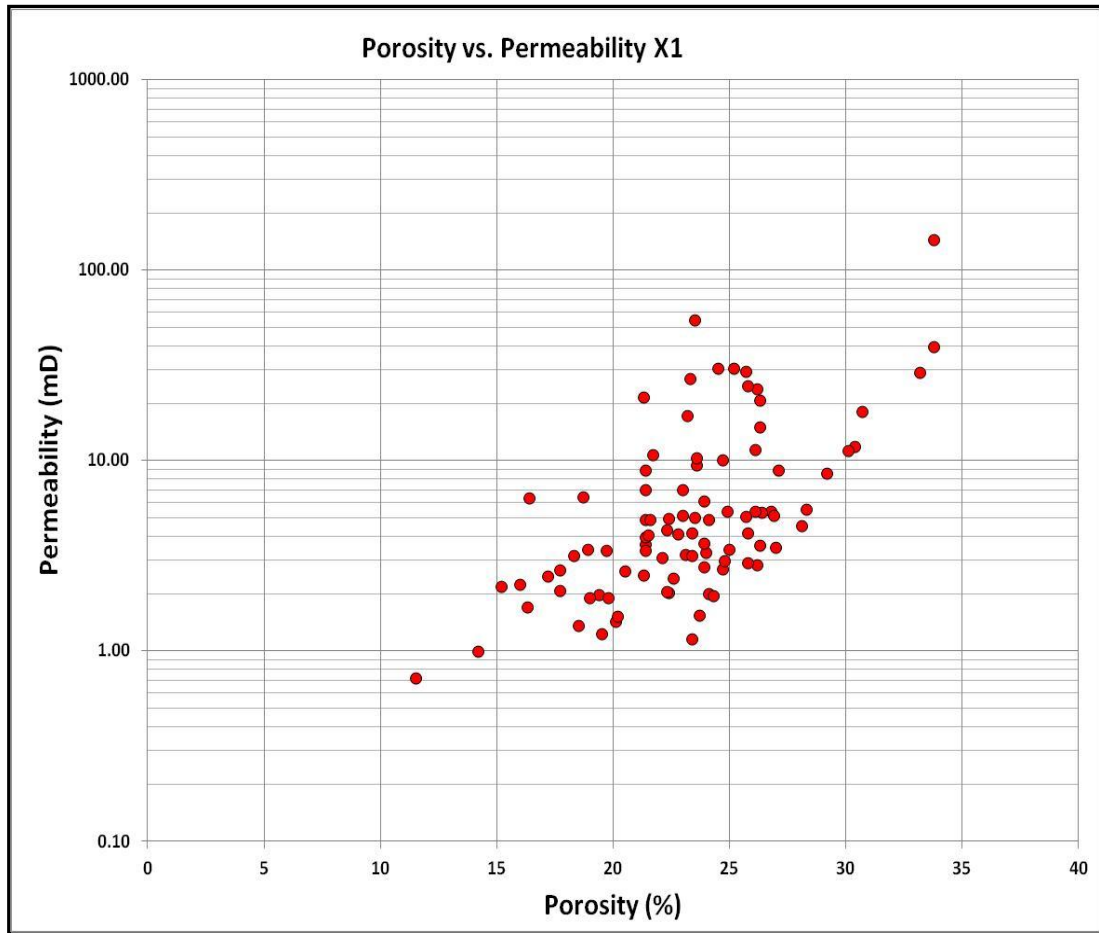


**Figure 3.14:** Core porosity - permeability cross - plot of well X-1.

### 3.3.2 Well X-2 core data

Well X-2 core data approximately cover the whole formation intervals. Except cores 6 and 7 almost 100% recoveries was achieved from the well (see Table 3.6). Table 3.6 shows the interval of the recovered cores from the existing well X-2 and Figure 3.15 shows the porosity – permeability cross - plot of well X-2 that obtained from X-2 core data. Note that difference between mKB to mss for well X-2 is 89.36 m (mKB = mss + 89.36).

**Table 3.6:** Recovered cores from well X-2.

No	Interval (mKB)	Meter	Recovery (%)
3	1401 - 1410	9.00	100
4	1410 - 1419	9.00	100
5	1419 - 1428	8.20	91
6	1433 - 1442	1.44	16
7	1442 - 1451	2.34	26
8	1451 - 1460	9.00	100
9	1460 - 1469	9.00	100

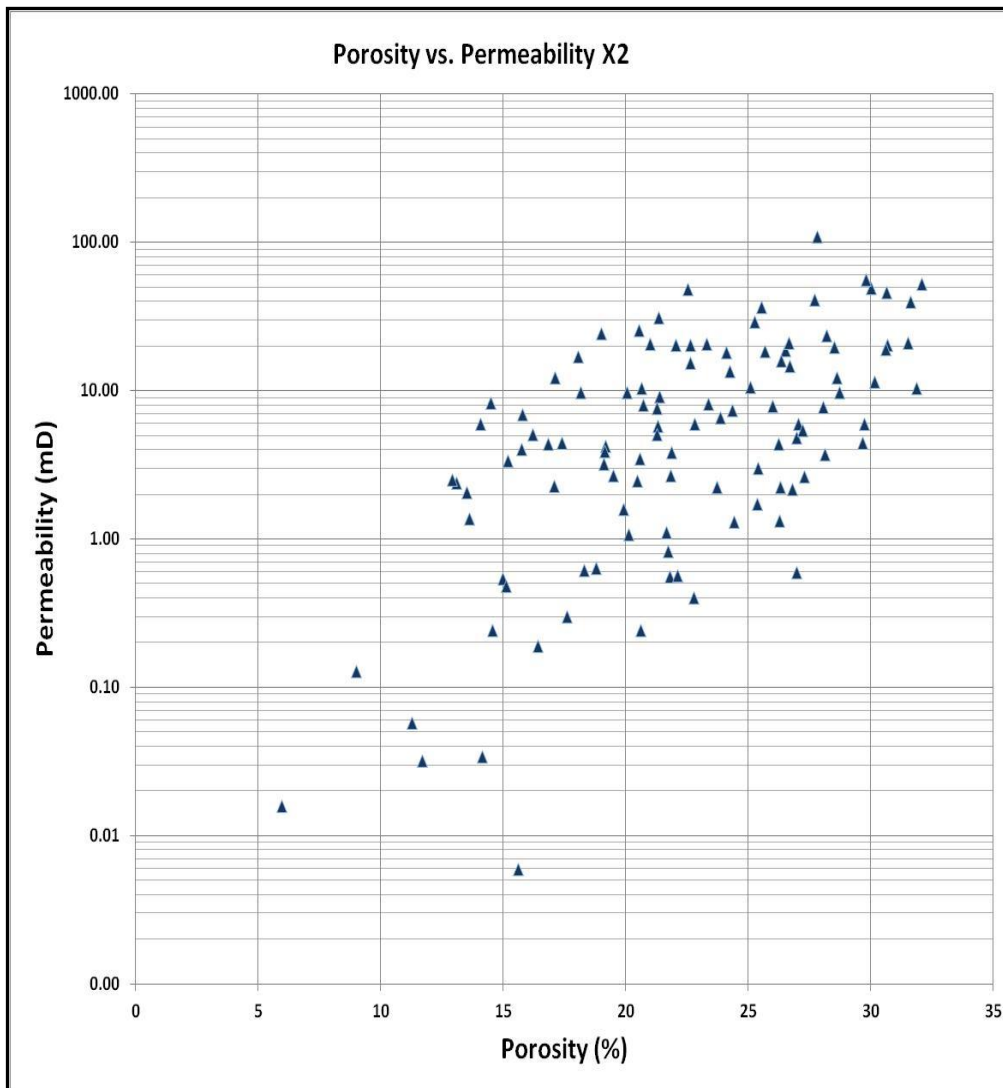


**Figure 3.15:** Core porosity - permeability cross - plot of well X-2.

### 3.3.3 Well X-3 core data

Well X-3 core data approximately cover the 20 m of formation in between 1360 to 1380 mss interval. In both cores 100% recoveries were achieved from the well (see Table 3.6). Table 3.7 shows the interval of the recovered cores from the existing well X-3 and Figure 3.16 shows the porosity – permeability cross - plot of well X-3 that obtained from well X-3 core data. Note that difference between mKB to mss for well X-3 is 90 m (mKB = mss + 90).

**Table 3.7:** Recovered cores from well X-3.

No	Interval (mKB)	Meter	Recovery (%)
1	1450 - 1459	9	100
2	1459 - 1468	9	100

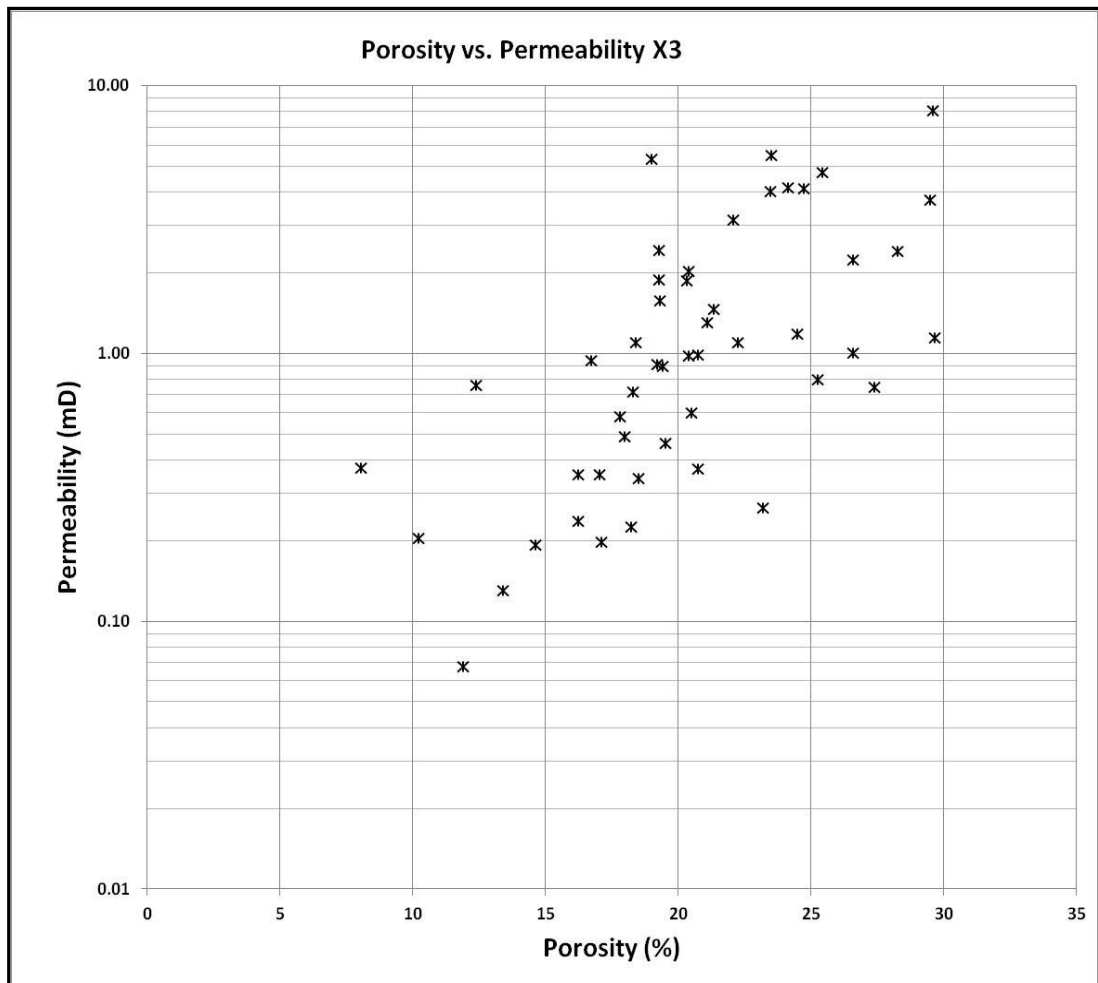


**Figure 3.16:** Core porosity - permeability cross - plot of well X-3.

### 3.3.4 Well X-4 core data

Well X-4 core data approximately cover the 40 m of the formation in between 1500 to 1540 mss interval. From the four cores 100% recoveries was achieved as can be seen in Table 3.7. Last 20 meter of the formation could not be cored. Table 3.8 shows the interval of the recovered cores from the existing well X-4 and Figure 3.17 shows the porosity – permeability cross - plot of well X-4 that obtained from well X-4 core data. Note that difference between mKB to mss for well X-4 is 136 m (mKB = mss + 136).

**Table 3.8:** Recovered cores from well X-4.

No	Interval (mKB)	Meter	Recovery (%)
3	1641 - 1650	9	100
4	1650 - 1659	9	100
5	1659 - 1668	9	100
6	1668 - 1677	9	100

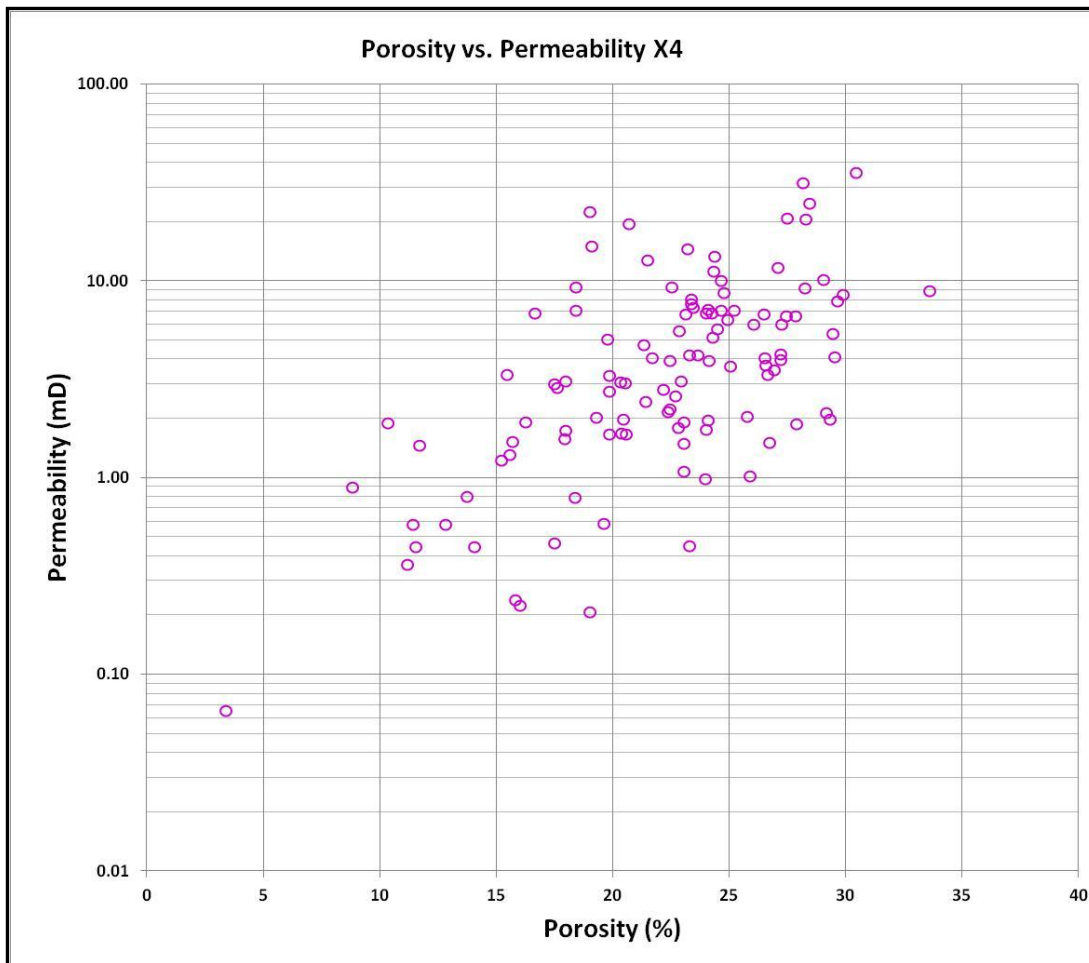


**Figure 3.17:** Core porosity - permeability cross - plot of well X-4.

### 3.4 PVT

PVT data are available from the existing three gas tested wells (Wells X-1, X-2 and X-3) in the field. No separation equipment was used during the testing operation except one sampling operation which was conducted recently on the well X-2. One of the major uncertainties in the field is the PVT data. There is hydrocarbon composition data on those samples: however, no experimental laboratory data available from any of the samples such as constant composition expansion (CCE), constant volume development (CVD), and dew point measurement except the recent one recovered from the well X-2. In this study, recent sampling data from well X-2 is used for fluid characterization because this is the only sample that has laboratory measurements although it is a surface sample and recombined for the PVT analysis. Compositional data and sampling conditions of the available samples are given in Table 3.9 except the recent well X-2 sample. Since the recent well X-2 sample is the

most recent and reliable data on hand in terms of PVT data, it was used for fluid characterization and it was analyzed in detail. Data given in Table 3.9 were not used in this study due lack of experimental data on the obtained samples and inconsistency on the data itself.

**Table 3.9:** Compositional data - sampling conditions.

Sampling Details / Components	Well X - 1	Well X - 1	Well X - 2	Well X - 2	Well X - 2	Well X - 3	Well X - 3
Sampling No	1	2	3	4	5	6	7
Sampling Pressure (psia)	90	280	400	250	3175	1000	3600
Sampling Condition	Surface	Surface	Surface	Surface	Surface	Surface	Surface
Sampling Interval	1259 - 1317	1320 - 1330	1306 - 1340	1453 - 1469	1325 - 1335	1343 - 1349	1343 - 1349
CO2	2.50	1.40	1.82	1.42	2.18	1.88	1.94
H2S	1.50	0.40	1.77	1.50	1.71	1.99	0.88
C1	86.80	88.01	85.34	85.60	84.87	79.93	81.36
C2	6.06	6.68	5.70	5.99	5.41	5.54	5.67
C3	1.83	2.02	2.53	2.85	2.48	2.86	2.91
i-C4	0.31	0.34	0.43	0.51	0.41	0.69	0.59
n-C4	0.58	0.63	0.80	1.01	0.96	1.25	1.22
i-C5	0.18	0.19	0.27	0.34	0.39	0.58	0.63
n-C5	0.15	0.18	0.27	0.33	0.36	0.66	0.67
C6	0.09	0.15	0.34	0.28	0.40	1.01	1.13
C7			0.27	0.13	0.35	0.97	1.19
C8			0.26	0.04	0.30	0.97	0.99
C9			0.15		0.05	1.03	1.62
C10			0.05		0.03	0.59	0.19
C11						0.07	0.01
Total (%)	100.00	100.00	100.00	100.00	99.90	100.02	101.00

As it was already mentioned, the only sample that has the laboratory measurements and experiments is the recent sample that recovered from well X-2. Due to operational problems, the flow period was very short and the sample recovered before the stabilization of the flow. This makes the sample questionable because it was a surface sample and recombination was made based on flow rate measurement on the surface. Figure 3.18 presents gas and oil rates measured during the surface test conducted in well X-2, and Table 3.10 summarizes the recombined sample that was analyzed in a PVT laboratory. That information will be used as main inputs of fluid

model that will be built in PVTi. Sampling was made when the CGR (condensate to gas ratio, bbl/MMscf) was around 82 stb/MMscf: however, as it was discussed already the well was not stable at the time of sampling. It is important to note that this instability on the flow created a lot of uncertainty on the recovered sample. Firstly, recombination was made based on GOR measurement reading from the field. Secondly, there is a possibility of losing heavier components of the fluid while taking the samples. It is needless to discuss and compare the quality of surface sample and bottom-hole sample, but the model has to be built based on available data on hand. From the recombined sample, the dew-point pressure was measured as 3853 psi by the CCE laboratory test at 138F. Flashed separator CGR was reported as 78.7 stb/MMscf. While constructing the EoS (Equation of state) model before starting the simulation, all of these findings and experiment will be evaluated in PVTi software which is a compositional PVT equation of state based program used for characterizing of fluid samples for use in reservoir simulators. Basic information about the available PVT data and sampling conditions are provided herein but, the detail analysis and discussion is made in the fluid characterization section.

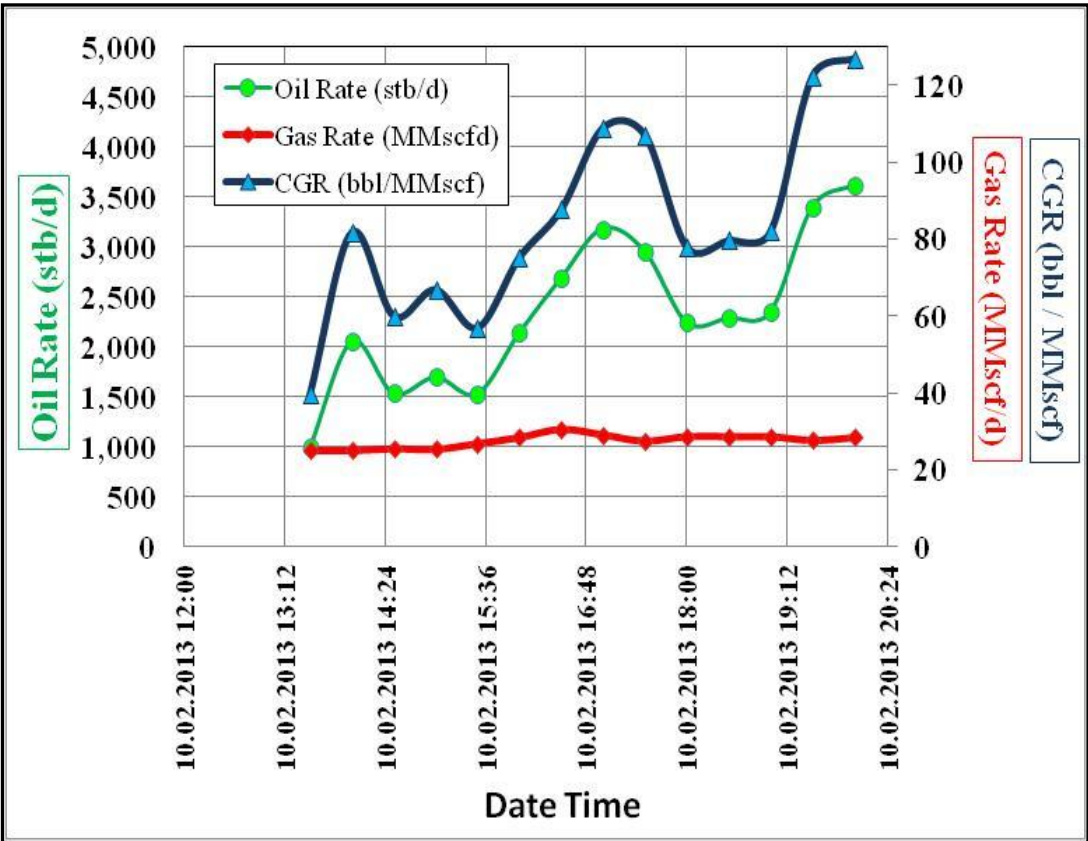


Figure 3.18: Separator flow rate measurement – well X-2.

**Table 3.10:** Compositional data – sampling conditions of well X-2 sample.

Sampling Details / Components	Sampling Conditions / Compositions (%)
Separator pressure (psia)	610
Separator temperature (F)	41
Well head pressure (psia)	2500
Well head temperature (F)	100
Sample Condition	Surface
Avg gas rate (MMscf/d)	28
Avg oil rate (bbl/d)	3000
Sampling interval (mss)	1259 - 1317
H <sub>2</sub>	0.00
H <sub>2</sub> S	1.46
CO <sub>2</sub>	2.22
N <sub>2</sub>	0.23
C <sub>1</sub>	78.78
C <sub>2</sub>	5.48
C <sub>3</sub>	2.94
iC <sub>4</sub>	0.69
nC <sub>4</sub>	1.47
C <sub>5</sub>	0.00
iC <sub>5</sub>	0.70
nC <sub>5</sub>	0.75
C <sub>6</sub>	1.02
M-C-Pentane	0.17
Benzene	0.05
Cyclohexane	0.14
C <sub>7</sub>	0.72
M-C-Hexane	0.21
Toluene	0.13
C <sub>8</sub>	0.66
E-Benzene	0.05
M/P-Xylene	0.13
O-Xylene	0.04
C <sub>9</sub>	0.47
1,2,4-TMB	0.03
C <sub>10</sub>	0.43
C <sub>11+</sub>	1.05
Total	100.00

### **3.5 Well Test**

From the existing four wells, there are both cased-hole and open-hole tests. Pressures were recorded with a bottom-hole pressure gauge: however, pressure build-up (PBU) tests were not conducted in all of the wells. Open-hole tests conducted with the standard drill stem tester (DST), and cased-hole tests were conducted after perforating different intervals as well as after successful acid operations. There are totally five PBUs from the field although all of the existing wells tested; four of PBU from well X-2 which is a gas well and one of them from well X-4 which is a water leg well. No surface separation equipment was used in any of the test. Therefore, there is no continuous rate measurement in the flow period. Reported rates contain uncertainty. All pressure data recorded with Amerada gauges which have low precisions. It is very difficult, if not impossible, to obtain any complex reservoir characteristic from those PBU except some permeability data which can be used for comparison purposes with available core permeability data and well productivity, and skin data which may give an idea about the well productivity. All well tests to be given here were analyzed by using the well-test software Ecrin from Kappa Engineering (Ecrin ver. 4.02.04).

#### **3.5.1 Well X-1 well tests**

One open-hole and one cased-hole test were conducted at the well X-1. However, PBU data do not exist on both tests. Although there is no PBU data to analyze, recorded pressure data will be used for water contact determination. Table 3.11 gives the pertinent data for well X-1 open-hole and cased-hole tests. As is seen from Table 3.11, open-hole and cased-hole tests were conducted on the different intervals and hence, provide pressure data from different depths. Obtained pressure data from different depths will be used together with gas and water gradients to obtain the gas water contact (GWC) (Kindly see section 3.6 for more information about GWC determination). Also note that 50 min. PBU data exists on the open-hole tests, and shut-in pressures were reported on the final well reports although there is no information on hand about the recorded pressure data or whether pressure data



recorded or not. These tests were conducted more than 30 years ago. Therefore, presumably recorded data were lost.

**Table 3.11:** Data for well X-1 open-hole and cased-hole tests.

Test	Open Hole Test	Cased Hole Test
Interval (mss)	1259-1317	1320 - 1330
Gauge depth (mss)	1235	1323
Temperature (F)	135	-
Flow period (min)	50	-
Flowing BHP (psi)	3956	-
Buildup Period (min)	50	-
Shut in BHP (psi)	4033	3987
Gas Rate (MMscf/d)	40	12.5

### 3.5.2 Well X-2 well tests

Two open-hole and two cased-hole tests were conducted at well X-2. PBU data were available from all of the four tests. Two acid operations was performed at the well and after each acid job, PBU data were recorded. Table 3.12 summarizes the pertinent data for well X-2 open-hole and cased-hole tests.

**Table 3.12:** Data for well X-2 open-hole and cased-hole tests.

Test	Open Hole Test	Open Hole Test	Cased Hole Test (First Acid)	Cased Hole Test (Second Acid)
Interval (mss)	1306-1340	1365-1381	1325-1335	1325-1335
Gauge depth (mss)	1280.5	1379	1314	1314
Temperature (F)	138	138		
Flow period (min)	30	25	370	510
Flowing BHP (psi)	3503	1815	1762	2386
Buildup Period (min)	100.000	50	100	110
Shut in BHP (psi)	4048	4012	3938	3888
Gas Rate (MMscf/d)	24.7	25.4	40	78

#### 3.5.2.1 Well X-2 open-hole test (1306-1340 mss)

The open-hole test was conducted at the well X-2 to test the interval of 1306-1340 m. After 30 minutes of flow period with an approximately 25 MMscfd gas rate, the well was shut in for 100 minutes, and the pressure data were recorded with an Amerada pressure gauge which has a low precision. Although as mentioned before it is very

difficult, if not impossible, to obtain any complex reservoir characteristics from such a short test and data obtained from a low resolution gauge. However, basic reservoir parameters such as permeability and skin were obtained from the pressure transient analysis (PTA). Such information will be used for the calibration of core data. Table 3.13 is the input data that used for PTA. It is worth to note that formation starts at 1311.7 m in well X-2, therefore, although the tested interval is 34 m (1340 m-1306 m = 34 m), pay zone is around 28 m (1340 m-1312 m = 28 m, approximately 90 ft). Additionally, the porosity value which was used for interpretation is the mean porosity value of the core data in the tested interval. The used compressibility and specific gravity values are obtained from PVT. The match of the observed data with the model, log-log diagnostic plots, and semi-log Horner plot are given in Figures 3.19-3.21, respectively.

It is important to note that the log-log diagnostic plots are based on the use of real gas pseudo-pressure of (Al-Hussainy et al., 1966) as the well is producing mainly single-phase gas. The model chosen to match the observed pressure data is the infinite-acting radial flow model with wellbore storage and skin effects (Bourdet, 2002). This model is an appropriate model for the real gas pseudopressure-derivative behavior observed in the lo-log diagnostic plot shown in Fig. 3.20. Note that the real gas pseudopressure change with respect to natural logarithm of elapsed time for drawdown tests, whereas with respect to the natural logarithm of the Agarwal's equivalent time for buildup portions (Agarwal, 1980 and Bourdet et al. 1989). Here and throughout this thesis, this derivative is called Bourdet derivative or real gas pseudopressure-derivative data. Also note that the real gas pseudopressure-derivative data in the time interval from 0.1 to 1 hr indicate a zero-slope line, which is typical of radial flow. The upward trend exhibited by the last few derivative data points (after 1 hr) in Fig. 3.20 is not due to any reservoir behavior. It is mainly due to the end-effects in numerical differentiation procedure (Onur and Al- Saddique, 1999). As can be seen from Fig. 3.19 and 3.20, the matches of the model real gas pseudopressure change and its Bourdet derivative data with the observed pressure change and pressure-derivative data are quite good. Also, a well-defined semi-log straight line passes through the observed data as can be seen in the Horner plot given by Fig. 3.21. A summary of the analysis results is given in Table 3.14.

**Table 3.13:** PTA inputs for well X-2.

Property	Value
Well radius (ft)	0.35
Pay zone (ft)	90
Porosity (%)	0.23
$c_t$ (1/psi)	$1.21 \times 10^{-5}$

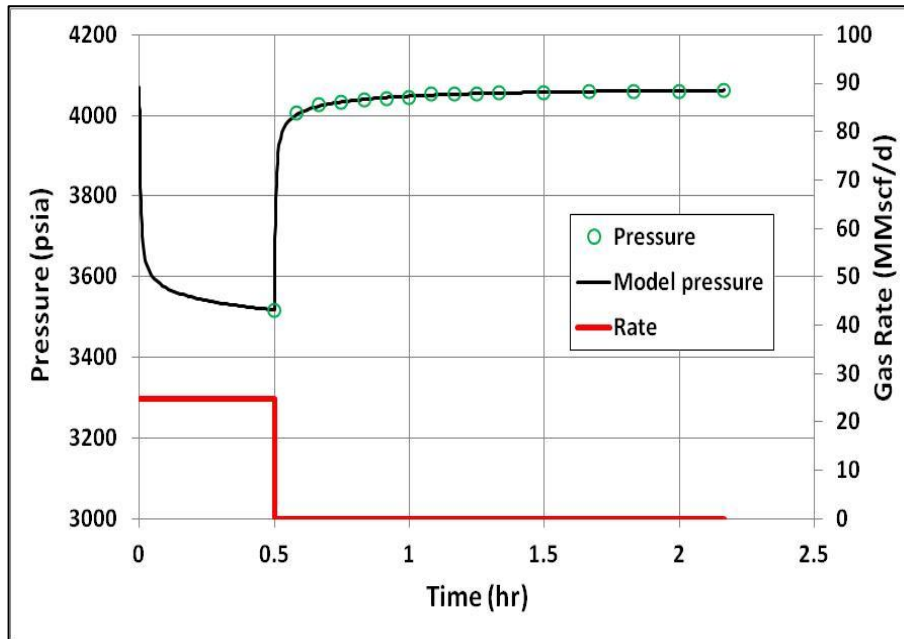


**Figure 3.19:** Pressure and rate history plot for well X-2 test (1306-1340 mss).

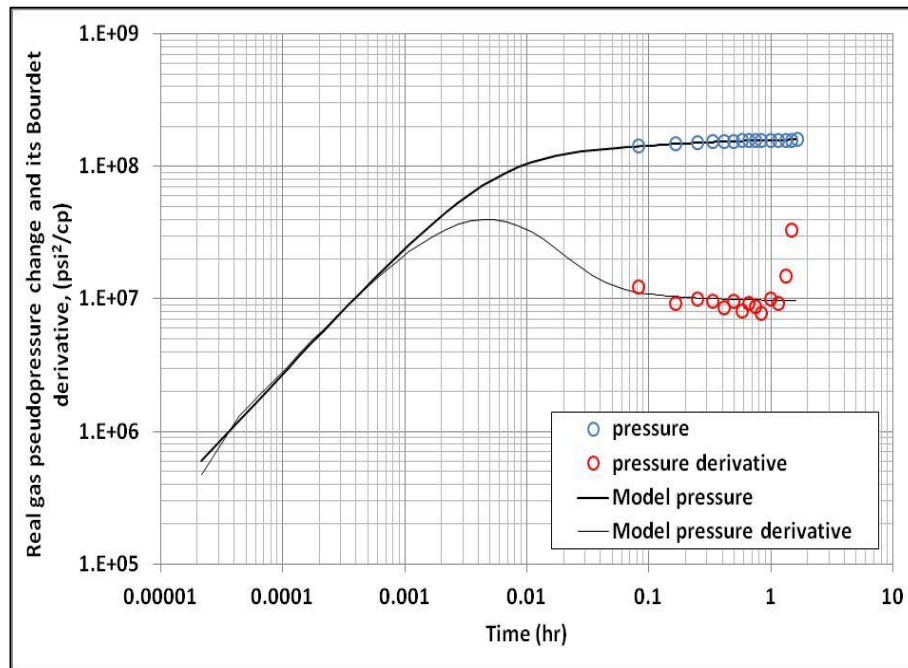


**Figure 3.20:** Log-log diagnostic plot (1306-1340 mss).

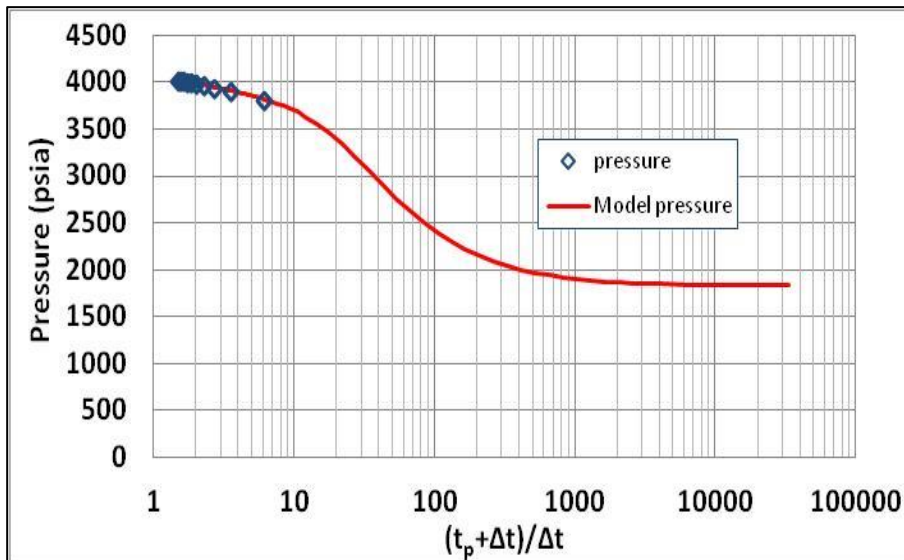


**Figure 3.21:** Semi-log Horner plot of well X-2 (1306-1340 mss).

**Table 3.14:** Test analysis result summary (1306-1340 mss)

Property	Interpreted result
Model Option	Standard Model
Well	Vertical
Reservoir	Homogeneous
Boundary	Infinite
Top/Bottom	No flow/No flow
TMatch	1440 [hr] <sup>-1</sup>
PMatch	5.21E-8 [psi <sup>2</sup> /cp] <sup>-1</sup>
C	0.00685 bbl/psi
Total Skin	3.33
k.h, total	1090 md.ft
k, average	12.2 md
p <sub>i</sub>	4071.22 psia
Skin	3.33
k.h	1090 md.ft
k	12.2 md
R <sub>inv</sub>	125 ft
Test. Vol.	0.00101528 bcf
Delta P (Total Skin)	220.738 psia

### 3.5.2.2 Well X-2 open-hole test (1365-1381 mss)

Another open-hole test was conducted in well X-2 to test the interval of 1365-1381. After 25 minutes flow period with approximately 25 MMscf/d gas rate, well was shut in for 50 minutes and the pressure data was recorded with an Amerada pressure gauge. The same PVT input data as given in Table 3.13 except the pay thickness

were used for interpretation. The pay thickness used for the analysis of this test is 22 ft. It is worth to note that formation end at 1372 m in well X-2, therefore, although the tested interval is 16m (1381 m-1365 m = 16 m), pay zone is around 7 m (1372 m-1365 m = 7 m, approximately 22 ft). Like in the previous test, the interpretation model chosen is the infinite-acting radial flow model with wellbore storage and skin effects and data analyzed using the real gas pseudo-pressure. The obtained match of the entire observed pressure, log-log diagnostic plots of real gas pseudopressure and its Bourdet derivative with the corresponding model curves, and the Horner plot of buildup real gas pseudopressure are shown in Figs. 3.22-3.24, respectively. Summary of the test analysis results is given in Table 3.15.

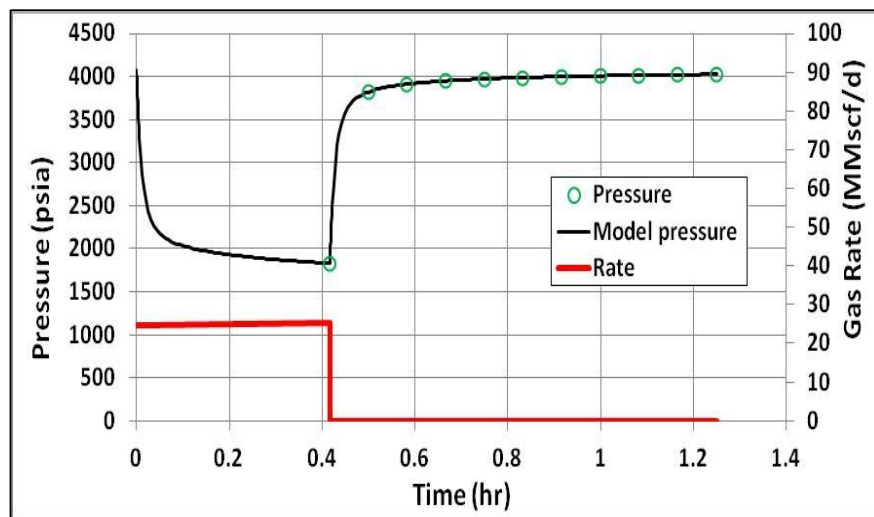


**Figure 3.22:** Pressure and rate history plot for well X-2 (1365-1381 mss).

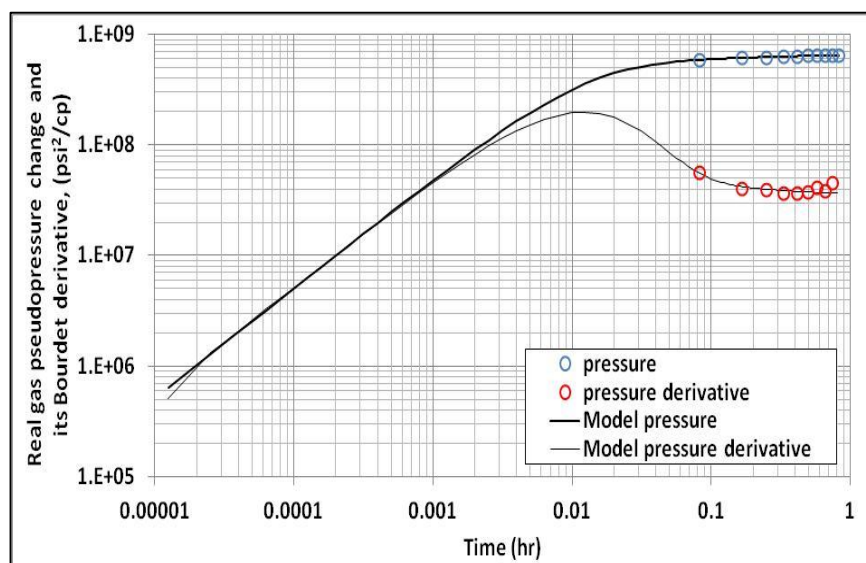


**Figure 3.23:** Log-log diagnostic plot (1365-1381 mss).

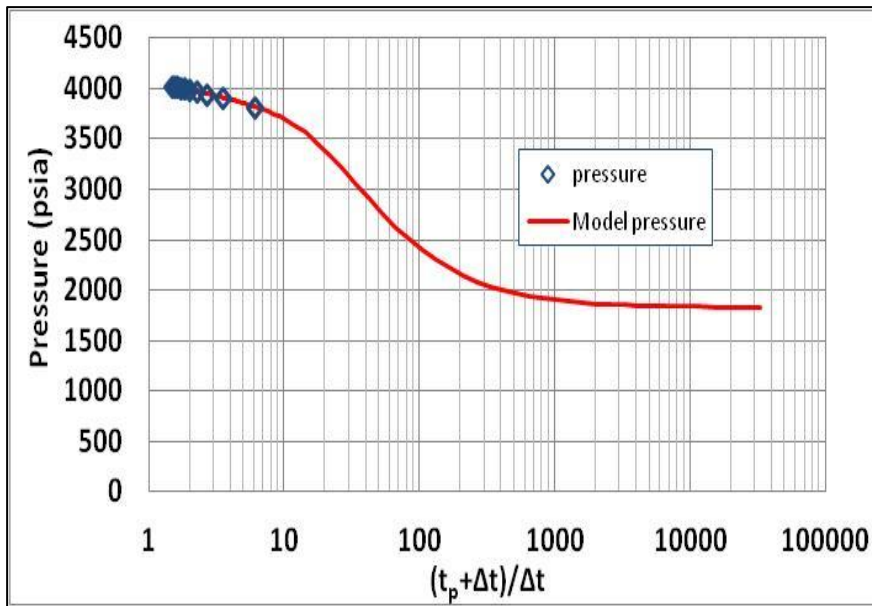


**Figure 3.24:** Semi-log Horner plot of well X-2 (1365-1381 mss).

**Table 3.15:** Summary of test analysis results (1365-1381 mss).

Property	Interpreted result
Model Option	Standard Model
Well	Vertical
Reservoir	Homogeneous
Boundary	Infinite
Top/Bottom	No flow/No flow
TMatch	734 [hr] <sup>-1</sup>
PMatch	1.44E-8 [psi <sup>2</sup> /cp] <sup>-1</sup>
C	0.00384 bbl/psi
Total Skin	4.51
k.h, total	312 md.ft
k, average	14.2 md
p <sub>i</sub>	4075.11 psia
Skin	4.51
R <sub>inv</sub>	95.3 ft
Test. Vol.	1.44498E-4 bcf
Delta P (Total Skin)	1058.77 psia

### 3.5.2.3 Well X-2 cased hole test – after first acid (1325-1335 mss)

A cased-hole test was conducted in well X-2 to test the interval of 1325-1335 after the first successful acid job. After 370 minutes flow period with approximately 40 MMscf/d gas rate, well was shut in for 100 minutes and the pressure data was recorded with an Amerada pressure gauge. The same PVT input data which was given in Table 3.13 except the pay thickness were used for interpretation. The pay

thickness used for the analysis of this test is 32.8 ft. The model chosen for interpretation and analysis is the infinite-acting radial flow model with wellbore storage and skin effects and data analyzed using the real gas pseudo-pressure. The obtained match of the entire observed pressure, log-log diagnostic plots of real gas pseudopressure and its Bourdet derivative with the corresponding model curves, and the Horner plot of buildup real gas pseudopressure are shown in Figs. 3.25-3.27, respectively. Summary of the test analysis results is given in Table 3.16.

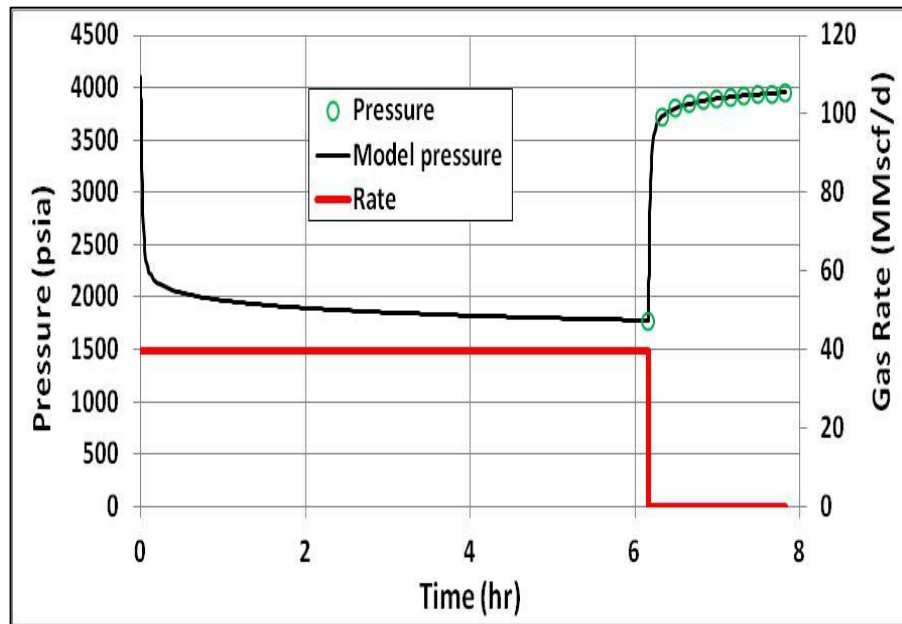


**Figure 3.25:** Pressure and rate history plot for well X-2-after first acid (1325-1335 mss).

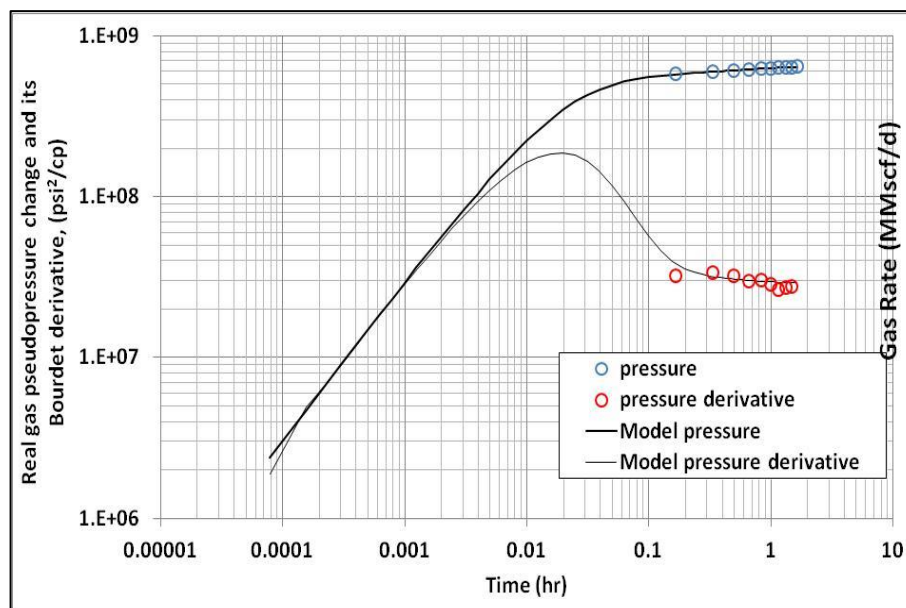


**Figure 3.26:** Log-log diagnostic plot after first acid (1325-1335 mss).

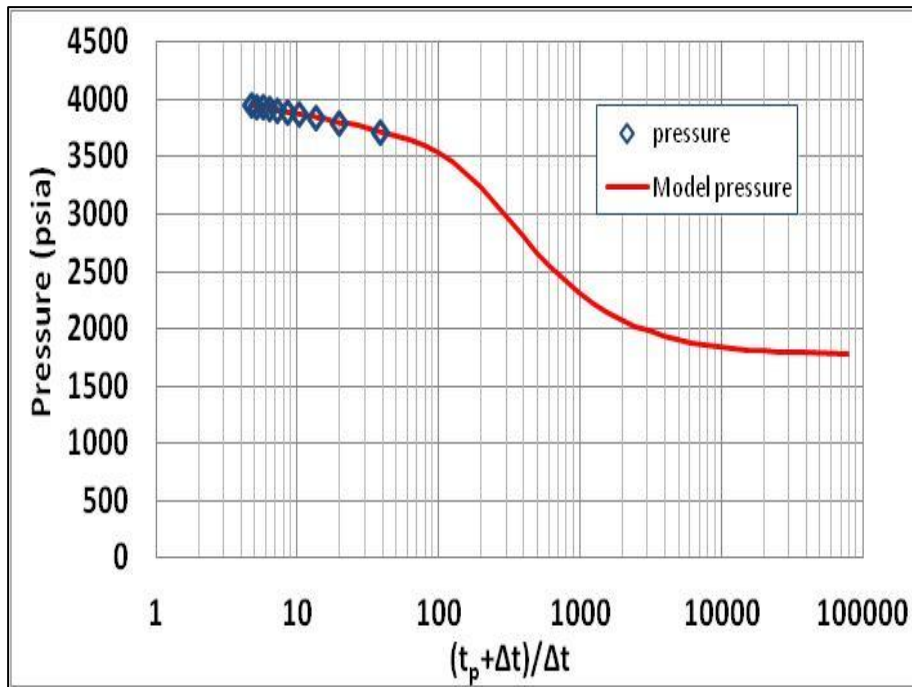


**Figure 3.27:** Semi-log Horner plot of well X-2 - after first acid (1325-1335 mss).

**Table 3.16:** Summary of test analysis results after first acid (1325-1335 mss).

Property	Interpreted result
Model Option	Standard Model
Well	Vertical
Reservoir	Homogeneous
Boundary	Infinite
Top/Bottom	No flow/No flow
TMatch	539 [hr] <sup>-1</sup>
PMatch	1.78E-8 [psi <sup>2</sup> /cp] <sup>-1</sup>
C	0.01 bbl/psi
Total Skin	5.67
k.h, total	599 md.ft
k, average	18.3 md
p <sub>i</sub>	4106.57 psia
R <sub>inv</sub>	147 ft
Test. Vol.	5.55126E-4 bcf
Delta P (Total Skin)	1082.62 psia

#### 3.5.2.4 Well X-2 cased-hole test – after second acid (1325-1335 mss)

A cased-hole test was conducted in the same interval after the second successful acid job in well X-2. After 510 minutes flow period with approximately 78 MMscf/d gas rate, well was shut in for 110 minutes and the pressure data was recorded. The same PVT input data as given in Table 3.13 except the pay thickness were used for



interpretation. The pay thickness used for the analysis of this test is 32.8ft. Like in the previous test' interpretation, the model chosen for interpretation and analysis is the infinite-acting radial flow model with wellbore storage and skin effects and data analyzed using the real gas pseudo-pressure. The obtained match of the entire observed pressure, log-log diagnostic plots of real gas pseudopressure and its Bourdet derivative with the corresponding model curves, and the Horner plot of buildup real gas pseudopressure are shown in Figs. 3.28-3.30, respectively. Summary of the test analysis results is given in Table 3.17. Reduction on the skin factor is expected after successful acid job as we observed here: however, improvement on permeability was also observed in this test. It is worth to note that although same interval was tested after first and second acid job, interpreted permeability was doubled as well as the significant skin effect reduction was observed. This could indicate possible chemical reaction on the carbonate and pumped acid which presumably cleaned up the fractures and improved the permeability. On the other hand, this could be due to wrong rate measurement. We assumed that the given rate (78MMscf/d) is wrong and we reduced the gas rate to 40 MMscf/d. Similar interpretation was performed to calculate the permeability and the skin factor where they are calculated as 18.86 md and 2.34, respectively. Deep investigation on answering of this phenomenon is required to make sure what the exact reason is.

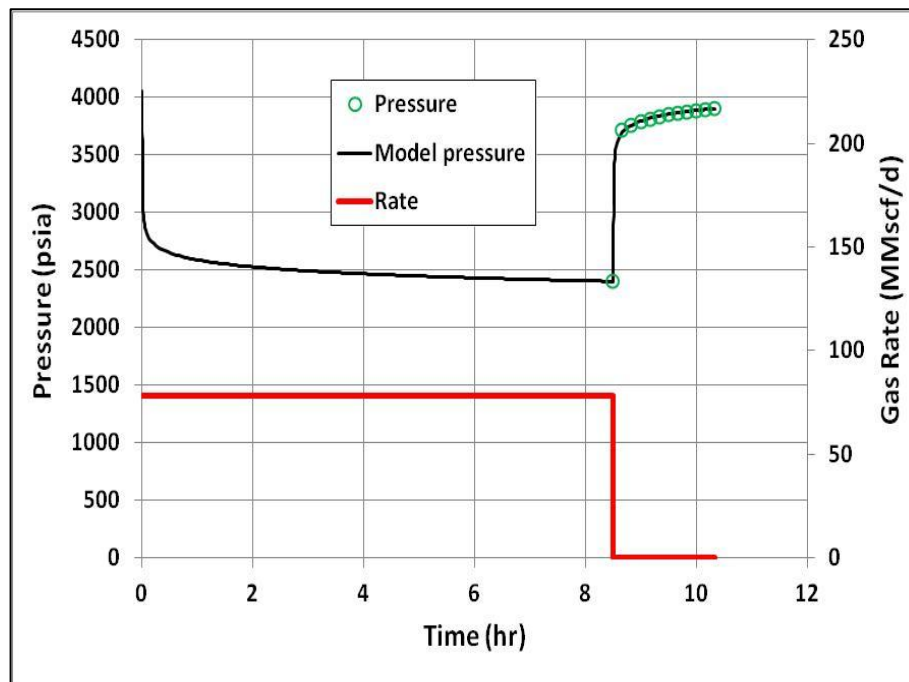


**Figure 3.28:** Pressure and rate history plot for well X-2 after second acid (1325-1335 mss).

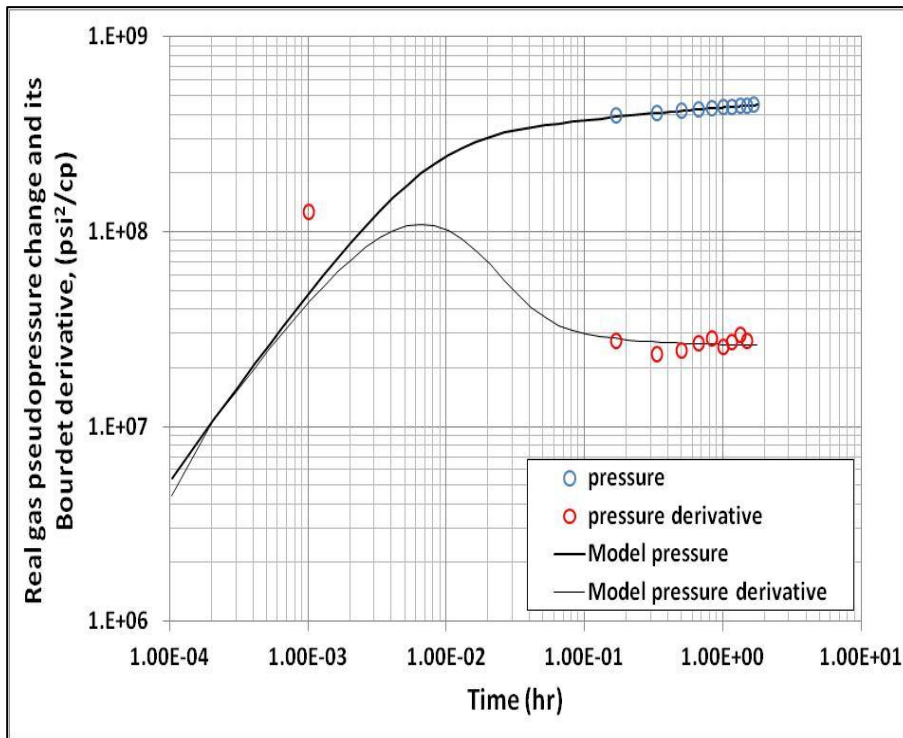


**Figure 3.29:** Log-log diagnostic plot after second acid (1325-1335 mss).

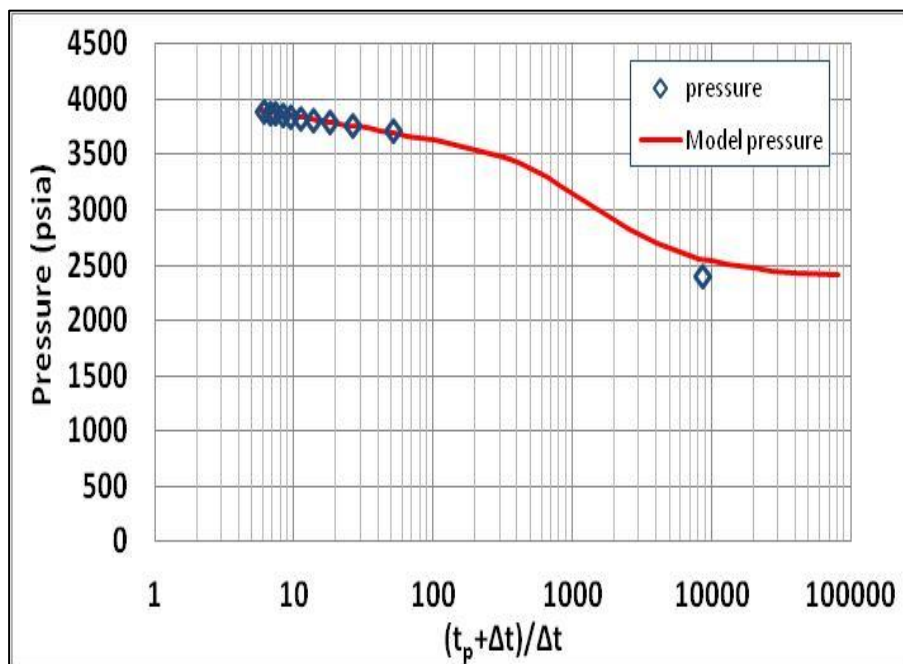


**Figure 3.30:** Semi-log Horner plot after second acid (1325-1335 mss).

In conclusion, two open-hole and two cased-hole tests were conducted in well X-2 and all of them interpreted as shown in the above sections. Figure 3.31 shows a comparison of all X-2 test data on log-log diagnostic plot. As it was given in section 3.3 and Table 3.2, the mean of the core permeability is 11 md. On the other hand

according to the performed well-test interpretation, permeability was calculated as 12.2 md and 14.2 md before the acid operation. It is needless to say that core measured permeability and well-test interpreted permeability values are in line with the each other. It is also worth to note that after first and second acid job, significant permeability improvement was observed. Further investigation is required to answer the reason of permeability increase after each acid job: however, presumably this is due to chemical reaction between carbonate and injected acid. No boundary effect was observed any of the tests due to short test periods. Also no complex reservoir phenomena were observed any of the conducted tests such as limited entry well behavior, double porosity/permeability reservoir behavior due to limitation on the test itself and used gauge quality which is low precision. Reservoir rock is carbonate and most probably it has some fractures. Therefore, it may be expected that the data should show double porosity and/or double permeability reservoir behavior on the conducted tests. Similarly, each of the tested intervals is limited and so, limited entry well behavior may expect to be observed in the recorded pressure data. None of these complex behaviors were observed in any of the tests: however, useful information on reservoir characteristics was gained on the interpretation of PTA data such as permeability, skin etc.

**Table 3.17:** Summary of test analysis results after second acid (1325-1335 mss).

Property	Interpreted result
Model Option	Standard Model
Reservoir	Homogeneous
Boundary	Infinite
Top	No flow
Bottom	No flow
TMatch	1030 [hr] <sup>-1</sup>
PMatch	1.93E-8 [psi <sup>2</sup> /cp] <sup>-1</sup>
C	0.0112 bbl/psi
Total Skin	2.45
k.h, total	1280 md.ft
k, average	39 md
p <sub>i</sub>	4056.68 psia
Skin	2.45
R <sub>inv</sub>	215 ft
Test. Vol.	0.00118651 bcf
Delta P (Total Skin)	435.109 psia

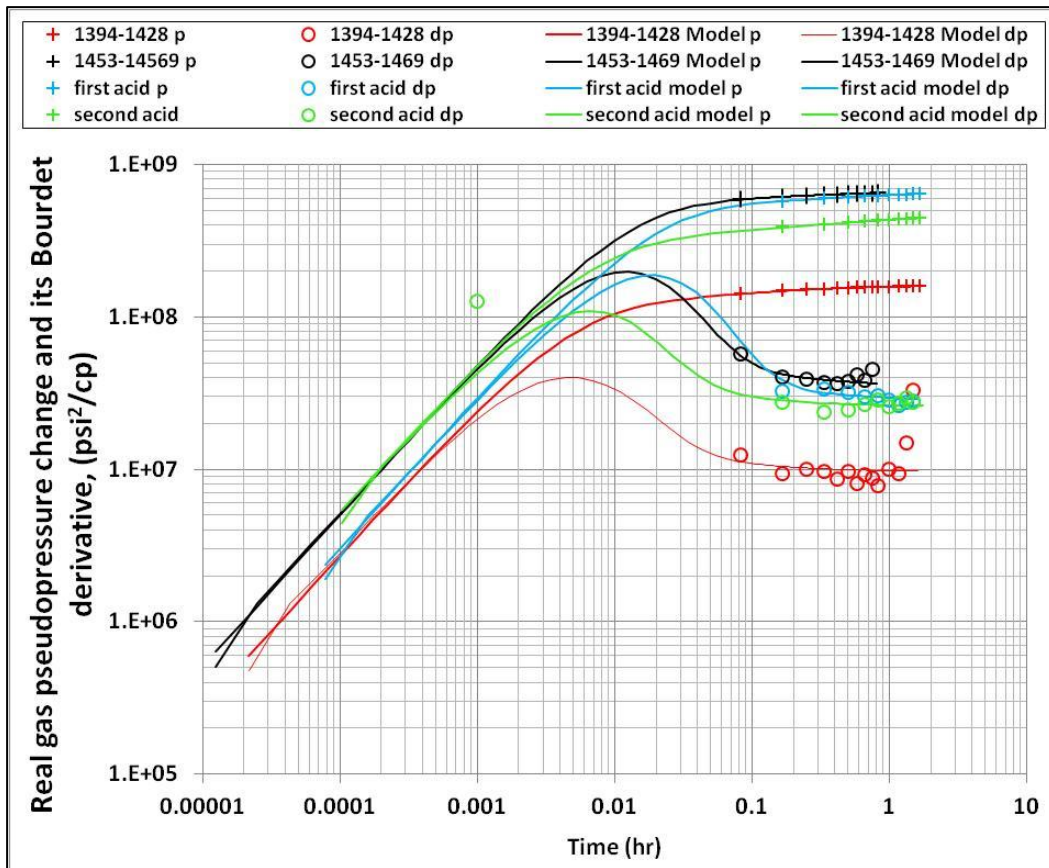


**Figure 3.31:** Well X-2 tests comparison, log-log diagnostic plot.

### 3.5.2.5 Well X-4 open hole test (1498-1554 mss)

An open-hole test was conducted in well X-4 to test the interval of 1498-1554. Recall that the well X-4 is a water leg well. After 1380 minutes flow period with approximately 400 bbl/d water production rate, well was shut in for 300 minutes. Table 3.18 gives the input data used for PTA. It is worth to note that formation starts at 1500.7 m in well X-4, therefore, although the tested interval is 56 m (1554 m-1498 m = 56 m), pay zone is around 53 m (1554 m-1501 m = 53 m, approximately 174 ft). Additionally, the porosity value which was used for interpretation is the mean porosity value (0.22) of the core data in the tested interval. As the well is a water leg well and we only produced water during the test, we analyze the pressure data by assuming single-phase flow of slightly compressible fluid of constant compressibility and constant viscosity. Hence, data were analyzed in terms of pressure, pressure change and its Bourdet derivative.

The model chosen for interpretation and analysis is the infinite-acting radial flow model with wellbore storage and skin effects. The obtained match of the entire

observed pressure, log-log diagnostic plots and its Bourdet derivative with the corresponding model curves, and the Horner plot of buildup are shown in Figs. 3.32-3.34, respectively. Summary of the test analysis results is given in Table 3.19.

**Table 3.18:** PTA inputs for well X-4.

Property	Value
Well radius (ft)	0.35
Pay zone (ft)	174
Porosity (%)	0.22
$c_t$ (1/psi)	$2.98 \times 10^{-6}$
$B_w$ (bbl/stb)	1.01152

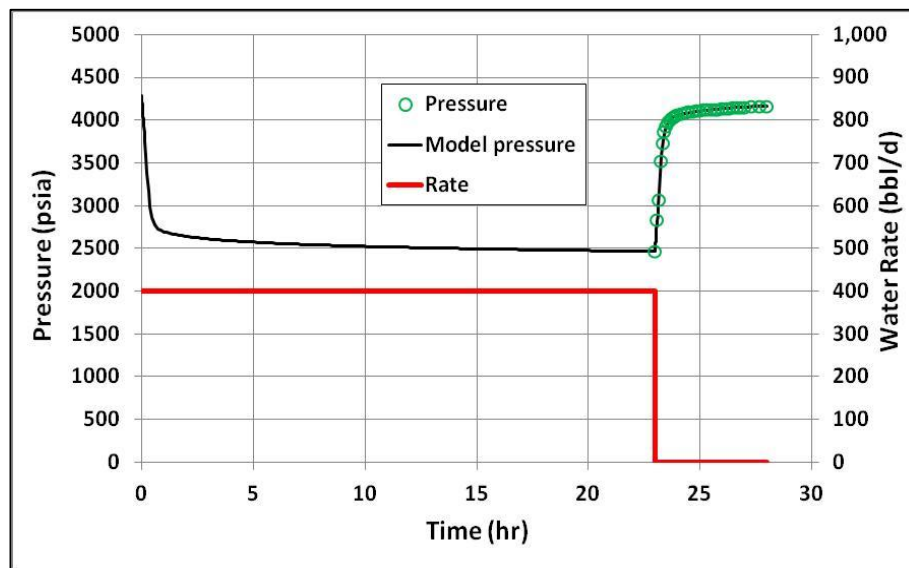


**Figure 3.32:** Pressure and rate history plot - well X-4 PBU test (1498-1554 mss).

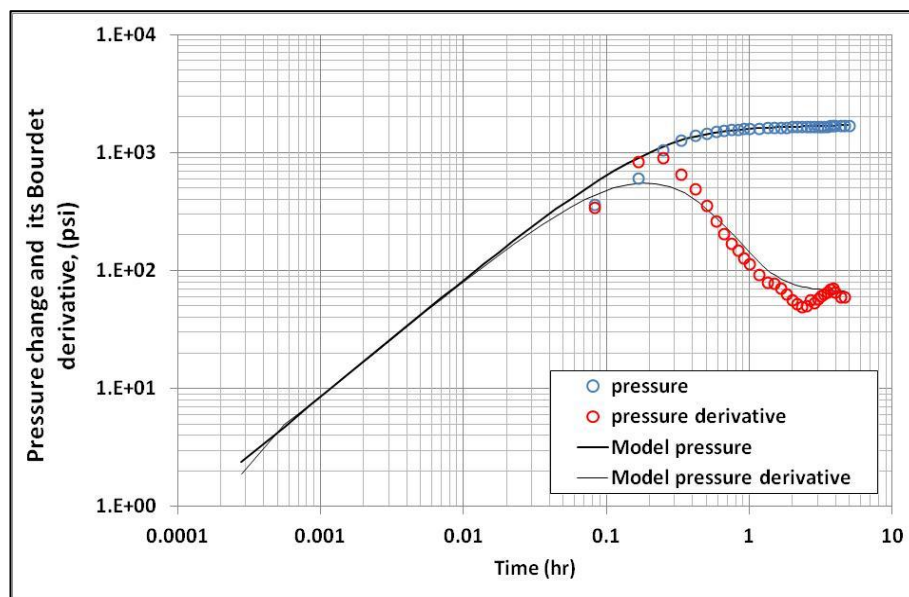


**Figure 3.33:** Log-log diagnostic plot for well X-4 (1498-1554 mss).

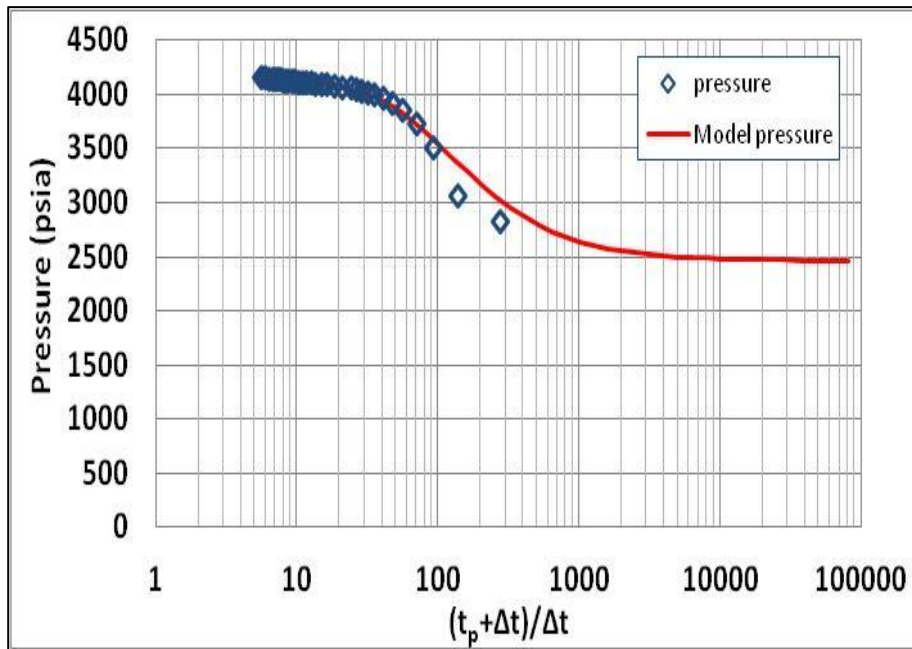


**Figure 3.34:** Semi-log Horner plot of well X-4 (1498-1554 mss).

**Table 3.19:** Summary of the test analysis results for well X-4 test (1498-1554 mss).

Property	Interpreted result
Model Option	Standard Model
Well	Vertical
Reservoir	Homogeneous
Boundary	Infinite
Top	No flow
Bottom	No flow
TMatch	71 [hr] <sup>-1</sup>
PMatch	0.00833 [psia] <sup>-1</sup>
C	0.00198 bbl/psi
Total Skin	8.6
k.h, total	476 md.ft
k, average	2.73 md
p <sub>i</sub>	4278.98 psia
R <sub>inv</sub>	132 ft
Test. Vol.	0.00210901 bcf
Delta P (Total Skin)	1033.03 psia

### 3.6 Gas-Water Contact (GWC)

Although there are four wells drilled in the field none of them tested GWC. As can be seen from the Figure 3.35, the lowest gas reading (gas down to – GDT) from the formation was observed from well X-3 log which was 1391 mss. On the other hand, water was tested from well X-4 and the shallowest water (water up to – WUT)

reading was 1502 mss. Therefore, GWC can be somewhere in between 1391 mss to 1502 mss. Pressure readings from the well tests and gas – water gradients will be used to estimate the gas water contact. Table 3.20 shows the pressure reading from the field, well-test interpreted pressures and the calculated pressure data from the gradients. Note that gas gradient (0.12psi/ft) given in Table 3.20 was calculated based on reservoir fluid density data given in well X-2 PVT report. Density of the reservoir fluid at reservoir condition is reported as 0.29 g/cm<sup>3</sup> (18 lb/ft<sup>3</sup>) that gas gradient can be calculated as 18lb/ft<sup>3</sup> x 1/144 ft<sup>2</sup>/inch<sup>2</sup> = 0.12 psi/ft. Also note that water gradient given in Table 3.20 (0.456 psi/ft) was calculated based on water salinity which is reported as 90000 ppm in well X-2 surface well-test report. Density of 90000 ppm saline water is 1.05 g/cm<sup>3</sup> (65.57 lb/ft<sup>3</sup>). Similar to the gas gradient calculation, water gradient can be calculated as 0.456 psi/ft. Figure 3.36 is showing the pressure versus depth plot. To be able to determine the GWC, trend lines were drawn for the gas zone pressure readings and water zone pressure readings. Interception between both trend lines gives 1460 mss gas water contact which will be used for the base case calculations.

**Table 3.20:** Pressure reading from the field.

Well	Pressure Data Source	Gauge Depth (mss)	Pressure (mss)
X - 1	Open-hole test	1235.0	4033.00
X - 2	Well test interpretation	1280.5	4071.22
X - 2	Well test interpretation	1379.0	4075.11
X - 2	Well test interpretation	1314.0	4106.57
X - 2	Well test interpretation	1314.0	4056.68
X - 3	Cased-hole test	1322.5	4089.00
Calculation from gradient	Calculation from gas gradient (ref. 1314 m - 4057 psi)	1600.0	4169.25
X - 4	Well test interpretation	1532.0	4289.57
X - 4	Open hole test	1532.0	4200.00
Calculation from gradient	Calculation from water gradient (ref. 1532 m - 4200 psi)	1400.0	4002.57

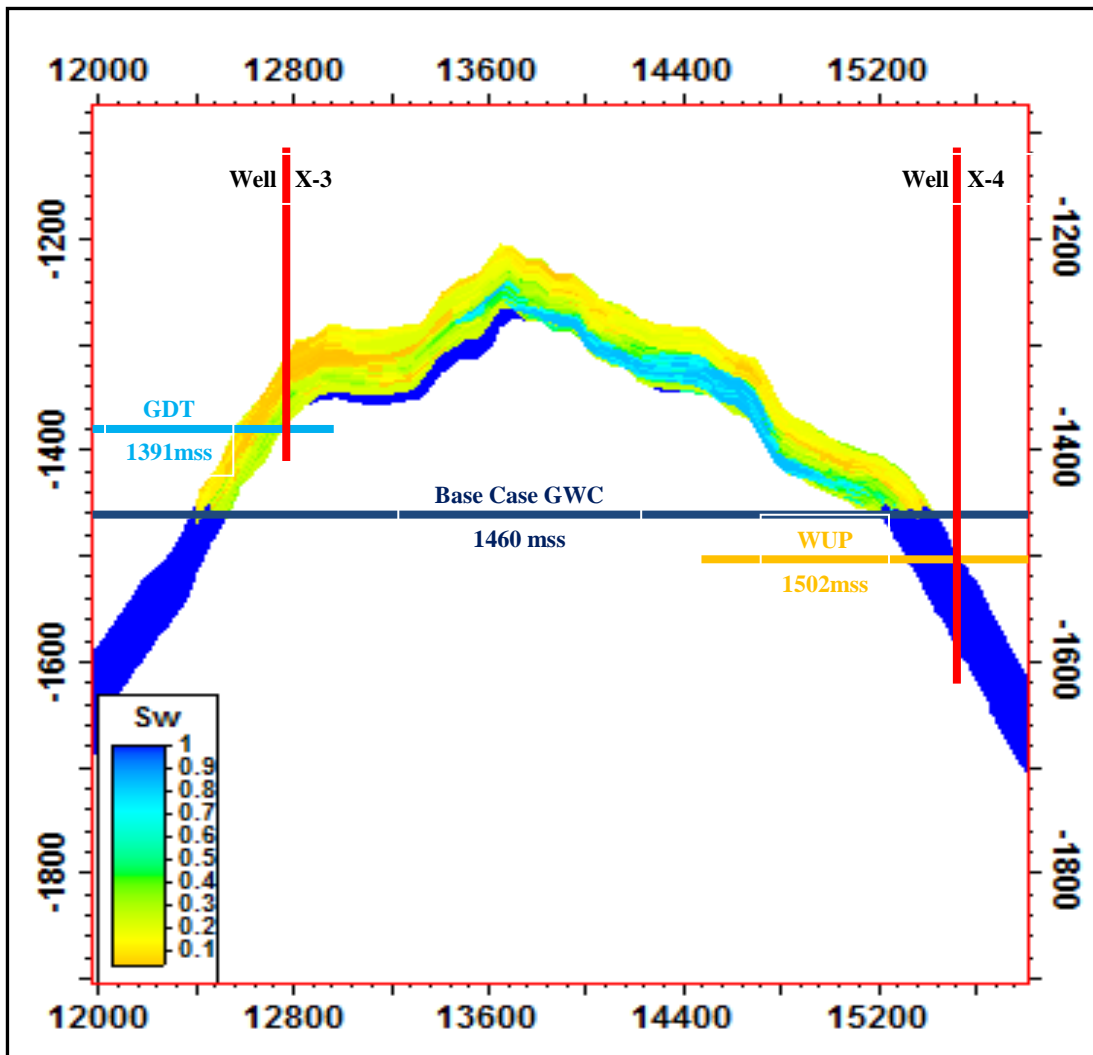


Figure 3.35: Cross sectional view of GDT (1391mss) and WUP (1502mss).

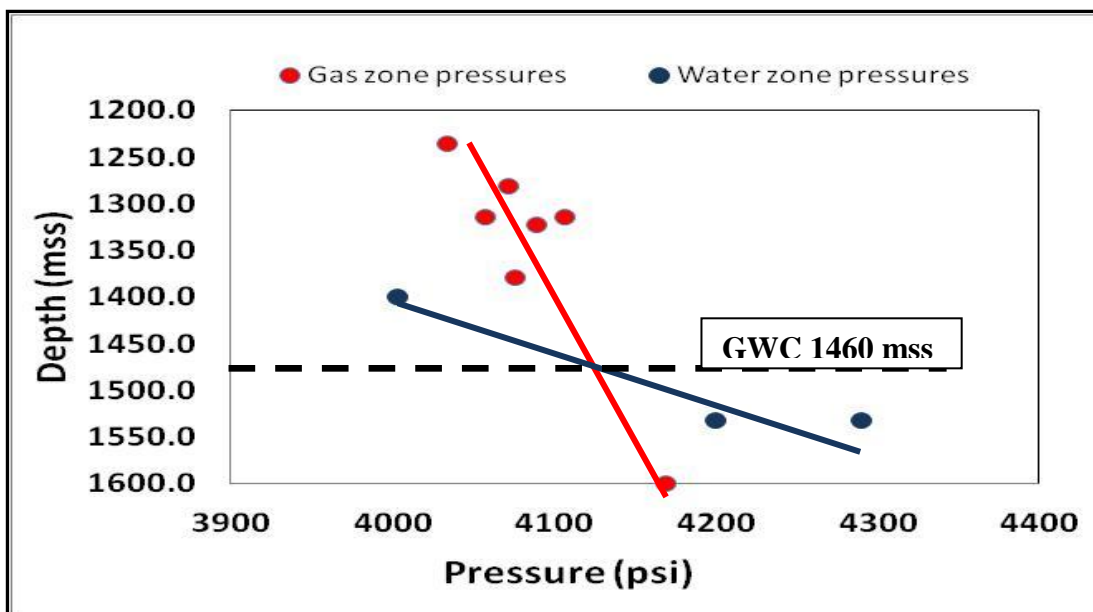
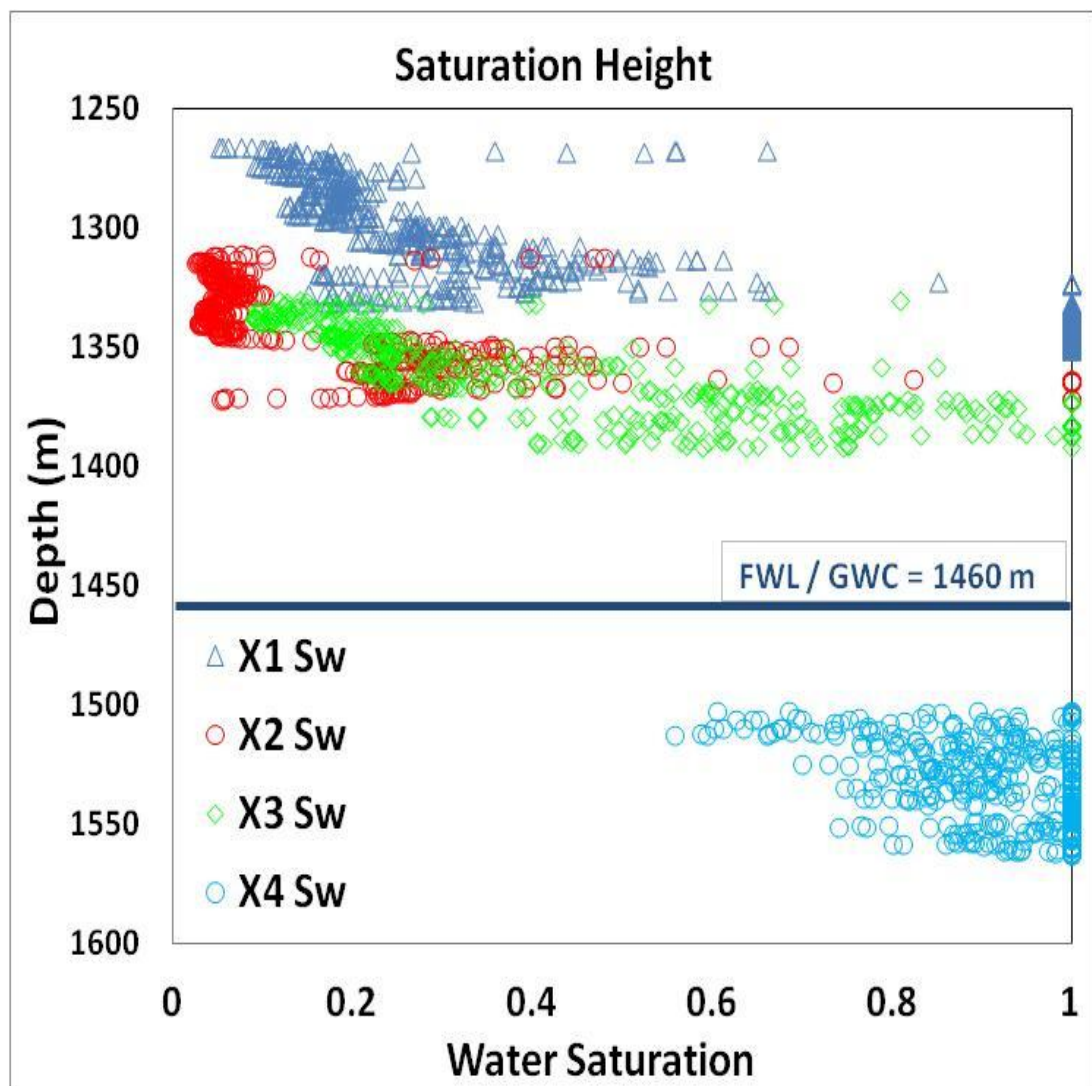


Figure 3.36: Pressure – depth & GWC.



Determination of GWC can be done with many different approaches. In this study as it was explained above, pressure data was used for determination of GWC due to limitation on the available data. However, different options have been studied in order to estimate the GWC such as analysis of saturation – height data. Well-log water saturation vs. depth for all existing wells drawn to see the trend of water saturation with depth. As it can be seen from the Figure 3.37, although there is a water saturation increase with depth, it is difficult to say that the behavior is obvious. Therefore, determination or predicting of gas water contact with the log data is impossible: however, determined GWC (-1460 m) by pressure data is not contradicting with saturation - height observation as can be seen from the below graph.



**Figure 3.37:** Water saturation vs. height.



#### **4. 3D GEOLOGICAL MODELING**

As mentioned previously, typical reservoir studies can be very complex due to requirement of integration of several disciplines that those have different data sources in different scales. Each of them has different perspective to look the problem and different tools to describe invisible underground structures. For instance, geophysicists have seismic data to model structures: Geologists have logs to describe formation properties, and reservoir engineers have well tests to predict reservoir parameters and reservoir performance. A 3D static reservoir model can be defined as a combination of the structural, stratigraphic, lithological and petrophysical modeling outputs. 3D geologic modeling starts with a structural modeling which consists of building formation top and bottom maps, defining and modeling the faults if there is any and calibration of those data with obtained information from the wells if any. After completion of the structural definition part, stratigraphic modeling part starts and it comprises the internal description of the formation such as dividing formation to sub zones where each of the zones represents different interval and dividing zones to sub layers not to lose the resolution of the data in the mathematical models. The final step in the geological modeling is the petrophysical modeling which includes assigning the petrophysical parameters, such as porosity, permeability and water saturation, to each grid block

As described above, geological modeling is a complex process that requires the integration and calibration of different data sources in a reservoir modeling suite. Collected data from the field that introduced in Chapter 3 were uploaded into PETREL and all required analysis and calibration were performed to obtain technically reliable static reservoir model which will be input of dynamic reservoir model. All the performed studies, analysis and modeling in PETREL are explained and presented in this chapter. The final product of this chapter will be 3D static reservoir model with the calculation of GIIP that will be the basis of the next section which is simulation model.

## 4.1 Structural Modeling

2D and 3D seismic data were used for obtaining the reservoir X formation top map. The constructed formation top map was imported to PETREL for structural modeling which is given in Figure 4.1. Similarly, formation base map which is given in Figure 4.2 was imported to PETREL. Note that there is not much difference between both figures except the depth of the surfaces because the base map is following the top map due the almost constant formation thickness observed from the existing wells throughout the field. As it was discussed in the Chapter 3.6, gas-water contact (GWC) is in 1460 mss and will be used for the base case model. Therefore, a flat surface was created by using the limits from structural surfaces at 1460 mss to use as a GWC in PETEL that is shown in Figures 4.1 and 4.2. Additionally, the field is bounded by a three main fault system that lies down on the south east – north west direction which is identified by seismic data. Fault sticks were imported into PETREL and prepared for the geological model by using the fault modeling module in PETREL. Final pillars after calibration and preparation of the fault sticks are shown in Figure 4.3. It is important to note that faults which have blue and yellow colors are crossing the formation below GWC, but the fault in the turquoise color is getting into the formation. Those faults are very important because most probably they are blocking the connection of the formation with aquifer if any or those are preventing active aquifer communication. If the reservoir pressure data are examined carefully, it supports that thesis because formation is significantly over pressured. Considering the depth of the formation which is less than 1500 mss, reservoir pressure would not be in the order of 4000 psi if there is any communication with active aquifer. Although that information gives some idea about aquifer, it is one of the unknown and uncertainty points in the field. Existence and strength of the aquifer can only be described and confirmed by well data which is considered as excessive expenditure most of the time. On the other hand, the field is anticline that formed due to compression from both side in the direction of NW-SE. Therefore, compression can cause to have sealing faults in the both side of the field and thus over pressured conditions can be observed. In conclusion, although there is no robust information about aquifer support on the field, due to above mentioned reasons, it is not expected to have strong aquifer support on the field.

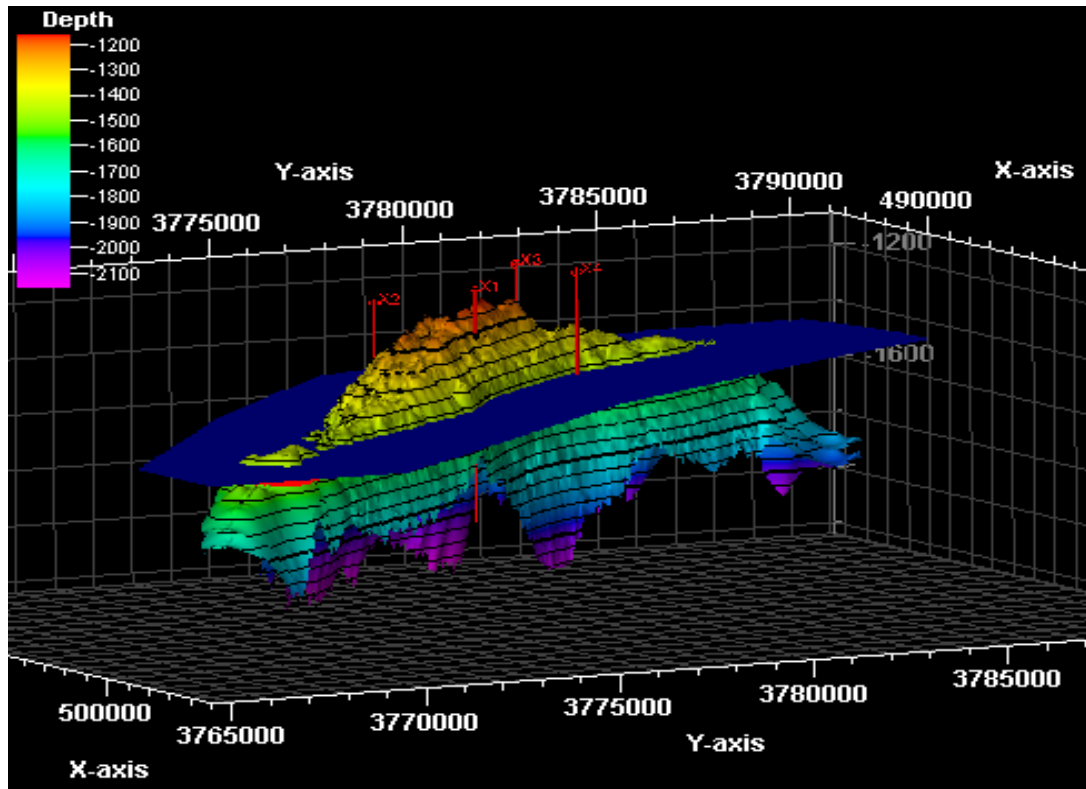


Figure 4.1: Formation structural top map & GWC.

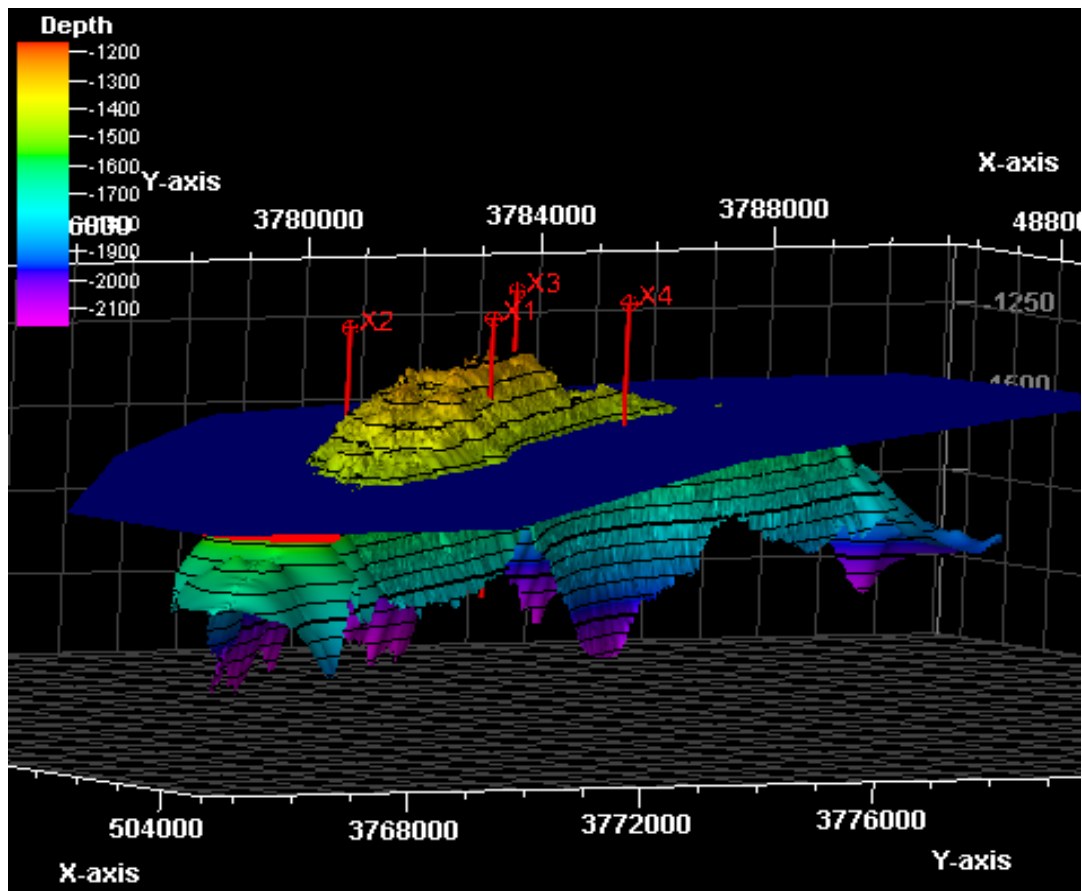
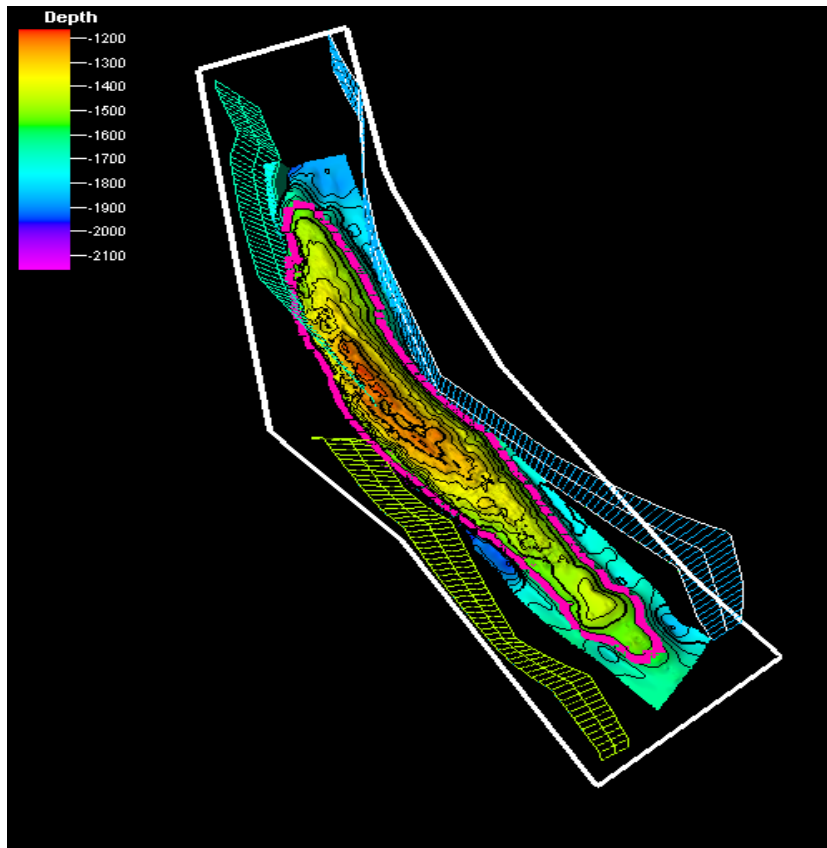


Figure 4.2: Formation structural base map & GWC.



**Figure 4.3:** Fault pillars.

## 4.2 Well Logs and Well Tops

One of the important steps in the structural modeling is calibration of the well tops with the structural surfaces. Most of the information obtained from the wells such as logs, cores...etc. will be used in geological modeling: therefore, the well tops have to tie with the created surfaces. Black balls in Figure 4.4 are the formation tops that should tie with the formation top and base surfaces. As it can be seen from Fig. 4.4, a very good match was achieved between well tops and the formation top - base surfaces for the each existing wells. On the other hand obtained match can be seen also from the existing wells logs given in Figure 4.5. As it was discussed in Chapter 3.3, recovered core data were analyzed carefully and 2D log was built in PETREL with available core data as shown in Figure 4.5 with the red color. Although the fact that core data are not covering whole formation, such data allows us to see the some intervals for the comparison purposes. As it can be seen from Fig. 4.5, log porosity (black colored line) and core porosity (red colored line) are overlapping, and the difference between them is quite small. Considering the fact that both well-log porosity and core porosity are matching quite well and that, the core data are not

covering the whole reservoir formation thickness, well-log porosity data will be used for petrophysical modeling of the porosity distribution for the field. In addition, the well-log water saturation shown in Fig. 4.5 will be used as a main input in the petrophysical modeling for distributing water saturation into the reservoir. Additionally, well-log porosity, core porosity, well-log water saturation histograms are given in Figures 4.6-4.8, respectively. Generally speaking, if the given histograms for porosity are compared, it can be seen that there is a good agreement between core and well-log porosity. Furthermore, log and core porosities show normal distribution, whereas the histograms of the water saturations exhibit skewed distributions; for instance, the histograms of water saturations for well X-1, X-2, and X-3 are like positively skewed or right-skewed (log-normal), whereas the histogram for well X-4 is like a negatively or left-skewed. However, all log property histograms and statistics will be evaluated deeply in petrophysical modeling section later for quality check purposes and making property distribution to the field.

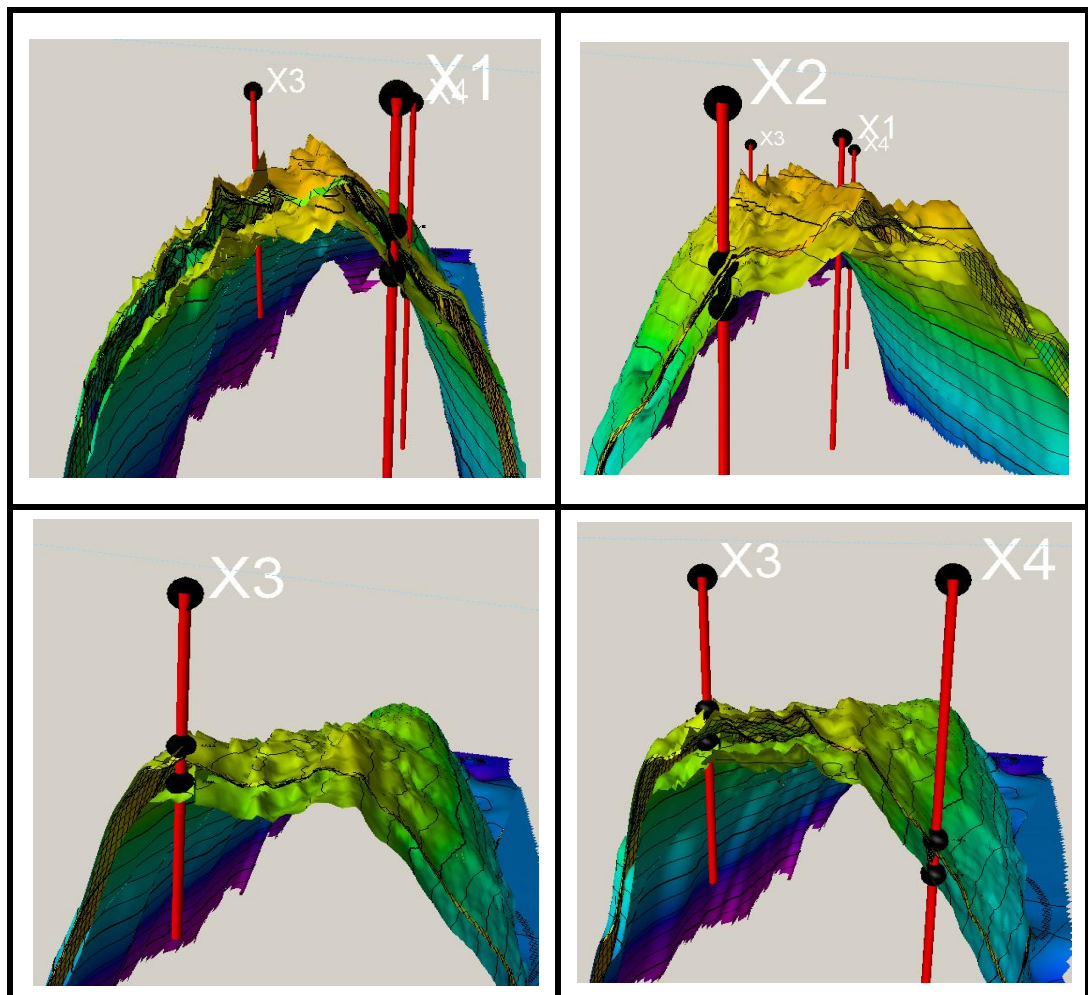


**Figure 4.4:** Well tops.

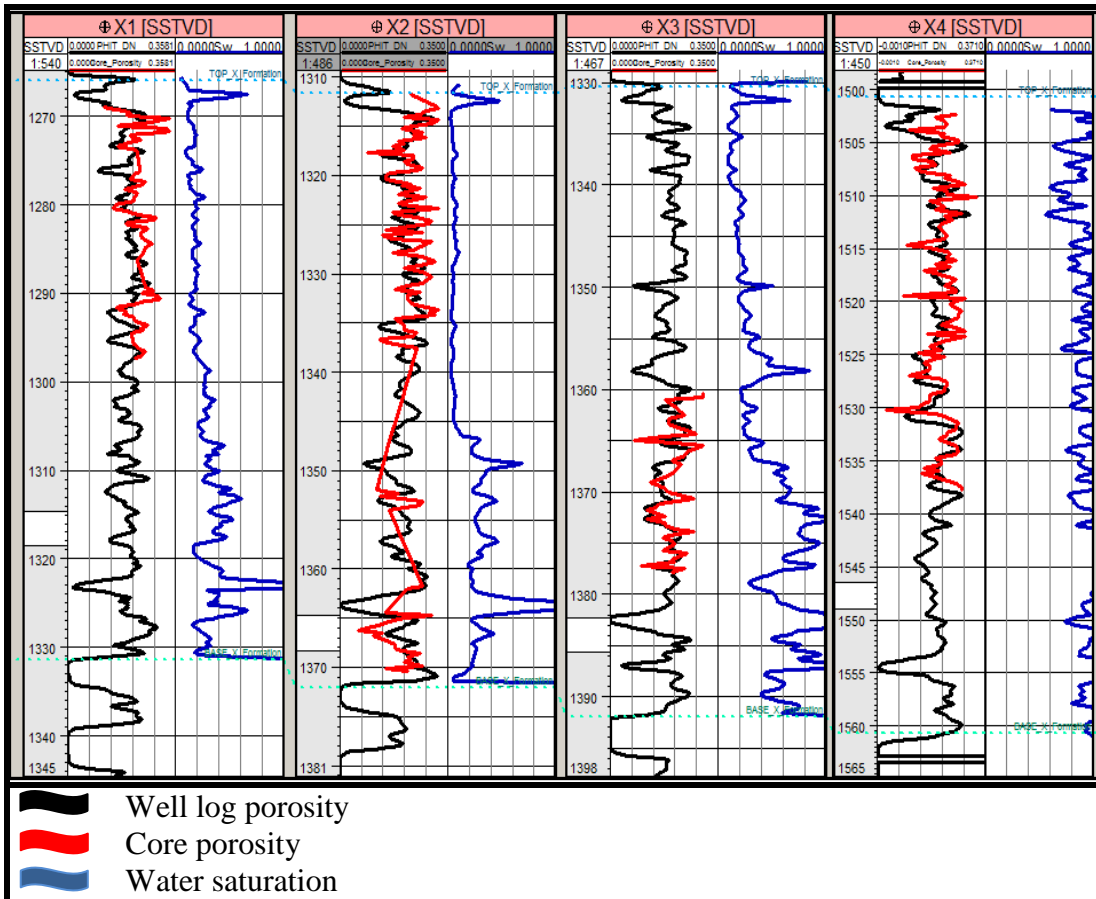


Figure 4.5: Well logs – all wells.

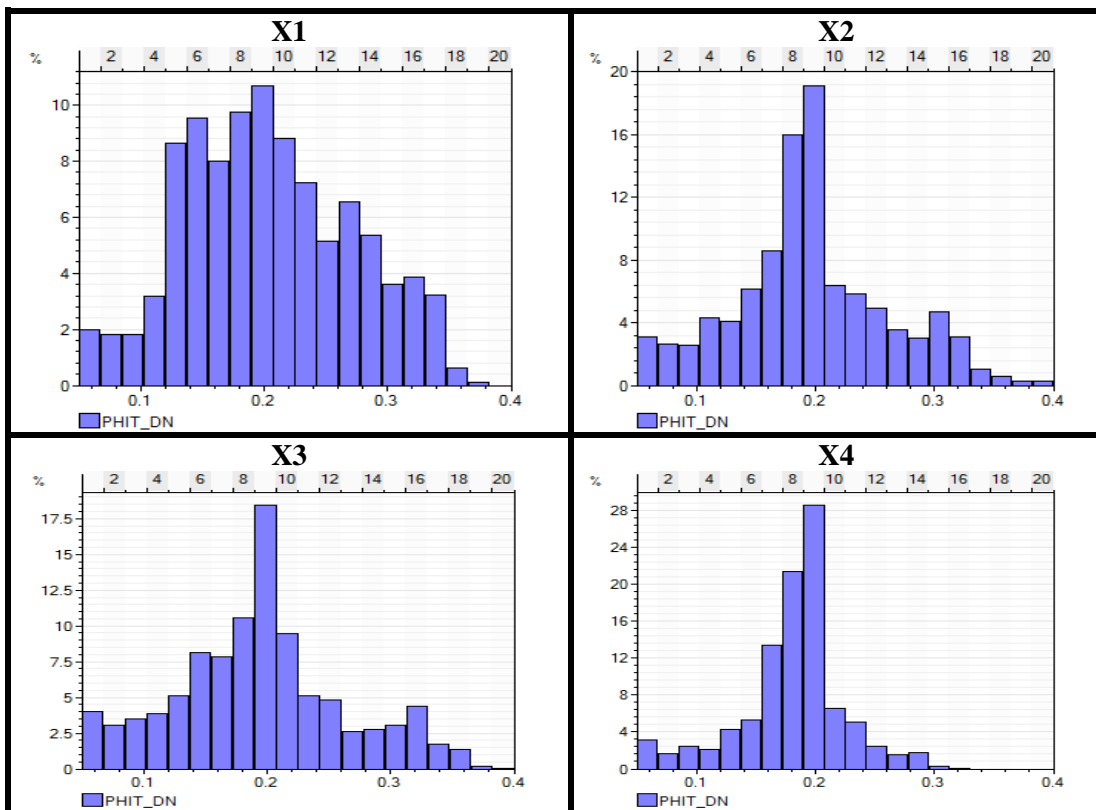


Figure 4.6: Well log porosity histograms – all wells.



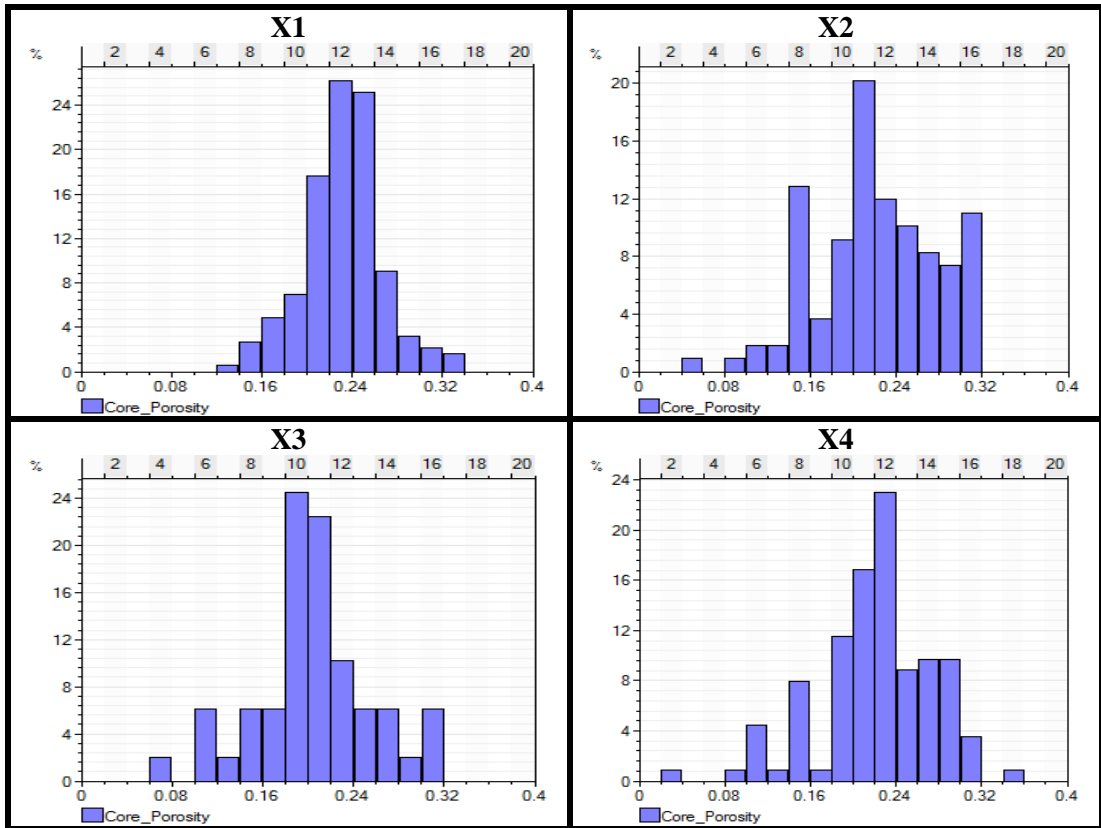


Figure 4.7: Core porosity histograms – all wells.

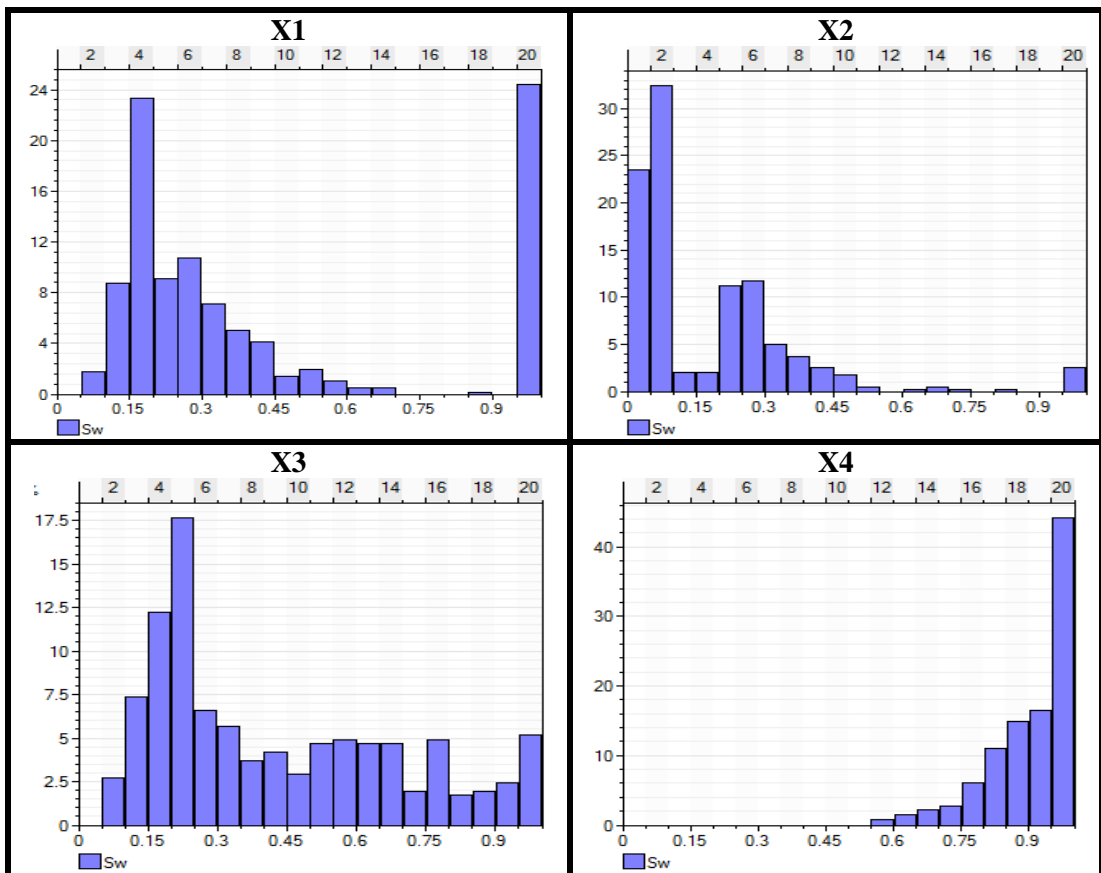
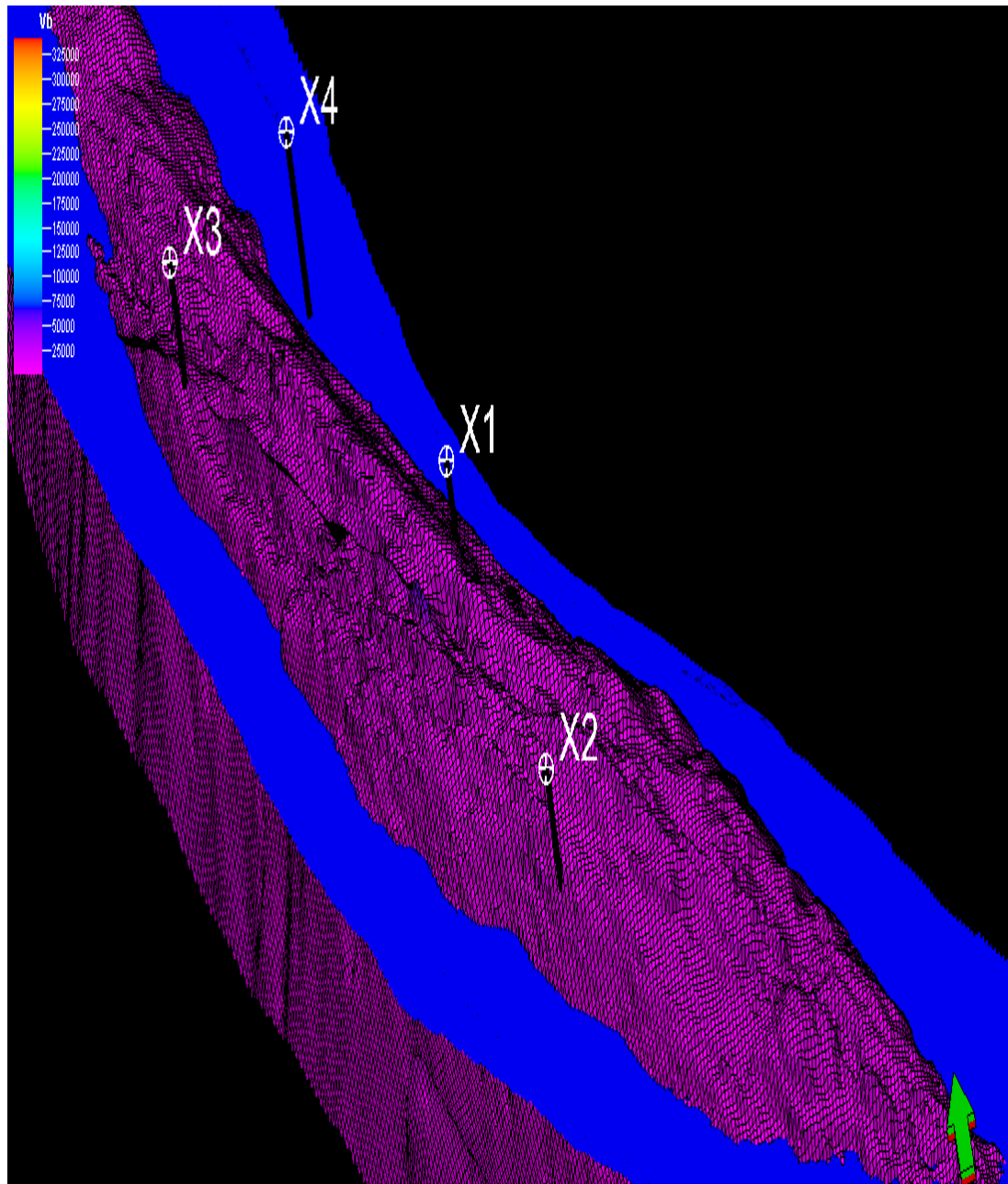


Figure 4.8: Water saturation histograms – all wells.

### 4.3 3D Grid Generation

While creating a 3D geological grid, the most important goal is to preserve the small features from well logs and seismic data as much as possible. These grids are designed to preserve the heterogeneity of the reservoir by typically subdividing it on a fine scale vertically, as well as keeping the XY-representation of the grid cells as small as possible. A geological grid often has millions of cells. Volume calculations are important in this type of grids. Therefore, a 50m grid-size was used in X and Y directions and the formation was divided into four major zones which were further divided into a total of 30 sub-layers not to lose well-log resolution. Note that vertical resolution of well-log is around 0.5 ft and modeling the 60m-65m thick reservoir by honoring the high resolution well-log data in vertical direction requires huge computational capability. Therefore, considering our limited computational capability and power of our computers, we tried not to lose well-log resolution by minimizing the number of sub-layers as much as possible to reduce computational time. In this context reservoir divided to main zones and sub-layers and well-log up-scaled which is averaging the well-log data points in the each layers. Applied zonation and layering are to be discussed in Section 4.3.2. As discussed in the previous sections, there are 3 major faults bounding the reservoir on the SE-NW direction. Therefore, these major fault directions used as a trend for 3D grid generation to reduce the risk of possible pinch out in the 3D grid and avoid the possible orthogonality problems. The constructed 3D grid model is shown in Figure 4.9 which was controlled carefully against above mentioned possible problems. The grid model has 439 grids blocks in the I-direction; 577 grids blocks in the J-direction and 31 grids blocks in the K-direction. Hence, the total number of grids blocks is 7,852,393. However, most of the grids are below the GWC and those will be deactivated while running simulation scenarios.

The simulation grid must have grid cell geometries which conform to the requirements of the specific flow simulator used. Using zigzag type faults is one option to keep the grid cells as orthogonal as possible. Therefore, zigzag type faults were used for grid generation. If the constructed fine scale geological model is not allowing the fast simulation run, even the cells below GWC deactivated which will reduce the active cells numbers significantly; fine scale model will be up scaled before simulation model initialization.



**Figure 4.9:** 3D Grids (50m x 50m cell size).

### 4.3.1 Horizons

The formation top and base structural maps were used for creating the horizons<sup>3</sup>. In this study, formation divided into four main zones, however, formation top and base surfaces are available which is interpreted from seismic data. Therefore, surfaces (horizons) were created for zones where the seismic interpreted surfaces not available based on formation top and base map. Figure 4.10 is the 3D view of

<sup>3</sup> In geology a horizon refers to either a bedding surface where there is marked change in the lithology within a sequence of sedimentary or volcanic rocks, or a distinctive layer or thin bed with a characteristic lithology or fossil content within a sequence (Rey and Galeotti 2008).

obtained horizons. After completion of the zone and layering process, the constructed top and base horizons as well as well tops used for creating the sub horizons for each zone. The formation top and base horizons are shown in Figure 4.10, and there are no surfaces for the sub zones as can be seen from the Figure 4.10. Therefore, specific depths (well tops) for the each zone where the formation starts and ends were determined by using the well-log data. Then, formation top map and base map used for geometry inputs of the horizons.

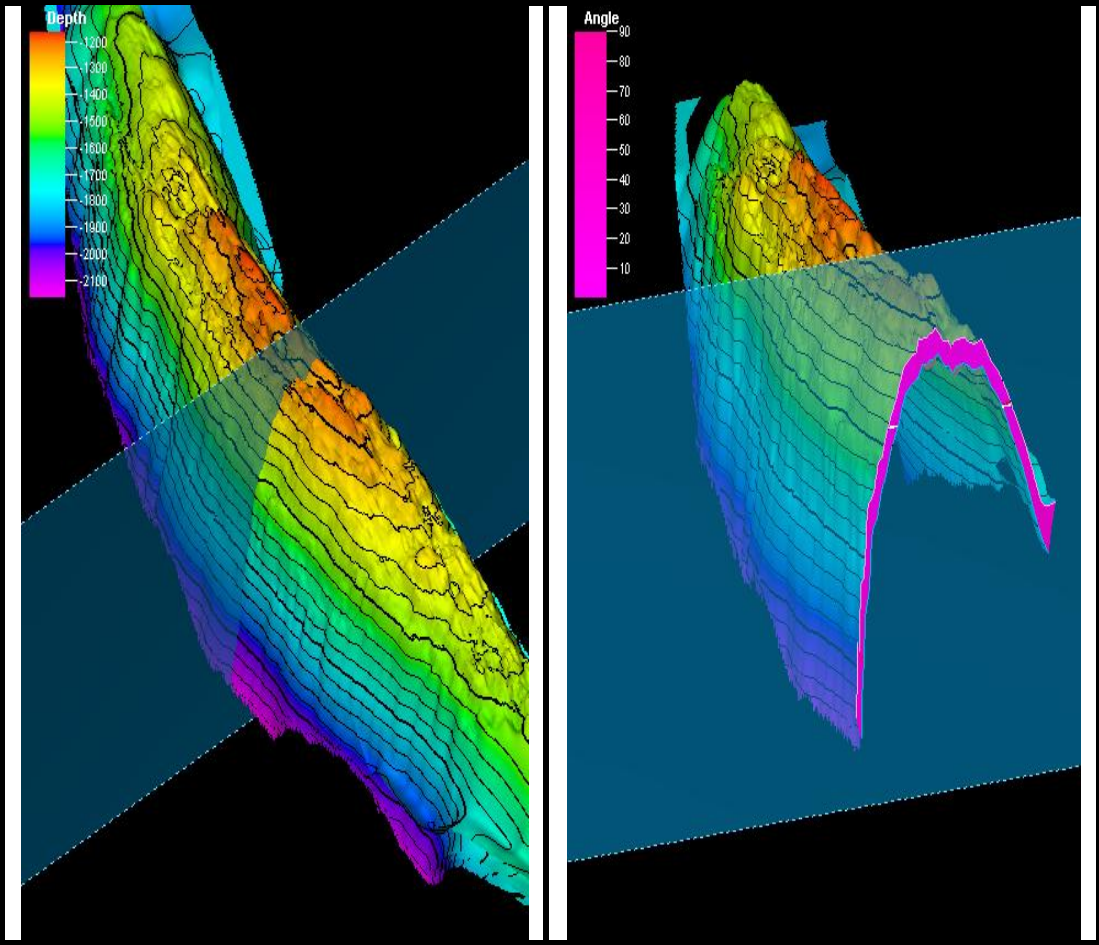


**Figure 4.10:** Horizon – 3D view.

**4.3.2 Zones – layering**

Considering the well-log data, zonation and layering were conducted for defining the vertical resolution of the 3D grid. Zonation is made for generally differentiation of facies, different sand packages, hydraulically disconnected formations etc. Although the fact that the formation X has no hydraulically disconnected units, different facies, we have divided the formation four zones due to having varying porosity, water saturation values in some of the intervals. As shown in Figures 4.11-4.13, the

formation was divided into the four main zones, and each zone is divided into sub-layers not to lose the resolution of well logs in the up scaled property. For instance, well log porosity is shown in Figure 4.11 where the low porosity intervals (top 2-4 meters) are identified as zone-1, high porosity intervals (next 20-25 meters after zone-1) are identified as zone-2, relatively lower porosity intervals than zone-2 are identified as zone-3 (next 30-35 meters after zone-3) and last 5 meters as zone with high porosity. Similarly, water saturation from each well-log was considered on the zonation. Water saturation value in the low-porosity intervals is higher than the high-porosity intervals. Therefore, zonation based on well-log porosity is somehow in-line for zonation based on well-log water saturation. To be able to create the identified zones, creating horizon map for each zone are necessary. Therefore, this will only be possible with isochor map<sup>4</sup> for the each zone. Table 4.1 gives the defined zones formation tops for each well that was used for horizon creation of each zone. After creating zones, each zone divided into sub-layers considering the vertical resolution of the log data (less than 0.5 ft) and variation on the properties in the vertical direction. As can be seen from the Figure 4.11, porosity values are not varying too much in the 2 meters intervals. Therefore, layering is made accordingly. However, thickness of each zone is different and it is impossible to have identical 2m layers in the each zone. Therefore, thickness of each layer is in between 1.5m - 2.0m depending on the thickness of zones. Created zones and layers thicknesses are shown in Tables 4.2 and 4.3, respectively.

As can be seen from the given Figures 4.11-4.13, vertical resolution of the 3D grid is enough to catch all the details of the original well logs by having a total of 30 layers and four zones. As a result, it can be concluded that model has enough number of layers to mimic the original well-log resolution.

After completion of zonation process, permeability – porosity cross plot of each zone from core data will be created in the petrophysical modeling part and obtained correlation equations will be used together with log porosity to create the permeability model.

---

<sup>4</sup> Isochor map is the variable thickness map of the zone which is constructed by the well data. It specifies the well tops and thickness of the specific zone from each well.

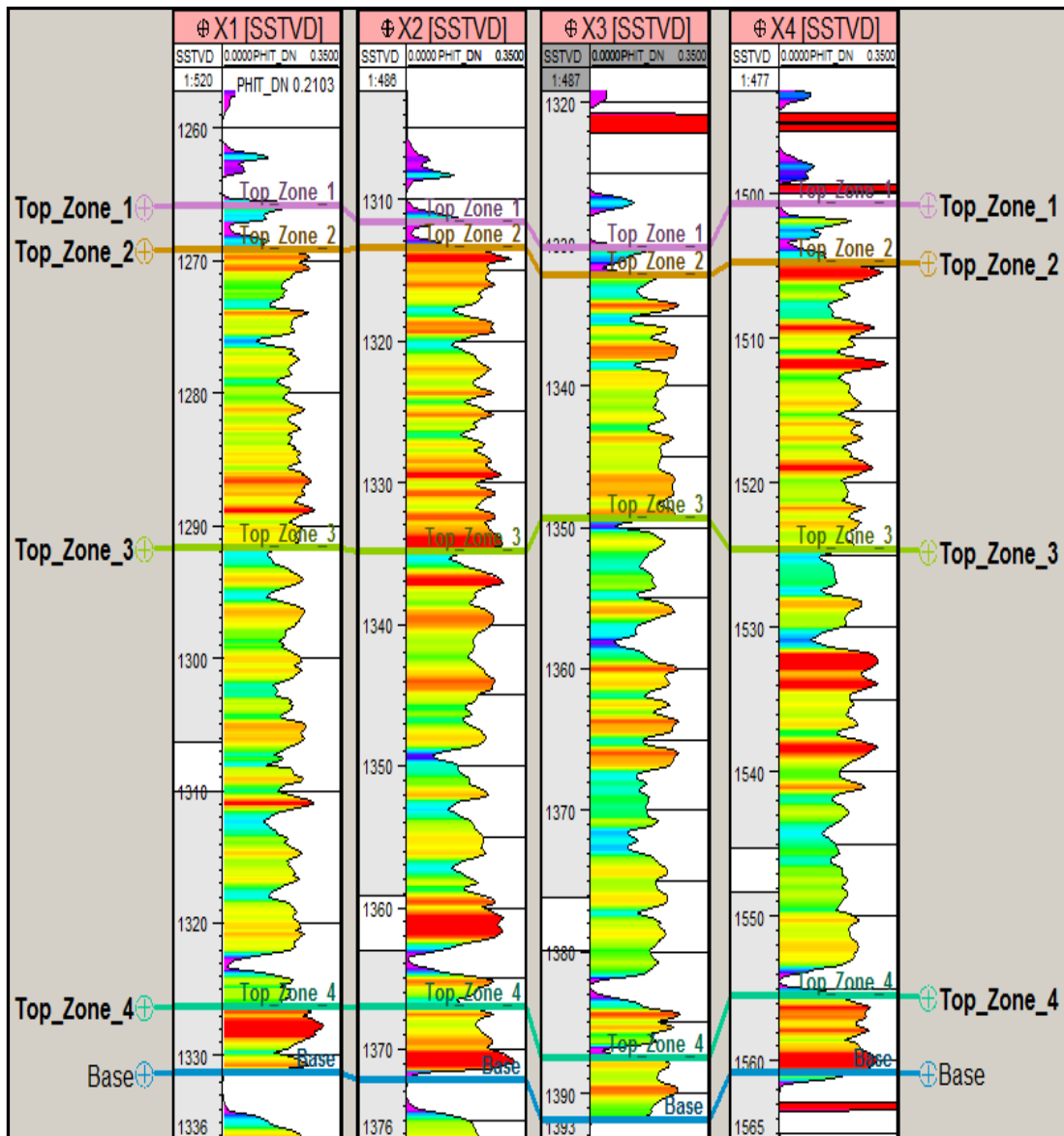


Figure 4.11: Zones – 2D well log porosity all wells.

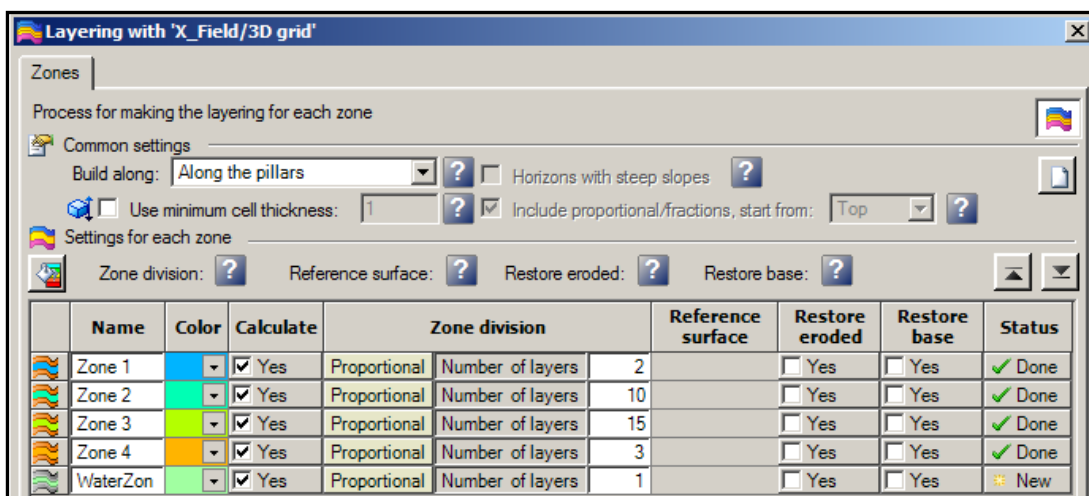
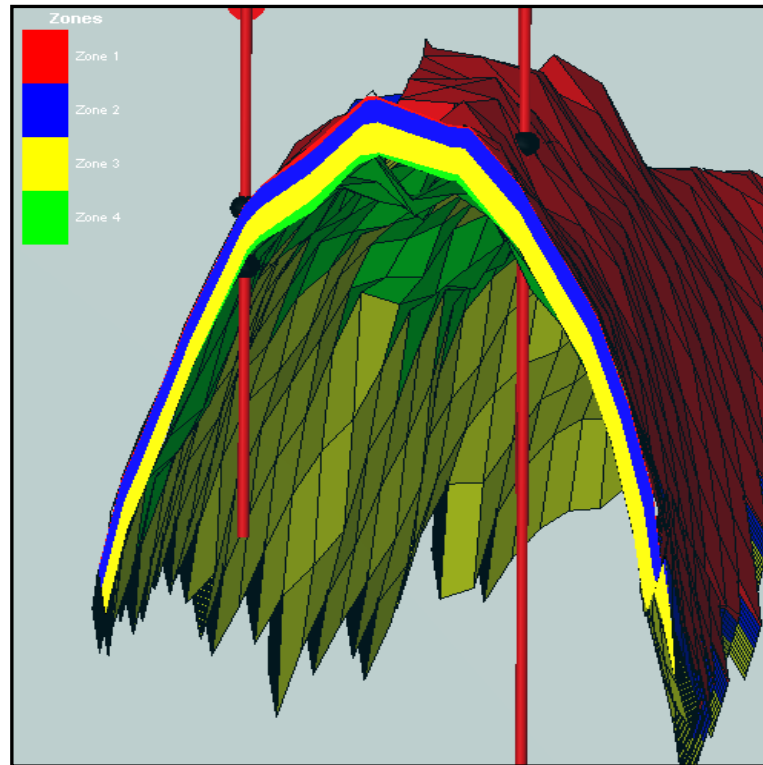


Figure 4.12: Each zone: number of sub-layers.



**Figure 4.13:** Zones – 3D view.

**Table 4.1:** Formation tops – all wells.

Zones	Formation	X-1 (m)	X-2 (m)	X-3 (m)	X-4 (m)
Zone 1	Top Zone 1	1265.90	1311.69	1330.26	1500.68
Zone 2	Top Zone 2	1269.19	1313.52	1332.22	1504.70
Zone 3	Top Zone 3	1291.69	1334.94	1349.43	1524.68
Zone 4	Top Zone 4	1326.29	1367.09	1387.47	1555.56
Base	Base	1331.32	1372.14	1391.86	1560.80

**Table 4.2:** Zone thickness.

Zones	X-1 Zone Thickness	X-2 Zone Thickness	X-3 Zone Thickness	X-4 Zone Thickness	Avg. Thickness (m)
Zone 1	3.29	1.83	1.96	4.02	2.77
Zone 2	22.5	21.42	17.21	19.98	20.28
Zone 3	34.6	32.15	38.04	30.88	33.92
Zone 4	5.03	5.05	4.39	5.24	4.93
Total	65.42	60.45	61.60	60.12	61.90

**Table 4.3:** Layer thickness.

Zone	Avg Zone Thickness (m)	Number of Layer	Avg Layer Thickness (m)
Zone 1	2.77	2	1.39
Zone 2	20.28	10	2.03
Zone 3	33.92	15	2.26
Zone 4	4.93	3	1.64

### 4.3.3 Fluid contacts

Gas-water contact (GWC) was determined by studying all well-test and pressure data which was discussed in detail in the Chapter 3.6. A flat surface was created at the depth of 1460 mss by using the limits of the structural surface of formation top map. Then, the 3D grid model was filled with water below 1460 mss as it can be seen from the Figure 4.14.

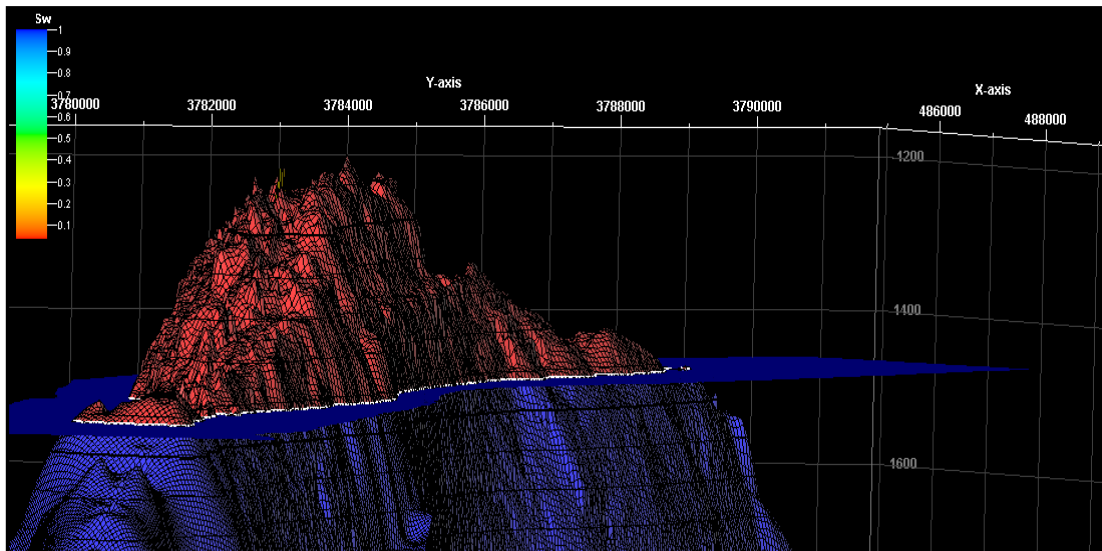


**Figure 4.14:** Gas water contact – 1460 mss.

## 4.4 Property Modeling

One of the major steps in 3D modeling is the property modeling which is a process of filling the cells of the grid with discrete (facies) or continuous (petrophysics) properties. The objective of the property modeling is to distribute the properties between the available wells so it realistically preserves the reservoir heterogeneity and matches the well data. In this process well data will be prepared for petrophysical modeling.

Porosity and water saturation logs are ready, and such log data can be used in petrophysical modeling after scale up well-logs process (see Section 4.3.3). However, permeability model needs to be obtained in this step. Permeability data from the field exist from two main sources. One of them is the well-test permeability obtained after PTA which was discussed in Chapter 3.5. However, this information is limited due to unavailability of the tests from the intervals where the core data are available. Therefore, additional information is required in order to make realistic



permeability model. Existing core data may be helpful but at the same time will be challenging to obtain a realistic model. All available core porosity and permeability were drawn firstly as shown in Figure 4.15. Then, porosity and permeability correlation equations were obtained for each zone as shown in Figure 4.16. Table 4.5 summarizes the results. After that those equations were used together with log porosity data to obtain permeability logs for the whole formation as shown in Figure 4.17. Green line in Figure 4.17 is the permeability derived by using core and log data together. On the other hand, the red lines in Fig. 4.17 represent the original core measured permeabilities. It is important to note that although core data are not covering the whole formation, a good match was obtained for the interval where the core data are available.

As mentioned previously, the reservoir has divided into four main zones. Therefore, data have been reviewed in accordance with reservoir zonation. Although the permeability derived from logs and core data are good enough, in some intervals it is less than the PTA interpreted permeability. Therefore, it may be necessary to modify the log permeability before simulation initialization to comply with the PTA derived permeability results.

Table 4.4 gives the statistical information of the core permeability for each well. As it can be seen from Table 4.4, permeability is around 1 md – 20md. However, it is important to note that core permeability is available from some intervals and not covering the whole formation. Table 4.6 shows the statistical information of continuous permeability-log which covers whole formation that produced using the equations (equations derived from log-porosity and core permeability data) given in Table 4.5. As can be seen from the Table 4.6, mean of permeability that will be distributed throughout the field is around 3 md: however, the PTA derived permeability was around in the range of 10 md – 20 md. Therefore, permeability multiplier of 4 will be used for the simulation to honor the well-test data.

**Table 4.4:** Statistics of core permeabilities (md).

Well	Min	Mean	Max
Well X-1	0.72	20.41	145.89
Well X-2	0.01	11.45	108.93
Well X-3	0.07	1.61	8.07
Well X-4	0.24	5.80	31.31

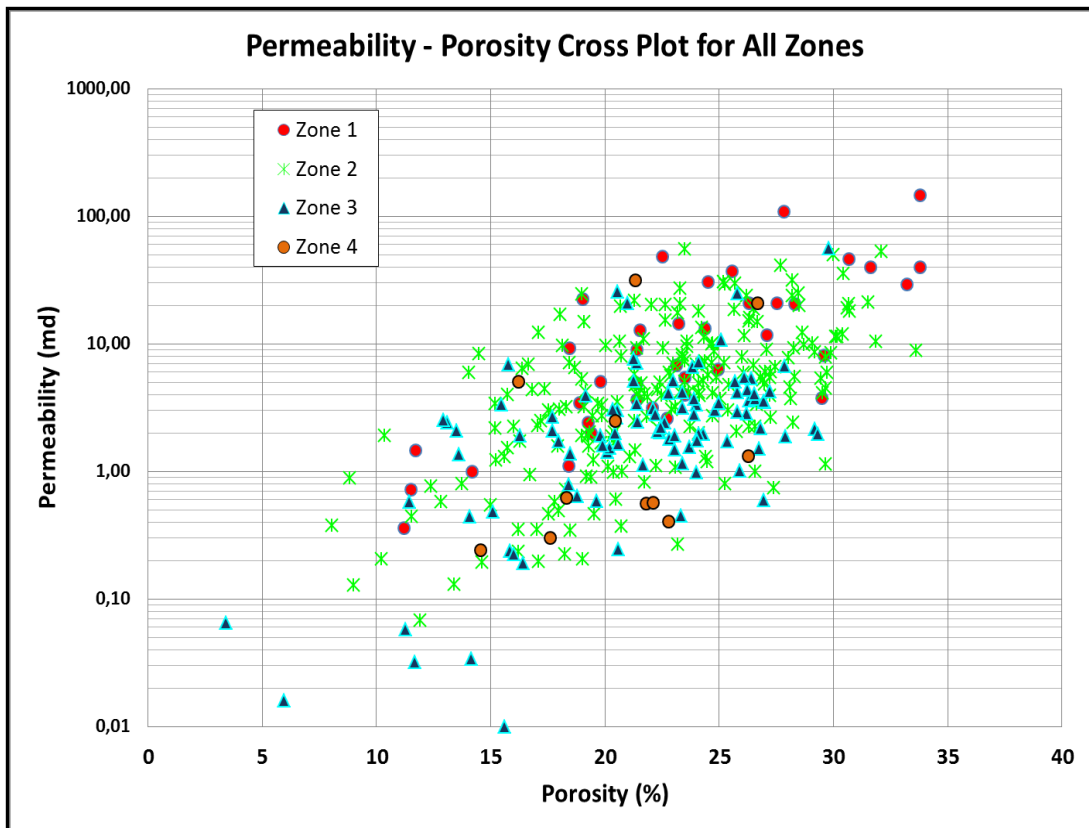


Figure 4.15: Permeability-porosity cross plot for all zones.

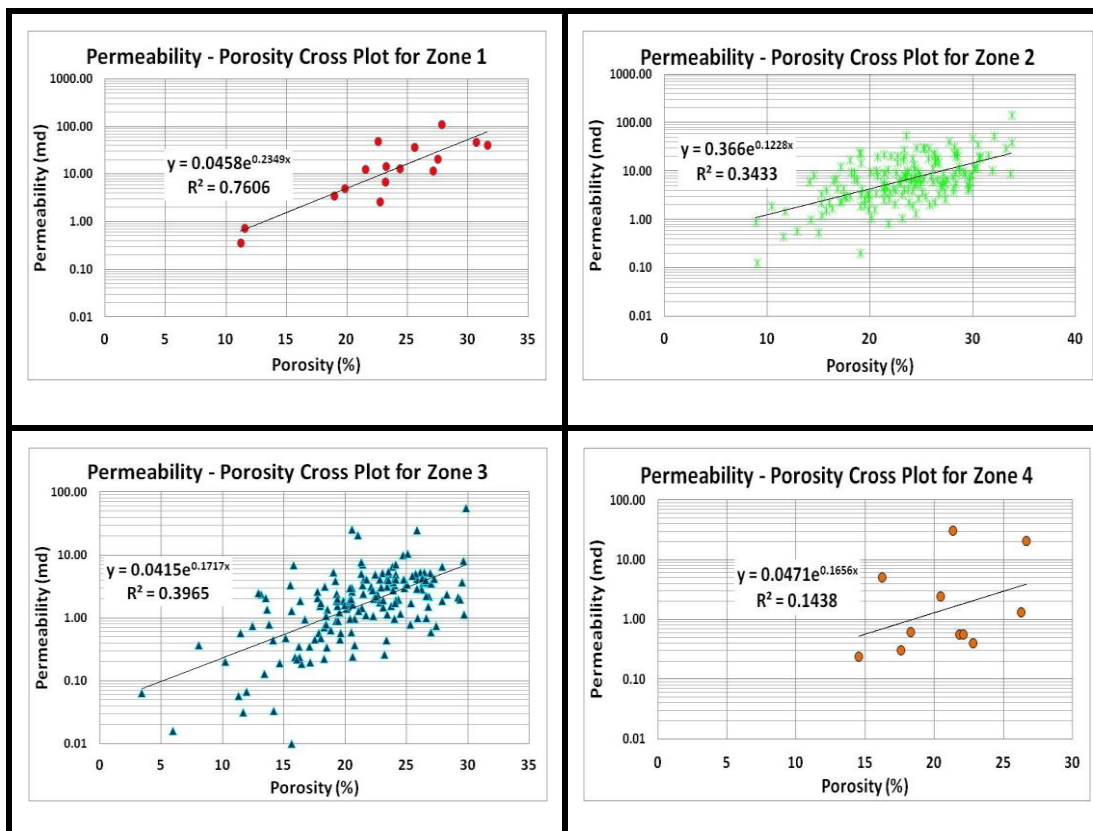


Figure 4.16: Permeability vs porosity each zone & correlation equations.

After drawing all available permeability and porosity cross plots, the equations describing the relationship between porosity and permeability for each zone were obtained (see Table 4.5). These equations will be used for permeability modeling after comparison with the available PTA derived permeability data.

**Table 4.5:** Permeability-porosity correlation equations.

Zone	Equation
Zone 1	Permeability = $0.0458e^{0.2349\text{porosity}}$
Zone 2	Permeability = $0.3660e^{0.1228\text{porosity}}$
Zone 3	Permeability = $0.0415e^{0.1717\text{porosity}}$
Zone 4	Permeability = $0.0471e^{0.1656\text{porosity}}$

As can be seen from Figure 4.17 with the green line, the continuous permeability logs were created by using above equations and log porosity data. Such porosity logs will be distributed throughout the field in the petrophysical modeling section. If any discrepancies exist between the obtained permeability model and the PTA derived permeability data from the wells, those discrepancies will be reduced by using permeability multiplier before initialization of simulation.

Purpose of trying to obtain continuous permeability log data is to have input data for petrophysical modeling for data distribution where the property will be distributed throughout the field by the help of constructed variogram model. Otherwise, the PTA data is provides only single permeability value where we can only assign the single value for the cells. However, assigning different permeability values to the each layer which obtained based on well-log and core data were achieved by doing above explained permeability modeling methodology. Variogram model will be used for distributing permeability data to the field and then will be calibrated with the PTA derived permeabilities that is superior than assigning same values for all the cells.

**Table 4.6:** Statistics of derived permeabilities based on log-porosity and core permeabilities (md).

Well	Min	Mean	Max
X - 1	0.06	2.72	10.08
X - 2	0.04	3.17	16.47
X - 3	0.04	2.23	8.91
X - 4	0.04	3.00	18.62

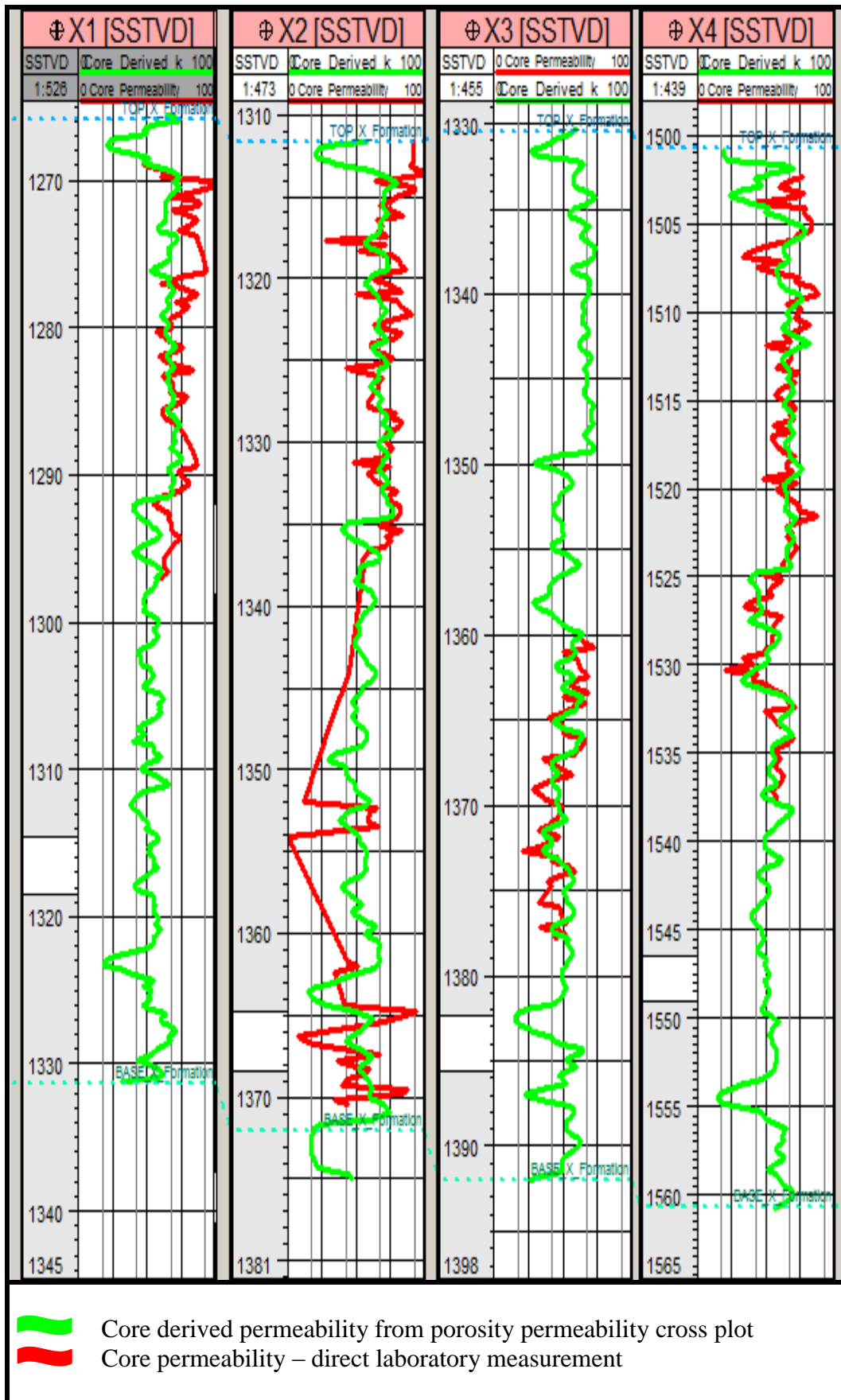


Figure 4.17: Permeability logs – all wells.

#### 4.4.1 Scaling up well-logs

While modeling the reservoir, the reservoir is divided into cells by generating a 3D grid which is generally less dense than well-log sample density. Each grid cell is filled with a single value for each property such as porosity, permeability, and water saturation. Therefore, well-log property data have to be scaled up to be able to assign the property to grid blocks. The importance of having enough number of layers can be observed in up scaling well-log process because number of layer is the main driver of up scaling well-log process not to lose resolution of well-log property. Up scaling well-log is a process that averaging the property values such as porosity, water saturation, and permeability within the each identified layers arithmetically. For instance, for the layer-1, there are almost 10 porosity values exist on the well-log data. In the up scaling of well-log process, arithmetic averaging of these 10 porosity values is taken and then single porosity value for layer-1 is obtained. Thus, single value for each property for the each layer is obtained after completion of this step. If necessary, the number of layers will be reduced before simulation due to computational limitation. However, for the sake of representing available data in the fine scale model, reservoir divided into 30 layers. If the up scaling of the structure is performed before simulation, up scaling will be performed according to the fine scale model. Actually, it is better to built fine scale geological model without performing any up scaling on the well-log data, but our computing power is not enough to perform such a modeling activities. Therefore, we had to up scale the well-log data to built fine scale model. The number of cells in the constructed model is more than 7 million which is even difficult to handle with the regular computers. Without up scaling on the well-log data, number of cells will reach almost 100 million cells which impossible to handle with the regular computers.

As can be seen from Figures 4.18-4.20, available well logs are up scaled according to the layers that created in the layering section for all wells. On the left hand side of the each figure, original (not up scaled) well-log is shown for each well and on the right hand side; the up scaled well log is shown. It is needless to say that up scaled well logs for each property which will be used in the model are representing original well logs very well and there is almost no loss of resolution of the data. After completion of that step, up scaled properties will be distributed whole field in the petrophysical modeling section.

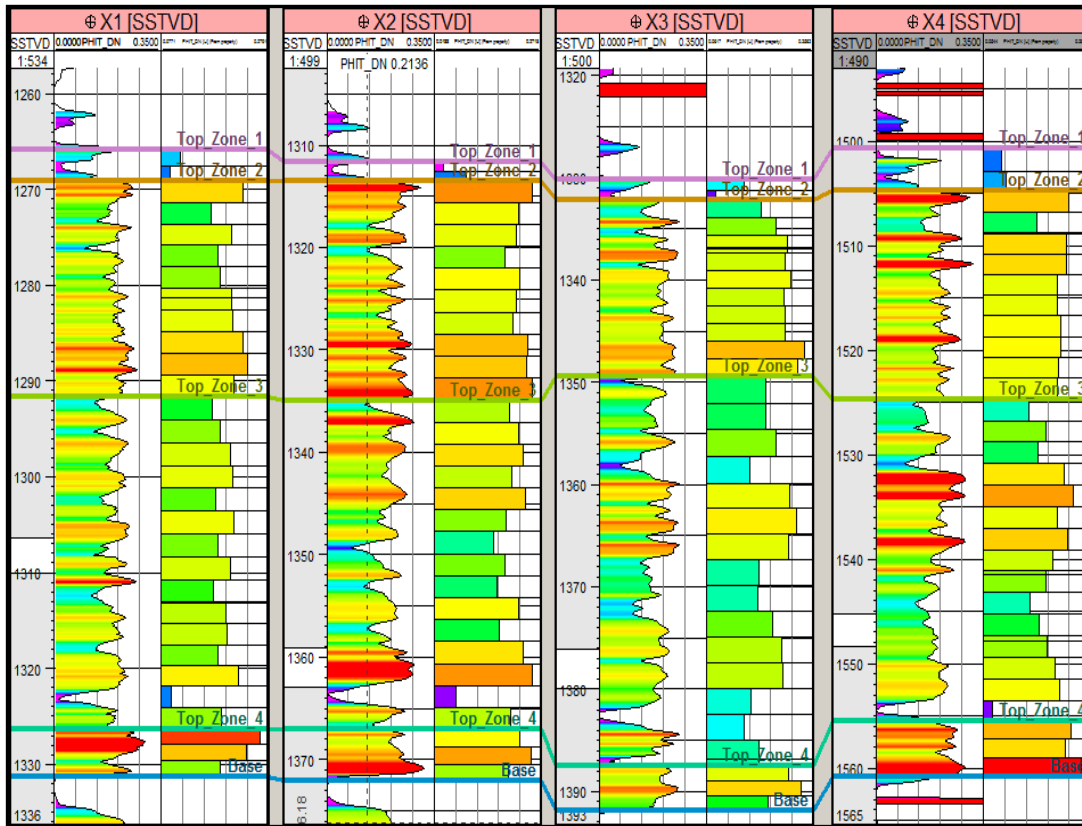


Figure 4.18: Up-scaled porosity for all wells.

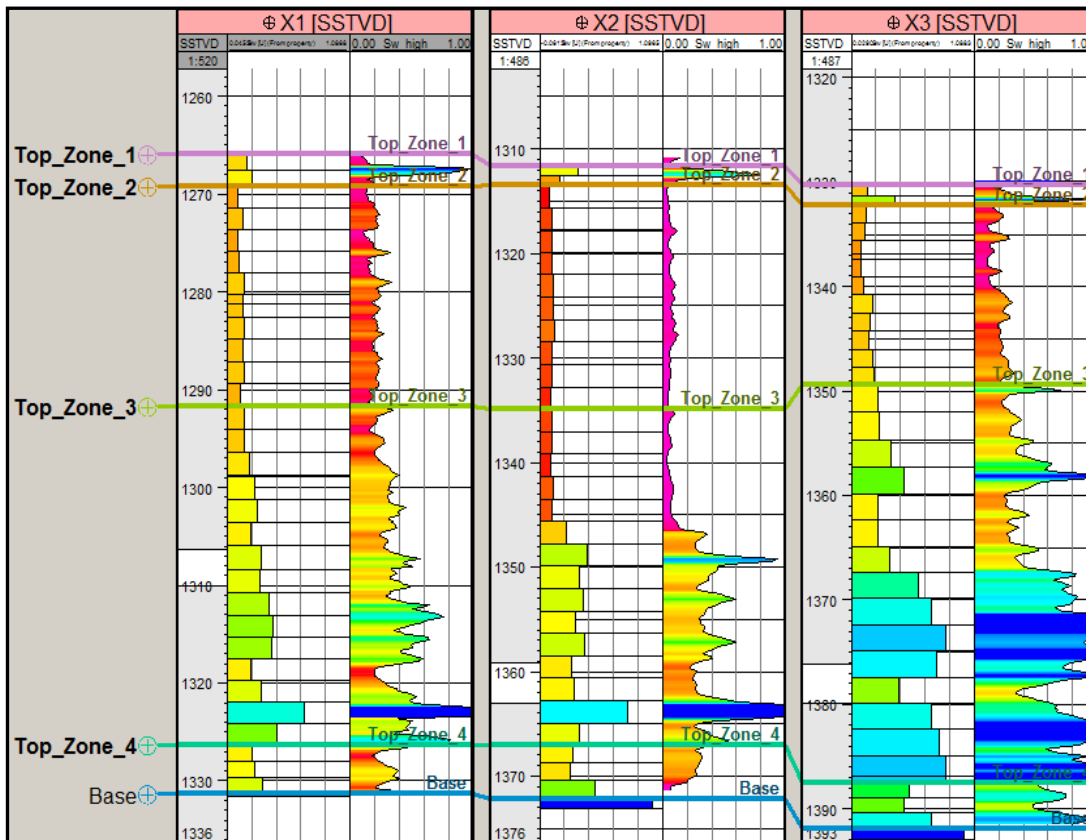
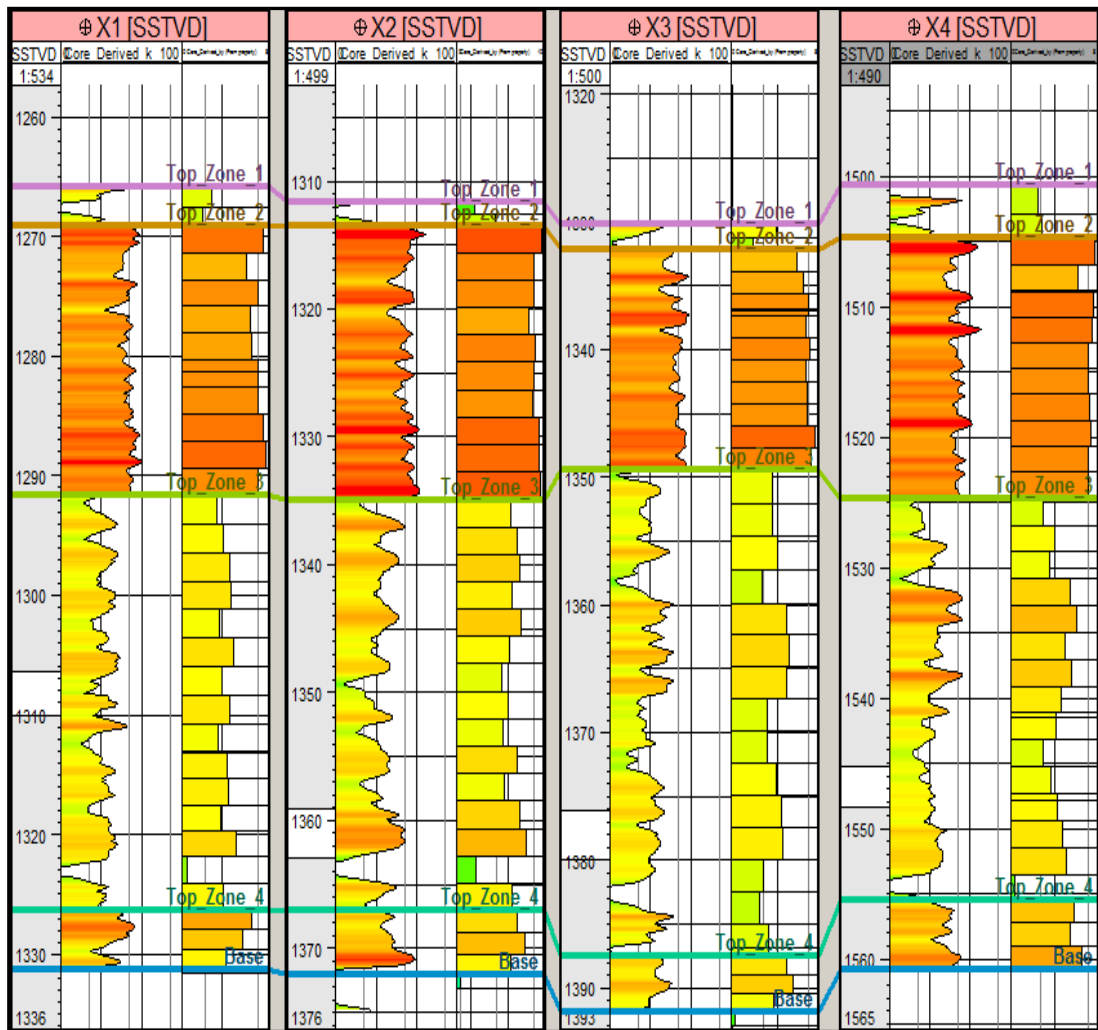


Figure 4.19: Up-scaled water saturation of X-1, X-2 and X-3.



**Figure 4.20:** Up-scaled permeability for all wells.

#### 4.4.2 Petrophysical modeling

Once the structural modeling is completed; that is one of the major steps in reservoir modeling, the next step is populating created cells with the reservoir properties. This property can be discrete data such as facies or continuous petrophysical data such as porosity, permeability, water saturation etc. Distribution of continuous petrophysical properties such as porosity, permeability and water saturation into the 3D model can be done by using an assortment of stochastic and deterministic algorithms. Geostatistical simulation is well accepted in the petroleum industry as a method for characterizing heterogeneous reservoirs stochastically. One of the most commonly used forms of geostatistical simulation for reservoir modeling is the sequential Gaussian simulation (SGS) for continuous variables like porosity. In this study, SGS (Caers 2005 and Remy et al. 2009) method was used for property distribution through the field.

Main inputs for controlling the simulation algorithm is existing well data. However, well data need to be evaluated and used every possible aspect. Any kind of statistical information of each well data that exist can play a major role in controlling the simulation algorithm. Besides, finding out the spatial characteristics of the data (how do they vary in space, is the variation smooth or sudden, is there any anisotropy in the data i.e. variation specific to any direction, is the distribution of data showing some patterns”) is also playing a very important role in controlling the simulation.

A variogram (more-precisely, semi-variogram) is a function for describing spatial variation of a reservoir property. It is based on the principle that closely spaced samples are likely to have a greater correlation than those located far from one another, and that beyond a certain point a minimum correlation is reached and the distance is no longer important (Kelkar and Perez 2002).

To be able to describe the spatial relationship of the data points, some parameters need to be supplied and are listed below:

- Variogram model type: Exponential, Spherical or Gaussian
- Nugget: Degree of dissimilarity at zero distance (experimental error).
- Sill: A unit Sill=1 is used in Petrel, i.e. the variogram is scale independent
- Range: This is the distance within which data can be correlated. Large range means greater continuity, Small range means less continuity. The larger the range the smaller the heterogeneity
  - Minor range: Defines the minor influence range, i.e. the range perpendicular to the azimuth
  - Major range: Defines the major influence range, i.e. the range parallel to the azimuth
  - Vertical range: Defines the vertical influence range, i.e. the vertical continuity. The larger the range, the thicker the beds will become in Petrophysical modeling
- Azimuth: The orientation of the major horizontal direction measured clockwise from north.

To be able to make petrophysical modeling of the X-Field considered in this study, a variety of data sources have been reviewed and prepared for distribution by creating



continuous log properties and up scaling them by considering the layers and zones as discussed in the above section such as log porosity, core permeability, well test data...etc. As can be seen from the Figure 4.21, the X-Field is elongated on the North – West direction and has some (-40) degree azimuth. Considering the shape of the field, it is obvious that major direction is NW – SE and minor direction is NE – SW. As it was mentioned above major and minor range needs to be determined to build a semi-variogram model by honoring well data and spatial variation of the existing data set. To find out the best variogram model that fits the experimental data, experimental variogram for the each property is constructed from the well data (see Section 4.4.2.1 – 4.4.2.3).

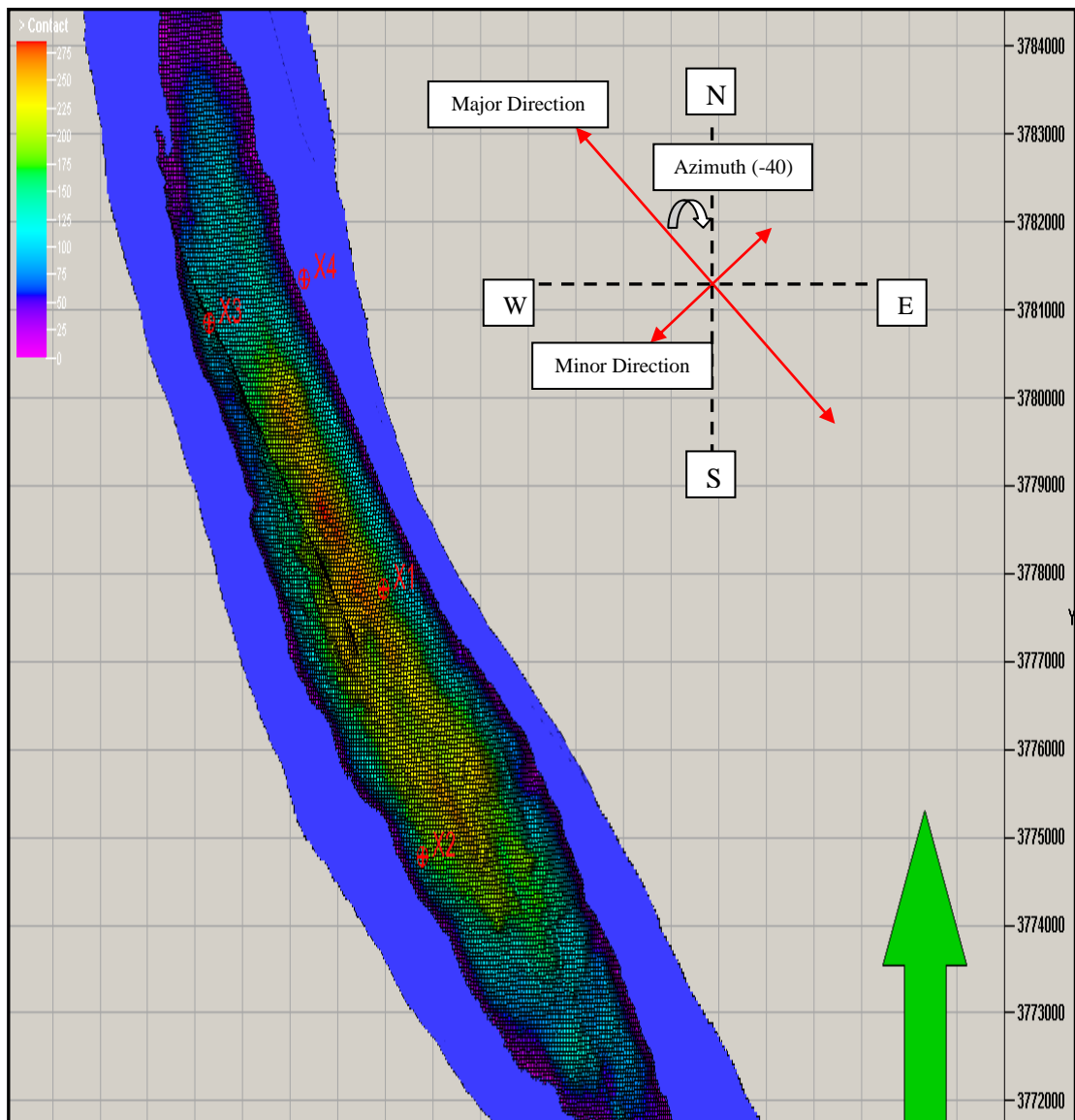


**Figure 4.21:** Orientation of the X-Field.

#### 4.4.2.1 Porosity distribution

The last step before making hydrocarbon volume calculation of the reservoir is distribution of the reservoir properties throughout the field. In this study well data are the only data source that was used for variogram modeling and considering the distance between the wells in the major and minor direction, major range is expected to be in the range of 2000 m - 4000 m while the minor range is expected to be in the range of 1000 m – 2000 m. Figures 4.22 - 4.24 show the experimental variogram and the match obtained with the chosen variogram model in the major, minor and vertical direction, respectively. Blue colored line and squares are the model data and the gray colored line and squares are the experimental data. As can be seen from the Figures 4.22 – 4.24, best fit was obtained with spherical type of variogram. Nugget effect was not considered and the ranges are found as 3126.2 m, 2174.8 m and 2.2 m in the major, minor and vertical direction, respectively.

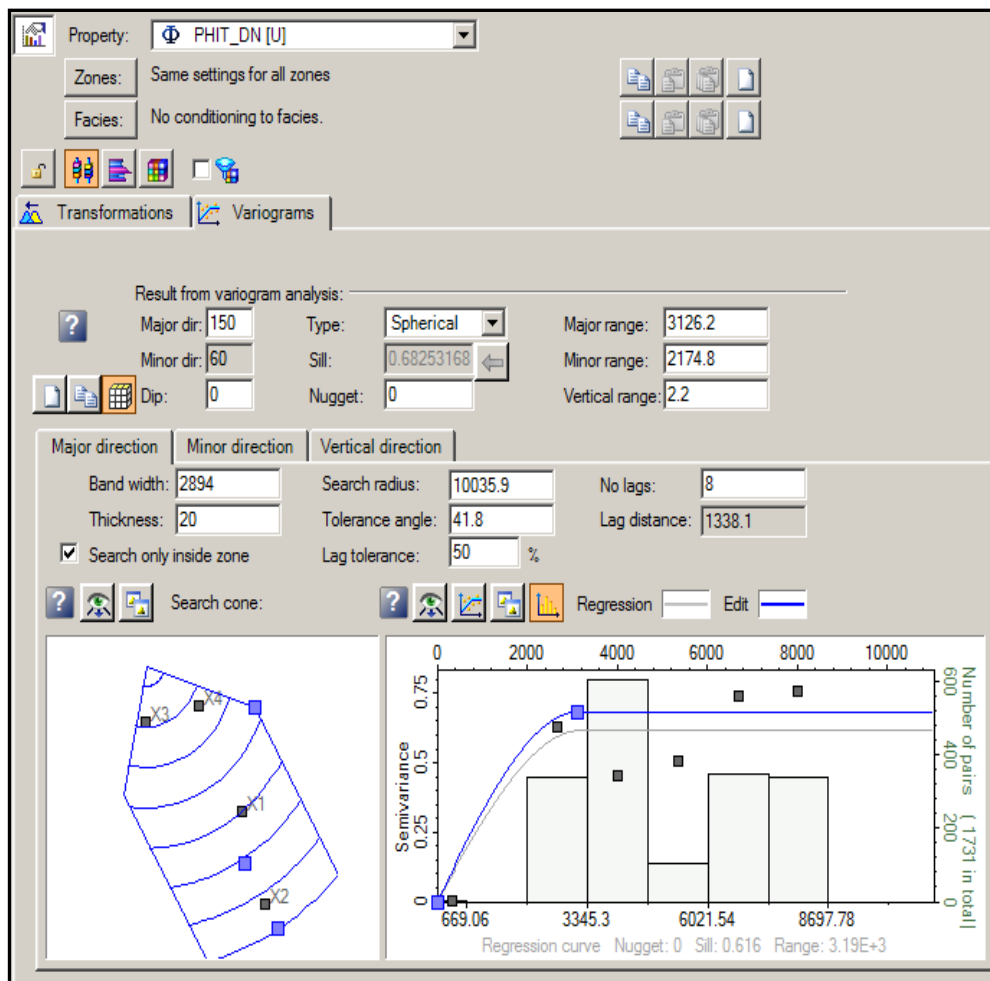


Figure 4.22: Variogram model for porosity – major direction.

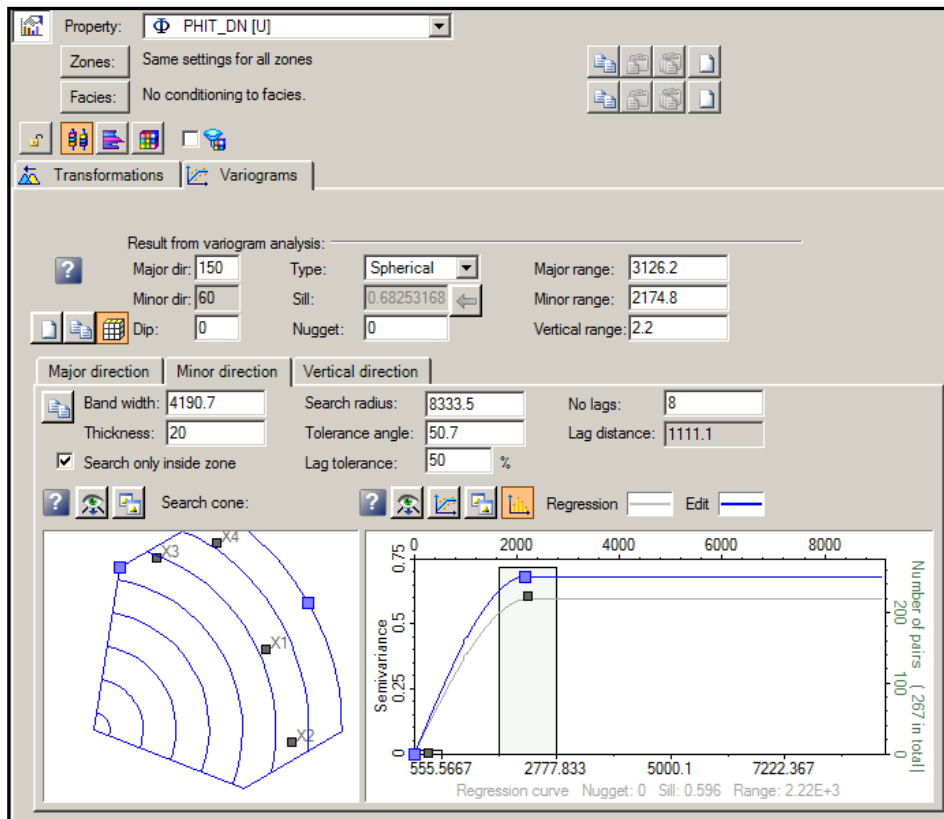


Figure 4.23: Variogram model for porosity – minor direction.

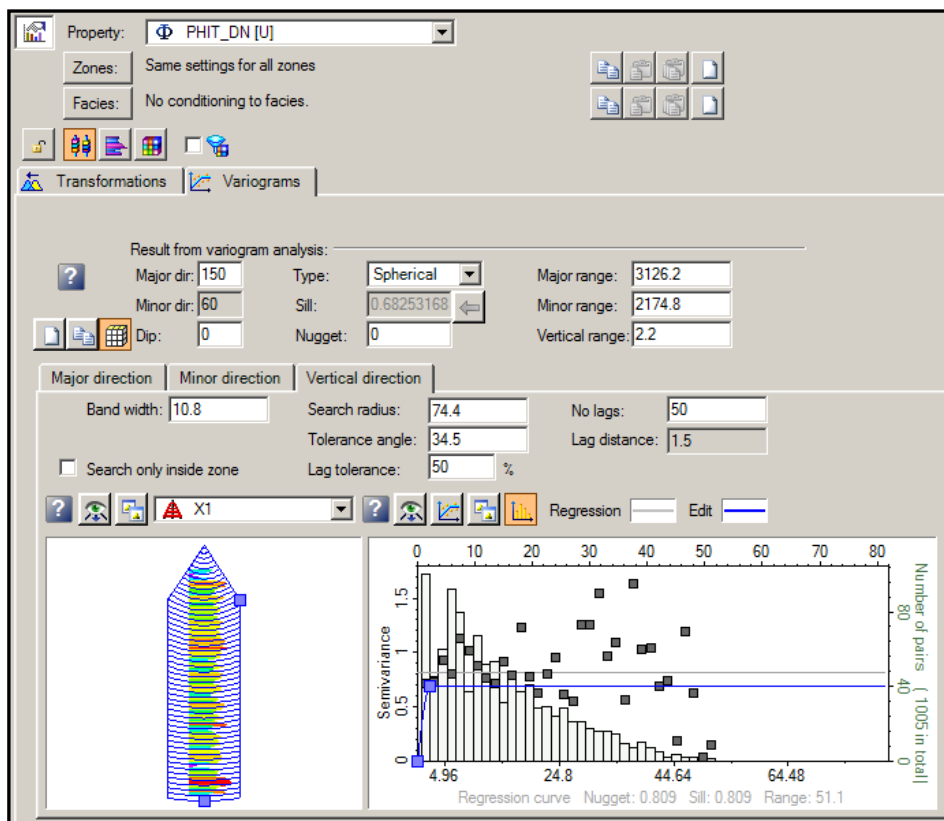
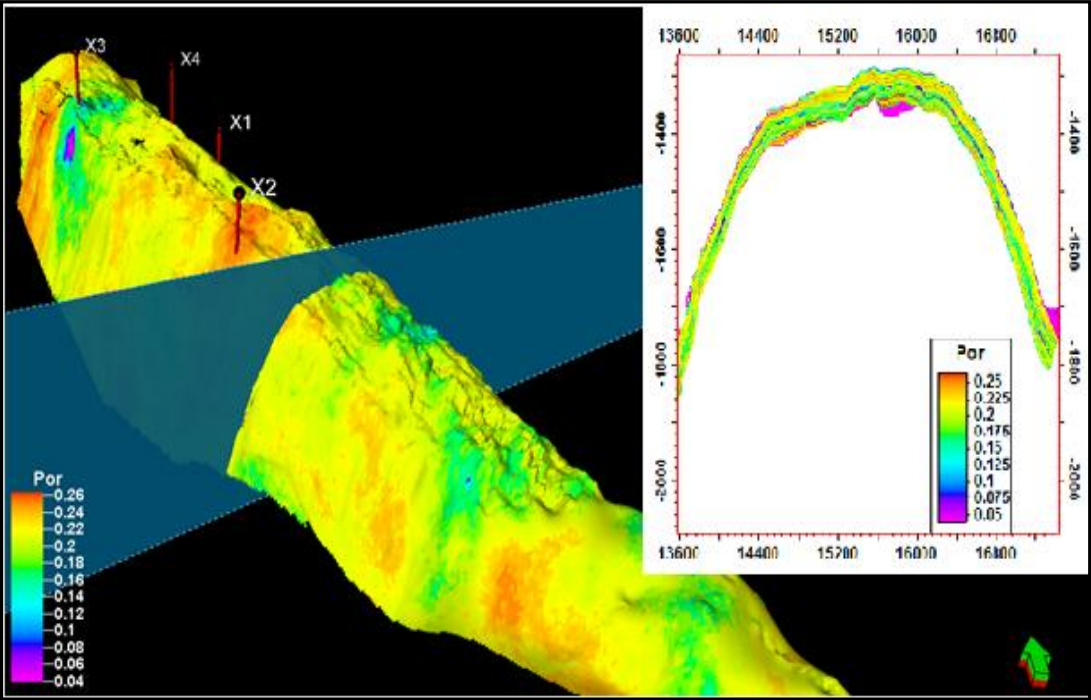


Figure 4.24: Variogram model for porosity – vertical direction.

As it was discussed in the above section 4.4.2, SGS was used for all property distribution by using the variogram model that gives the best fits with experimental data. A 3D and cross sectional views of the obtained porosity distribution model are shown in Figure 4.25. On the other hand statistical information of the porosity distribution is given in Table 4.7. It is important to note that mean value of the original well log (0.1946 %), scaled up well log (0.1933 %) and distributed property (0.1913 %) is almost the same which is proving the successful property distribution as the mean is preserved. Additionally, histogram of the obtained porosity model is given in Figure 4.26. In Figure 4.26, well log porosity is shown in red colored bar, while the up scaled one and property models are shown in green colored bar, and blue colored bar respectively. As can be noticed from the Figure 4.26, porosity histogram is negatively skewed due to having relatively low porosity intervals (Zone1, 2-4 m) at the top of the formation.



**Figure 4.25:** Porosity distribution 3D- cross sectional view.

**Table 4.7:** Statistical information of porosity distribution.

Name	Min	Max	Mean	Std
Property	0.0399	0.2645	0.1913	0.0439
Upscaled	0.0399	0.2645	0.1933	0.042
Well logs	0	0.3176	0.1946	0.0535

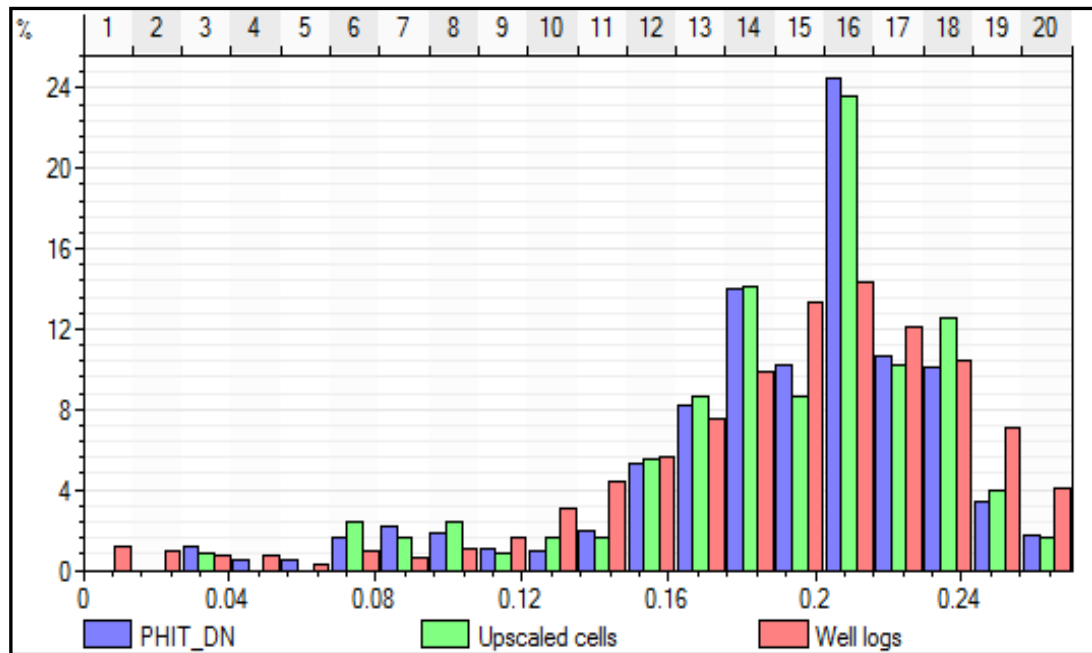


**Figure 4.26:** Porosity distribution histogram.

#### 4.4.2.2 Water saturation distribution

The same methodology with the porosity modeling, applied in the water saturation property modeling. Figures 4.27 - 4.29 shows the experimental variogram and obtained match with chosen variogram model in the major, minor and vertical direction, respectively. Blue colored line and squares are the model data and the gray colored line and squares are the experimental data. As can be seen from the Figures 4.27 – 4.29, best fit was obtained with spherical type of variogram. Nugget effect was not considered and the ranges are found as 7129.2m, 542.4m and 25.7m in the major, minor and vertical direction, respectively. It is important to note that well X-4 data was not used either in variogram modeling or petrophysical property distribution. As it was previously mentioned, well X-4 is water leg well and the well-log water saturation readings are almost unity. Therefore, if this well is used for property modeling, it will change the statistics of the water saturation. For instance, it will increase mean value of water saturation. We are trying the preserve the mean value of the property while making property modeling. Therefore, if the well X-4 is used for property modeling, it will miss lead the water saturation distribution. Additionally, also note that after completion of property modeling of water saturation, the cells below GWC will be filled full of water before starting simulation activities.

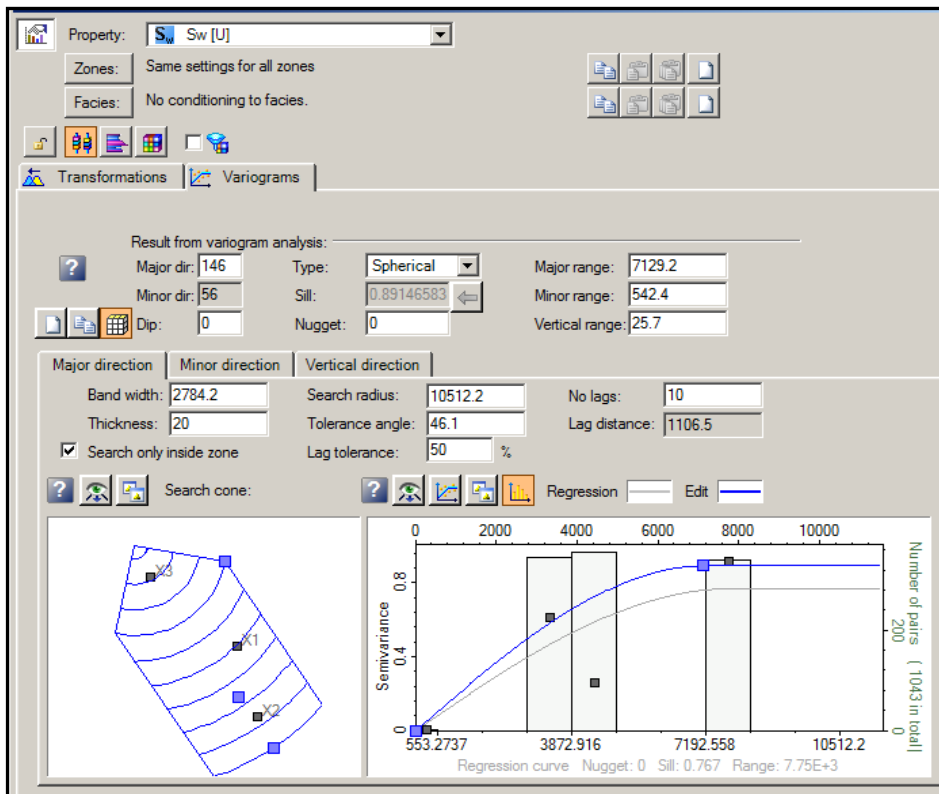


Figure 4.27: Variogram model for water saturation – major direction.

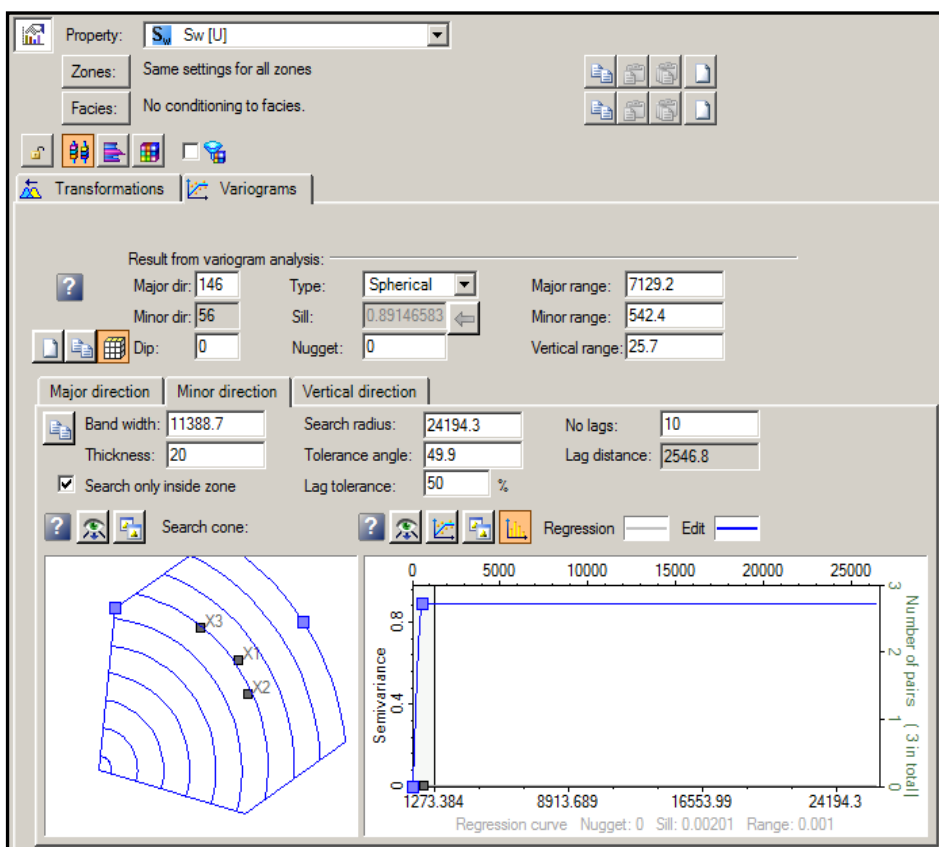
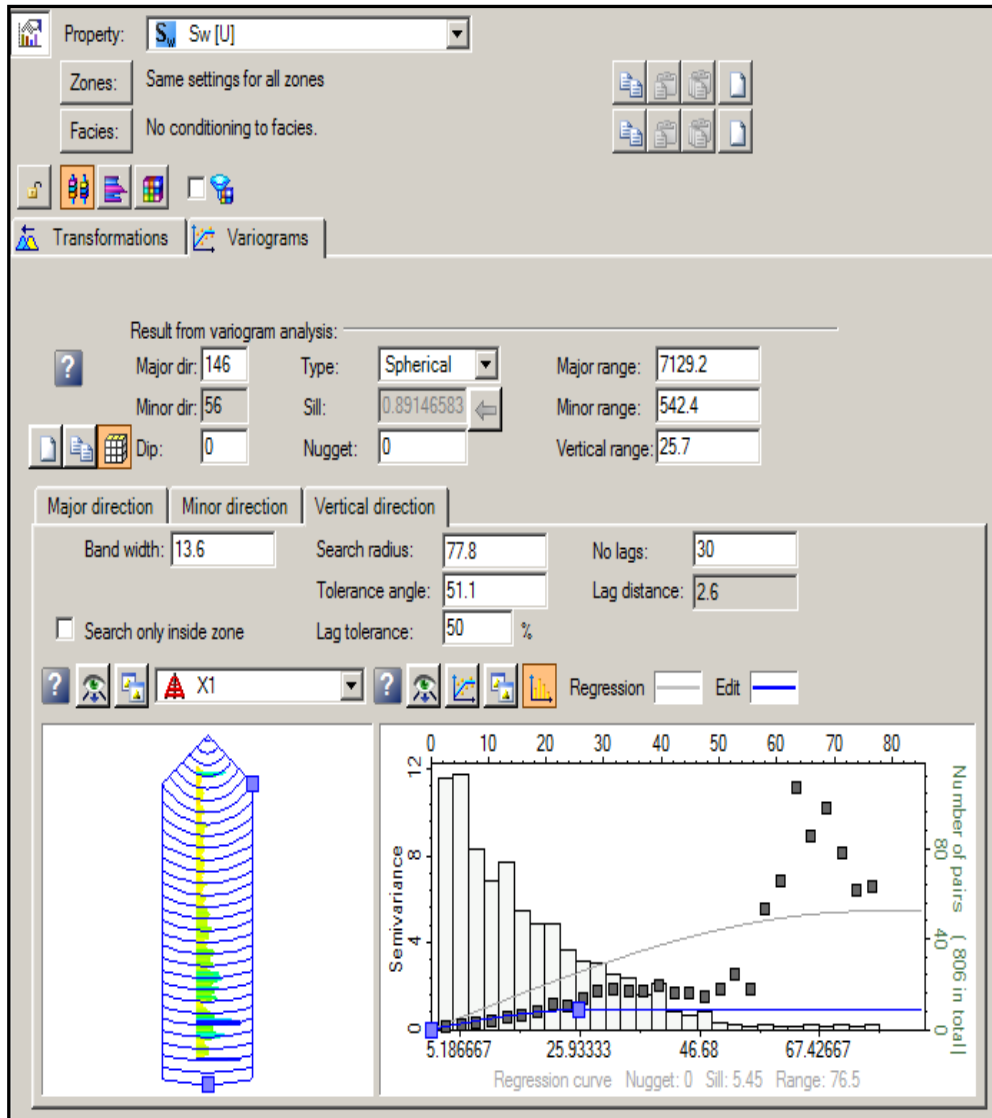
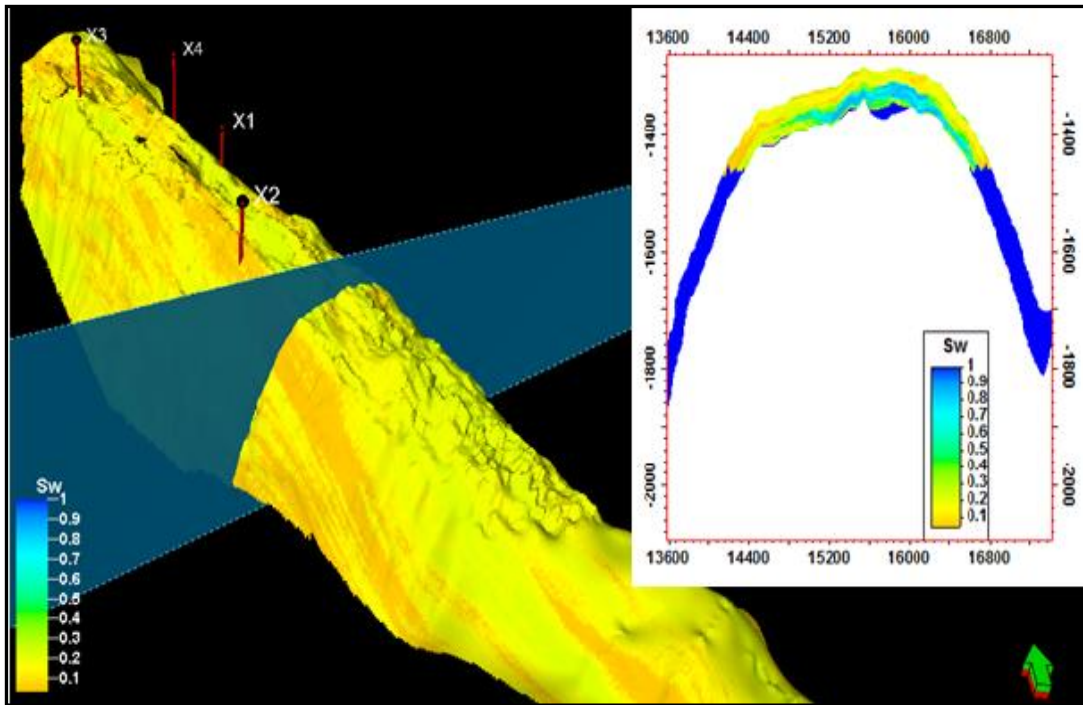


Figure 4.28: Variogram model for water saturation – minor direction.



**Figure 4.29:** Variogram model for water saturation – vertical direction.

A 3D view and cross sectional view of the obtained water saturation distribution model is shown in Figure 4.30. On the other hand statistical information of the water saturation distribution is given in table 4.8. It is important to note that mean value of the original well log (0.2929 %), scaled up well log (0.2983 %) and distributed property (0.2986 %) is almost the same which is proving the successful property distribution as the mean value is preserved. Additionally, histogram of the obtained water saturation model is given in Figure 4.31. In Figure 4.31, the well log water saturation is shown in red colored bar, while the up-scaled one and property model is shown in green colored bar and blue colored bar respectively. As can be noticed from the Figure 4.31, water saturation histogram is positively skewed due to having relatively high water saturation intervals (Zone3, 3-5 m) at the end of the zone.



**Figure 4.30:** Water saturation distribution 3D – cross sectional view.

**Table 4.8:** Statistical information of water saturation distribution

Name	Min	Max	Mean	Std
Property	0.0349	1	0.2986	0.2189
Upscaled	0.0349	1	0.2983	0.2360
Well logs	0.0264	1	0.2929	0.2311

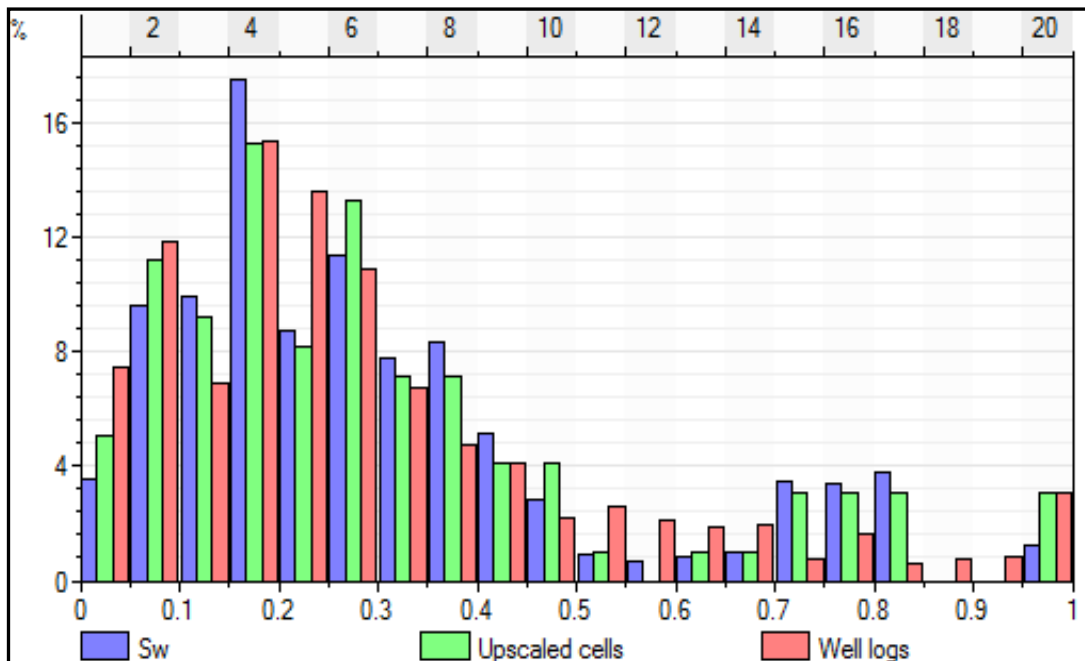


**Figure 4.31:** Water saturation distribution histogram.



#### 4.4.2.3 Permeability distribution

The same methodology with the porosity and water saturation modeling, applied in the permeability property modeling. Figures 4.32 - 4.34 shows the experimental variogram and obtained match with chosen variogram model in the major, minor and vertical direction, respectively. Blue colored line and squares are the model data and the gray colored line and squares are the experimental data. As can be seen from the Figures 4.32 – 4.34, best fit was obtained with spherical type of variogram. Nugget effect was not considered and the ranges are found as 3014.4m, 2229.6m and 8.8m in the major, minor and vertical direction, respectively. Note that we assumed that permeability is isotropic in the X and Y direction and permeability on the Z direction is equal to the half of the permeability on the X and Y direction. Shown variogram models in the Figures 4.32-4.34 is the variogram model that constructed for permeability-X. Then, permeability distribution was made based on determined variogram model for permeability-X. Once the permeability distribution is made for permeability-X, same property model assigned for permeability-Y. On the other hand, permeability-X model multiplied by 0.5 to obtain the permeability-Z model by using the property calculator in PETREL. As it was previously mentioned, there is no robust data for modeling permeability-Z. Therefore, vertical permeability is made based on the given assumption as permeability-Z is equal to half of the permeability-X. On the other hand, 3D and cross sectional views of property distribution for each permeability model (permeability-X; permeability-Y, and permeability-Z) are shown in Figures 4.35-4.37, respectively.

Recall that as previously discussed, distributed permeability values are less than PTA derived permeability values. Therefore, obtained permeability models will be multiplied by constant 4, to be able to match with PTA interpreted permeability. Then, obtained model will be calibrated with the production test data by matching the pressures data obtained from the production test and pressures of the constructed simulation model. After checking the simulation model pressure matches with the observed data, permeability model will be calibrated by changing the permeability multiplier accordingly. Then, the uncertainty on the constructed permeability model can be reduced by the appraisal data which will be available in the later stage of the project.



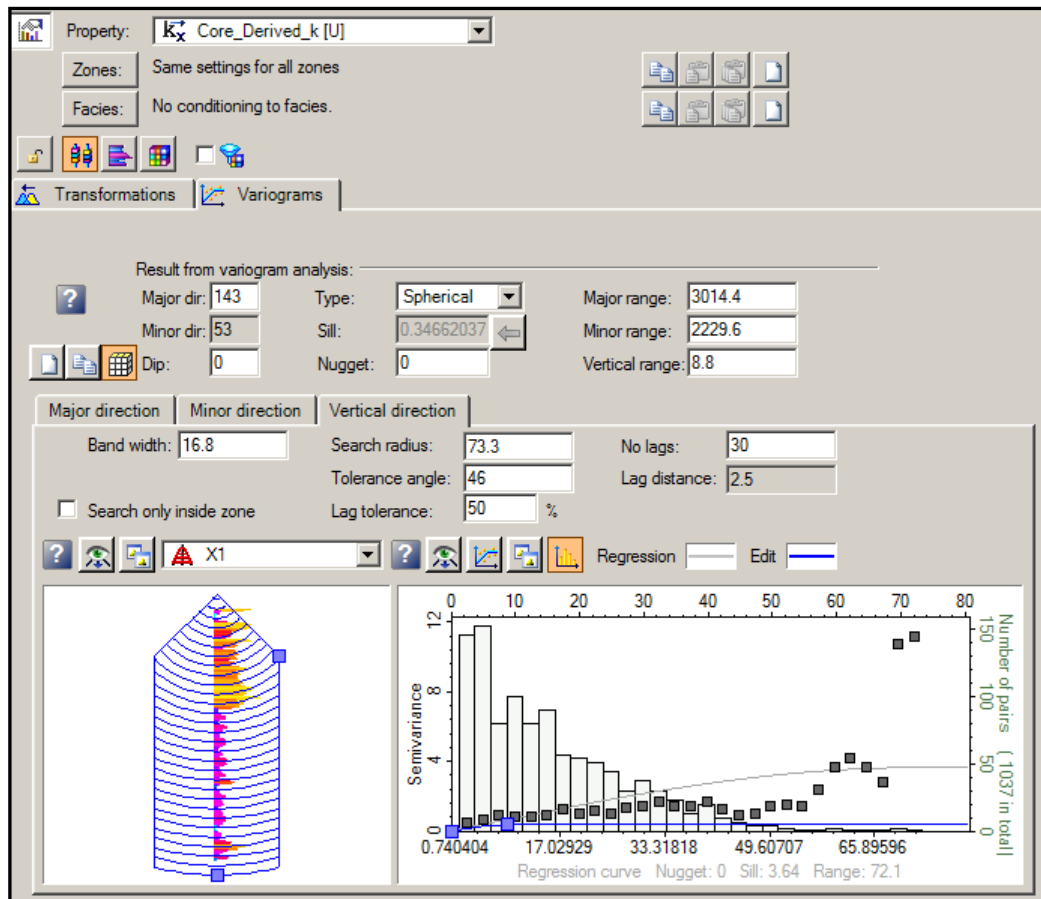


**Figure 4.34:** Variogram model for permeability – minor direction.

A 3D view and cross sectional view of the obtained permeability distribution models are shown in Figures 4.35-4.37 for the permeability X, Y, and Z, respectively. On the other hand statistical information of the permeability X, Y, and Z distributions are given in Table 4.9. There is no statistical information given for the well-log and up-scaled permeability for the distribution of permeability Y and Z because permeability distributions of Y and Z were made by property calculator in PETREL based on permeability-X distribution. It is important to note that mean value of the original well log (3 md), scaled up well log (3 md) and distributed property (3 md) for permeability-X is same which is proving the successful property distribution. Additionally, histograms of the obtained permeability models are given in Figure 4.38-4.40. In Figures 4.38, well log is shown in red colored bar, while up scaled well log and property model are shown in green colored bar and blue colored bar respectively. Besides, in Figures 4.39-4.40, distributed property (permeability) is shown in blue colored bars. Also note that, while making permeability distribution, logarithmic distribution option was used in PETREL.

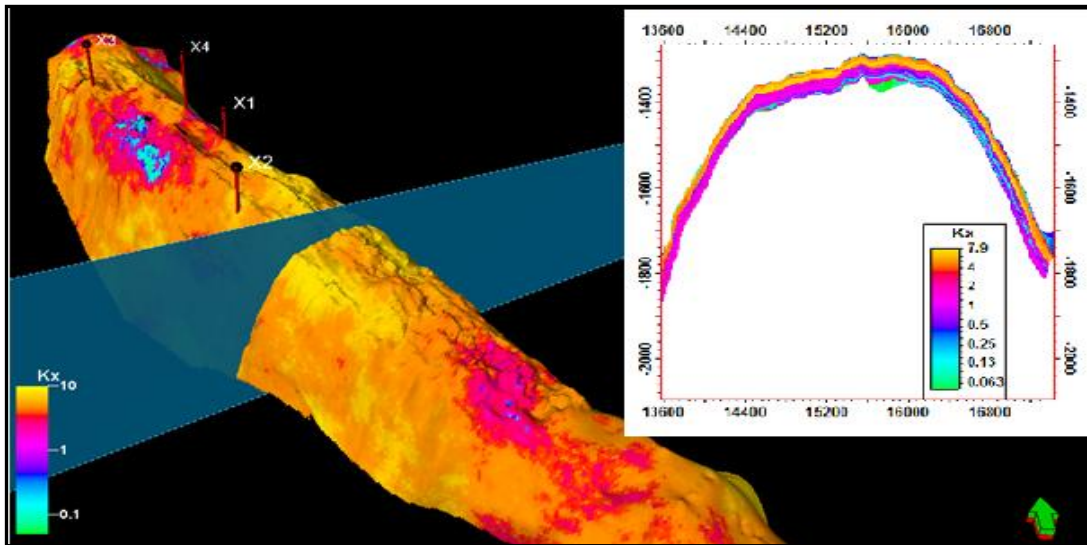


Figure 4.35: Permeability-X distribution 3D – cross sectional view.

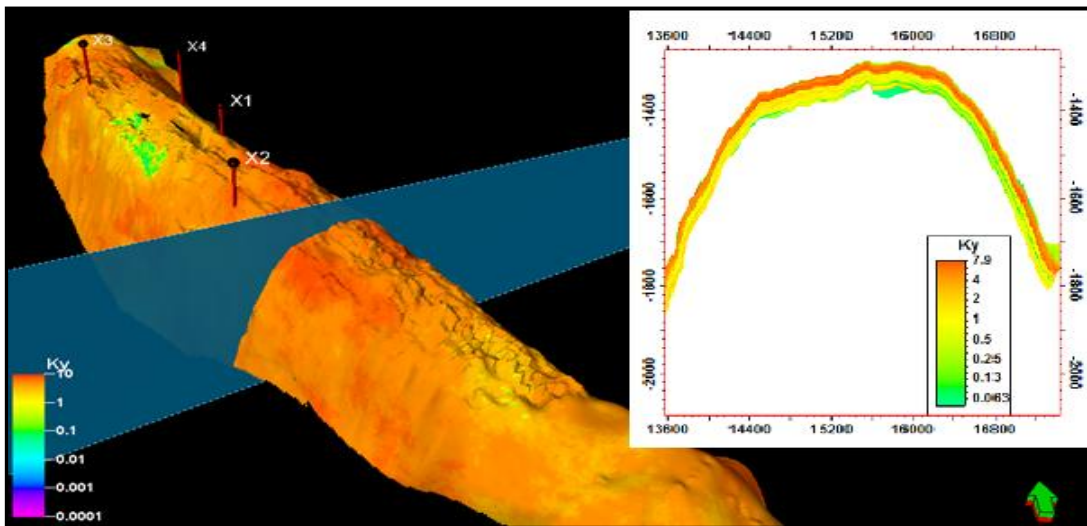


Figure 4.36: Permeability-Y distribution 3D – cross sectional view.

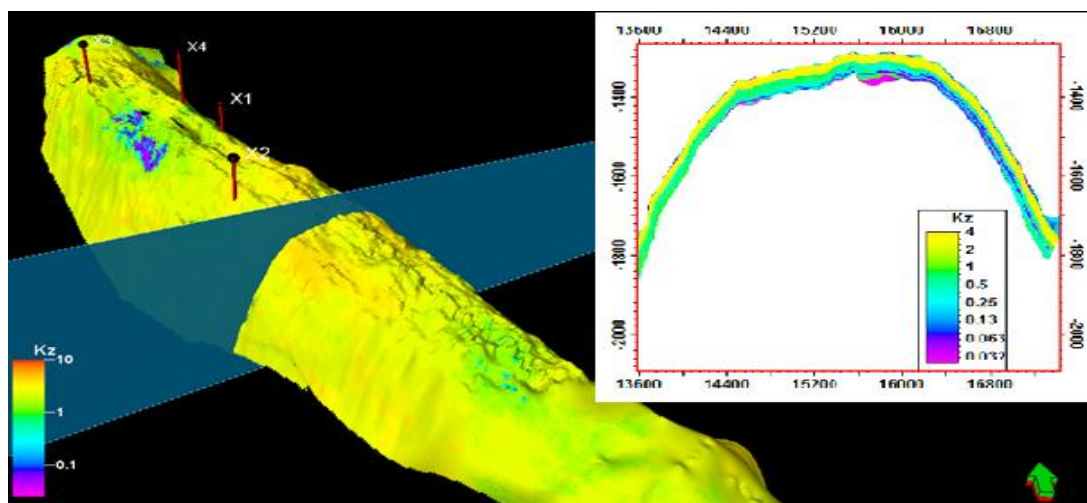
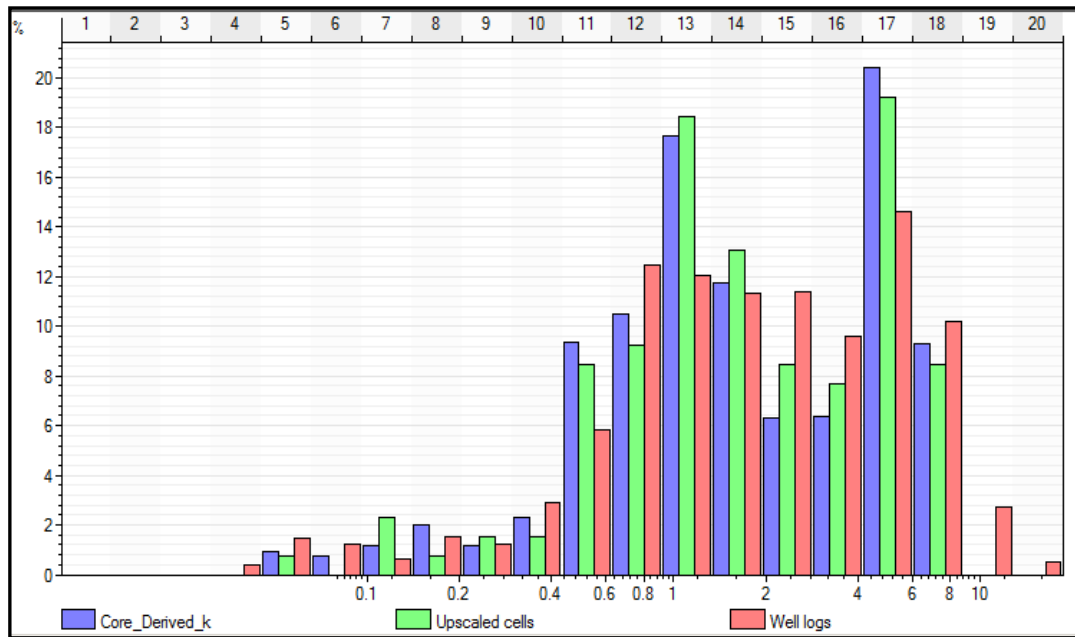


Figure 4.37: Permeability-Z distribution 3D – cross sectional view.

**Table 4.9:** Statistical information of permeability X, Y, and Z distribution.

Permeability	Name	Min	Max	Mean	Std	Var
Perm-X	Property	0	8	3	2	5
Perm-X	Upscaled	0	8	3	2	4
Perm-X	Well log	0	19	3	2	6
Perm-Y	Property	0	8	3	2	5
Perm-Z	Property	0	4	1	1	1



**Figure 4.38:** Permeability-X distribution histogram.

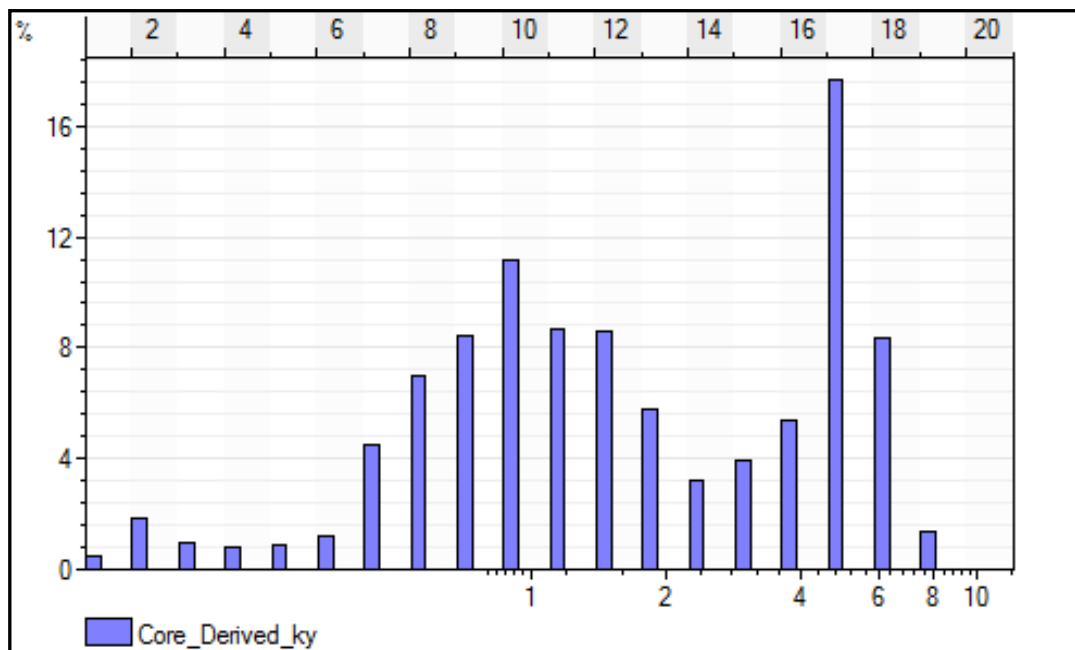


**Figure 4.39:** Permeability-Y distribution histogram.

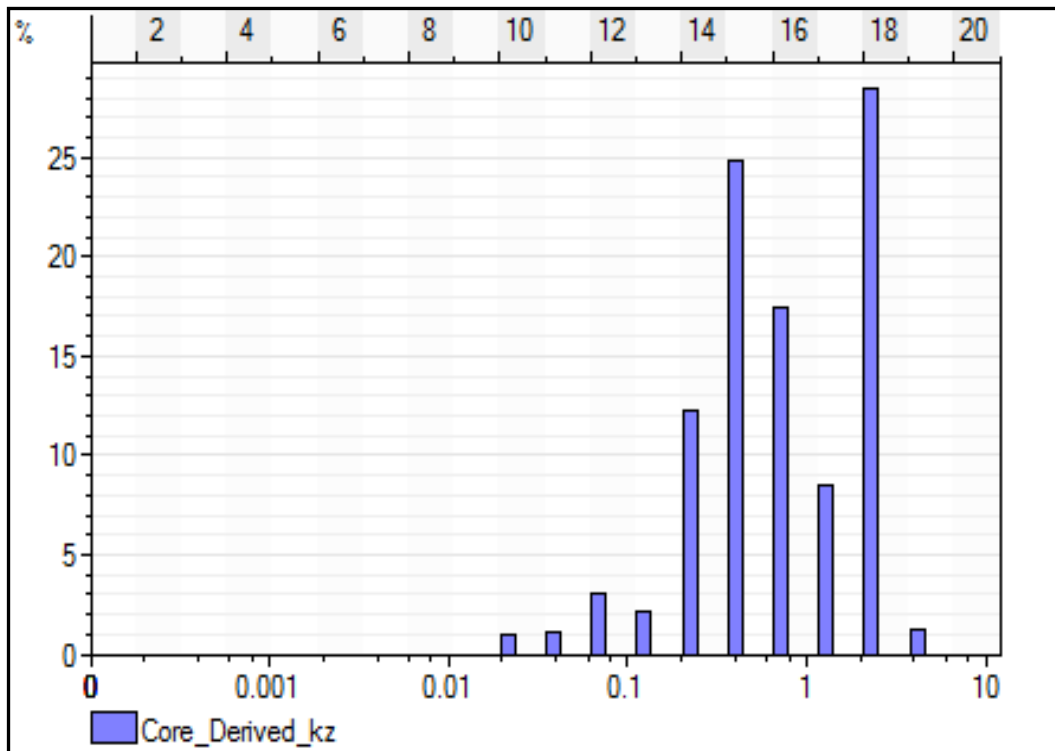


**Figure 4.40:** Permeability-Z distribution histogram.

#### 4.4.2.4 Net to gross

In petroleum industry, a net to gross (NTG) ratio is used for elimination of non-productive reservoir rock units if there is any. However, the X-Field is petrophysically clean carbonate reservoir and there is no shale barrier and/or non-productive rock intervals identified in the formation. Besides, the formation thickness is almost the same throughout the field, and there are no facies changes in the field. In addition, while making petrophysical modeling, effective porosity well logs was used and distributed to the field. Therefore, net to gross ratio was set to unity for the volume calculation due to above explained reasons.

Note that NTG can be used for deactivating the cells below any specific depths such as GWC by assigning NTG value as zero into cells which are located below GWC. In this study, to deactivate the cells below GWC, we have assigned NTG value as zero below 1460 mss where the GWC is. Thus, all the cells are deactivated below GWC by performing this operation: however, cells below GWC need to be activated again if aquifer model is required to be connected to the reservoir. Figure 4.41 is the constructed 3D and cross sectional view of NTG model. As can be seen from the Figure 4.41, NTG is assigned to zero for the cells located below GWC to deactivate the cells below contact.

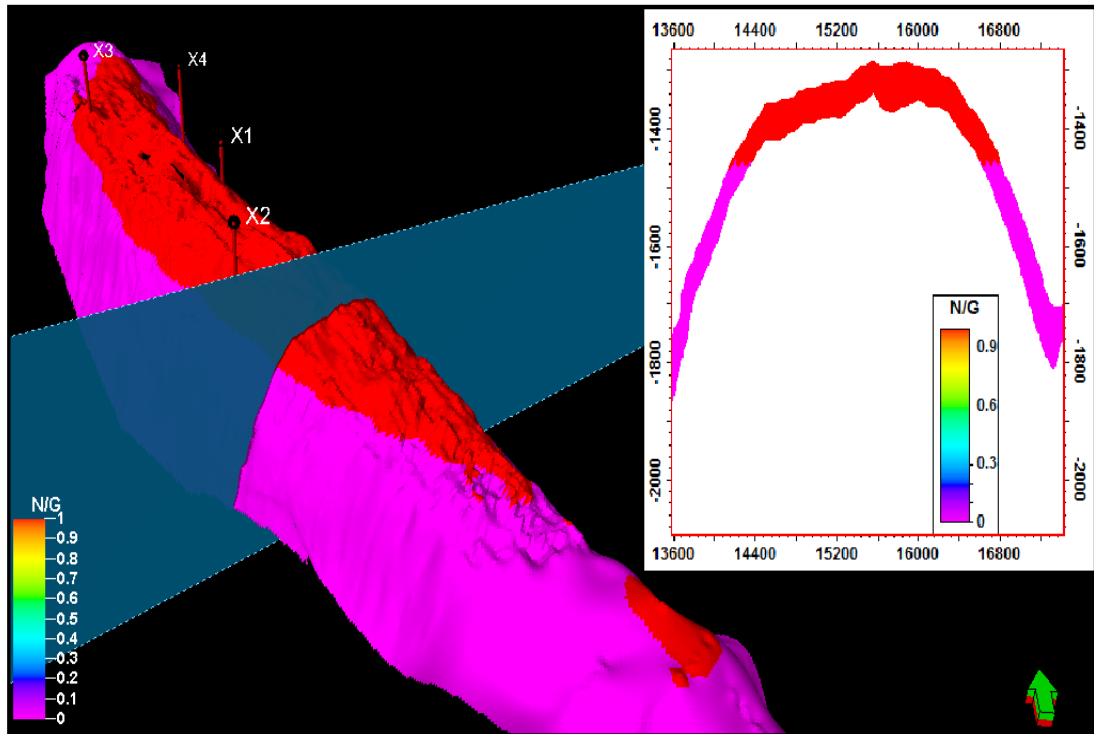


**Figure 4.41:** NTG model, 3D and cross sectional view.

#### 4.5 Volume Calculation & GIIP

The last stage of 3D geological modeling process is the calculation of the original hydrocarbon volume and assessing the associated uncertainty in the calculation. During the course of this study, variety of data was analyzed and incorporated to build an integrated geological model. The base case model defined by formation top and base map, four main zones, and 30 sub-layers, petrophysical analysis of all properties and gas water contact determination. Gas formation volume factor that was obtained from laboratory PVT analysis is used as  $0.00381679 \text{ (rm}^3\text{/sm}^3\text{)}$  to calculate hydrocarbon volume initially in place in standard conditions. Final output of the all these complex studies is the hydrocarbon in place calculation which is summarized in Table 4.10. Bulk volume, net volume, pore volume, hydrocarbon pore volume and gas initially in place (GIIP) for each zone were calculated in PETREL. As can be seen from Table 4.10, calculated GIIP is 0.0074 tcf for zone-1: 1.272 tcf for zone-2: 1.032 tcf for zone-3: 0.0308 tcf for zone-4 and totally **2.686 tcf**: however, associated uncertainty on the calculation is assessed in Section 4.6. As previously mentioned, main uncertainty on the X-Field is the GWC that is estimated as 1460 mss for the base case but it may be in between 1390 mss – 1500 mss.

**Table 4.10:** Volumetric report of base case.

Zones	Bulk volume [*10 <sup>6</sup> m <sup>3</sup> ]	Net volume [*10 <sup>6</sup> m <sup>3</sup> ]	Pore volume [*10 <sup>6</sup> m <sup>3</sup> ]	HCPV gas [*10 <sup>6</sup> m <sup>3</sup> ]	GIIP [*10 <sup>6</sup> MSCF]
Zone 1	1281	99	10	8	74
Zone 2	2977	771	164	137	1272
Zone 3	4883	1091	203	112	1032
Zone 4	714	216	48	33	308
Base Case	11501	2541	487	290	<b>2686</b>

#### 4.6 Uncertainty Analysis

Presented models and volume calculation have some uncertainty due to complexity of performed work, integration of data from different source, scale difference on the existing data and limits on the available data etc. It is very well known fact that there will be always limits on the available data and it is impossible to remove all these uncertainty but those can be reduced by additional data gathering campaign from the field. On the other hand while constructing the reservoir model many kind of data sources were used that those have some degree of uncertainty itself and those are indirect data sources such as seismic (geometry of field), well test data, core data etc. Therefore, determination the level of uncertainty on the model and calculation is one of the critical tasks in order to be able to make robust planning and predictions.

2D and high resolution 3D seismic data are available from the field; therefore, the level of uncertainty is not much on the structural model. However, as it was discussed in Section 3.6, the major uncertainty in the model is the GWC. The lowest gas reading depth (Gas Down To, GDT) from the field is 1390 mss and the highest water reading depth (Water Up To, WUP) is 1502 mss. Therefore, while running uncertainty cases, these depths were used for minimum and maximum GWC depth. Besides, +/- 5% uncertainty range was studied in the uncertainty runs. Table 4.11 gives the minimum and maximum ranges that were used while running uncertainty cases. 100 realizations were run with Monte Carlo Sampler by using the ranges given in Table 4.11 on the stochastic GIIP calculation. Probability plot of the obtained realizations is given in Figure 4.28 and P10, P50 and P90 GIIP values is given in Table 4.12. Note that SPE definitions were used while reporting the P10 and P90 GIIP values which is opposite in the statistics terminology (Etherington et al. 2005).



**Table 4.11:** Uncertainty range of the reservoir parameters.

Parameter	Min	Base Case	Max
GWC (m)	1390	1460	1500
Porosity	0.1817	0.1913	0.2008
Sw	0.2836	0.2986	0.3135
Bg	0.0036	0.00381679	0.0040

**Table 4.12:** Probabilistic GIIP range.

Probability	GIIP (bcf)
P10	3609
P50	2937
P90	2369

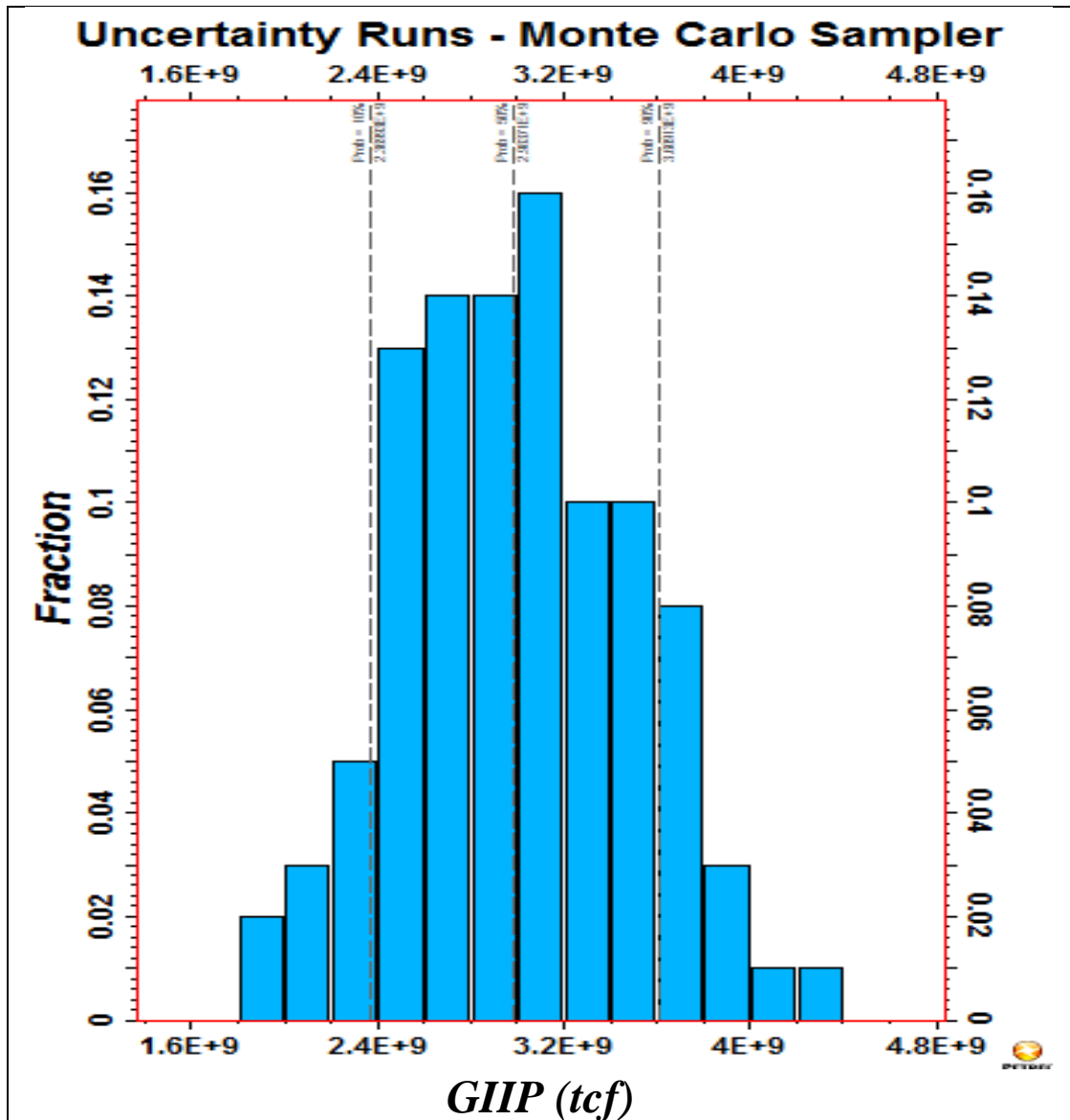


**Figure 4.42:** GIIP uncertainty.



## 5. SIMULATION MODEL

The aim of reservoir simulation model is to construct a numerical model able to simulate the dynamic behavior of reservoir and fluid flow in porous media. The main components of the reservoir simulation models are the 3D static geocellular model, fluid (Equation of State, EoS) model, rock-fluid interaction model, well model, equilibration (i.e., initial conditions) model and if exist historical production data. As previously discussed in Chapter 4, fine scale description of the reservoir was made on the basis of seismic (2D-3D seismic) and well (well-log, core, well-test) data in the 3D geological reservoir modeling suite PETREL.

Well test data are evaluated and interpreted in PTA software SAPHIR and discussed in Section 3.5. To able to start simulation, fluid model, rock-fluid interaction model, and equilibration model needs to be constructed. In this section, fluid model is constructed in PVTi which is an EoS based software for generating PVT data to simulators from the laboratory analysis of oil and gas samples. (PVTi, 2011). Then, rock-fluid interaction model is constructed in PETREL based on Corey correlation and saturation end-point data from cores (Brooks and Corey 1966).

Final step before starting simulation is to define initial conditions (equilibration) based on fluid contact and well-test pressure data which will be made in PETREL as well.

Considering the reservoir is gas condensate, ECLIPSE 300 compositional reservoir simulator (ECLIPSE, 2011) is used for performing all the simulation studies in the field that presented herein.

There is no historical production data available from the field; therefore, it is impossible to perform history matching activities to calibrate the constructed simulation model. However, once the field starts producing and production data gathered from the field, constructed geological model and simulation model can be calibrated accordingly.

## 5.1. Upscaling Fine Scale Geological Model

Geological reservoir models are generally constructed by using geostatistical approaches based on well data from the different scales, as discussed before. To be able to describe the reservoir characteristics in detail while creating a 3D geological model, size of the created grids has to be very small to preserve the small features from well logs and seismic data as much as possible. These grids are designed to preserve the heterogeneity of the reservoir by typically subdividing it on a fine scale vertically, as well as keeping the XY-representation of the grid cells as small as possible. A geological grid often has millions of cells. The number of grids in geological model is often exceeding the capabilities of standard reservoir simulators and requires huge computational powers to run. Therefore, reservoir descriptions made by fine scale geocellular model has to be coarsen (up-scale) to the scales that are suitable for flow simulation (Darman et al. 2002; Durlofsky et al. 1999; Arbogas et al. 2001). However, although up scaling the geological reservoir model is an inevitable step for the reservoir simulation considering the computational power of regular computers, recent technological development allows running such a big reservoir models with a parallel computing systems which was not available on hand in the course of this study.

As discussed in Chapter 4, generated geological model of Field-X has more than eight million cells (50m x 50m in X-Y direction). Considering the computational capability of computer that is used for this study, the geological model has to be up scaled so that the computer used for this study can be used. Before making any up scaling in the model, the cells below GWC were deactivated by assigning zero NTG to the cells below GWC as shown in Figure 5.1, but it reduced the active cell numbers to approximately 1.95 million cells which is still exceeding the computational power of the computer. Therefore, up scaling was performed either in cell size in the X-Y direction or in layering (vertical resolution) of the model. No optimization study was performed while deciding the optimum cell size and number of layers that should be in the up scaled model due to time constraints of the study. However, representation of the reservoir characteristics in the up scaled model is carefully examined with the fine scale model.

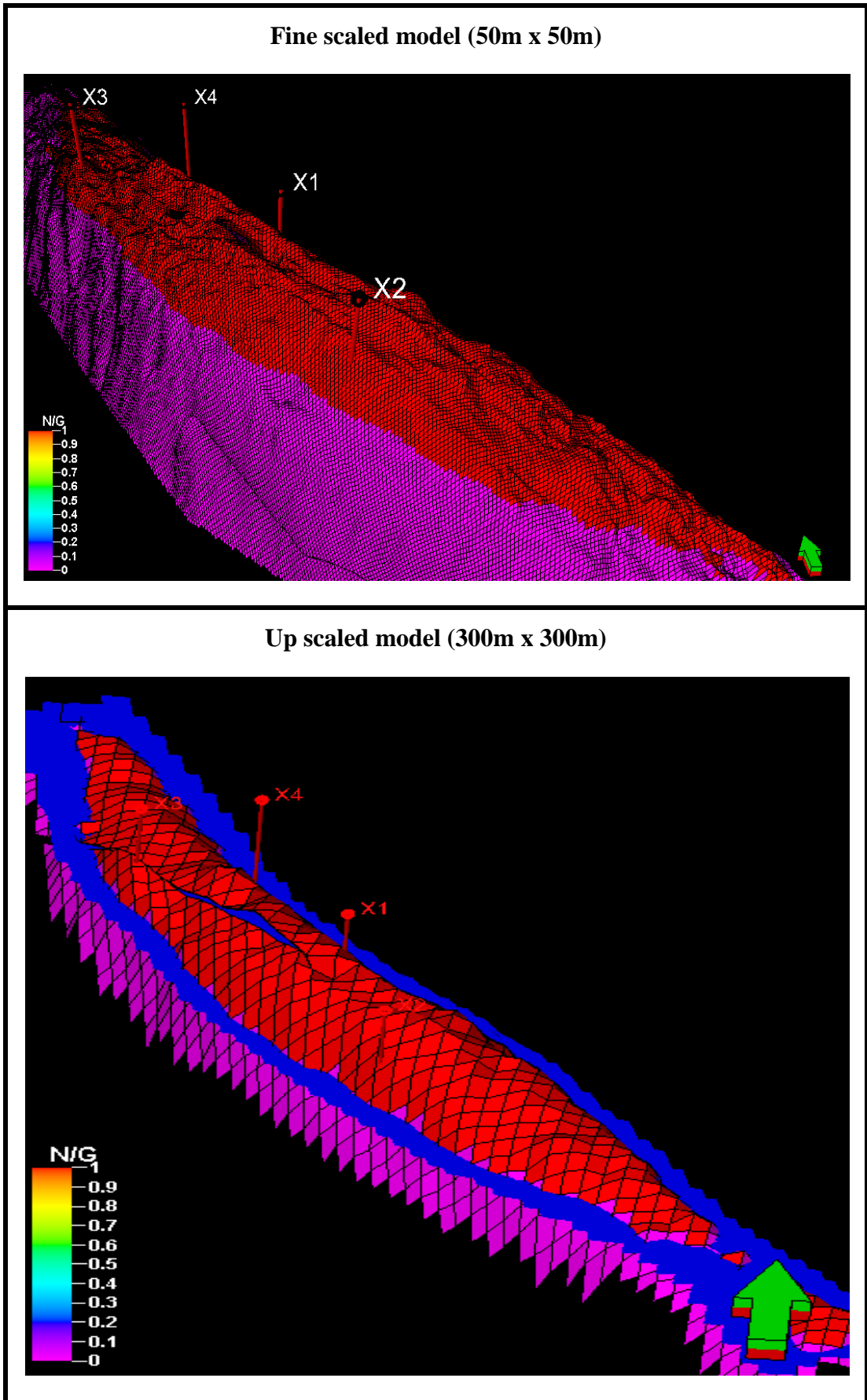


**Figure 5.1:** 3D view of NTG - fine scaled model (top), up scaled model (bottom).

The size of the cells in the model increased to 300 m in the X and Y direction which was 50m in the geo-cellular model. Additionally, as previously discussed, vertical resolution of the reservoir is represented with four main zones and 30 sub-layers in the geological model which is reduced to 15 layers in the up scaled model. Figure 5.2 is showing the number of layers that each zone divided into. Layer thickness is in between 4-5m for each layer in the up scaled model.

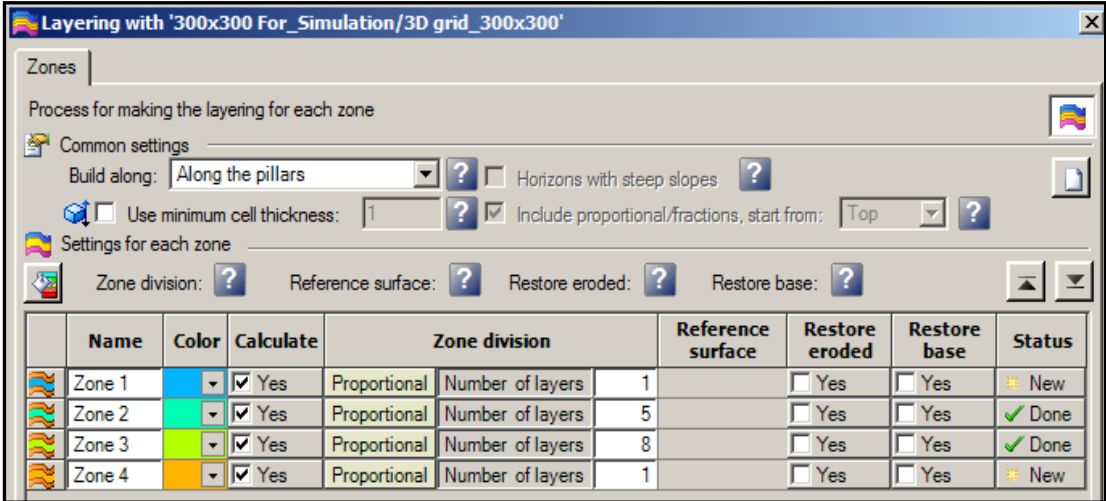


**Figure 5.2:** Layers of up scaled model.

Although, thickness of the layers are coarse, representation of reservoir features are good enough with the 15 layers, as can be seen in Figures 5.3-5.4. In Figure 5.3, the original well-log (no up scaling) porosity is shown by black lines for the each well and up scaled model porosity is shown by colored bars. Similarly, in Figure 5.4, the original well-log (no up scaling) water saturation is shown by blue lines for the each well and up scaled model porosity is shown by colored bars. As can be seen from the Figures 5.3-5.4, some details on the well-log porosity and water saturation are lost due to up scaling the model but it can be said that the reservoir properties representations with the 15 layers are good enough based on statistical information compared to fine scaled model.

Note that similar methodology which was discussed in Sections 4.4-4.5, is applied for the up scaled simulation grid while making property models and calculating reservoir volumes (GIIP). Generated property models for simulation grids are carefully reviewed and compared with fine scaled geo-cellular model properties. All of the constructed property models, comparisons figures, and statistical information are presented hereafter.

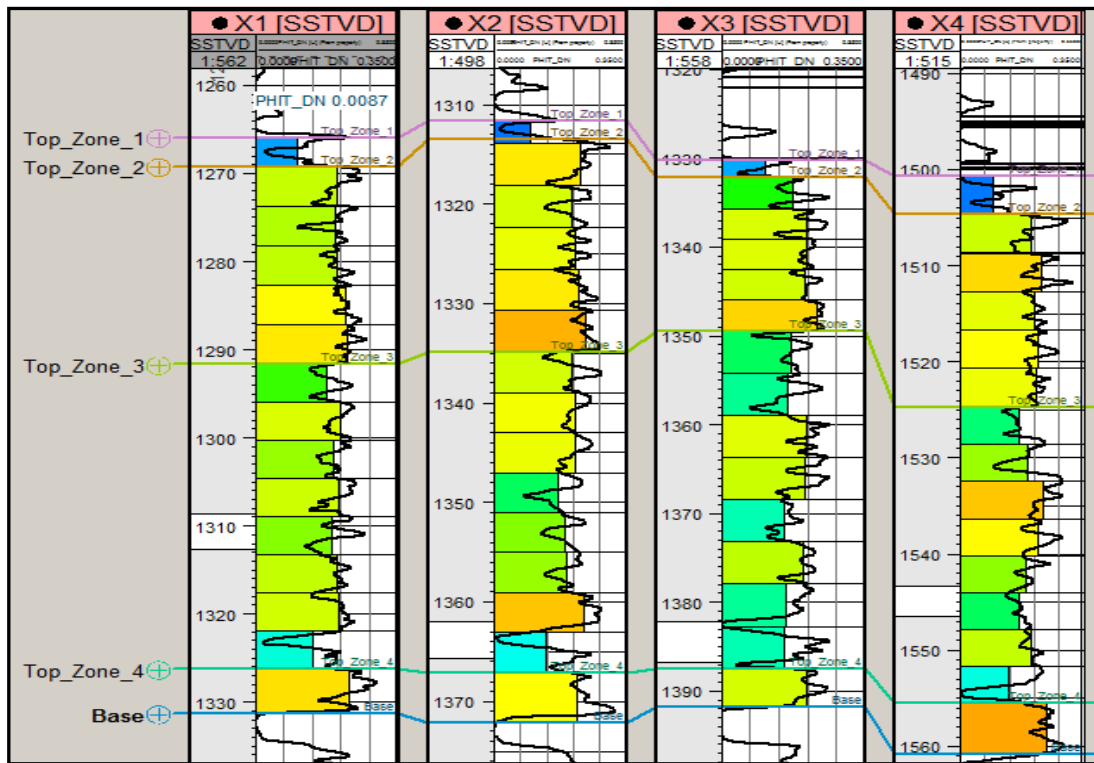


**Figure 5.3:** Original well-log porosity (black line) versus up scaled model porosity (colored bars).

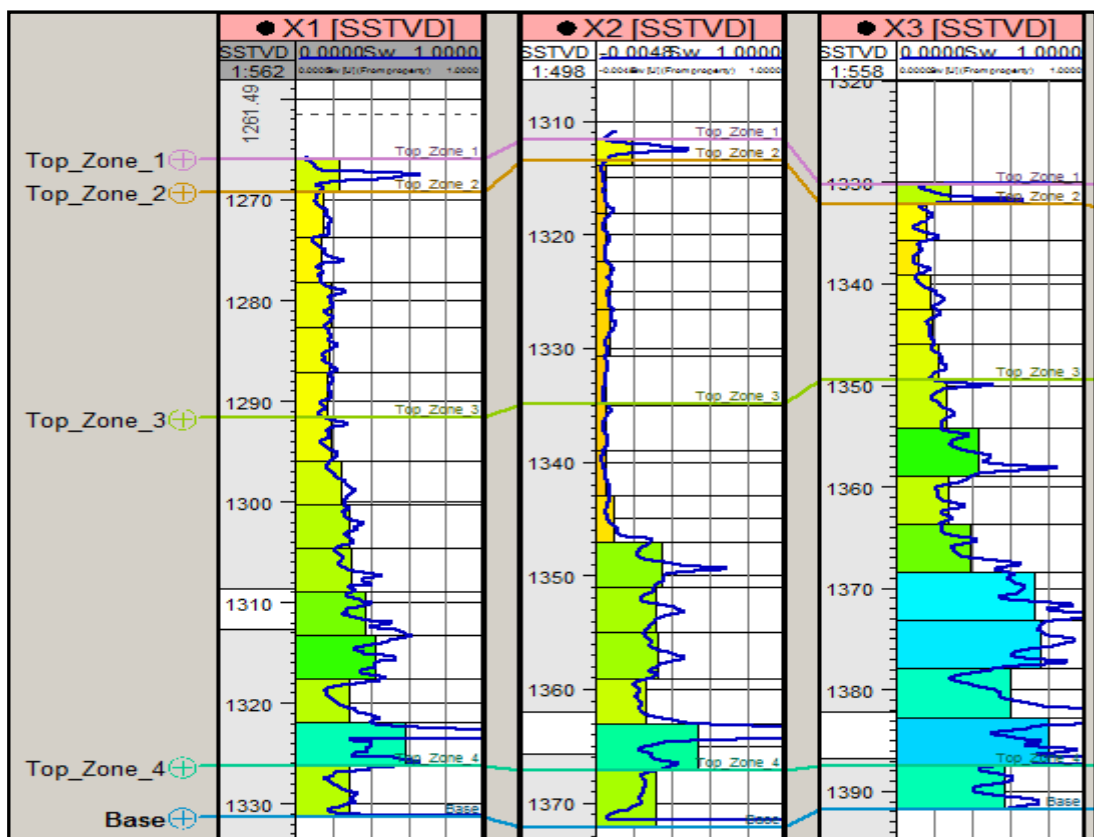


**Figure 5.4:** Original well-log water saturation (blue line) versus up scaled model water saturation (colored bars).

After generating up scaled simulation grids, the next step is populating created cells with the reservoir properties. As it was mentioned previously, similar approaches which was discussed in the Section 4.4.2, is used for populating cells with reservoir properties. Similar to the geological reservoir model, all property distribution made with SGS by using the variogram model that gives the best fits to the experimental data. A 3D and cross sectional views of the obtained porosity distribution model for up scaled reservoir model are shown in Figure 5.5. Note that for the comparison purposes, previously presented fine scaled model landscapes are given herein on the top of each figures.

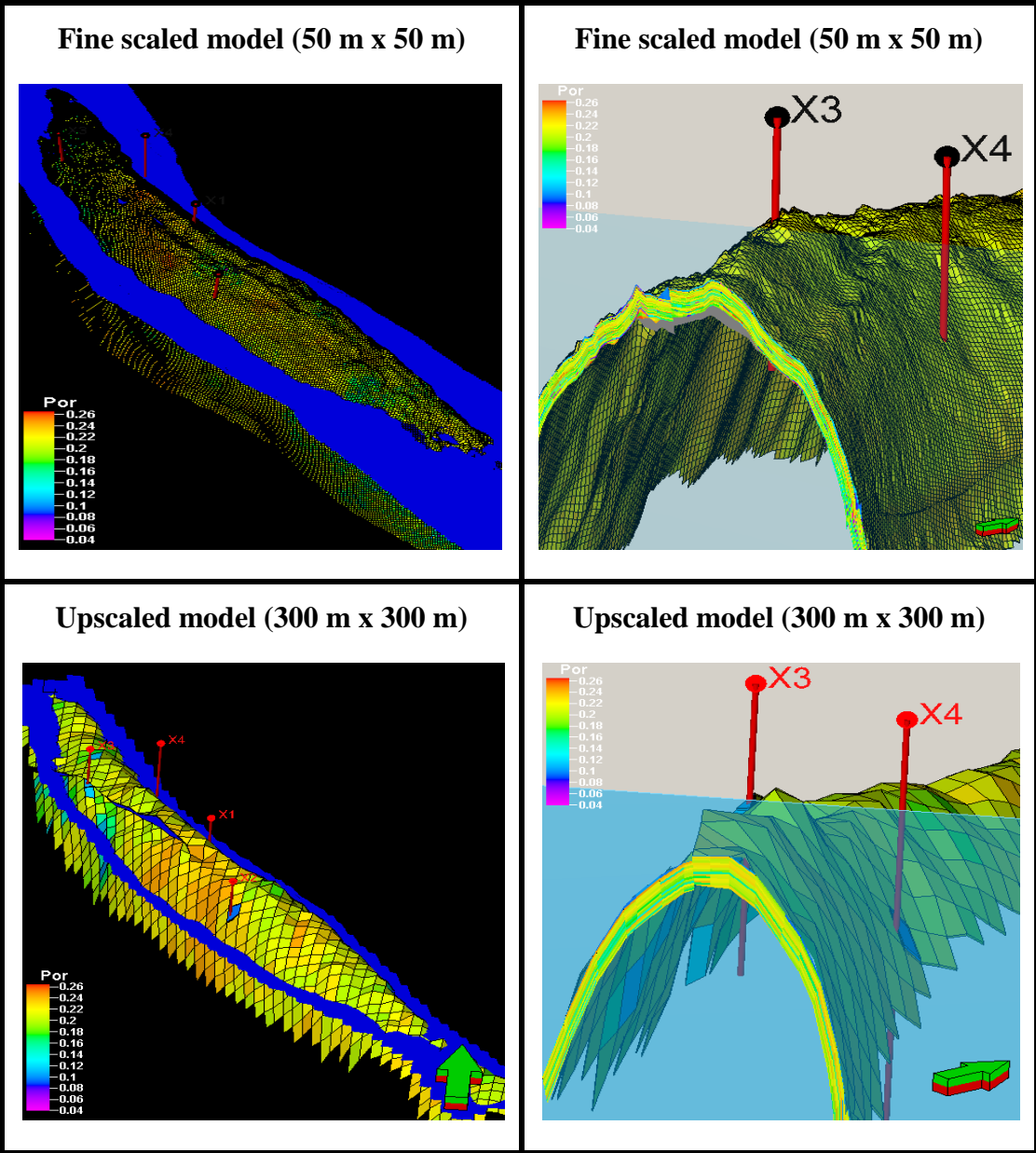


**Figure 5.5:** 3D and cross sectional view comparison of porosity distribution – fine scaled model (top) and up scaled model (bottom).



Porosity histograms and their statistical information are given in Figure 5.5. On the left, fine scaled model porosity histogram and statistical information is shown while the up scaled simulation grid model details is given on the right. The fine scaled geological model (50 m x 50 m) has almost eight million cells and up scaled simulation model (300 m x 300 m) has approximately sixty thousand cells. Although the fact that there is a huge difference in the grid numbers, mean values of distributed porosity is preserved (fine scaled model 0.1925: up scaled model 0.1930) and property histograms are very similar.

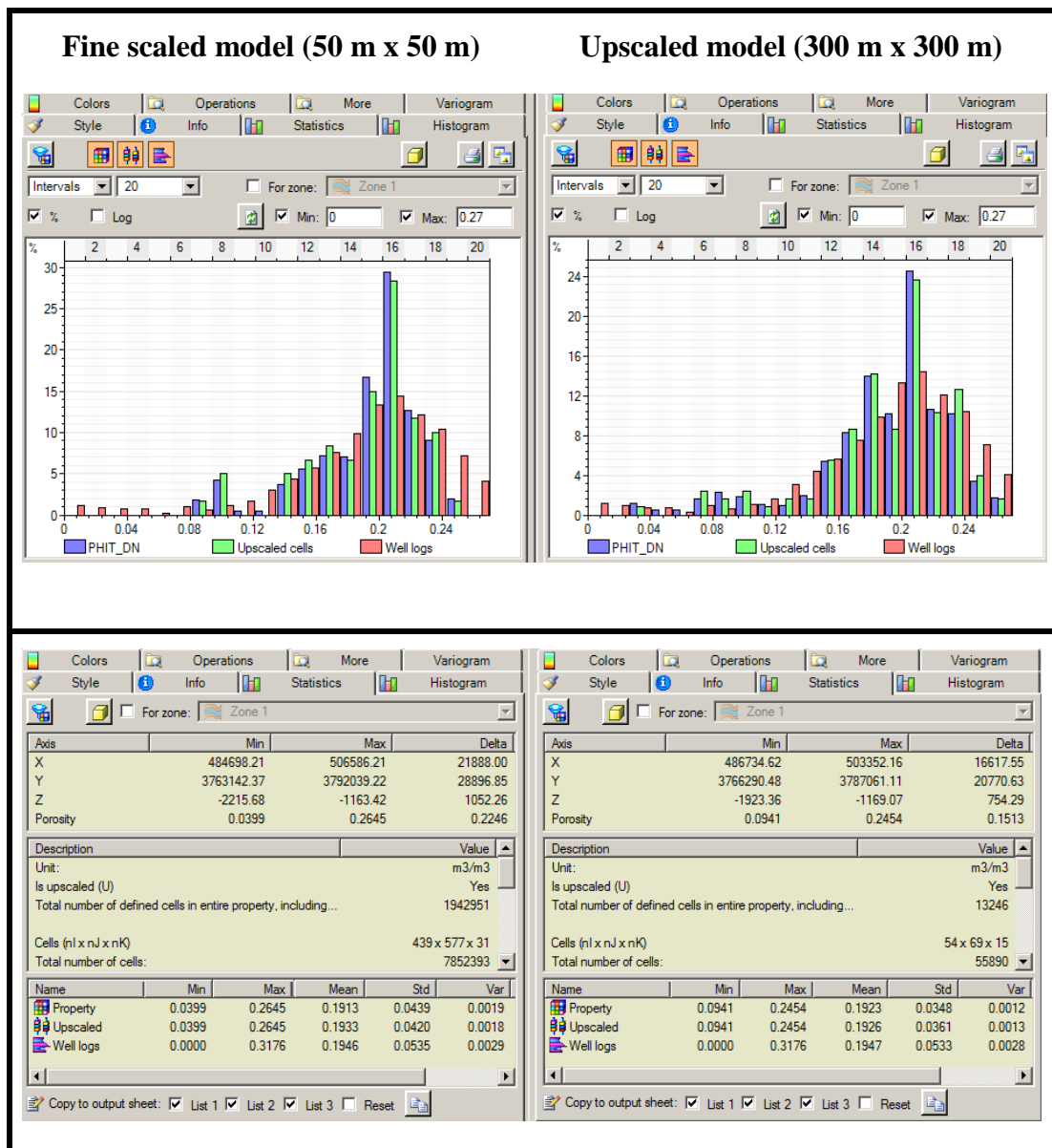


**Figure 5.6:** Porosity histogram – statistics comparison of fined scaled model (on the left) and up scaled model (on the right).

Similar to the porosity distribution, the same approaches which was discussed in the Section 4.4.2, were used for populating cells with water saturation. A 3D and cross-sectional views of the obtained water saturation distribution model for up scaled reservoir model are shown in Figure 5.7. As aforementioned for the comparison purposes, previously presented fine scaled model water saturation landscapes are given herein on the top of Figure 5.7.

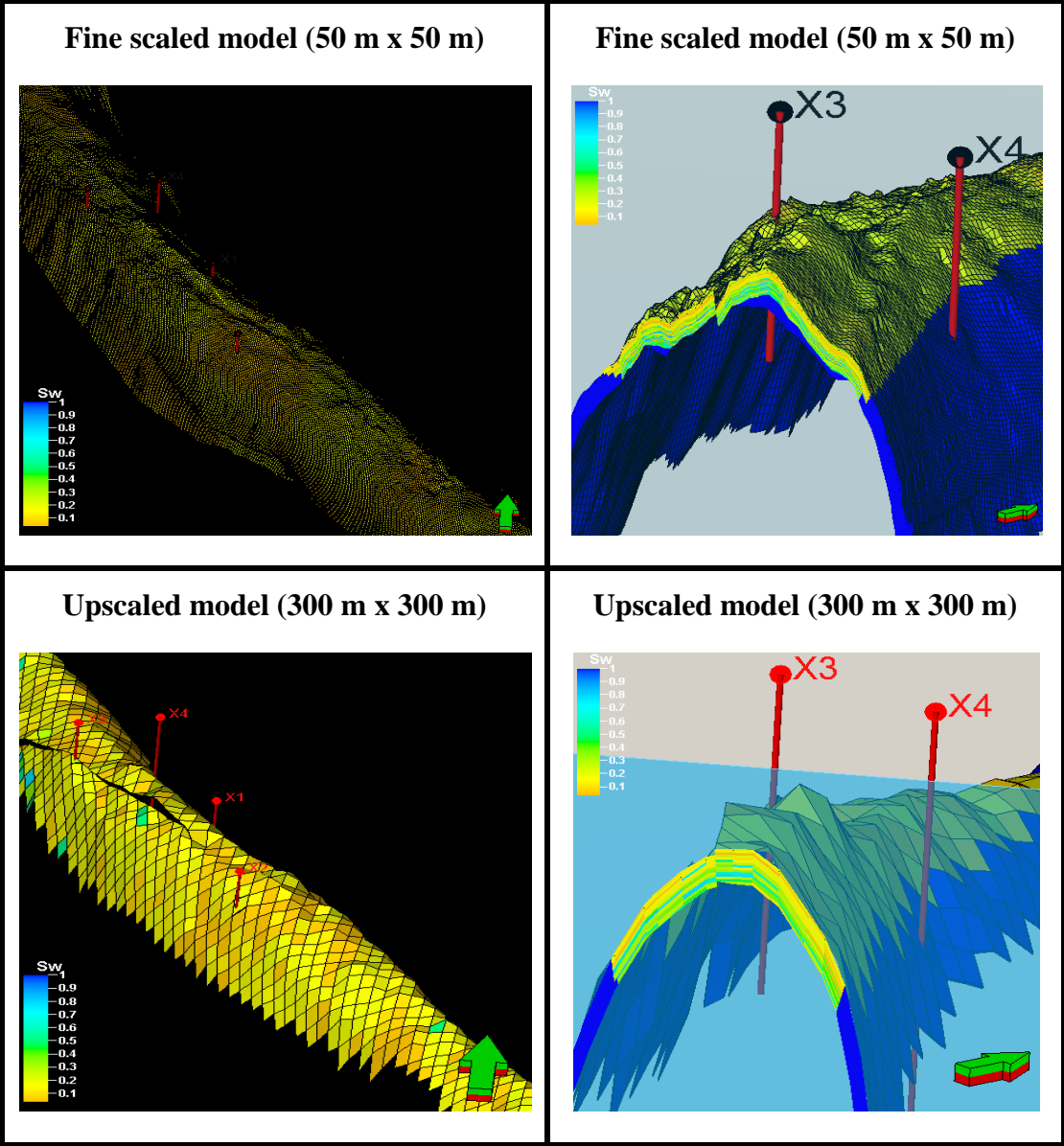


**Figure 5.7:** 3D and cross sectional view: comparison of water saturation distribution – fine scaled model (on the top) and up scaled model (on the bottom).

Water saturation histograms and their statistical information are given in Figure 5.8. On the left, fine scaled model water saturation histogram and statistical information is shown while the up scaled simulation grid model details is given on the right. As

can be seen from the Figure 5.8 mean values of distributed water saturation is almost preserved (fine scaled model 0.2986: up scaled model 0.3098) and property histograms are similar.

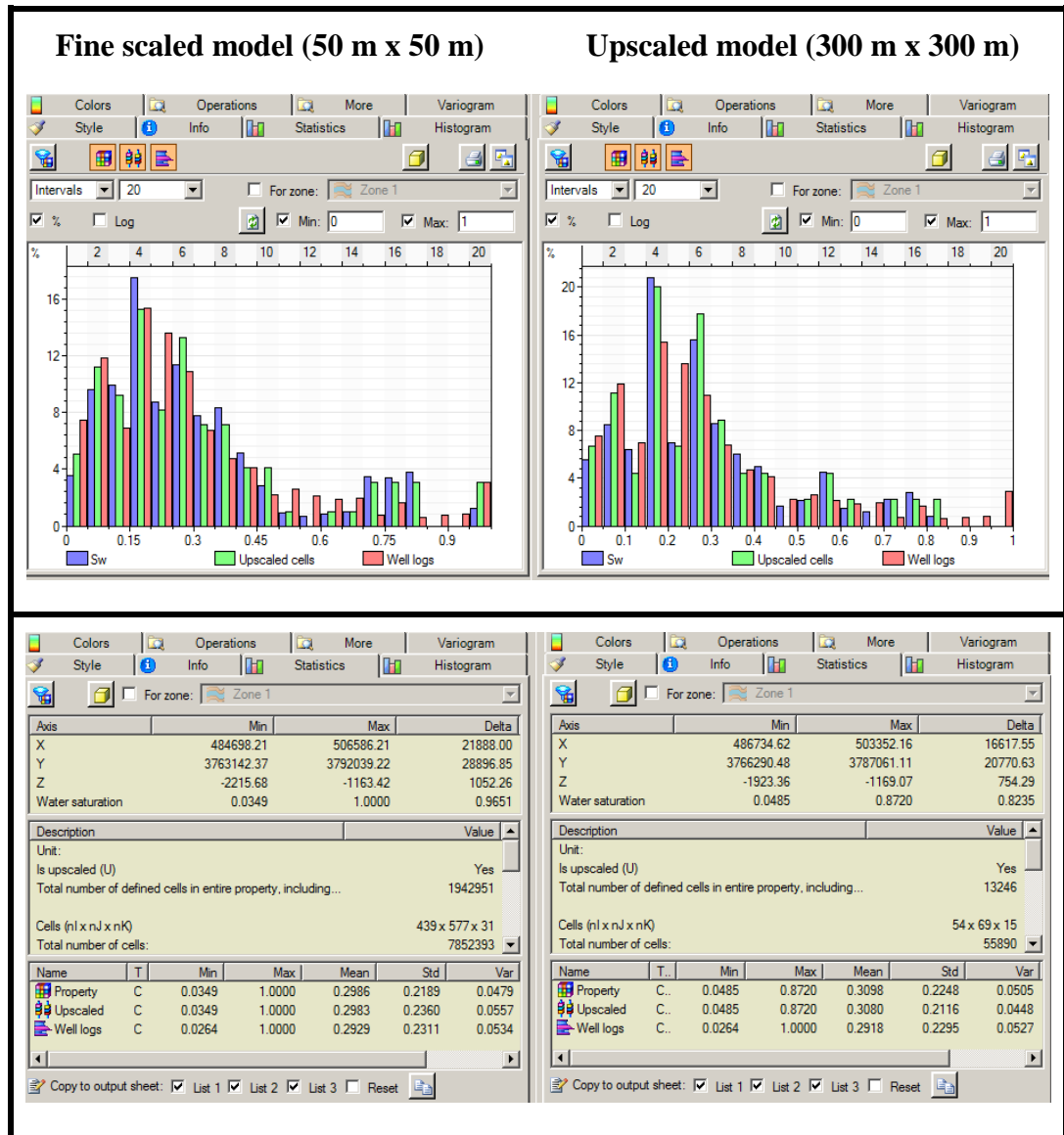


**Figure 5.8:** Water saturation histogram – statistics comparison of fined scaled model (on the left) and up scaled model (on the right).

Similar to the porosity and water saturation distribution, the same approaches which was discussed in the Section 4.4.2, were used for populating cells with permeability. A 3D and cross sectional views of the obtained permeability distribution model for up scaled reservoir model are shown in Figure 5.9. As aforementioned for the comparison purposes, previously presented fine scaled model permeability landscapes are given herein on the top of Figure 5.9. Note that permeability-X distribution is shown in Figure 5.9: however, same procedure was followed that was

discussed in Section 4.4.2.3 for constructing permeability model in Y and Z direction. Recall that permeability models will be multiplied by constant four as discussed before to calibrate permeability models with PTA findings.

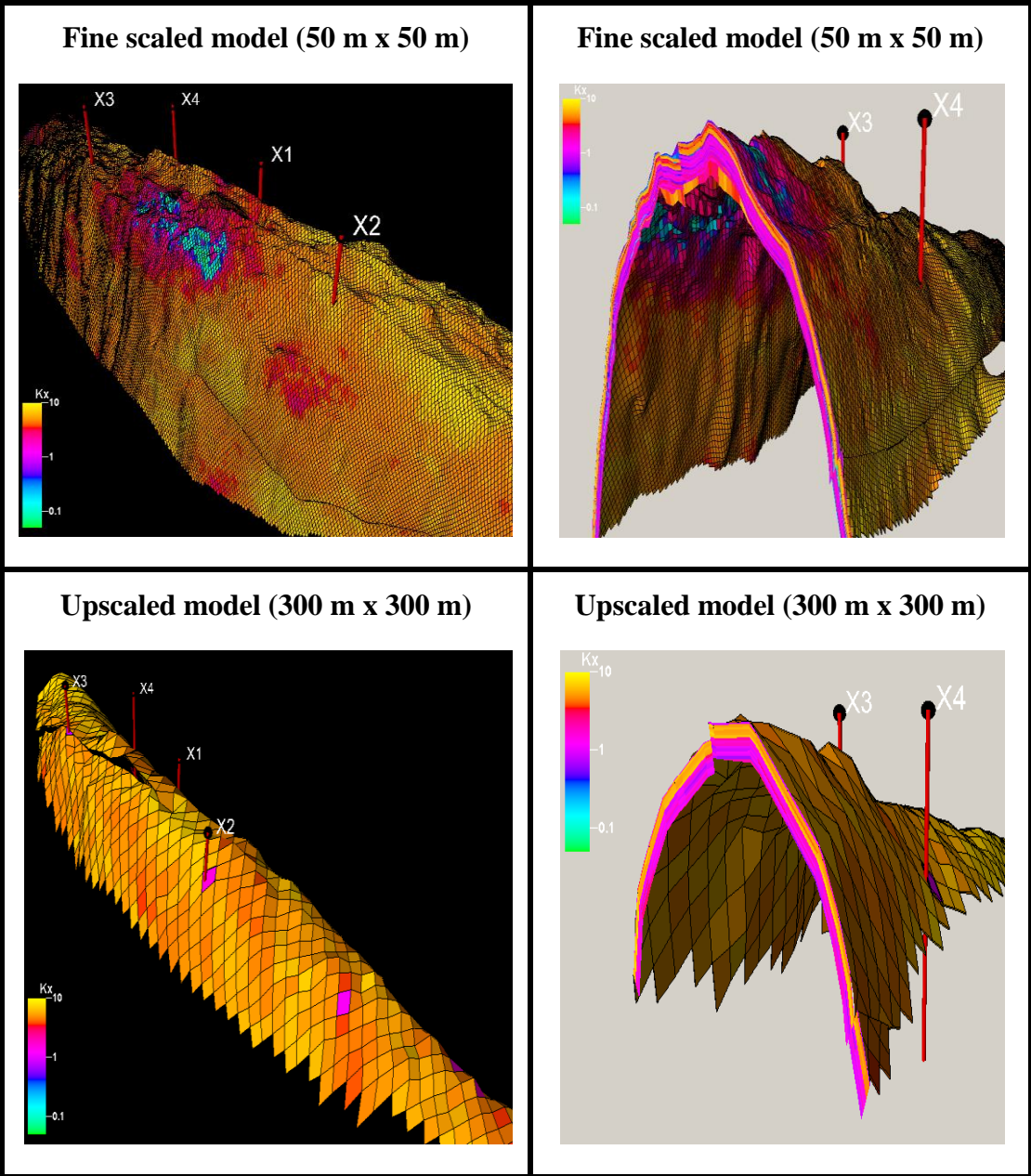


**Figure 5.9:** 3D and cross sectional view: comparison of permeability-X distribution – fine scaled model (on the top) and up scaled model (on the bottom).

Permeability distribution histograms and their statistical information are given in Figure 5.10. Similar to others, on the left fine scaled model permeability-X histogram and statistical information is shown while the up scaled simulation grid model details is given on the right. As can be seen from Figure 5.10 mean values of distributed

permeability-X is preserved (fine scaled model 3md: up scaled model 3md) and property histograms are barely similar.

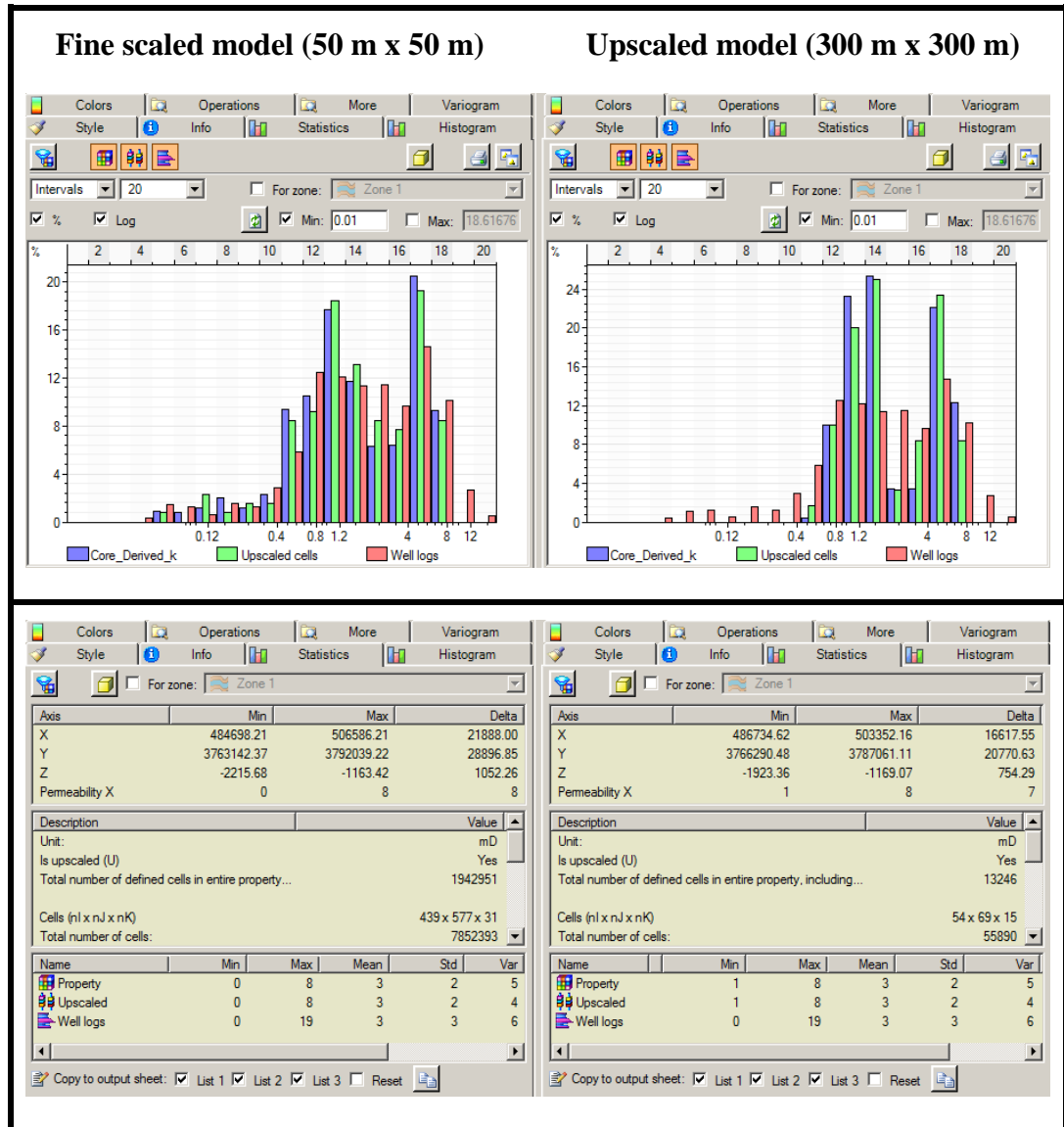


**Figure 5.10:** Permeability histogram – statistics comparison of fined scaled model (on the left) and up scaled model (on the right).

The last stage of upscaling geo-cellular model process is the calculation of the original hydrocarbon volume for the value scaled model and comparing the result with fine scaled model. During the course of upscaling process, size of the grids increased to 300m in the X and Y direction and number of sub-layers reduced to 15 layers. Petrophysical modeling of all properties performed again by considering the fine scaled model findings. Gas initially in place (GIIP) for up scaled model was calculated in PETREL as **2.732 tcf**: however, for the fine scale model, GIIP was calculated as **2.686 tcf** (see section 4.5). Although the difference between two

calculations is less than 50 bcf, it needs to be considered while performing further studies. There could be numerous reasons behind these results, but most probably it is due to size of the grids in the up scaled model. As can be seen from Figure 5.12, a cell that exceeds the GWC is bigger in the up scaled model than fine scaled model which creates an extra volume of hydrocarbon in the volume calculation. To be able to avoid such problems, it is better to use powerful computers that capable of running simulation with fine scaled model. However, as mentioned before, computational power of used computer for the study is limited and upscaling the model is inevitable. It is important to note that GIIP of the dynamic model will be checked before starting the simulation and if the GIIP value of the dynamic model is not close to the fine scaled model calculation, pore volume multiplier can be used to match the GIIP values.

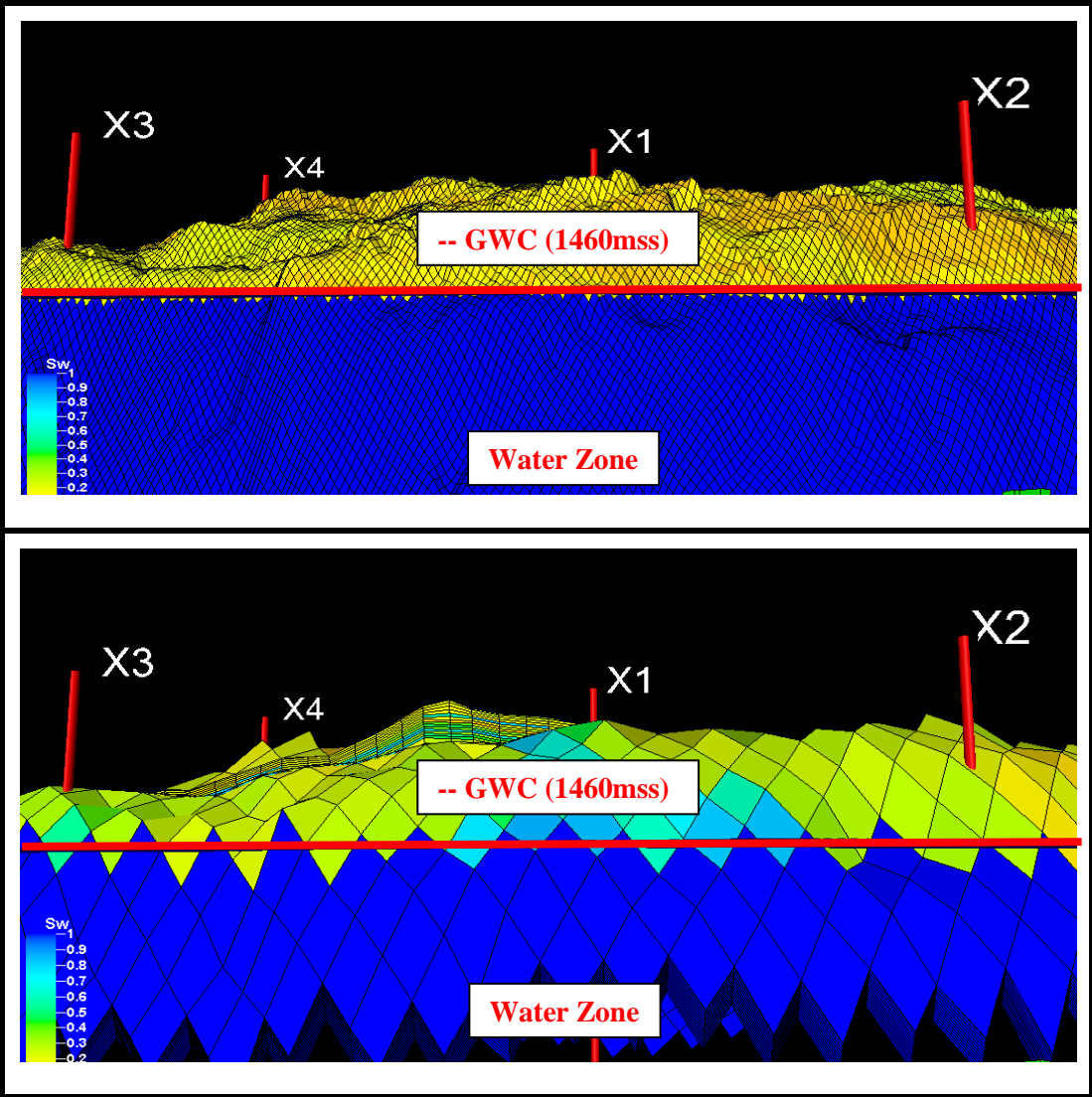


**Figure 5.11:** 3D View of the cells below GWC (fine scaled – up scaled).

### 5.1.1. Quality check of up scaled model

Created cell geometry needs to be checked before starting simulation because it may cause a problem if there are many distorted cells exist in the model. Such kind of problems generally occurs once the orientations of the faults are discarded when a grid is generated. For instance if a fault in the model has a direction in the NW-SE, grid orientation need to be arranged accordingly. Orientation of the grid needs to be either in the same direction with the fault or perpendicular (i.e. NE-SW) to it. However, sometimes number of faults could be more than one and the directions of them can be different. In such a case that creating a grid can be very problematic. Therefore, the grid geometry has to be checked carefully before conducting any simulation activities.

As previously discussed in Chapter 3, there are three main faults in the model. Two of them are bounding the reservoir from both sides in the NW-SE direction but both of them crossing the formation below GWC where the cells are deactivated. Besides, the other is crossing through reservoir as can be seen from Figure 5.13.

The quality of the generated grid can be assessed by checking the apparent cell angle and cell inside-out. Cell angle property can be generated in PETREL that calculates the deviation (from 90degrees) of the angles in each cell (absolute values) to get a measure of the apparent cell angle. It can be used as a measure of the internal skewness in each cell. For a certain plane, a cell has eight internal angles, one for each corner. The deviation angle is the deviation from 90 degrees (i.e. regular cell will have deviation angles of 0 deg.). The criteria for checking the model is to have fewer cells which have the cell angle more than 50 deg. The generated cell angle property and its statistical information are shown in Figure 5.13. As can be seen from Figure 5.13, the numbers of cells that have angle more than 50 degree are fewer. The cells nearby the fault has bigger cell angle as it is expected. Therefore, in terms of cell angle, no problem is observed for the simulation. On the other hand, to calculate the cell inside-out, PETREL uses a temporary fine grid of microcells which the resolution can be specified by user. Assume that resolution of micro grid specified as integer A, then PETREL constructs the micro grids temporarily inside the each simulation grid block that has a dimension  $A \times A \times A$ . Then, PETREL calculates the Jacobian at the eight corners and at the center points of the microcells. Once the calculation completed, the total number of times that the Jacobian is negative is then

reported. The criteria for checking the model is to have cell inside-out as zero or at least fewer cells that have the value different than zero. In most cases, the values are all, or almost all, zeros. A grid is not good when the result is different in different grid blocks. The generated cell inside-out property and its statistical information are shown in Figure 5.14. As can be seen from Figure 5.14, almost all of the generated simulation grids have zeros. Similar to the cell angle, a few of the cells have different than zeros nearby the fault. Therefore, it is concluded that there is no problem regarding generated grids in terms of cell inside-out.

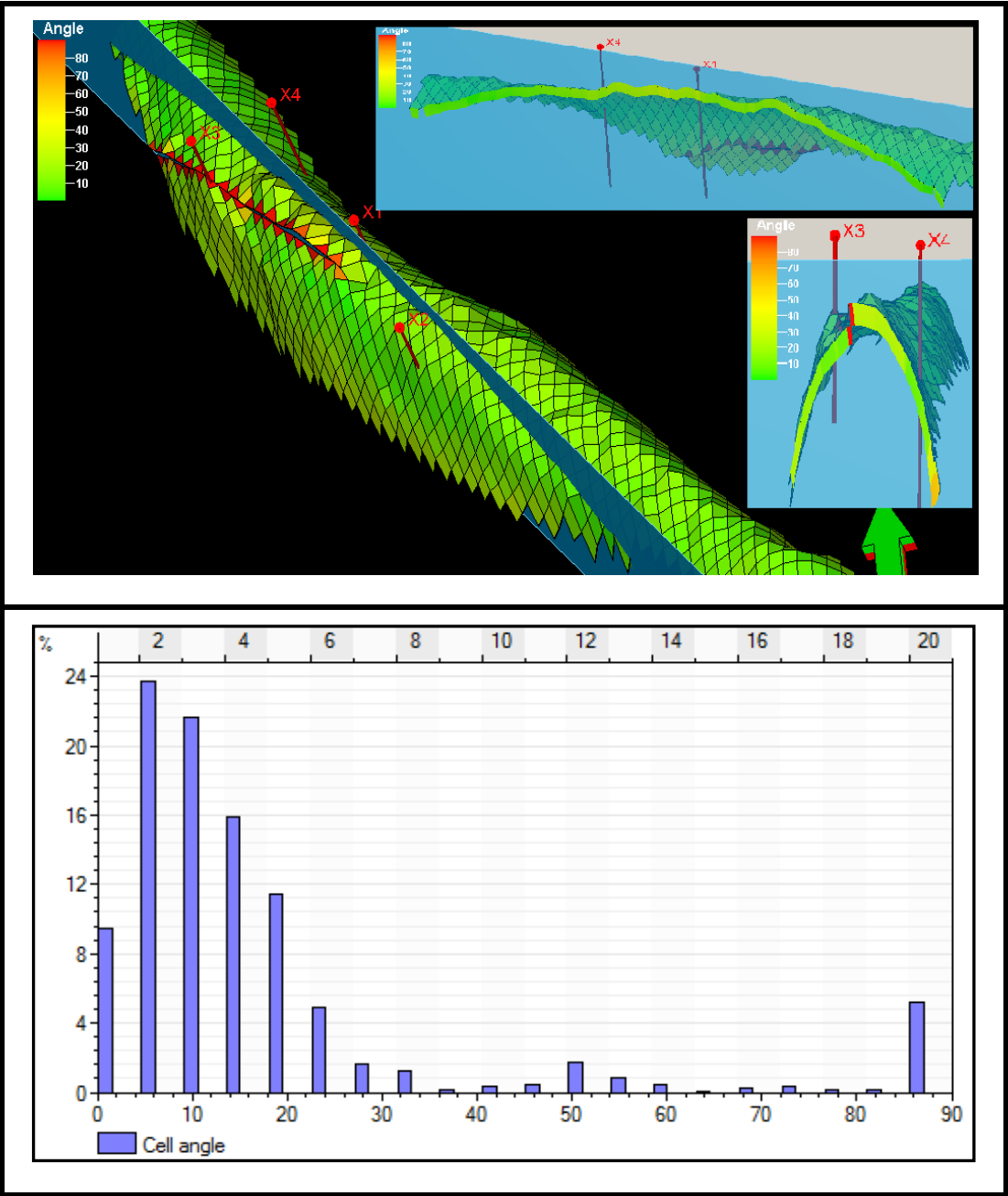
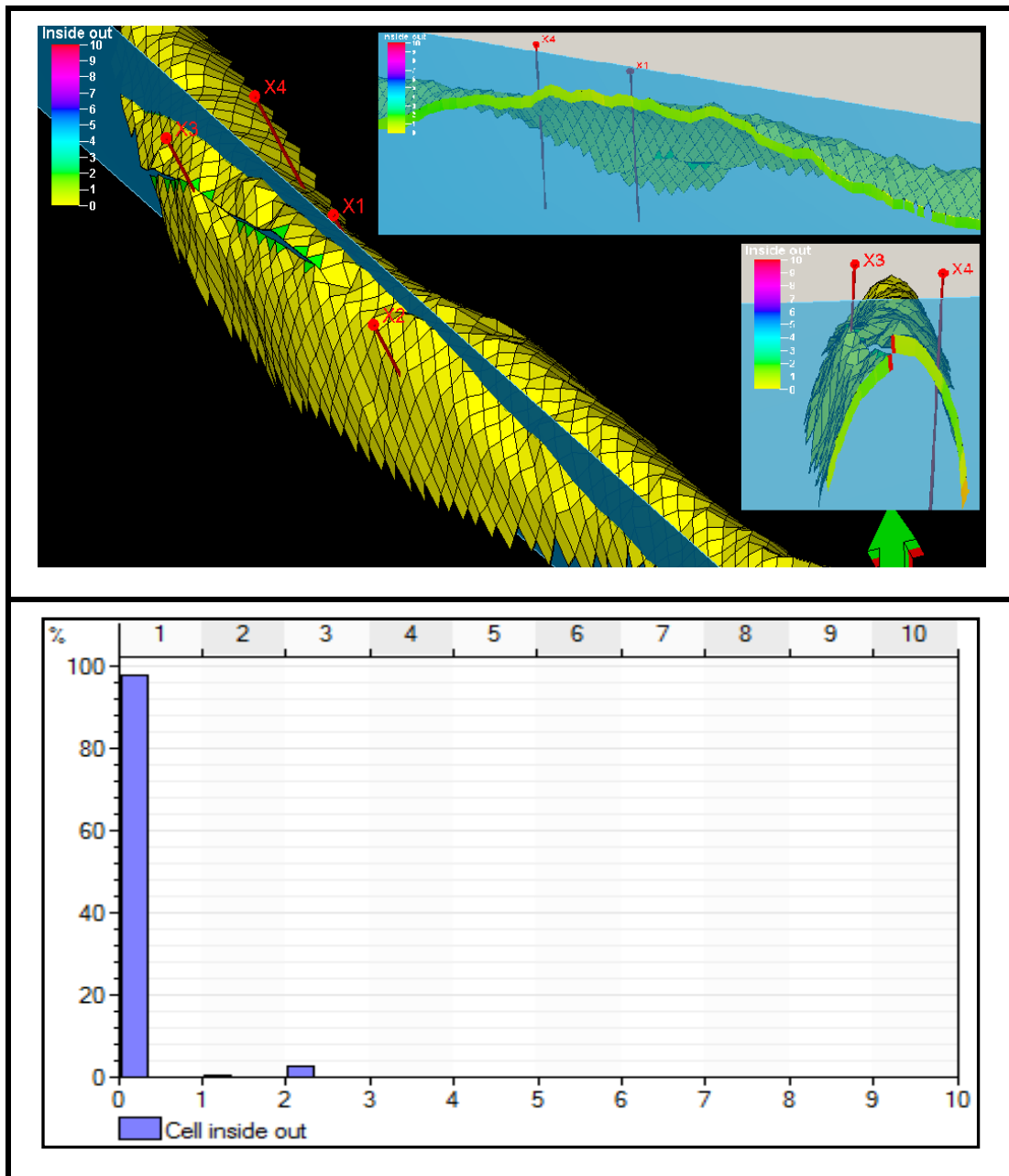


Figure 5.12: Quality check of cell angle.





**Figure 5.13:** Quality check of cell inside out.

## 5.2. Fluid Model

Before production starts from a field, one of the important goals is to obtain representative reservoir fluid sample at the initial condition of the reservoir to be able to predict the behavior of the reservoir fluid with development. The phase and volumetric behaviors of reservoir fluid can simulated with black oil fluid model or compositional fluid model (Aziz and Settari, 1979). Black oil fluid model do not consider the changes in composition whereas compositional models consider the changes in composition during the development. Considering the nature of the gas

condensate reservoir, where the changes in composition with development is playing a major role on reservoir fluid behavior, characterizing such kind of reservoir fluid with a compositional fluid model can give better result than modeling with black oil fluid model. Therefore, compositional fluid model is preferred for characterization of the reservoir fluid considering the fact that it is supercritical gas-condensate reservoir where the dew point pressure is very close to the reservoir pressure. A compositional fluid model represents the hydrocarbon fluid by a set of components (typically 6-12 for reservoir simulation). To be able to determine the physical properties of mixtures of these components as a function of pressure and temperature and the properties of the individual components, an equation of state (EoS) model is used. To make EoS calculations such as dew point pressure, pressure-temperature phase envelope, depletion PVT experiments (i.e. CCE, CVD), separator gas oil ratio (GOR), and densities-compressibilities of oil-gas phases, the minimum required inputs are molar composition of the each component, molecular weight and specific gravity of the heaviest fraction (i.e.  $C_{7+}$  or  $C_{11+}$ ). As previously discussed in Chapter 3.4, in this study, recent sampling data from well X-2 is used as an input for EoS modeling because this is the only sample for which there are laboratory measurements although it is a surface sample and recombined for the PVT analysis. Since the recent well X-2 sample is the most recent and the most reliable data on hand in terms of PVT data, it is used for fluid characterization and analyzed in detail to create PVT tables for simulation. The well X-2 sample quality, sampling conditions and how it represents the reservoir fluid was discussed in Section 3.4. Therefore, no more further discussions are made herein. Additionally, note that well X-2 sample is the only sample that laboratory test like constant composition expansion (CCE)<sup>5</sup>, constant volume depletion (CVD)<sup>6</sup>, and separator test data are available. Recall that as previously mentioned, to construct and tune the EoS model PVTi (Schlumberger 2011.1, 2011) is used. Given fluid composition in Chapter 3.4 is used on the EoS

---

<sup>5</sup> **Constant composition expansion (CCE)** test is used to measure dew point pressure, single-phase gas Z-factors, and oil relative volume (liquid dropout curve) below the dew point pressure. A sample of reservoir fluid is charged in a visual PVT cell and brought to reservoir temperature and a pressure sufficiently high to ensure single-phase conditions. Pressure is lowered by increasing cell volume until a liquid phase is visually detected. Total cell volume and liquid volume are monitored from the initial reservoir pressure down to a low pressure.

<sup>6</sup> **Constant volume depletion (CVD)** test is used to monitor the phase and volumetric changes of a reservoir gas sample as the pressure drops below the dew point and equilibrium gas phase is removed. The CVD test simulates closely the actual behavior of a gas condensate reservoir undergoing pressure depletion, and results from the laboratory measurements can be used directly to quantify recoveries of surface gas and condensate as function of pressure below the dew point.

model and for calibrating the EoS model with the laboratory experimental data (i.e. CCE, CVD, flash calculation, GOR, and dew point) numerous regressions was conducted on the  $C_{11+}$  properties. All below listed correlations are used for EoS modeling and viscosity modeling to obtain the best fits with the experimental data.

EoS Modeling Correlations:

- 2-Parameter Peng-Robinson
- 2-Parameter Soave-Redlich-Kwong
- Redlich-Kwong
- Zutkevitch-Joffe
- 3-Parameter Peng-Robinson
- 3-Parameter Soave-Redlich-Kwong
- Schmidt-Wenzel

Viscosity Correlations:

- Lohrenz-Bray-Clark
- Pedersen
- Aasberg-Petersen
- Lohrenz-Bray-Clark (Modified)

Best fits with the laboratory experimental observation and calculations are obtained with “3-Parameter Peng-Robinson” correlation for EoS model and “Lohrenz-Bray-Clark” correlation for viscosity model. Figure 5.15 shows the phase envelope of the constructed model. Detail information about the fluid model is given in Appendix A.

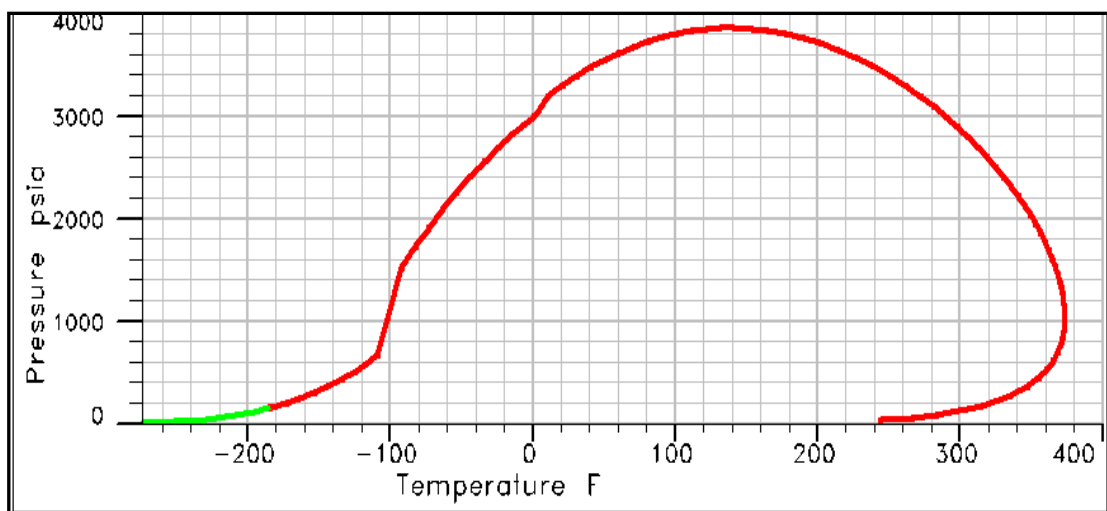


**Figure 5.14:** Phase envelope.

As previously mentioned regression was only performed on the  $C_{11+}$  properties to match the model with the observations. While performing the regression to match the model with laboratory experimental calculation, the first and most important calculation that needs to be checked is the dew point pressure calculation. According to the laboratory experiment, dew point is observed as 3853 psi. The constructed EoS model with 3-Parameter Peng-Robinson correlation, the dew point pressure is calculated as 3855.56 psi which is very similar to laboratory calculation. On the other hand, similar to dew point pressure, a good match was obtained for GOR. Laboratory GOR calculation is reported as 8.32 Mscf/bbl whereas it is calculated as 8.49 Mscf/bbl on the EoS model. Additionally, a good match on the laboratory CCE test observations of liquid saturation, relative volume (liquid dropout) and vapor Z-factor is obtained with the constructed fluid model as shown in Figures 5.15-5.17, respectively. In Figures 5.15-5.17, laboratory observation is represented with red colored dots whereas the model calculation is shown with the blue lines.

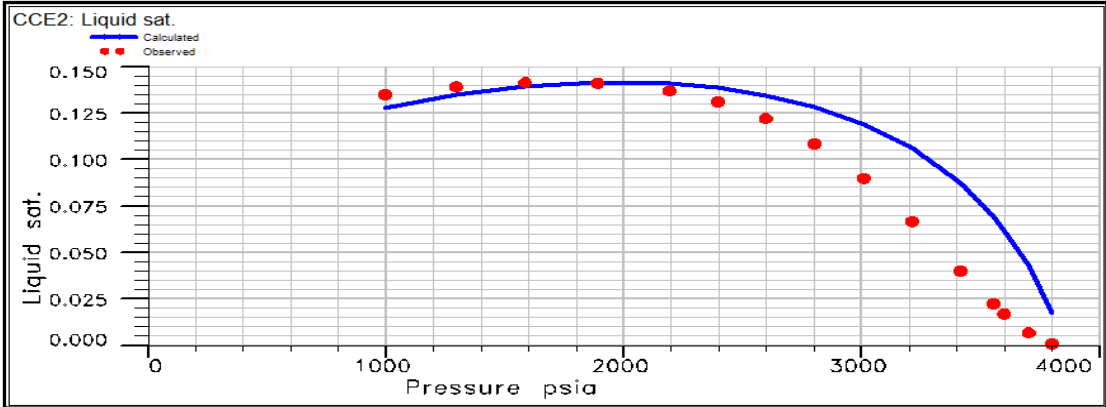


**Figure 5.15:** EoS model versus CCE observations – liquid saturation.

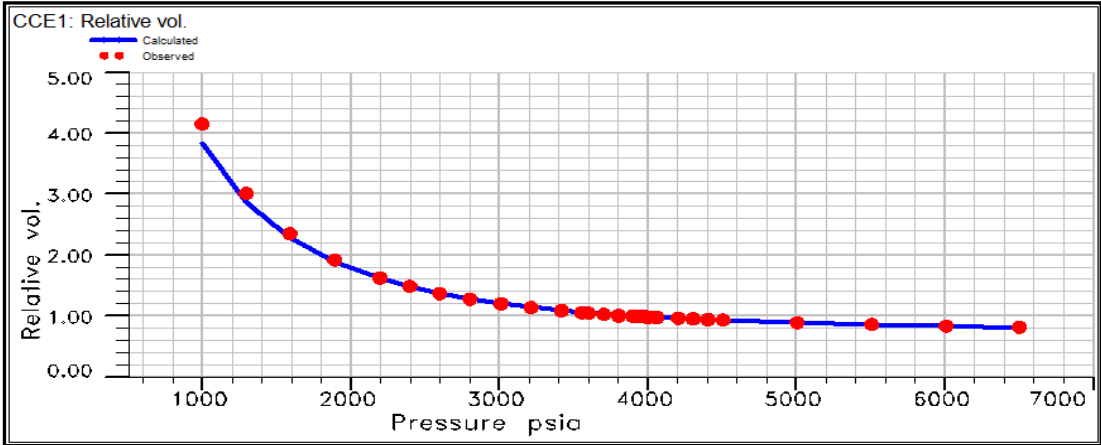


**Figure 5.16:** EoS model versus CCE observations – relative volume.

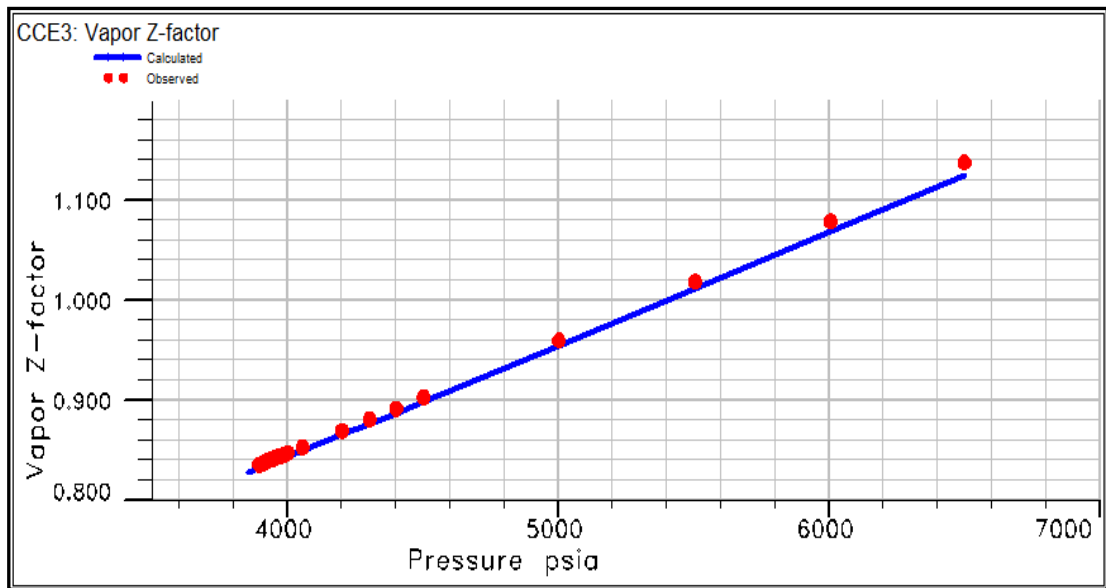


**Figure 5.17:** EoS model versus CCE observations – vapor Z-factor.

Similar to the CCE test, a good match on the laboratory CVD test observations of liquid saturation, 2-phase Z-factor, vapor Z-factor, and vapor viscosity is obtained with the constructed fluid model as shown in Figures 5.18-5.21, respectively. In Figures 5.18-5.21, laboratory observation is represented with red colored dots whereas the model calculation is shown with the blue lines.

After the EoS characterization has been completed, a primary application of the EoS is to generate compositional PVT tables for reservoir simulation. Constructed fluid model is exported as a compositional fluid model that is compatible with ECLIPSE 300 compositional simulator to generate the compositional PVT tables in simulator.

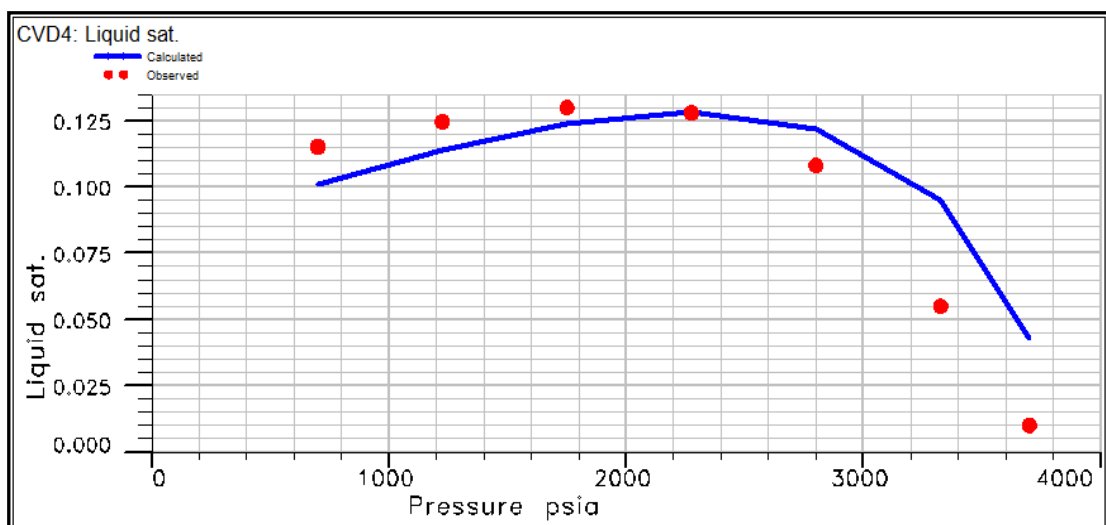


**Figure 5.18:** EoS model versus CVD observations – liquid saturation.

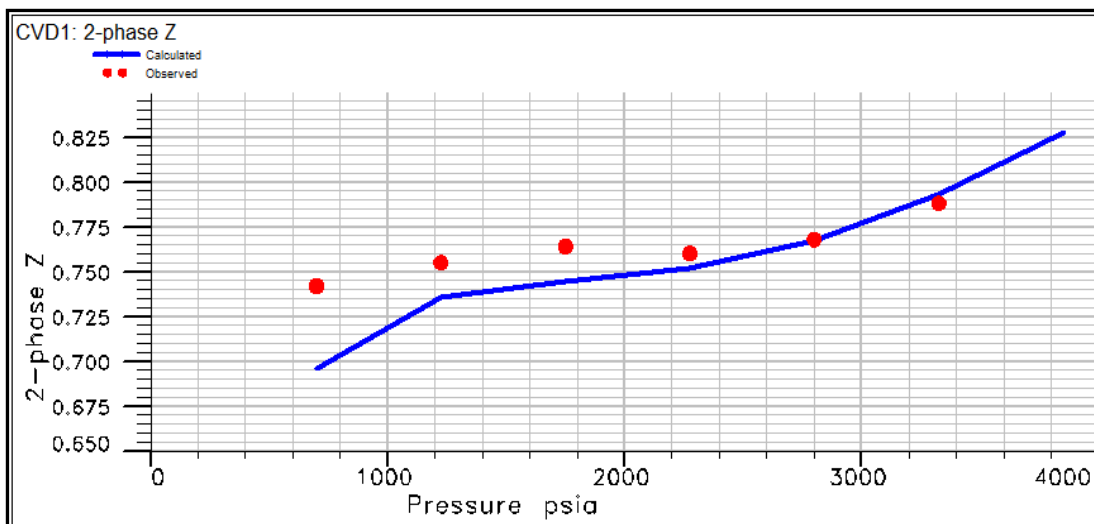


**Figure 5.19:** EoS model versus CVD observations – 2-phase Z-factor.

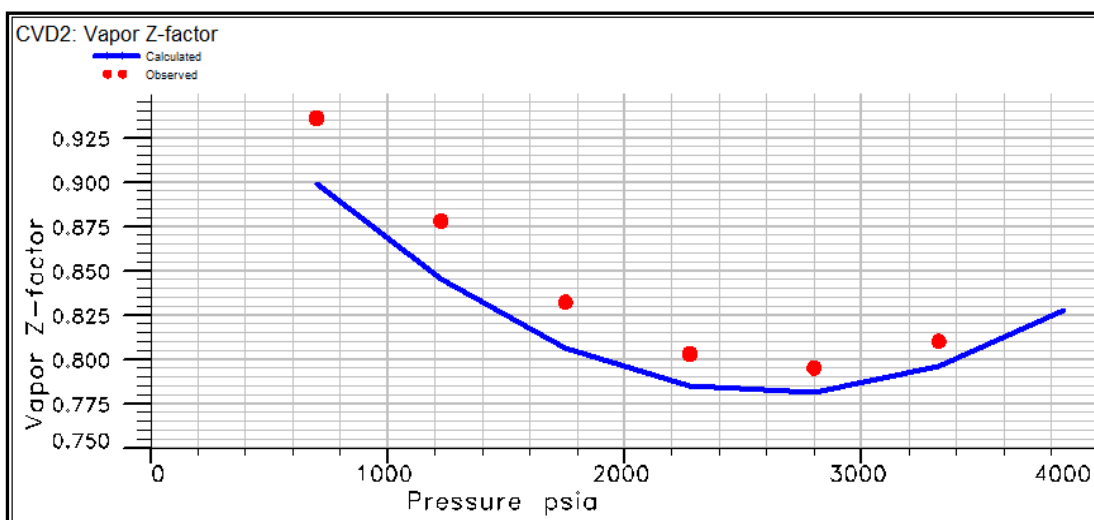


**Figure 5.20:** EoS model versus CVD observations – vapor Z-factor.

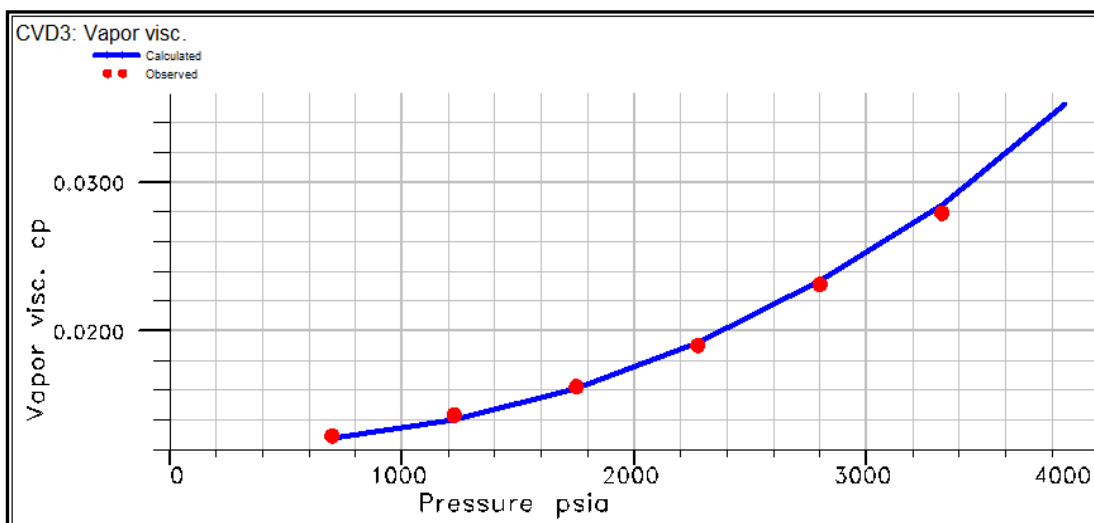


**Figure 5.21:** EoS model versus CVD observations – vapor viscosity.

### 5.3. Rock Physics Function

One of the most challenging tasks in reservoir modeling activities is to construct reliable and accurate rock physics model which is consisting of relative permeability, capillary pressure, and rock compaction modeling. The challenges is not only related with generation of relative permeability data in reservoir studies but also related with having enough samples from the field for evaluation. Generally, coring from the field is limited due to increasing drilling time effect of the operation. Additionally, even the core data are available, scarcity and scale of the performed tests with a small core plugs in the laboratory create a lot of difficulty to characterize the reservoir rocks accurately with such a small plugs, especially where the variation on the vertical and horizontal direction is often observed. Another challenge is restoring the reservoir conditions on laboratory to be able to perform tests in reservoir conditions. Even people with long years' of experience can be lost on the applicability of laboratory tests, correlating data to the whole field, and manipulating data accurately. All in all, this has been one of the major challenges of the reservoir engineering activities. It is very well known fact that reliable relative permeability and capillary pressure data and modeling are one of the inevitable requirements of successful field development planning.

Laboratory experiments of 2-phase flow on the core plug is the best way to obtain 2-phase relative permeability data. There are three main and widely accepted techniques that applied in laboratory for measuring relative permeabilities. These are Steady State, Unsteady State and Centrifuge Method (Honorpour et al., 1987 and Feigl, 2011). The unsteady state method is widely used, fast and cheap method where relative permeability can be measured down to  $10^{-3}$  and it is representative for reservoir situations. On the other hand, the steady state method can measure the relative permeability down to  $10^{-3}$  but it has low accuracy near end-point saturations. The other widely used laboratory experiment is the Centrifuge Method where the relative permeability of only displaced phase can be measured with this technique. To be able to get better relative permeability data applying one of these techniques will not be sufficient; therefore, combination of these methods such as centrifuge – steady state or centrifuge – unsteady state is generally used in the industry. It is unavoidable fact that at the early stage of the field development; generally core data

from the field is not enough to fully characterize the reservoir rocks. Therefore, if the available data on hand is not enough to model the rock physics at the early stage of the field development, analogy from the surrounding field and/or correlation methods are often used to meet the needs of engineering calculations.

As previously discussed, core data is available from the existing four wells but special core analysis where the relative permeability tests are conducted is limited. There is no three phase relative permeability measurement on the available cores from the field. However, two phase relative permeabilities for water-oil and gas-oil are obtained with the Centrifuge method in the laboratory. The measured relative permeabilities are given in Figures 5.22 – 5.23. However, before plotting the water-oil relative permeability measured data, normalization<sup>7</sup> was performed on the water saturation ( $S_w$ ), relative permeability of oil phase ( $k_{ro}$ ) and relative permeability of water phase ( $k_{rw}$ ). Normalization was made based on Eqs. 5.1-5.3 and laboratory measurements used in normalization are given in Table 5.1.

$$(S_w)_{normalized} = \frac{S_w - S_{wc}}{1 - S_{wc} - S_{oc}} \quad (5.1)$$

$$(k_{ro})_{normalized} = \frac{k_{ro}}{(k_{ro})_{S_{wc}}} \quad (5.2)$$

$$(k_{rw})_{normalized} = \frac{k_{rw}}{(k_{rw})_{S_{or}}} \quad (5.3)$$

**Table 5.1:** Special core analysis data that used in normalization.

Well	Core	Depth (m KB)	$S_{wc}$	$S_{or}$	$K_{rw}$ ( $S_{or}$ )	$K_{ro}$ ( $S_{wc}$ )
X-1	1	1350.5	0.5523	0.2414	0.3398	0.2286
X-1	2	1358.6	0.3490	0.4690	0.2516	0.3863
X-1	4	1371.2	0.6780	0.0390	0.2560	0.3890
X-1	4	1384.7	0.4687	0.1207	0.3038	0.9114
X-2	4	1413.7	0.3701	0.3224	0.1396	0.2738
X-2	5	1423.6	0.2634	0.3863	0.0915	0.3534
X-3	1	1456.3	0.3656	0.1830	0.2070	0.2670
X-3	2	1463.8	0.3709	0.0560	0.1710	0.3100
X-4	4	1653.2	0.1195	0.4049	0.1080	0.6420
X-4	5	1660.7	0.2095	0.3264	0.1860	0.6260

<sup>7</sup> Normalized relative permeability defines the oil relative permeability at the critical water saturation (water becomes mobile) as a value of one (1.0), and defines the absolute permeability as the effective at the critical water saturation.



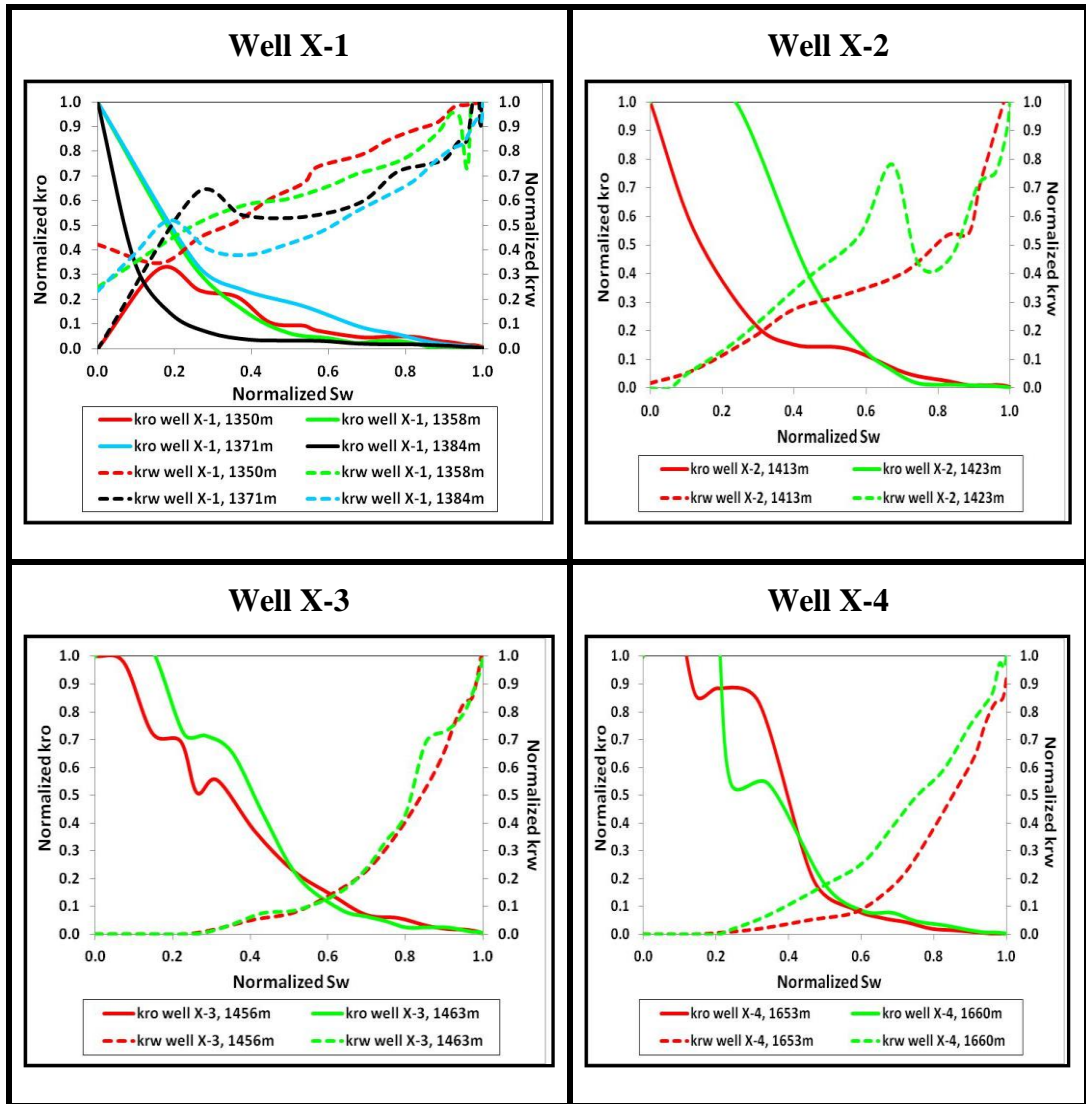


**Figure 5.22:** Water-oil relative permeability laboratory measurements.

As can be seen from Figures 5.22-5.23, it is almost impossible to use the laboratory measured relative permeabilities directly due to numerous reasons such as unexpected shapes of curves ( $k_{ro}$ ,  $k_{rw}$ , or  $k_{rg}$  goes up and down with  $S_w$  and  $S_g$ ), having core measurement from some specific depths only, serious shape variation on the obtained curves from different intervals. As it was discussed previously, if the direct usage of the laboratory measured data is not sufficient to obtain reliable relative permeability model, analogy from nearby field and/or using proposed relative permeability correlations in the literature is the best way to construct the relative permeability model for the field. There is no data set on hand for making analogy from the surrounding fields; therefore, the well-known Corey correlation was used to obtain relative permeabilities based on available data set given in Table

5.1 and Figures 5.22-5.23. The model parameters of the Corey correlation<sup>8</sup> are given in Figure 5.24. Moreover, obtained two-phase relative permeability curves based on the Corey correlation for water-oil and gas-oil are given in Figures 5.25-5.26.

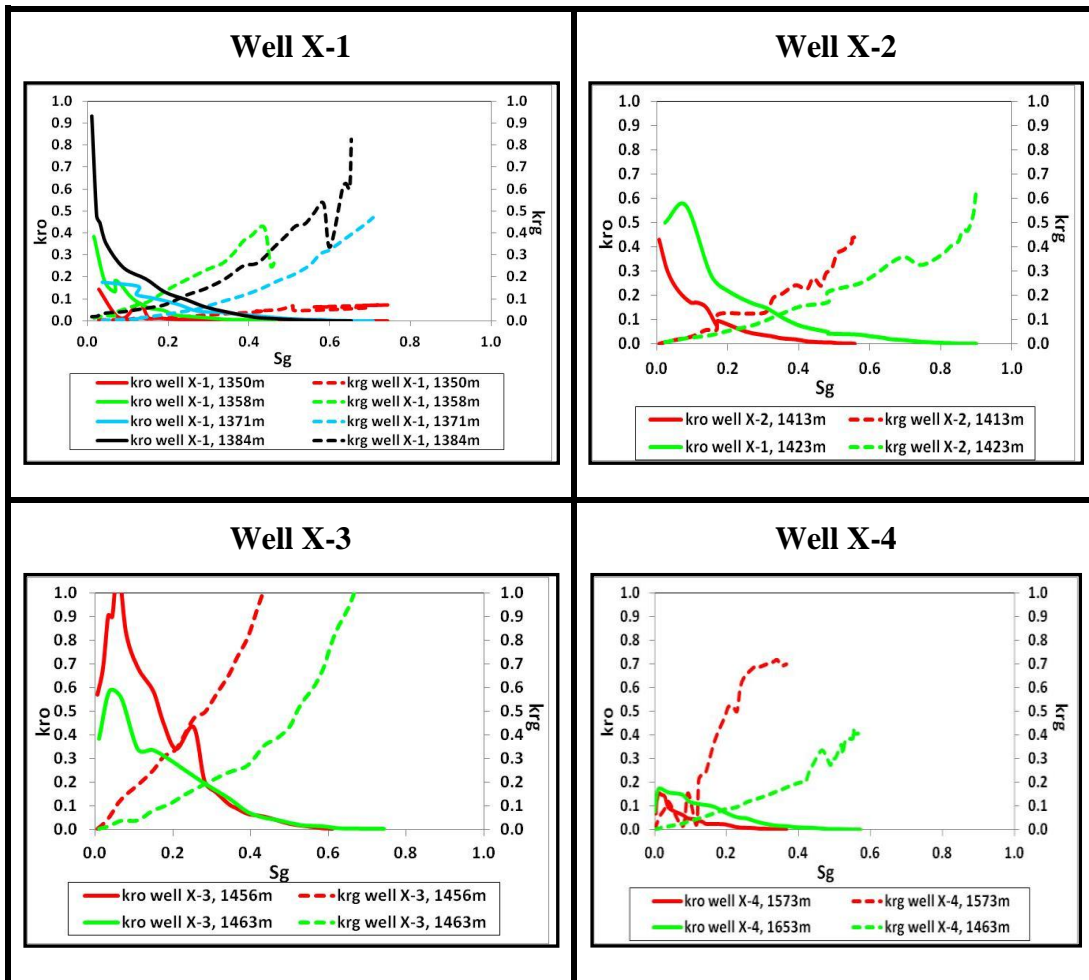


Figure 5.23: Gas-oil relative permeability laboratory measurements.

<input checked="" type="checkbox"/> Gas <input checked="" type="checkbox"/> Oil <input checked="" type="checkbox"/> Water              ?					
Rel. Perm./Cap. Pre					
Table entries: 11					
Gas:		Oil:		Water:	
Sgcr:	0.1	Sorw:	0.15	Swmin:	0.052
Corey gas:	2	Sorg:	0.1	Swcr:	0.06
Krg@Swmin:	1	Corey O/W:	2.5	Corey water:	2.5
Krg@Sorg:	1	Corey O/G:	2	Krw@Sorw:	0.4
		Kro@Somax:	1	Krw@S=1:	1

Figure 5.24: Corey model input parameters.

<sup>8</sup> Corey model assumes the wetting and non-wetting phase relative permeabilities to be independent of the saturations of the other phases and requires only a single suite of gas/oil relative permeability data.

Note that during the laboratory experiments a maximum 60 psi capillary pressure was applied using the air-brine system. Considering the stratigraphically deepest gas (1391m) producing from well X-3, minimum capillary pressure at the base of the formation at reservoir conditions can be calculated as 74.78 psi (5.16 bar) by using Eq. 5.4. Recall that density of water ( $\rho_w$ ) is 65.57 lb/ft<sup>3</sup>; density of gas ( $\rho_g$ ) is 18 lb/ft<sup>3</sup> and height ( $h$ ) is 69 m (GWC- stratigraphically deepest gas: 1460-1391m). Similarly, maximum capillary pressure at the top of the formation (1265 m) at reservoir conditions can be calculated as 211.34 psia (14.57 bara). Considering the calculated minimum capillary pressure and the applied capillary pressure in the laboratory tests which is less than the calculated minimum capillary pressure, it is obvious that the end point observations is not reliable and needs some modifications. Therefore, observed laboratory end points are adjusted accordingly in the Corey model as seen at the Figures 5.24-5.26. Additionally, as discussed, there are no reliable capillary pressure measurements because the maximum applied pressure in laboratory tests is around 60 psi which is lower than the minimum calculated capillary pressure. However, capillary pressure curve given in Figure 5.27 was constructed based on above capillary pressure calculations which then will be used in simulation. Furthermore, all these data are adjusted according to the volume calculation of the dynamic model. It is very well known fact that capillary pressure has an important effect on hydrocarbon saturations which is directly related with hydrocarbon volume in place calculations. On the other hand, rock compaction is also having relatively small effect on the GIIP comparing the capillary pressure effect but it is also modeled with Newman Correlation (Newman,1973) based on porosity data, minimum pressure (40bar), maximum pressure (400bar) and reference pressure (283 bar) as shown in Figure 5.28. Gas initially in place (GIIP) calculation result of the fine scale geo-cellular model, the up scaled model and the dynamic reservoir model are tabulated in Table 5.2. As can be seen from the Table 5.2, a very good match on the gas initially in place (GIIP) calculation of the fine scale geo-cellular model (2.686 tcf) and dynamic reservoir model (2.697 tcf) is obtained.

$$(P_c)_{@res\ cond} = \frac{(\rho_w - \rho_g) * h}{144} \quad (5.4)$$

**Table 5.2:** Comparison of GIIP calculations.

Fine scale geo-cellular model GIIP (tcf)	Up scaled model GIIP(tcf)	Dynamic model GIIP (tcf)
2.686	2.732	2.697

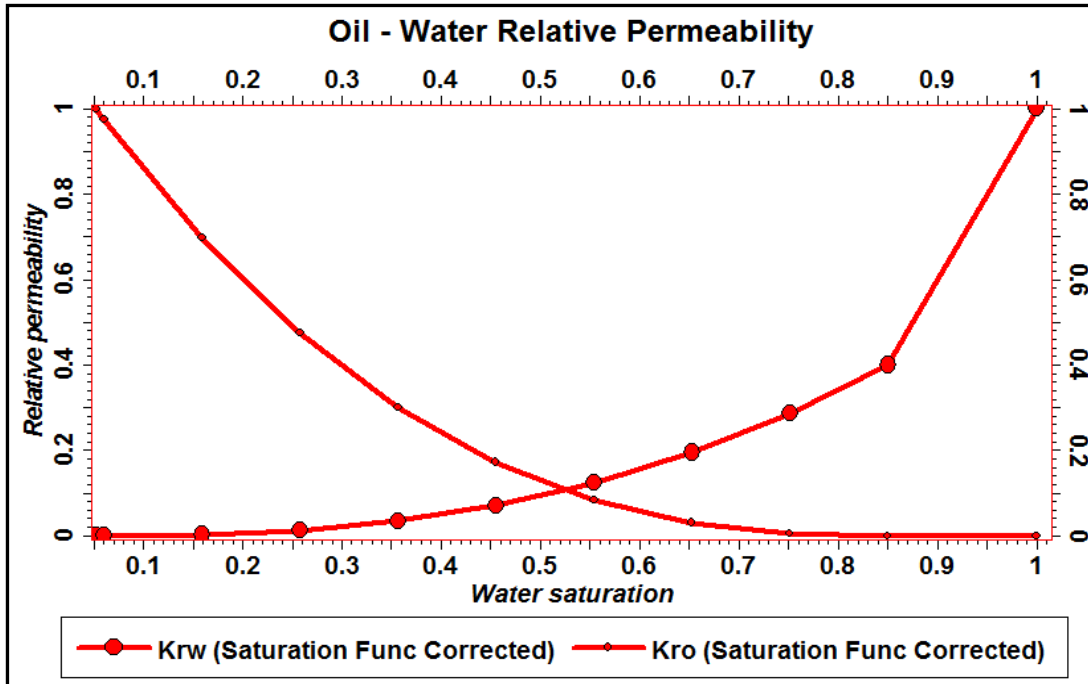


**Figure 5.25:** Oil-water relative permeability – Corey model.

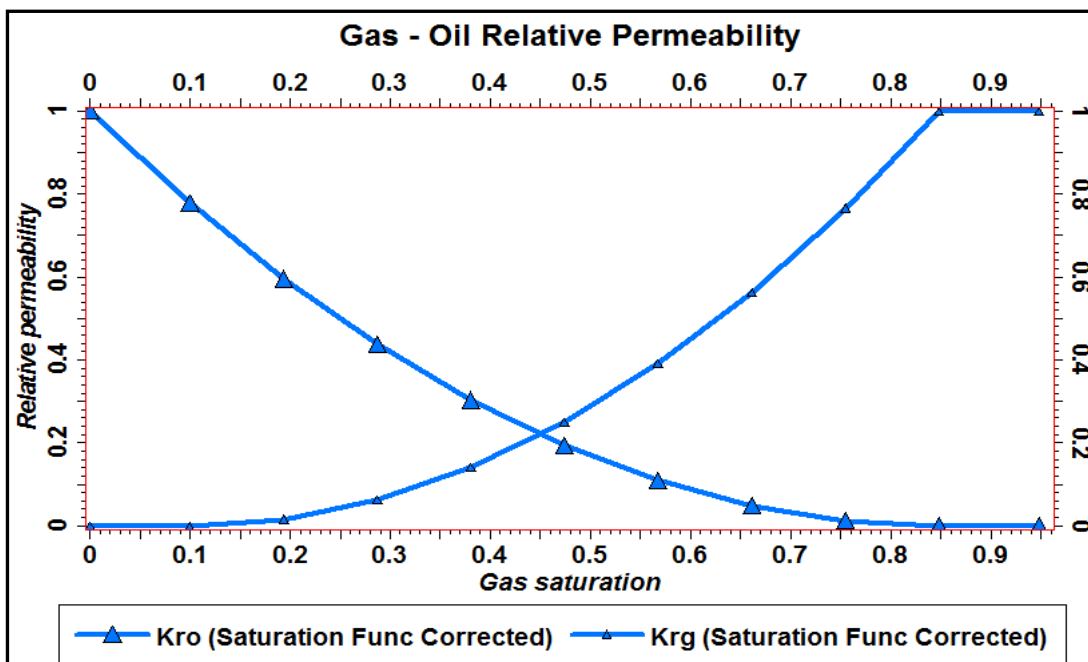


**Figure 5.26:** Gas-oil relative permeability – Corey model.

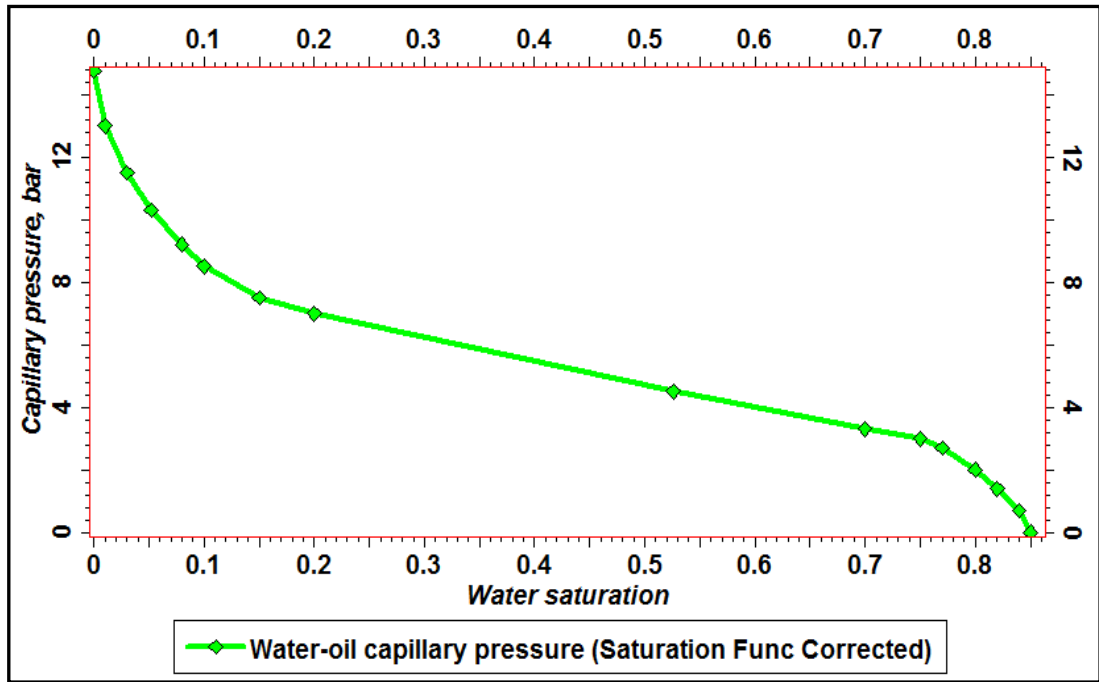


Figure 5.27: Capillary pressure.

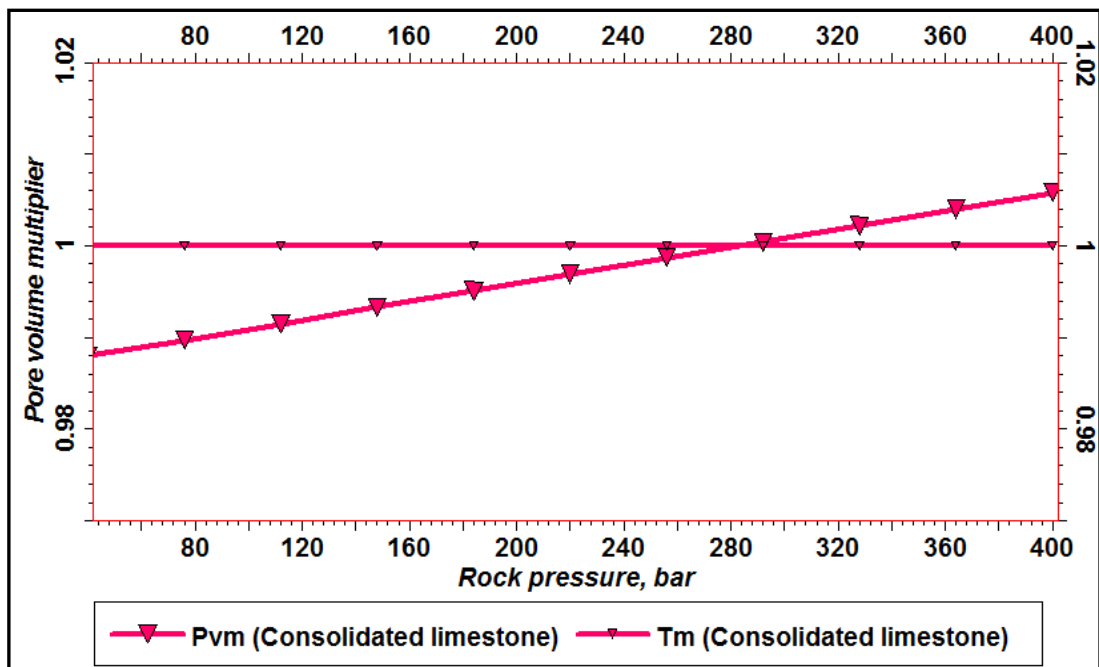


Figure 5.28: Rock compaction.

As previously discussed, core data are available from the existing four wells but special core analysis where the relative permeability tests are conducted is limited. There is no three-phase relative permeability measurement on the available cores from the field. Therefore, after obtaining two-phase relative permeabilities for water-oil and gas-oil, obtained data is then used for the calculation of three-phase relative permeabilities. Although there are many approaches suggested in literature

for calculation of three-phase relative permeabilities such as Stones’s first model, Stone’s second model (modified), IKU method, Baker method, and ODD3P method, the default model that proposed in ECLIPSE for obtaining three-phase relative permeabilities from two-phase relative permeability models is used for the calculation. The schematic view of the assumed model is given in Figure 5.29. In the model oil saturation is assumed to be constant and equal to the block average value ( $S_o$ ), throughout the cell. The gas and water are assumed to be completely segregated, except that the water saturation in the gas zone is equal to the connate saturation ( $S_{wco}$ ). The full breakdown, assuming the block average saturations are  $S_o$ ,  $S_w$  and  $S_g$  (with  $S_o+S_w+S_g=1$ ) is as follows:

In a fraction  $S_g/(S_g+S_w-S_{wco})$  of the cell (the gas zone), the oil saturation is  $S_o$ , the water saturation is  $S_{wco}$ , the gas saturation is  $S_g+S_w-S_{wco}$ . In a fraction  $(S_w-S_{wco}) / (S_g+S_w-S_{wco})$  of the cell (the water zone), the oil saturation is  $S_o$ , the water saturation is  $S_g+S_w$  the gas saturation is zero. The oil relative permeability is then given by Eq. 5.5:

$$k_{ro} = \frac{S_g * k_{rog} + (S_w - S_{wco}) * k_{row}}{S_g + S_w - S_{wco}}, \tag{5.5}$$

where  $k_{rog}$  is the oil relative permeability for a system with oil, gas and connate water which is tabulated as a function of  $S_o$  and  $k_{row}$  is the oil relative permeability for a system with oil and water only also tabulated as a function of  $S_o$  as well.

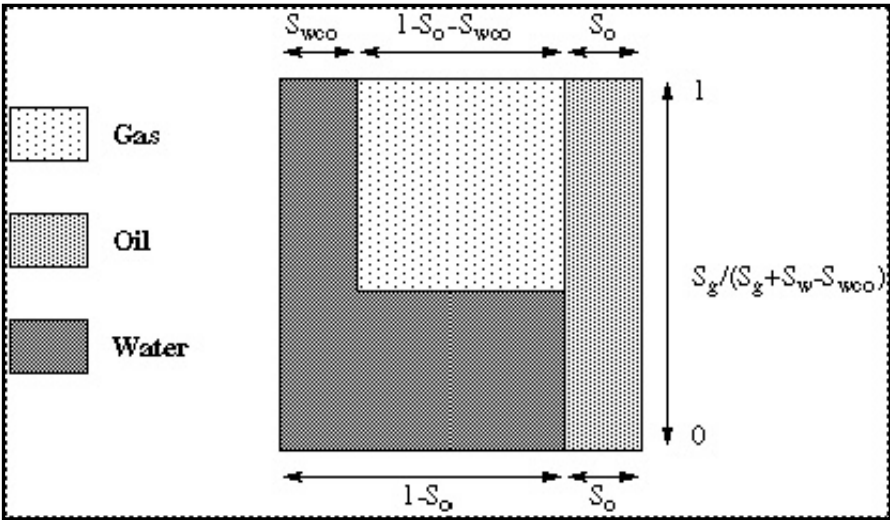


**Figure 5.29:** Three-Phase relative permeability model assumed by ECLIPSE (ECLIPSE Reference Manuel, 2011).

#### 5.4. Well Modeling

A single-branch well model was constructed in PIPESIM to be able to determine the inflow performance of the wells that will be used in the simulation. PIPESIM is a steady-state<sup>9</sup>, multiphase flow simulator used for the design and analysis of oil and gas production systems. PIPESIM is generally used for modeling well performance, performing nodal analysis, designing artificial lift systems, model pipeline networks (infield oil/gas gathering network, export pipelines etc.) and facilities, field development plans and optimize production. In this study, PIPESIM was used for determining the well deliverability and performing nodal analysis to determine optimum tubing size. The Well X-2 was chosen since it is the best candidate for performing mentioned studies because there are two cased-hole test data and one surface production test data from the well. Additionally, as it was discussed, most reliable PVT data were obtained from the well X-2. The well test data and completion string data were used as main inputs of the constructed model. Also well X-2 PVT data were used for making compositional fluid model in PIPESIM. As shown in the Figure 5.30, reservoir conditions and completion string properties were defined to perform nodal analysis. Nodal analysis point was positioned in between the perforation and completion string as can be seen from Figure 5.30.

Once the model is constructed, production test data such as production rates, down-hole flowing pressures, and reservoir pressure are needed to be able to determine the well deliverability (productivity index, PI). Surface well test was conducted recently but down-hole pressure gauge was not installed in the test. Therefore, surface production rates and wellhead pressure were recorded in the test. Average gas rate on the conducted six hours production test was measured as 28.58 MMscf/d where the wellhead pressure measured as 2500 psia. Since there was no down-hole pressure gauge data in the test, wellhead pressure converted to down-hole pressure to be able to use the production test data in the estimation of productivity index. Wellhead shut in pressure was recorded as 3500 psia in the test. Considering the reservoir pressure is 4114 psia, hydrostatic head can be calculated as 614 psia ( $p_r - p_{wh}$ ; 4114 psia – 3500 psia) at the static conditions. Wellhead pressure measured as 2500 psia during production test which then bottom-hole pressure can be approximated as 3114 psia

---

<sup>9</sup> Steady-state flow simulation implies that the mass flow rate is conserved throughout the system which means there is no accumulation of the mass within any component in the system.

(2500 psia + 614 psia if the pressure losses due to frictions are discarded in the dynamic flow conditions. Actually, this approximation is conservative (if the friction losses added on top of hydrostatic pressure, bottom-hole pressure will then be calculated more than 3114 psia where the PI will be calculated higher than the estimated value) but maximum well deliverability will be defined with this calculation so being in safe side is preferable.

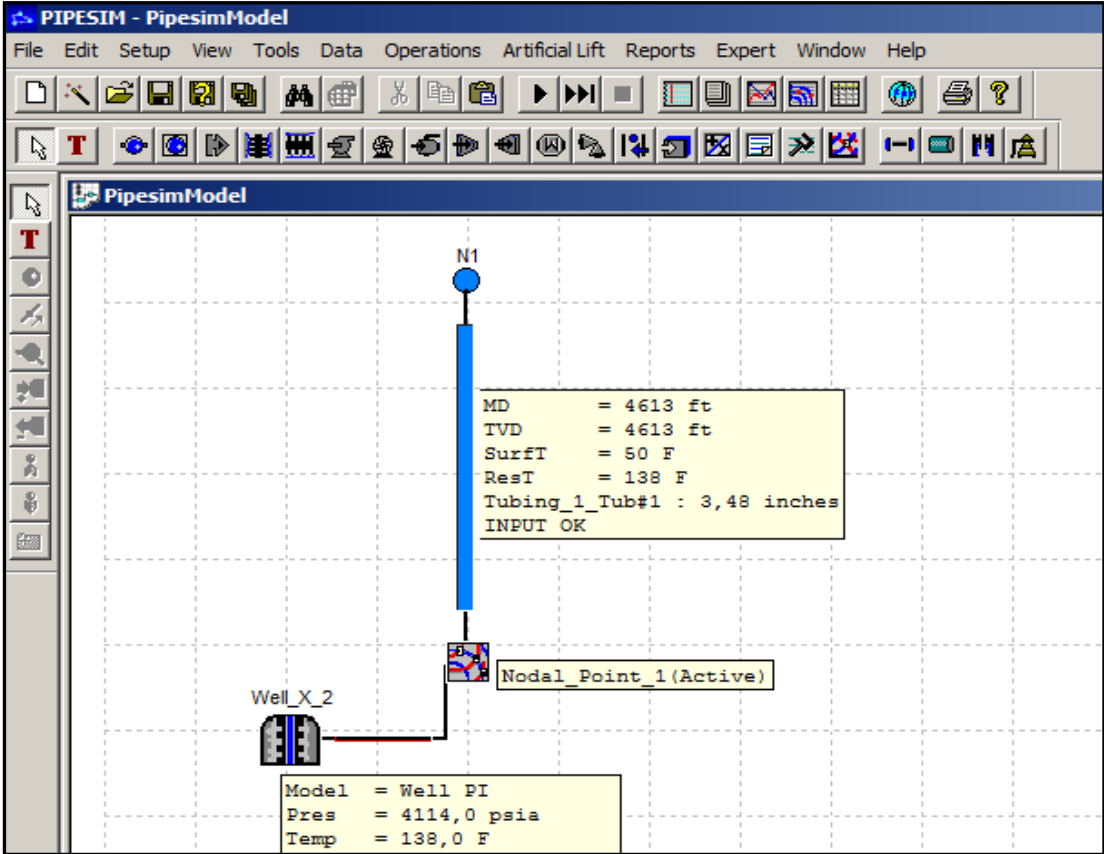


**Figure 5.30:** Single branch PIPESIM model.

Furthermore, as discussed previously, two cased-hole well test conducted in well X-2; in the first test, well produced 40 MMscf/d gas where the flowing bottom hole pressure measured as 1762 psia, in the second test, well produced 78 MMscf/d gas where the flowing bottom hole pressure measured as 2386 psia. It is needless to discuss the inconsistency on the conducted tests results but these are the only available data on hand for constructing inflow performance relationship (IPR) curve and estimating the PI of the well. Although, all the mentioned inconsistency on the data, it seems that the well can deliver 50 MMscf/d gas easily at the early stage of the production from the field based on available test data and constructed IPR shown in Figure 5.31. Straight line option was used in PIPESIM to approximate the gas PI



where PI is equal to  $Q/(p_{ws}^2 - p_{wf}^2)$ . As can be seen from Figure 5.31, the PI is calculated as  $4.52 \times 10^{-6}$  MMscf/d/psi<sup>2</sup>. Therefore, maximum gas production rate target is defined as 50 MMscf/d for each of well in the base case simulation model.

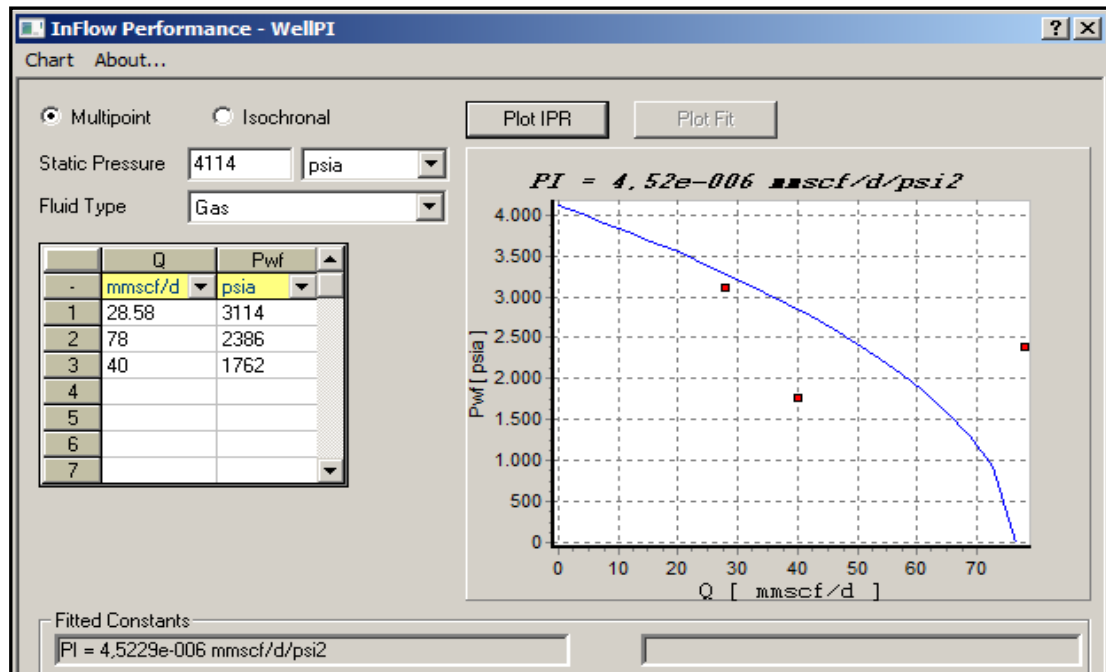


**Figure 5.31:** IPR curve and well productivity index.

On the other hand, nodal analysis was performed to determine the optimum tubing size. Therefore, several sensitivity cases simulated based on different tubing diameters (3", 3.5", 4.5", and 7" tubing). Early life reservoir pressure defined as 4100 psia, mid-life reservoir pressure defined as 3000 psia, and late life reservoir pressure defined as 2000 psia as shown in Figure 5.32. Inflow and outflow curves were plotted each of the mentioned cases. Comparing the operating point<sup>10</sup> of the each case, it is obvious that production capacity is not increases much with the increase on the tubing size after 4.5 inch tubing. However, there is considerable difference between 3"-3.5" tubing and 3.5-4.5" tubing. For instance, at the early stage of the reservoir depletion (4100 psia IPR, shown with red colored line), the well production is 42 MMscf/d for 3" tubing (turquoise colored line); 50MMscf/d for 3.5" tubing (dark blue colored line); and 58 MMscf/d for 4.5" tubing (light green colored line) whereas production rate increases 1-2 MMscf/d with the increasing tubing diameter after 4.5" tubing. Although the optimum tubing size is determined

<sup>10</sup> Operating point is the intersection of the inflow and outflow curves, that is, flow rate and pressure at the specified node.

with nodal analysis, for the base case simulation runs pressure control is used as bottom-hole pressure (BHP) where the vertical lift performance (VLP) curves is not necessary. However, pressure control can be defined as well head pressure (WHP) where the selection of the optimum tubing size is necessary.

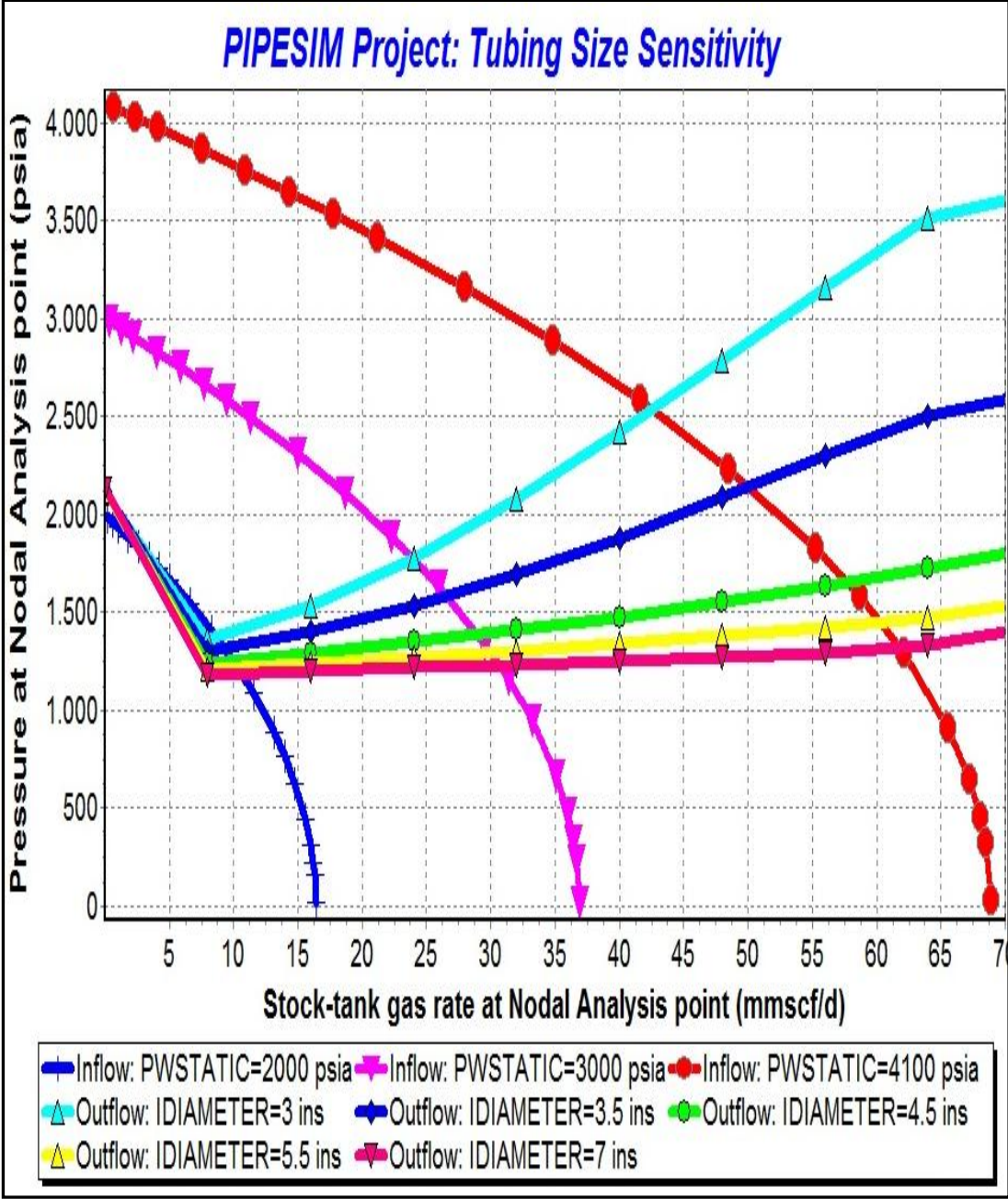


Figure 5.32: Tubing size sensitivity, inflow-outflow curves for different tubing sizes.

5.4.1. Location and number of wells – base case

Determination of the number and locations of the wells is one of the complex problems and the solution may vary case to case based on exposed constraints in the

development plans. Sometimes, same recovery from the field can be achieved with less number of wells if there is no constraint on the project life. In some cases increasing the number of wells to reduce production life of the field can be more economical than reducing number of wells by increasing the depletion duration if the operational cost is high in the field. Sometimes maximization of the recovery can kill the project economy if the field is small; therefore, incremental production of any proposed well is evaluated according to the contractual terms and conditions. On top of all these complexities, gas development projects can bring additional constraints such as gas sales agreements since the gas storage is very difficult and expensive. Therefore, development plan and number of wells should be optimized according to the committed gas amount in the sales agreements.

In this study to define the base case well numbers/locations, three main scenarios are considered to honor the defined production targets and constraints in Chapter 2. The first scenario assumes equally spaced 16 wells where the distance between the two wells is approximately 1400m. Recall that well X-4 is water-leg well; therefore, it will not be used as a producer in simulation runs while existing other three wells are used as producers. As a result, for the first scenario, production targets and technical-commercial constraints are tried to be fulfilled by drilling additional 13 wells as shown in Figure 5.33. Note that red line in the Figure 5.33 representing the closure contour of 1460 mss and blue colored closed polygon is the location of the central gas processing facility (CPF) where drilling a well in that location impossible and there should be at least 800 m safety distance between the wells and the facility. Also note that as discussed in the previous sections, no conspicuous property changes was observed in the field, no distinct variation on the formation thickness, no compartmentalization is exist due to faults and/or baffles and there are no facies changes observed from the existing well data throughout the field. Additionally, there is no data to make discrete fracture network model although the field is carbonate and most probably fractured. Therefore, equally spacing the wells based on available data set is the best that can be doable. Since the field is gas condensate and it is mobility is higher than the mobility of the oil, applied equally well spacing approaches is the best that can be doable based on the available dataset. Note that all the proposed wells located on the crest of the field, so water coning problem is not expected.

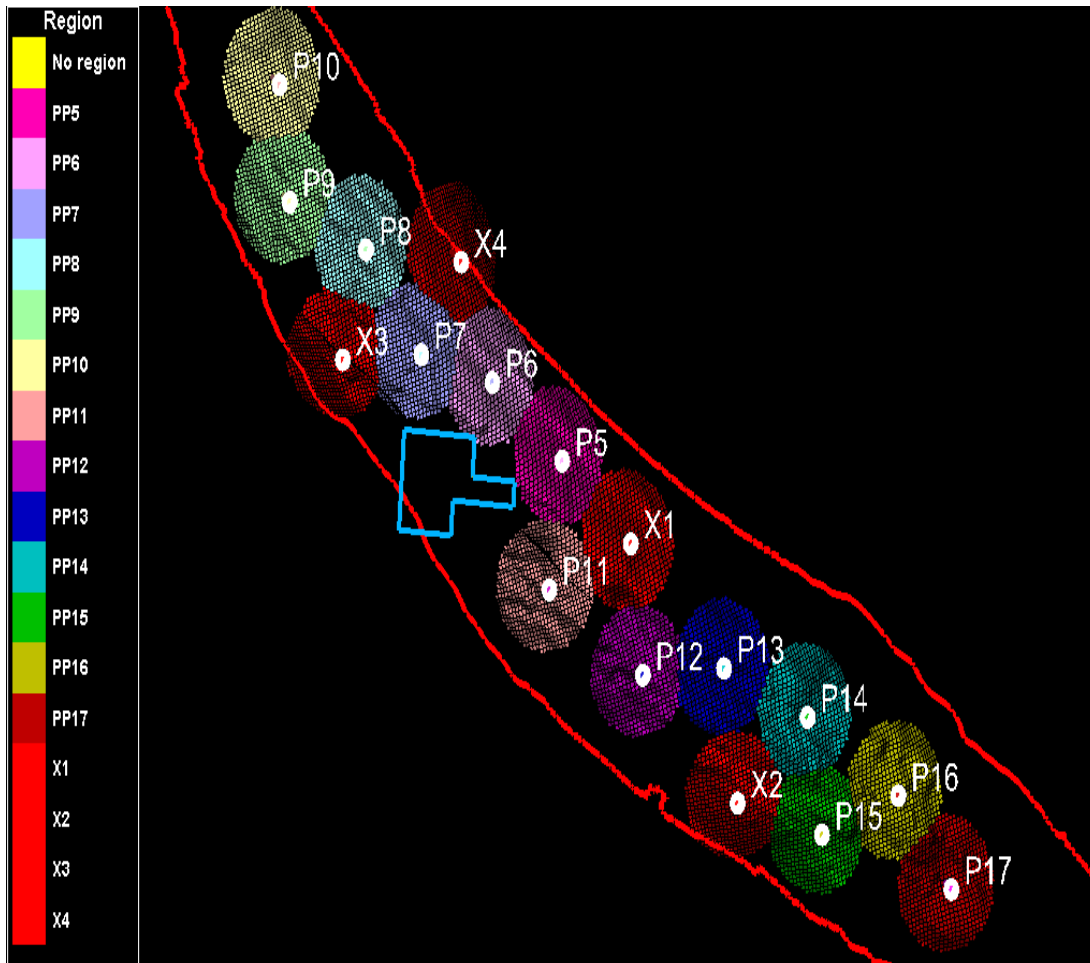


**Figure 5.33:** Proposed wells - 700m radius.

In the second case, equally well placement was made by keeping the distance as 1000 m between the wells where additional 19 wells needs to be drilled as shown in Figure 5.34. Similarly, 800 m equally spaced 31 wells proposed in the last scenario to achieve the production targets. As can be seen from Figure 5.36, additional 28 wells are required to be drilled. After running simulation with these well placement options, base case well numbers and locations are determined (see Section 5.6). Note that according to the well modeling study as discussed previously, well production targets of the each well are defined as 50 MMscf/d. Automatic well drilling command is used in ECLIPSE where the drilling queue of the proposed wells are defined and the simulator putting the next well into production from the drilling queue if the defined group production target is not achievable by the existing wells. To be able to plan the sequence of drilling campaign that needs to be applied in the field to achieve the planned production targets, automatic drilling is a good practice to show the required timing of drilling.

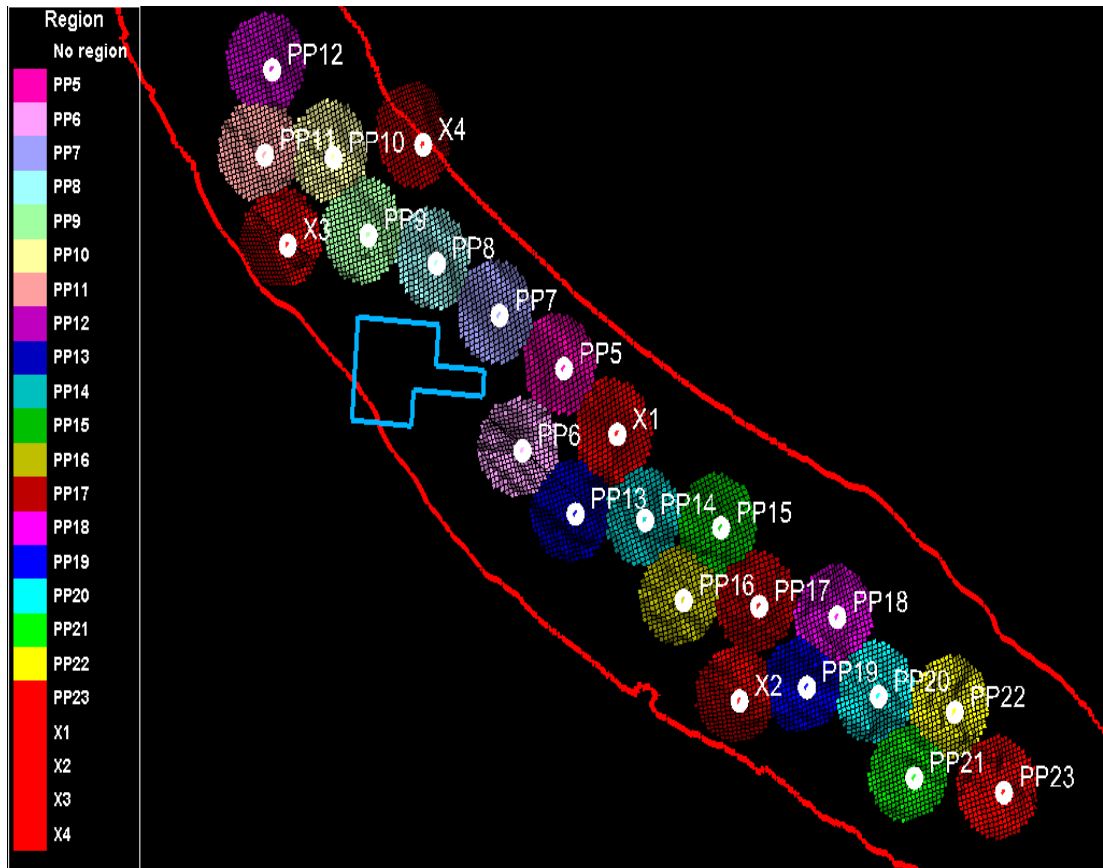


**Figure 5.34:** Proposed wells – 500 m radius.

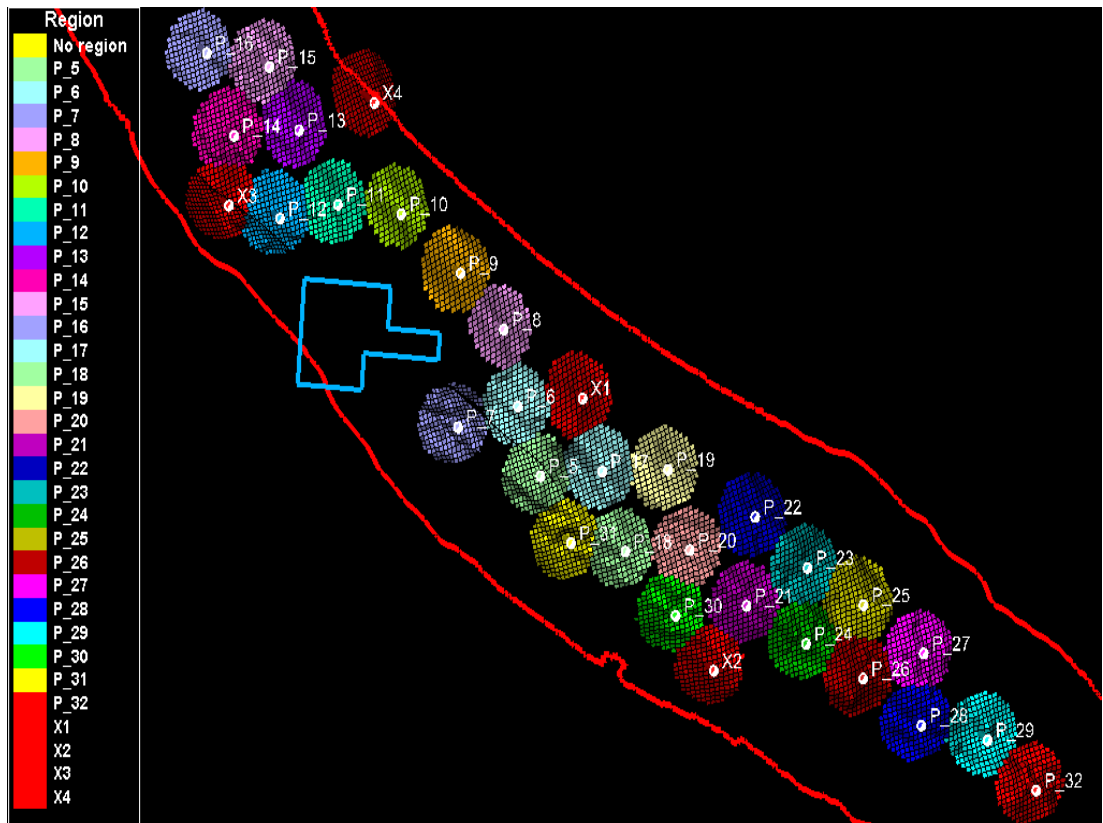


**Figure 5.35:** Proposed wells – 400 m radius.

#### **5.4.2. Well completions – base case**

No completion string is used in the base case simulation model. Therefore, open-hole well completion with zero skin assigned all of the wells. Well pressure control (limit) is defined as the bottom-hole pressure (BHP). As mentioned in Chapter 2, according to the gas processing facility design, inlet pressure of the central gas processing facility designed as 1015 psia (70 bara). The longest distance between the wells and CPF is less than 10 km. Therefore pressure loses from wells to CPF will be very less considering the distance and type of hydrocarbon (gas). Besides, as it was discussed previously, pressure loses inside the wellbore due to friction and hydrostatic head is around 600 psi. Considering all these, for the base case simulation run, well minimum bottom-hole pressure (BHP) constraint is defined as 1600 psia. However, to meet the minimum facility inlet pressure requirement, compressor can be installed in the late life of the plateau production. Thus, BHP constraint of the wells can be reduced as low as the hydrostatic head pressure. In other words, well head pressure can be reduced to zero where the BHP constraint can be defined as 600 psia.

#### **5.5. Development Strategy – Base Case**

Development strategy of a field is generally determined by considering the technical and contractual constraints. The technical and contractual constraint of the field is discussed in Section 2. Three different well placement options were considered to determine base case development strategy. To honor the technical and contractual constraints of the field, base case development strategy is defined as follows:

- Simulation commences date Jan 2016 - end date Jan 2037 (20 years contract).
- Production wells (16 wells – 1400 m equally spaced; 22 wells – 1000 m equally spaced; 31 wells – 800 m equally spaced).
- Open-hole well completion with zero skin factor,
- Early production with constant 150 MMscf/d gas rates commencing on January 2016 and maintained until the end of 2018.
- Plateau production with constant 400 MMscf/d gas rates commencing on January 2019 and desired plateau length at least 10 years.
- Minimum BHP control is 1600 psia for each of the proposed wells.
- Maximum gas production target of each individual well is 50MMscf/d.

- Minimum gas production rate (economical minimum production limit) of the each individual well is 1 MMscf/d.
- Automatic drilling from the defined wells pool and defined drilling queue which will enable us to see right time of drilling the next well and arrange drilling program accordingly.

## **5.6. Definition of Simulation Case – Base Case**

The ECLIPSE 300 compositional simulator is used to predict the reservoir performance. Constructed fine scale geological model which has approximately 8 million cells (1.9 million active cells above GWC) was up-scaled to build simulation grids geometry. As discussed, up-scaled simulation model has 55890 cells (54x69x15) where the grid size on X-Y direction is around 300m and on the z direction approximately 4 m thick. All the reservoir properties such as porosity, permeability, water saturation, and NTG which were generated in the geological modeling part were imported into simulation model. As discussed in Section 5.2, EOS model was constructed in PVTi based on well X-2 fluid sample to generate the compositional fluid model which was then imported into simulation model. Rock physics functions were generated by the Corey correlation (relative permeabilities) and Newman correlation (rock compaction) based on special core analysis data which was discussed in Section 5.3. Generated rock physics models were also imported to simulation model as well. Then well model which was discussed in Section 5.4 were used for the proposed wells. After integration all the analyzed data in simulation model, model initialized by defining the pressure and temperature at GWC as 4114 psia (well test data) and 138 F respectively.

Before running any simulation case, the model tested by the well X-2 surface production test data. Actually, using this test for calibrating/matching simulation model is very challenging and inappropriate due to several reasons. First of all, stabilization on the oil rate could not be achieved although the gas rate stable (28Mscf/d) on the conducted test. Secondly, down-hole pressure gauge was not installed in the test where the well head pressure measurements are only available. Additionally, conducted test were very short which was around seven hours. However, it is the only test data that the surface flow rates and pressure measurements were recorded together. Therefore, it was used to calibrate the model

by designing the same test in the simulation model. At the well X-2 production test, surface rates measured by separator where the average gas rate measured as 28 MMscf/d as shown in Figure 5.36. Wellhead pressure was constant throughout the test since the critical flow<sup>11</sup> is achieved between the separator and wellhead on the test. Thus, changes on flow rates have no effect on the downstream pressure. Measured wellhead pressure (2500 psia) used for the calculation of the down hole pressure. As discussed previously, the sum of the pressure losses and hydrostatic head is around 600 psi in this well which then bottom-hole pressure can be calculated as 3100 psi. As a result, to be able to simulate the test, 28 MMscf/d gas rate is defined as gas production target where the simulator calculated the bottom-hole pressure and oil rate. As can be seen from Figure 5.36, a good match on the pressure data was achieved. Besides, obtained match on the oil rate is acceptable at the beginning of the test although the measured oil rate is higher than simulated values at the last four hours of the test. Simple answer of the question why the oil rates is not matching is related with the PVT sample itself that obtained at the beginning of this test. Recombination on the surface sample was made based on sampling conditions where the condensate to gas ratio (CGR) was around 80 bbl/MMscf. Since the sampling was made at the first 3 hours of this test, measured CGR was lower than the last four hours CGR (120 bbl/MMscf). Therefore, it is obvious that calculated oil rates will be based on PVT sample obtained at the beginning of this test. However, since the stabilization in oil rates could not be achieved, nobody can guarantee that the real CGR is higher than the measured value (80 bbl/MMscf). Actually, it can be concluded that predicted oil rates will be lower than the reality if the CGR is higher than 80 bbl/MMscf. Therefore, it means that simulation model will give conservative predictions on the oil rates which is better than being optimistic. This issue was discussed in Section 3.4 but it is important to note that obtaining representative fluid sample is the key issue in the full field development for predicting the oil production correctly. Since there is only one sample that has PVT analysis which was used for this study, prediction will have to be made on this basis by putting the question mark on the oil rate predictions. It is suggested to obtain representative fluid sample to

---

<sup>11</sup> In gas flow through an orifice there is an occasion where the gas velocity reaches sonic conditions. This occurs for air flow when the absolute pressure ratio is 0.528, i.e. when the downstream absolute pressure (P2) is %52.8 of the upstream absolute pressure (P1). When the air velocity reaches sonic velocity (P2/P1 < 0.528) further increases in upstream pressure do not cause any further increase in the air velocity through the orifice. This phenomenon is called as critical gas flow.



improve the reliability of simulation model prior to start production and thus, facility can be designed accordingly to make sure facility has enough capacity to handle oil production.

Although predicted oil rates are questionable, a good match was obtained on the pressures. Since there is nothing to do in this stage for improving the quality of simulation model in terms of fluid model, constructed simulation model is used for full field reservoir performance prediction runs. Figures 5.37-5.39 are the result of the prediction runs with the 16-22-31 wells, respectively. Red colored line represents field gas production rates; light green colored line represents oil production rates; dark green colored line represents cumulative oil production; black colored line represents cumulative gas production and turquoise colored line represents the count of the number of wells flowing in the simulation model. Since the dew point pressure (3850 psia) is very close reservoir pressure (4114 psia), CGR decreases rapidly and hence oil rates starts to decrease at the beginning of the production throughout the life of the field production as it is expected.

As can be seen from the Figures 5.37-5.39, none of the case achieved to deliver desired 10 years gas plateau length. Plateau production with 400 MMscf/d maintained only 2.5 years with the simulation case run by 16 wells. On the other hand, simulation case with 22 wells improved plateau length 2 years and simulation case with 31 wells delivered 400 MMscf/d for a period of 6 years. According to contractual obligations, plateau production has to be maintained at least ten years; therefore, either the number of wells needs to be increased or gas compressors needs to be installed to decrease the BHP limit.

As can be seen from the 5.37-5.39, increasing number of wells extends the plateau length but to achieve the desired 10 years plateau, a lot of wells need to be drilled. Therefore, installing the gas compressors at 2025 to reduce the BHP limit is suggested to maintain the plateau production rather than drilling additional wells. As can be seen from the Figure 5.40, we assumed the gas compressors are online at the beginning of the 2025 and hence BHP limit lowered to 600 psia in this year which helped to maintain plateau more than 4 years. Desired 3 years early production with 150 MMscf/d and 10 years plateau with 400MMscf/d is achieved with 31 wells by installing gas compressors at 2025. It is important to note that installing gas compressors will increase the fuel gas consumption. However, considering the

advantages of the gas compressors on the field gas recovery, the gas consumption of the compressors can be neglected. The improvement on the gas recovery by the help of gas compressors is significant as can be seen from the Fig 5.40. Therefore, simulation case with 31 wells is chosen as a base case with the assumption of installing gas compressors at 2025 and the constructed simulation model will be used for applications to investigate the effects of completion (full perforation; 40m perforation); changing well locations etc. Although full field production performance is shown here, analysis on well basis on the chosen base case is made in Chapter 6.1, to see the contribution/performance of each individual wells, to investigate the wells with high water cut.

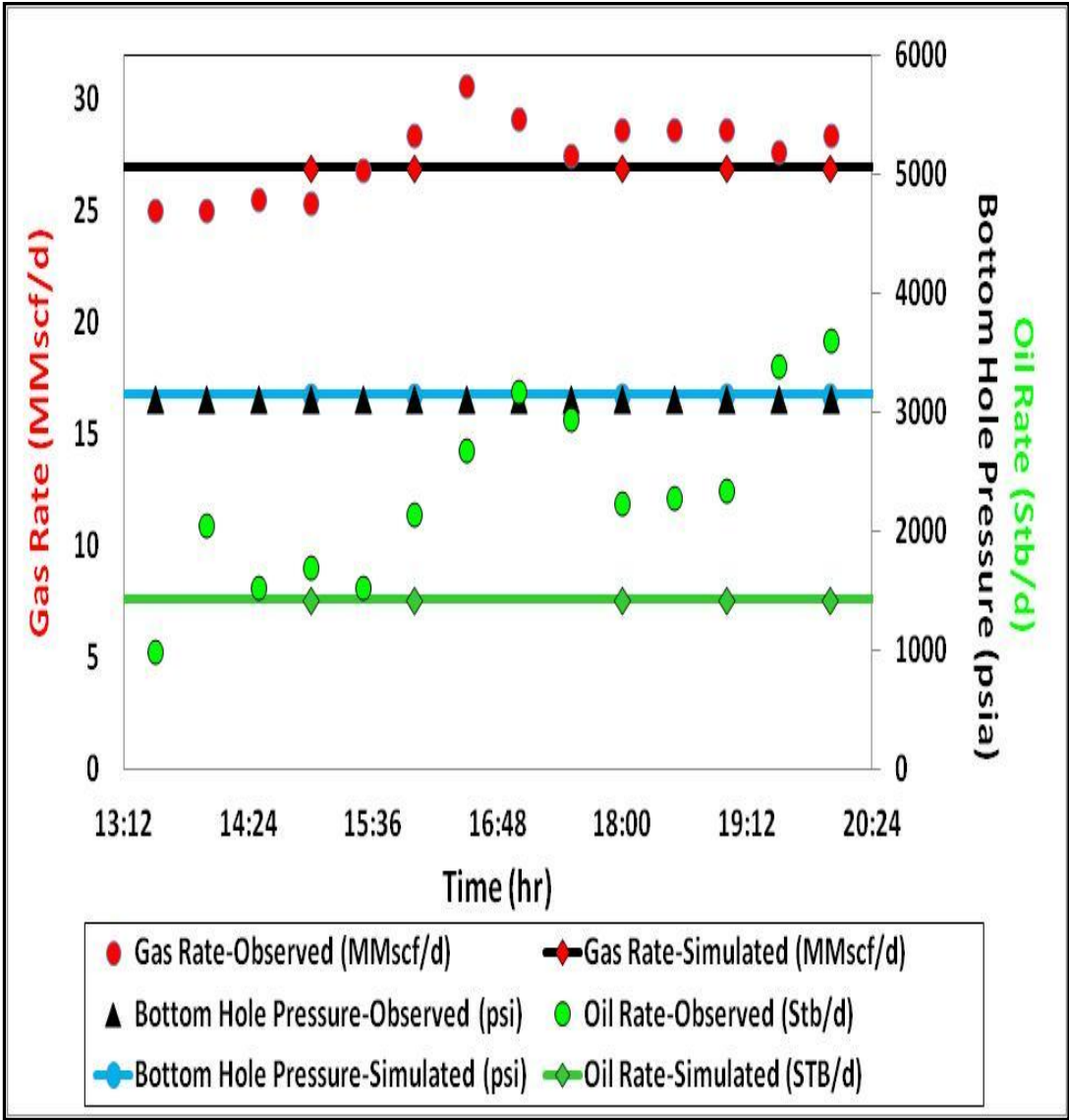


Figure 5.36: Well X-2 production test history match with simulation model.

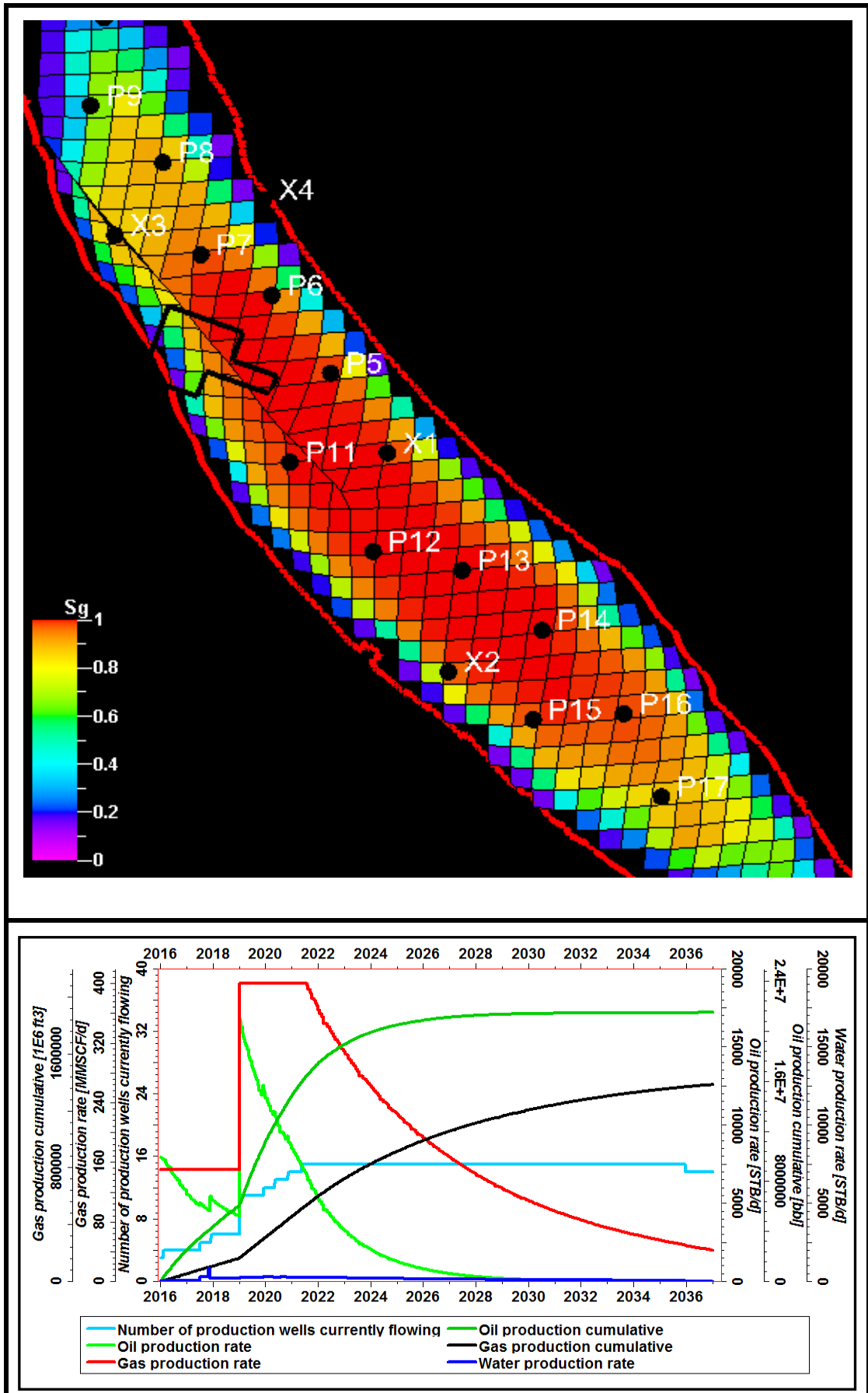


Figure 5.37: Simulation result of the base case with 16 wells.

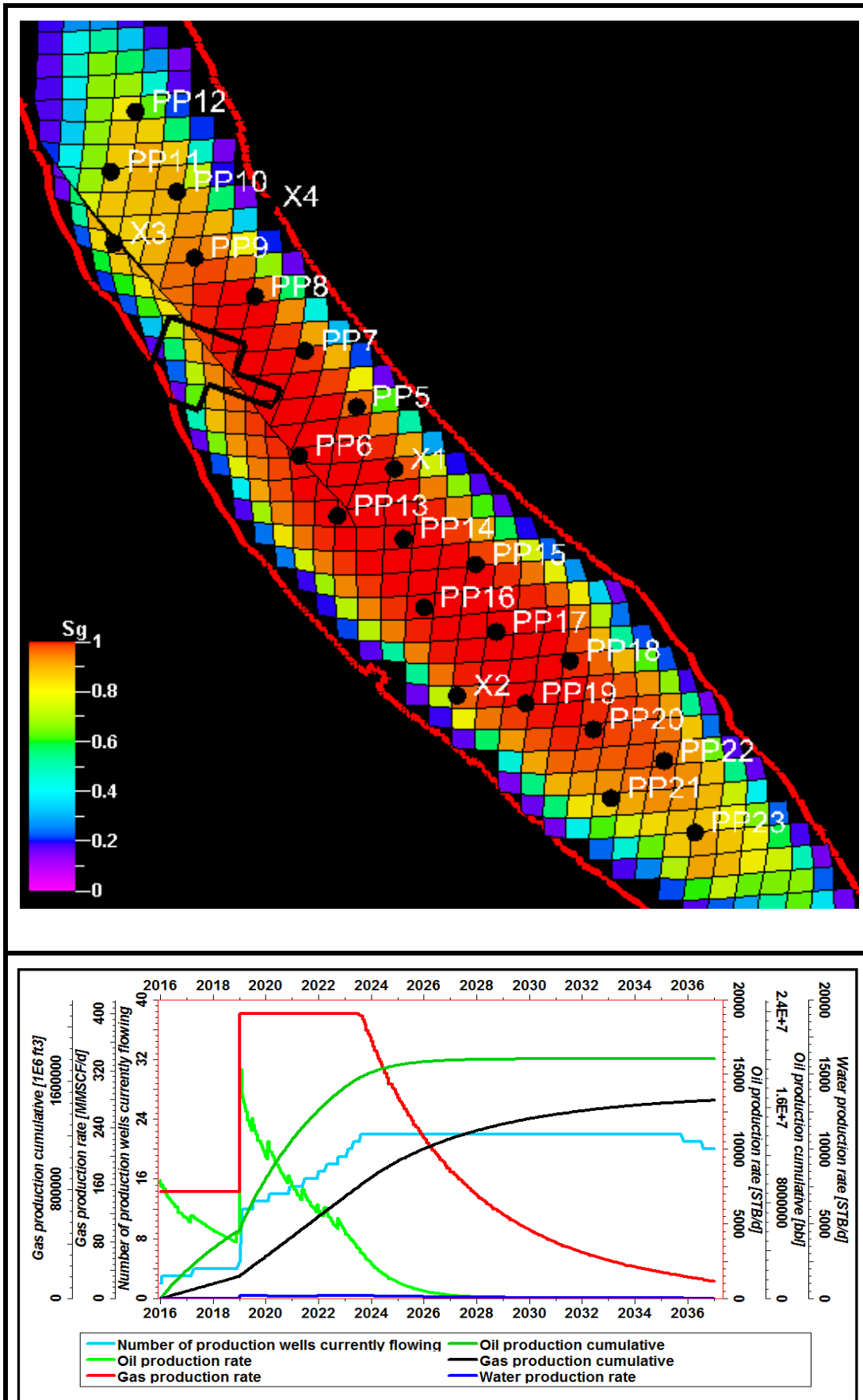


Figure 5.38: Simulation result of the base case with 22 wells.

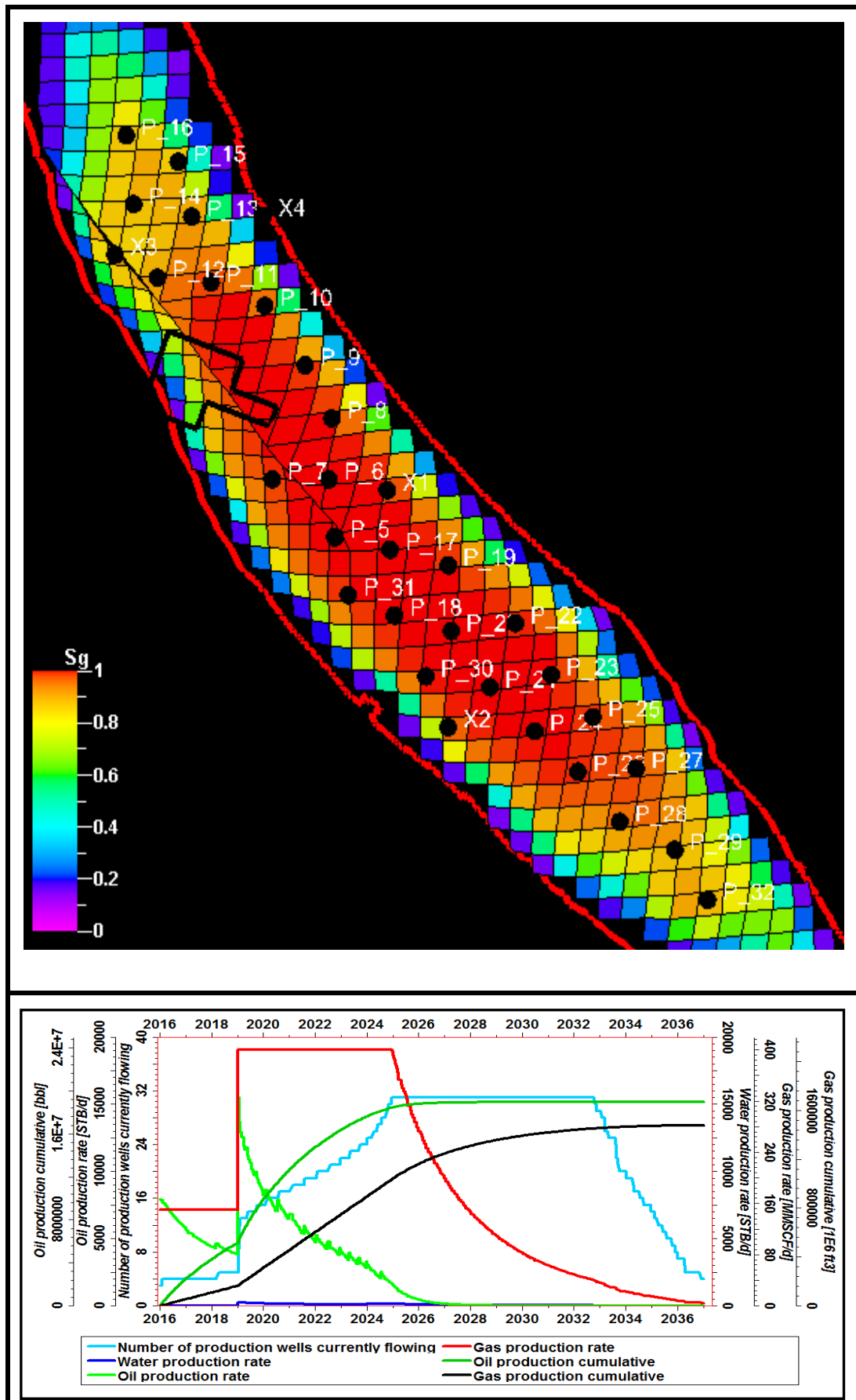
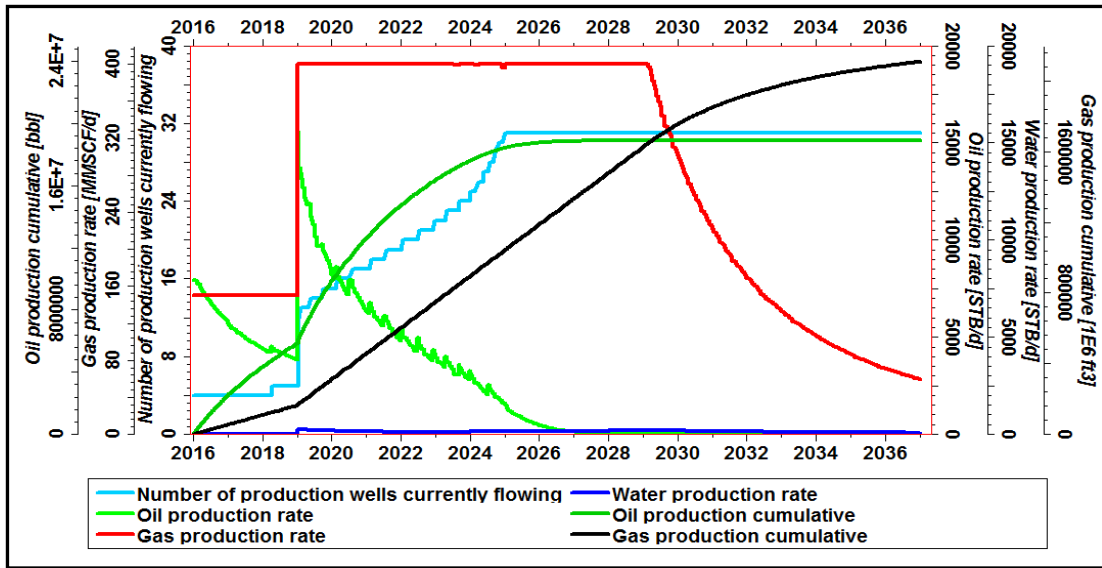


Figure 5.39: Simulation result of the base case with 31 wells.



**Figure 5.40:** Simulation result of the base case with 31 wells – gas compressors installation at 2025 (BHP limit reduced to 600psi).

## 6. APPLICATIONS

The simulation case with 31 wells assuming the gas compressor installation on 2025 gives the desired early production target (3 years constant gas production with a rate of 150 MMscf/d) and plateau production target (10 years constant gas production with a rate 400 MMscf/d). However, further analysis on the base case can give some opportunity to increase recovery from the field such as changing the well locations which are producing relatively lower gas than others and/or changing the location of wells which are producing relatively more water than others. Moreover, the effects of perforation length need to be investigated. Considering the operational difficulties of perforating high pressure gas wells, reducing the perforation length of the wells will bring considerable easiness on the operation if the reduced perforation length does not have important effect on the production. Therefore, the base case was analyzed on the well basis to determine the candidates that the location changes may have some positive effect. Then, the effects of perforation length were studied to see the impact of the perforation length on the production.

### 6.1. Analysis of Base Case

To investigate the contribution of each individual well on the field production and determine the best candidate wells that the location change may have a positive impact on field production, base case simulation results analyzed carefully. Proposed wells tried to be located on the crest of the field as much as possible by considering the constraints on the well placements such as keeping 800 m safe distance to facility, and keeping 800 m distance between each wells. Figure 6.1 is showing the height above GWC property and locations of wells. As can be seen from Figure 6.1, none of the wells were placed closer to GWC except well X-4 which is existing water leg well. Figures 6.2-6.4 show the gas production rates, cumulative gas production and water production rates of each well, respectively. As can be seen from the Figure 6.3, cumulative gas productions of the wells are varying in between  $125 \text{ bm}^3 - 35 \text{ bm}^3$ . Although all of the wells can be considered as a good producer in

terms of cumulative gas productions, some of the wells produced relatively lower gas than others. For instance, X1, X2, X3, P15, P29, and P32 are produced around 35 bcm. Since the X1, X2 and X3 are the existing wells and changing their locations is not possible, P15, P29 and P32 can be considered as a good candidate for replacing their locations to improve field production. On the other hand, as can be seen from Figure 6.3, most of the wells produced less than 5 STB/d water, although a few of the wells produced in the range of 35-40 STB/d such as P13, P14, P15, P16 and P19. It obvious that in terms of water production, none of the wells seem problematic and there is no need to replace any of the wells due to water production only.

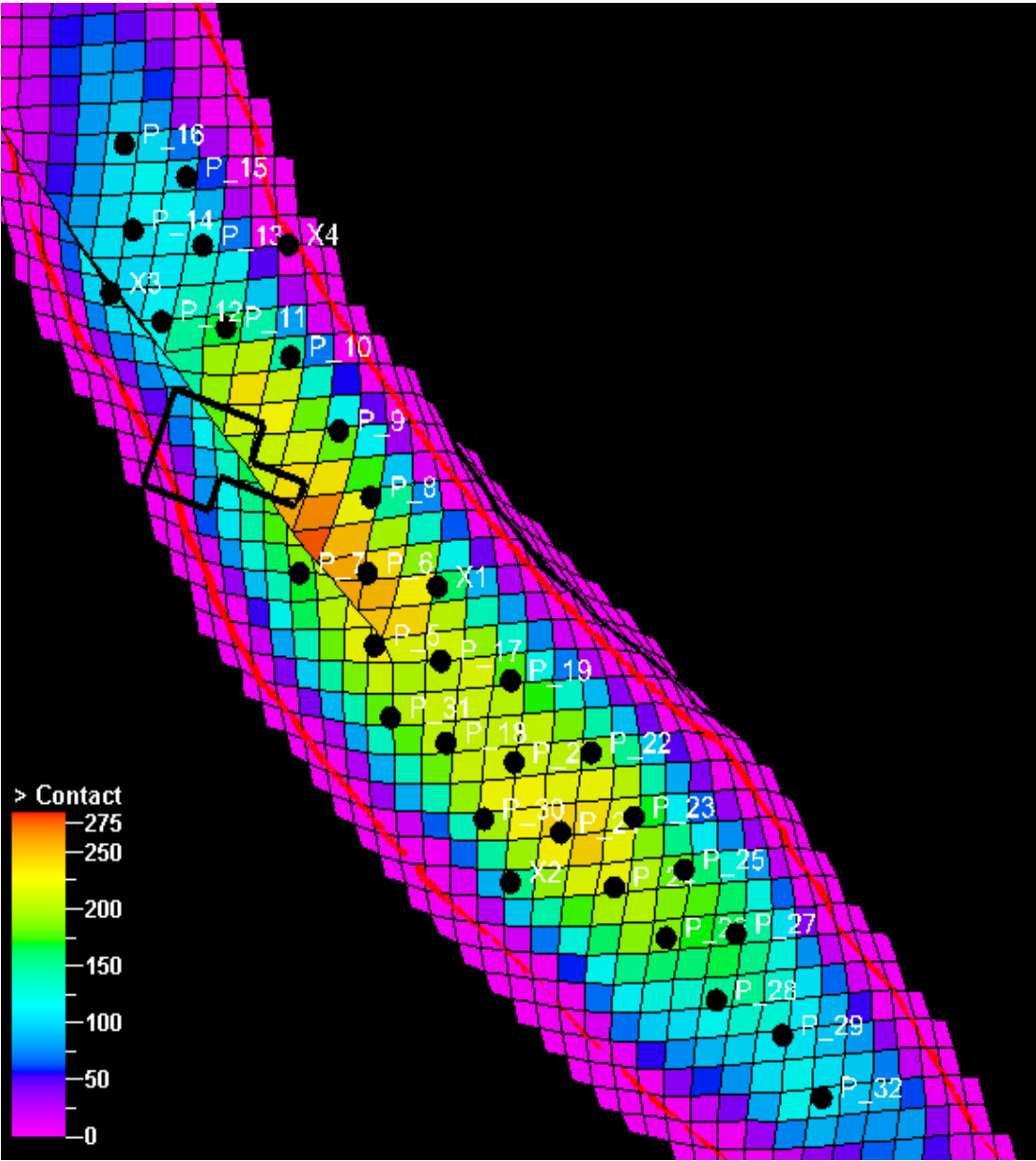


**Figure 6.1:** Height above GWC – base case well locations.



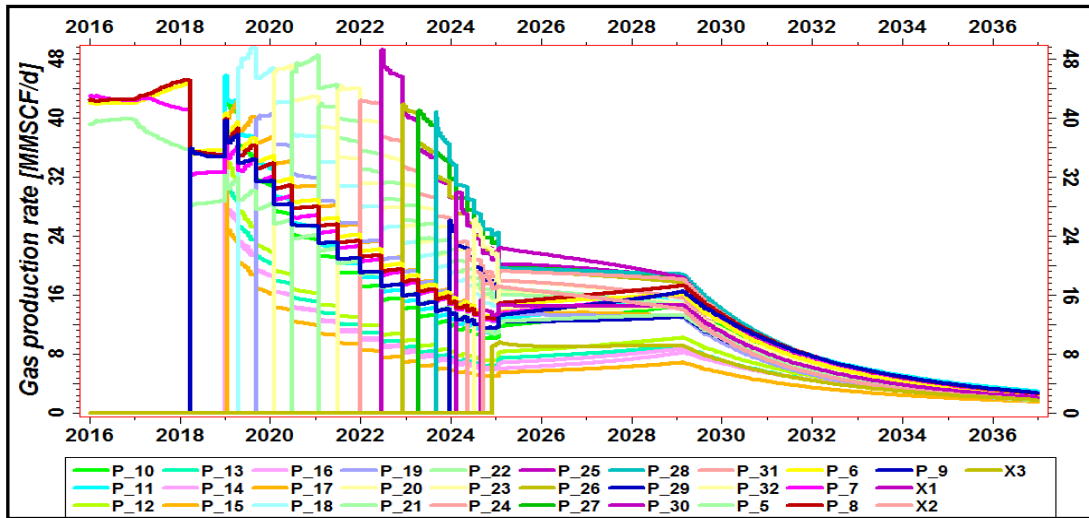


Figure 6.2: Gas productions rates of the wells.

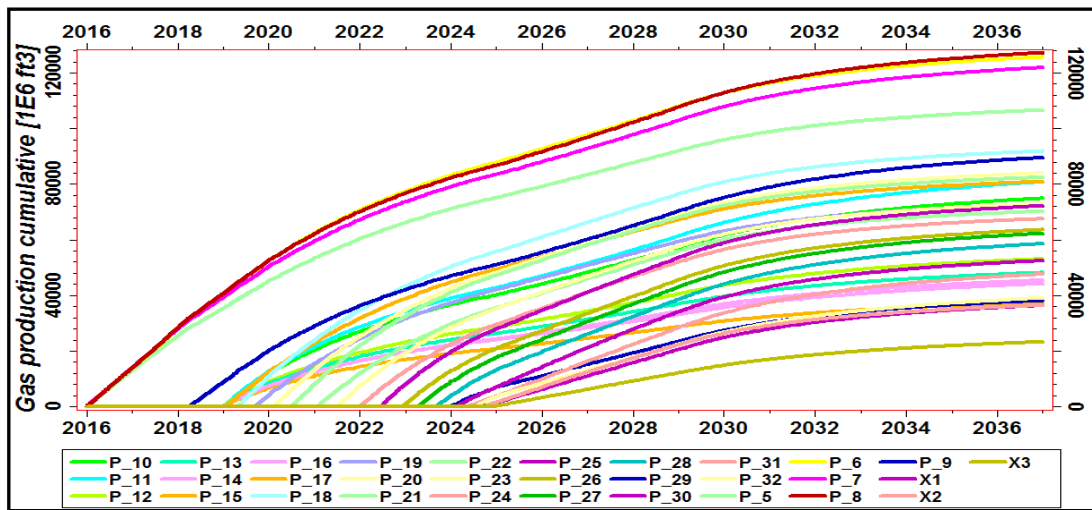


Figure 6.3: Cumulative gas production of the wells.

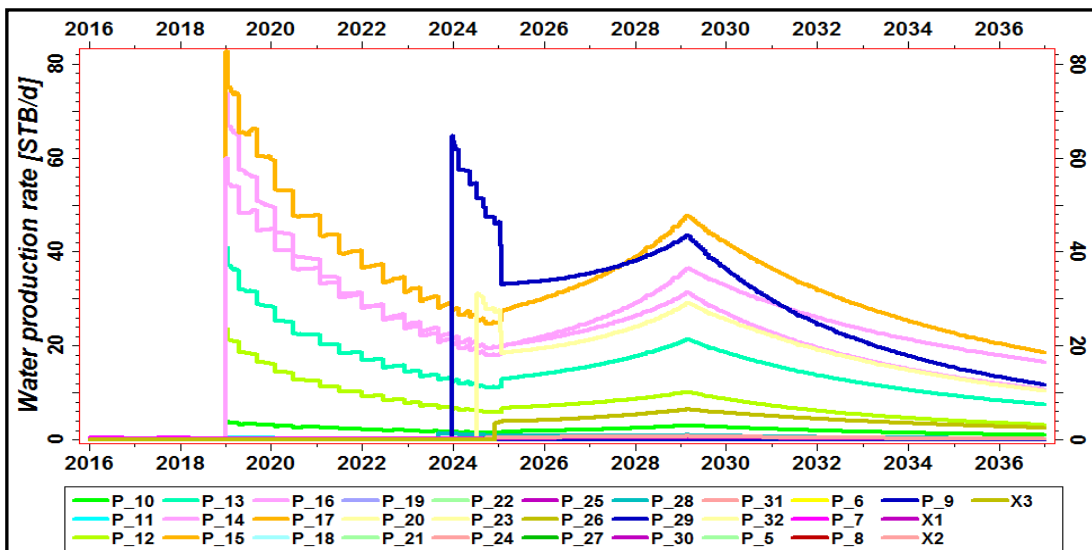


Figure 6.4: Water production rates of the wells.

In conclusion, a summary of the values of the field gas, oil, and water production is given in Table 6.1. Approximately 78% recovery was achieved by 31 wells by installing gas compressor at the beginning of 2025. Recall that dynamic model GIIP was 2.697 tcf.

**Table 6.1:** Base case - cumulative field productions.

Field Gas Production Cumulative (tcf)	Field Oil Production Cumulative (MMbbl)	Field Water Production Cumulative (STB)	Recovery Factor (%)
2.108	18.9	902,397	78

**6.2. Well Locations**

As it was discussed in Section 6.1, the proposed wells P15, P29, and P32 have lower gas productions than others. Since the wells P29 and P32 are located in the extreme south east end of the field and their locations are close to each other, we replaced only P32 to the crest and central location as shown in Figure 6.5. On the other hand, P15 was replaced from the extreme north east location to central location in between P7 and P5 as also shown in Figure 6.5. All the other well locations were kept the same to see the effects of these location changes.

After running the simulation case with the new locations of P15 and P32, no significant changes in production histories were observed. Production profiles pertinent to this case are shown in Figure 6.6. A summary of cumulative field productions is given in Table 6.2. As can be seen from Table 6.2, although the field cumulative water production was decreased more than 0.2 MMSTB, gas and oil productions decreased slightly as compared to the base case simulation result. Although further optimization cases can be studied on the well locations, it is better to wait for appraisal data campaign to improve the reliability of the simulation model and finalize the well locations by further optimization studies prior to production starts.

In conclusion, since the field is in the early life of development and the data is limited, proposed well locations are good enough based on constructed model results.

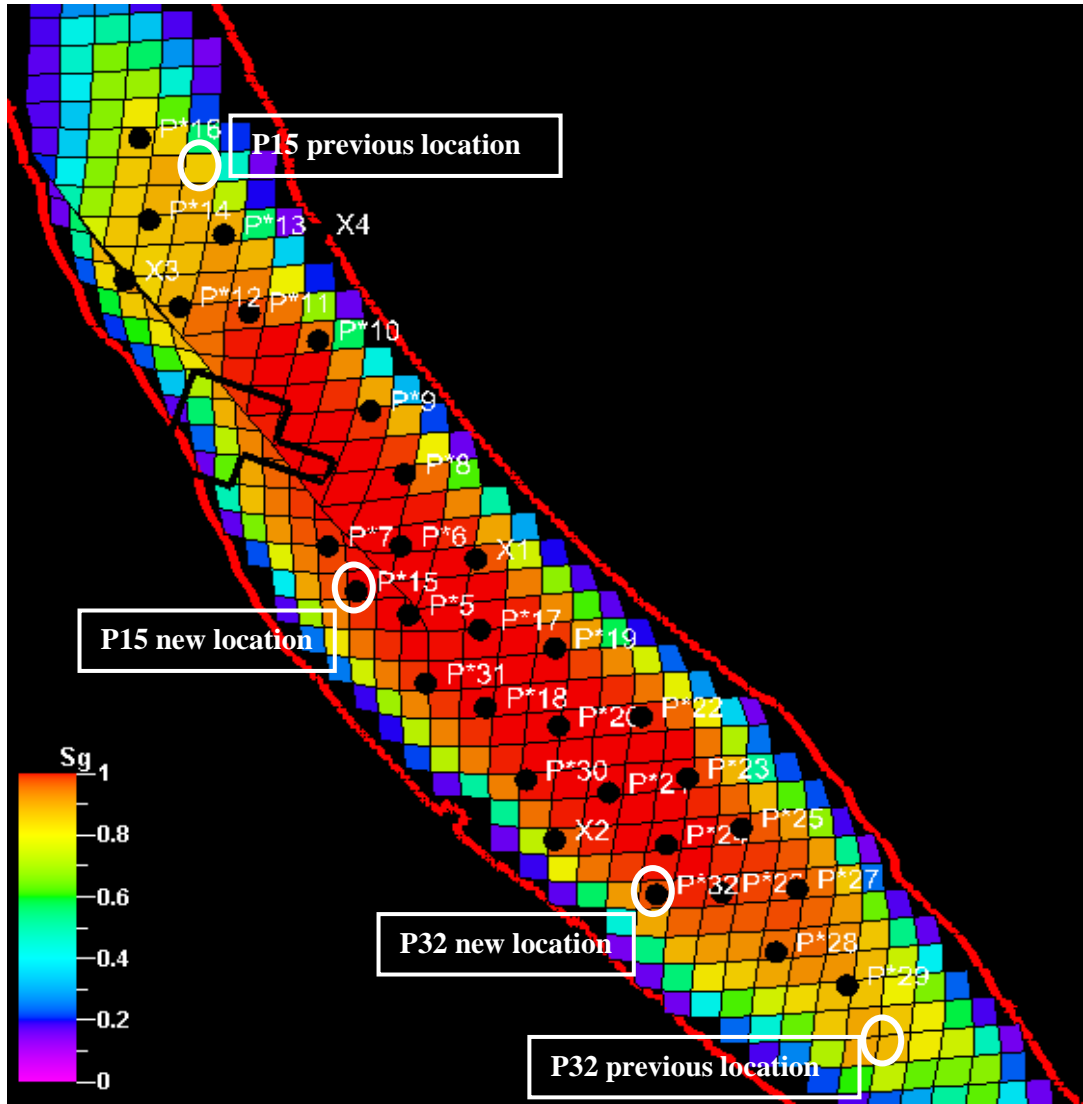


Figure 6.5: New locations of P15 and P32.

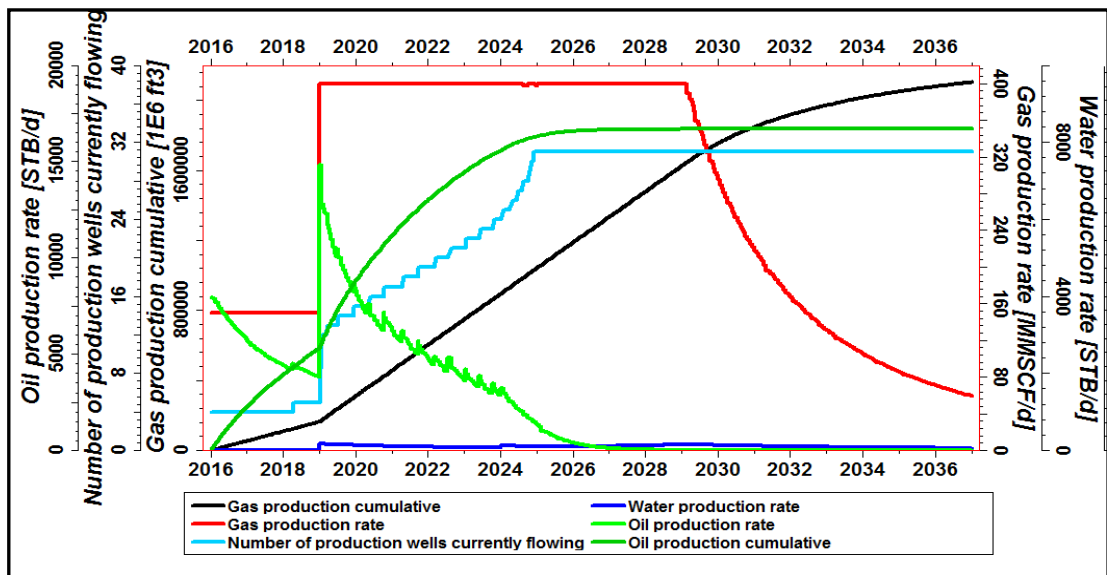


Figure 6.6: Simulation result of the base case after the replacement of P15 and P32.

**Table 6.2:** Cumulative field productions after the replacement of P15 and P32.

Field Gas Production Cumulative (tcf)	Field Oil Production Cumulative (MMbbl)	Field Water Production Cumulative (STB)	Recovery Factor (%)
2.102	18.3	669,398	78

### 6.3. Optimization of Well Completion

In the base case simulation for the simplicity we assumed that the wells are fully open to flow and zero skin: however, in reality wells will be completed as a cased hole and the wells will be perforated with the workover operation. Considering the operational difficulties associated with perforating high pressure gas wells, reducing the perforation length will be cost effective and easier if this reduction on the perforation length does not have material impact on the production of the wells. Perforating 20 m thick interval is the maximum limit of the tubing conveyed perforation operation. Therefore, if the whole interval which is approximately 60m thick needs to be perforated, three runs into hole are required. Additionally, after perforating the first interval, controlling the high pressure gas wells to perforate the second interval will be very challenging. On the other hand, reducing the perforation interval will have negative impact on the possible condensate blockage problem. In the industry, to be able to avoid such a drastic effect (condensate blockage) on the production, the used criterion as a rule of thumb is to have at least 1000 md-ft permeability thickness product. Considering the average permeability of the field is around 10-12 md and if the perforated interval has 40m (131ft) length, permeability thickness product will be around 1300 – 1500 md-ft which will not create condensate blockage problem if the rule of thumb applies. Therefore, to see the impact of reducing the length of perforations, all the wells completed as a cased-hole and upper 40m is perforated. Figure 6.7 is an example completion that performed for all the wells. As can be seen from Figure 6.8, reducing the perforation interval has big impact on the production. Before 2024, plateau production starts to decline since the field pressure hit the minimum BHP limit. Although gas production resumes the plateau production target with the installation of gas compressors at 2025, it remains in the plateau until the year 2028. It means that gas compressors need to be online

after 2023. Even the gas compressors installed in 2023, maintaining the desired 10 years plateau will not be achievable by perforating 40m interval. Table 6.3 gives a summary of the cumulative field productions for this case. To sum up, it is suggested to perforate the whole formation although it has mentioned operational difficulties.

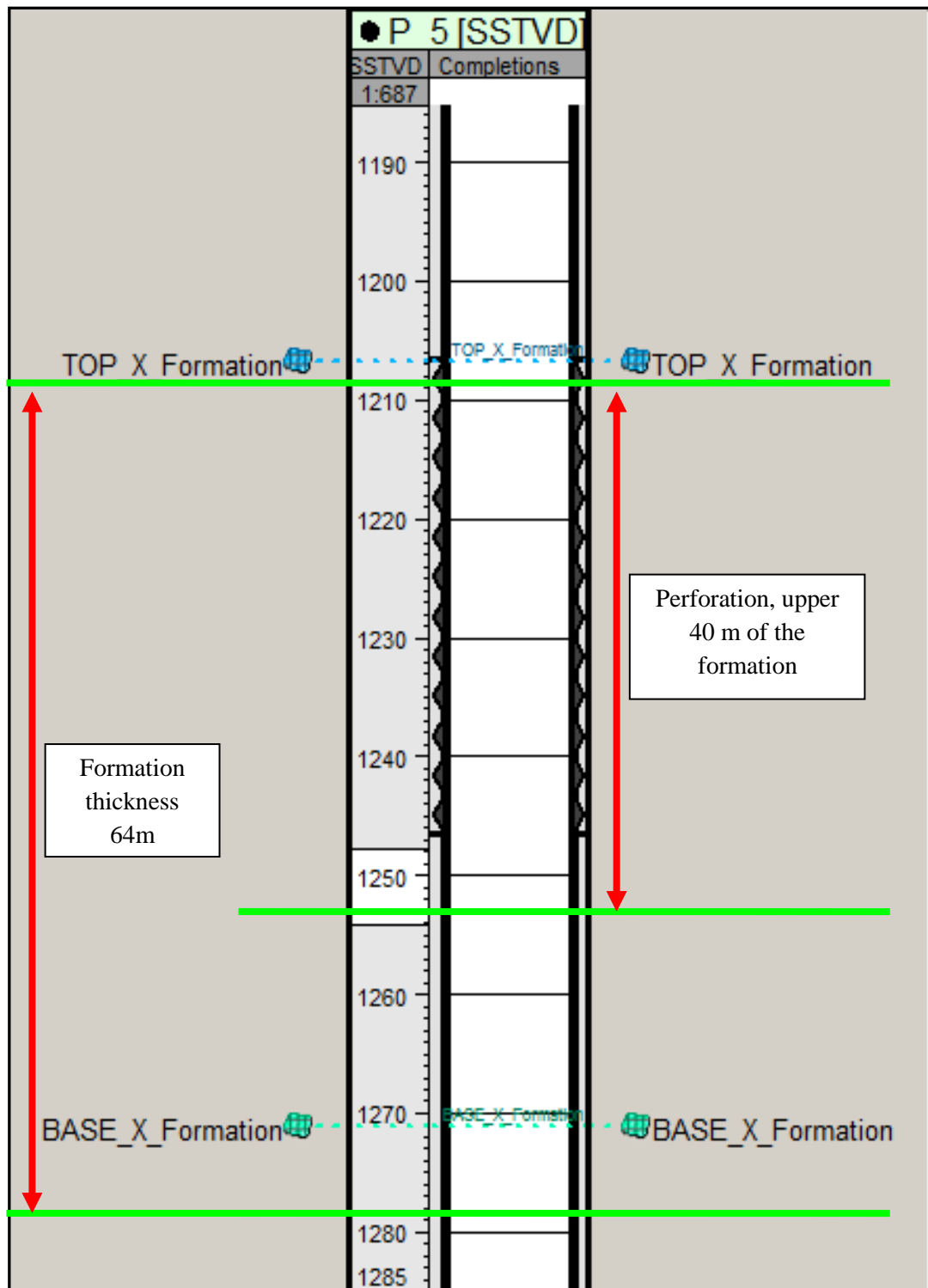
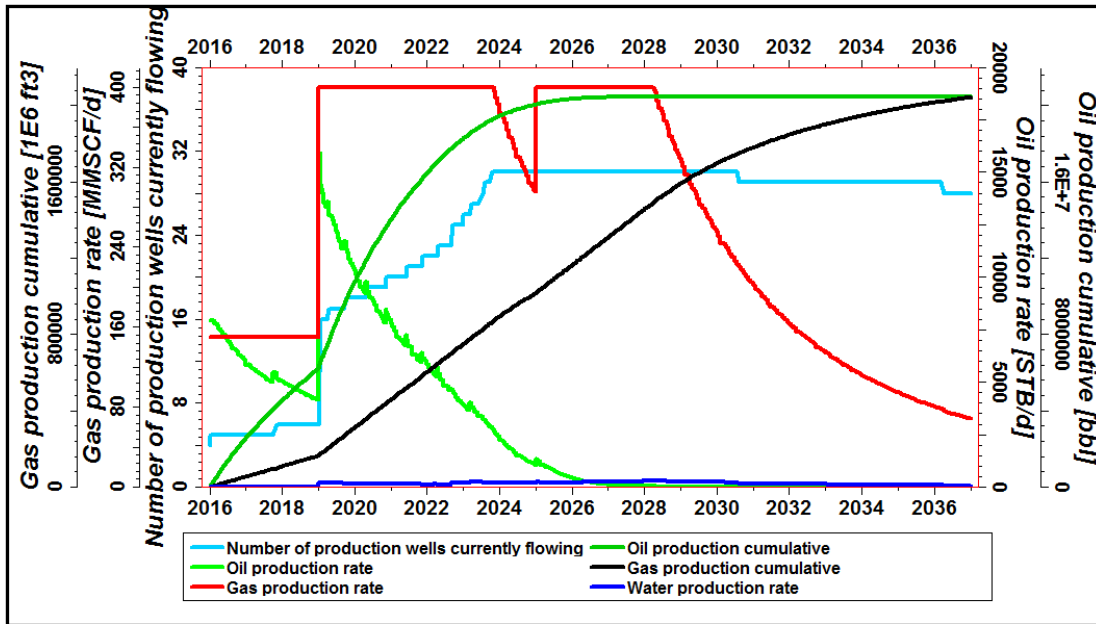


Figure 6.7: Well completion of well P5.



**Figure 6.8:** Simulation result of the base case with 40m perforation.

**Table 6.3:** Cumulative field productions the case 40m perforation.

Field Gas Production Cumulative (tcf)	Field Oil Production Cumulative (MMbbl)	Field Water Production Cumulative (STB)	Recovery Factor (%)
2.042	20.5	571,175	76

## 7. CONCLUSIONS

### 7.1 Concluding Remarks

All the available data collected from the field until now such as 2D-3D seismic, core, well-log, well-test, and PVT were reviewed carefully and used for reservoir characterization purposes.

3D reservoir modeling (fine-scaled geo-cellular model) was constructed with PETREL by using all the available data that fit for study purposes. Structure shape and boundaries were defined by the formation top and base surfaces that interpreted from 2D-3D seismic. Similarly the faults were modeled by using fault sticks which were also obtained from seismic data. While creating a 3D geological grid, the most important goal is to preserve the small features from well logs and seismic data as much as possible. Therefore, a 50m grid-size was used in X and Y directions and the formation was divided into four major zones which were further divided into a total of 30 sub-layers not to lose well-log resolution. Reservoir property distribution/modeling was made by using core, well-log and well-test data by constructing variogram model for each of the property that matched with experimental data. Fluid contact was determined by using well-test pressure data and gas-water pressure gradient that calculated based on PVT data. Gas initially in place was calculated as 2.686 tcf on the fine scale geo-cellular model.

Level of uncertainty on the constructed geo-cellular model was assessed by defining +/-5% uncertainty range on the reservoir properties and defining min/max GWC as 1390-1502 mss. 100 realizations were run with Monte Carlo Sampler by using the ranges given above for calculating GIIP. Probabilistic P10, P50, and P90 were calculated as 3.609 tcf, 2.937 tcf, and 2.369 tcf, respectively.

The number of grids in geological model is often exceeding the capabilities of standard reservoir simulators and requires huge computational powers to run. Therefore, reservoir descriptions made by fine scale geo-cellular model has to be coarsen (up-scaled) to the scales that are suitable for flow simulation. Therefore,

considering the computational capability of computer that used for this study, the geological model up scaled to a scale that computer used for this study can handle. The size of the cells in the model increased to 300 m in the X and Y direction which was 50m in the geo-cellular model. Additionally, vertical resolution of the reservoir is represented with four main zones and 30 sub-layers in the geological model which was reduced to 15 layers in the up scaled model.

Compositional fluid model was preferred for characterization of the reservoir fluid considering the fact that reservoir is supercritical gas condensate reservoir where the dew point pressure is very close to the reservoir pressure. To be able to determine the physical properties of mixtures as a function of pressure and temperature and the properties of the individual components, an equation of state (EoS) model was used. In this study, recent sampling data from well X-2 were used as input for EoS modeling because this is the only sample that has laboratory measurements although it is a surface sample and recombined for the PVT analysis. Since the recent well X-2 sample is the most recent and the most reliable data on hand in terms of PVT data, it was used for fluid characterization and analyzed in detail to create PVT tables for simulation. To construct and tune the EoS model PVTi (Schlumberger, version 2011.1) is used. Best fits with the laboratory experimental observation and calculations were obtained with “3-Parameter Peng-Robinson” correlation for EoS model and “Lohrenz-Bray-Clark” correlation for viscosity model. Constructed fluid model in PVTi was exported as a compositional fluid model that is compatible with ECLIPSE 300 compositional simulator to generate the compositional PVT tables in the simulator.

The well-known Corey correlation was used to obtain two-phase relative permeabilities based on available core data. There are no three-phase relative permeability measurements on the available cores from the field. Therefore, after obtaining two-phase relative permeabilities for water-oil and gas-oil systems, these two sets of relative permeability data were then used for the calculation of 3-phase relative permeabilities. Although there are many approaches suggested in literature for calculation of three-phase relative permeabilities such as the Stones’s first model, the Stone’s second model (modified), the IKU method, the Baker method, and the ODD3P method, the default model of ECLIPSE for obtaining three-phase relative



permeabilities from two-phase relative permeability models was used for the calculation. On the other hand, there are no reliable capillary pressure measurements because the maximum applied pressure in laboratory tests is around 60 psi which is lower than the minimum calculated capillary pressure. Considering the stratigraphically deepest gas (1391m) producing from the Well X-3, minimum capillary pressure at the base of the formation at reservoir conditions was calculated as 74.78 psia. Similarly, maximum capillary pressure at the top of the formation (1265m) at reservoir conditions was calculated as 211.34 psia. Then capillary pressure versus water saturation curve was obtained based on this calculation which is then imported to the simulator. Additionally, rock compaction was modeled with Newman Correlation based on porosity data, minimum pressure (40 bar), maximum pressure (400 bar) and reference pressure (283 bar).

A single-branch well model was constructed in PIPESIM to be able to determine the inflow performance of the wells to be used in simulation. Maximum gas production rate target was defined as 50 MMscf/d for each of the well in the base case simulation model based on constructed model outputs. On the other hand, nodal analysis was performed to determine the optimum tubing size. Therefore, several sensitivity cases simulated based on different tubing diameters (3", 3.5", 4.5", and 7" tubing). Inflow and outflow curves were plotted for each of the tubing size and optimum tubing size were determined as 4.5" tubing.

To be able to produce the desired 150 MMscf/d gas for three years and 400 MMscf/d plateau for ten years, 31 vertical wells which are 800 m equally placed were proposed as a base case. The minimum BHP control was defined as 1600 psia for each of the proposed wells. Maximum gas production target of each individual well was determined as 50MMscf/d where the minimum gas production rate (economical minimum production limit) of the each individual well was defined as 1 MMscf/d. To be able to maintain the desired 10 years plateau length, installation of gas compressors at 2025 was suggested.

The ECLIPSE 300 compositional simulator was used to predict the reservoir performance. A very good match on the gas initially in place (GIIP) calculation of the fine scale geocellular model (2.686 tcf) and dynamic reservoir model (2.697 tcf)

was obtained. Approximately 78% recovery was achieved by drilling 31 wells and installing gas compressors at the beginning of 2025.

### **7.3 Recommendation for Future Works**

Here recommendations are given for the field considered in the study. Although the name of the field was not revealed to the readers, the recommendations given here will be useful and can be considered by those conducting similar simulation and reservoir development strategies for their specific fields.

As to the field, the structural uncertainty was less since 2D and 3D seismic covered almost the whole structure. Therefore, no further seismic activities are recommended rather than calibrating constructed surfaces by the well data that will be available after drilling a new appraisal and/or development wells.

Although there are four wells drilled in the field none of them tested GWC. The stratigraphically deepest gas reading (gas down to – GDT) from the formation was observed from well X-3 which was 1391 mss. On the other hand, water was tested from well X-4 and the shallowest water (water up to – WUT) reading was 1502 mss. Therefore, there is no information in between 1391 mss to 1502 mss. Although GWC was determined as 1460 mss according to the pressure test data, there is a significant possibility to have 20-30m oil rim in the formation. The biggest uncertainty in the field is unknown GWC and/or possibility of having oil rim. Therefore, drilling a appraisal well/wells on the flank of the field is strongly recommend to explore the interval of 1391mss-1502mss. Having 20-30 m thick oil column will have material impact on the development strategies of the field such as targeting to produce oil first by keeping the gas production as low as possible to be able to keep the reservoir energy, drilling the wells on the flank of the field rather than drilling on the crest, resizing the facility accordingly, and perforating the intervals where the oil is exist etc. Therefore, it is strongly suggested to obtain appraisal data prior to making any major decision on the field development.

Although there is no direct information about the existence of the fractures, most probably formation has natural fractures considering the mud loses occurred in the drilling operations and observed permeability differences in between the PTA and core derived permeabilities. Formation was treated as a single porosity reservoir in

this study due to lack of information: however, it is suggested to acquire relevant data sets for fracture characterization and in situ stress model such as core, fracture logs, production logs, borehole image logs, extended well test, formation integrity test, and drilling records (mud losses) etc. To be able to construct reliable discrete fracture network model those data suggested to be collected at least upcoming five wells.

Significant permeability improvement was interpreted from the well X-2 test data collected after the second acid job which could be indication of chemical reaction between acid and reservoir rock and/or wrong rate measurement on the conducted test. This issue needs to be investigated by conducting long term well test and conducting special laboratory test to see the interaction of the acid and reservoir rock.

Another major uncertainty on the field is the fluid characteristics where the information is very limited in terms of PVT data. Therefore, it is strongly suggested to obtain single phase pressurized reservoir fluid sample from at least two wells and conduct regular PVT experiments on the collected samples to be able to make robust fluid model. It is also strongly suggested to design facility after fully characterizing the reservoir fluid to avoid any kind of sizing problems that may be occurred if the facility is designed based on current fluid data.

Special core analysis from the existing for wells for obtaining the robust relative permeability and capillary pressure data are very limited. Therefore, it is suggested to perform special core analysis test on the cores that collected at least from 3 different locations to be able to model rock physics functions to the full extend.

There is no information available about the existence and strength of the aquifer. Since reservoir is bounded from both side in the direction of SE-NW with major faults and reservoir is significantly overpressure reservoir, we assumed that there is no active aquifer in the field. However, data need to be collected from the field to investigate the existence and strength of the aquifer.

Further optimization studies are suggested to be conducted on the well locations after updating simulation model based on collected datasets from the field in the appraisal phase.



## REFERENCES

- Agarwal, R. G.** (1980). A New Method to Account for Producing Time Effects When Drawdown Type Curves are Used to Analyze Pressure Buildup and Other Test Data". Presented at the 55<sup>th</sup> Annual Fall Technical Conference and Exhibition of the Society of Petroleum Engineers of AIME, Dallas, Texas, September 21-24, Paper SPE 9289.
- Ahmed, T.** (2001). *Reservoir Engineering Handbook*. 2nd edition, Butterworth-Heinemann, Gulf Professional Publishing.
- Al-Hussainy, R., Ramey H.J. and Crawford P.B.,** (1966). The Flow of Real Gases Through Porous Media. *J. Pet. Technol*, 18 (5), 624-634.
- Arbogast, T. and Bryant, S.L.** (2001). "Numerical Subgrid Up Scaling for Waterflood Simulations. Paper SPE 66375 presented at the SPE Reservoir Simulation Symposium, Houston, 11-14 February.
- Aziz, K. and Settari, A.** (1979). *Petroleum Reservoir Simulation*. London: Applied Science Publishers Ltd.
- Bourdet, D., Ayoub J.A. and Pirard Y.M.,** (1989). "Use of Pressure Derivative in Well-Test Interpretation". *SPE Formation Evaluation* 4(2), 293-302.
- Bourdet, D.** (2002). *Well Test Analysis: The Use of Advanced Interpretation Models*. Boston: Elsevier Science.
- Brooks, R.H. and Corey, A.T.** (1966). Properties of Porous Media Affecting Fluid Flow. *J. Irrigat. Drainage Div.*, Proc. ASCE: 92, No. IR2, 61.
- Caers, J.** (2005). *Petroleum Geostatistics – An Interdisciplinary Approach to Topics in Petroleum Engineering and Geosciences*. Richardson, TX, USA, Society of Petroleum Engineers.
- Christoforos, B. and Dario, V.** (2010). Fully Integrated Hydrocarbon Reservoir Studies: Myth or Reality? *American Journal of Applied Sciences* 7 (11), 1477-1486.
- Darman, N.H., Pickup G.E. and Sorbie K.S.** (2002). A Comparison of Two-Phase Dynamic Up Scaling Methods Based on Fluid Potentials. *Computational Geosciences* 6 (2002), 5-27.
- Durlofsky, L.J.** (1998). Coarse Scale Models of Two Phase Flow In Heterogeneous Reservoirs: Volume Averaged Equations and Their Relationship to Existing Up Scaling Techniques. *Computational Geosciences* 2 (1998), 78-92.
- Durlofsky, L.J.** (2002). Upscaling of Geological Models for Reservoir Simulation: Issues and Approaches, *Computational Geosciences* 6 (2002), 1-4.

- Durlofsky, L.J.** (2005). Upscaling and Gridding of Fine Scale Geological Models for Flow Simulation, paper presented at the 8<sup>th</sup> International Forum on Reservoir Simulation Iles Borromees, Stresa, Italy, June 20-24.
- Eclipse 2009.1.** *Schlumberger Reservoir Simulation Software Manuel*, USA.
- Ecrin 4.02.04**, (2007). *Kappa Engineering Sophia Antipolis*, France.
- Elena, M., Leticia R.B., Guilermina S., Anthony R.T., Marta V. and Jose L. M.** (2012). 3D Static and Dynamic Modeling of a Carbonate Reservoir: Case Study from the Lower Cretaceous La Tosca Unit (Neuquen Basin, Argentina). *Search and Discovery Article*, 50699.
- Ertekin, T., Abou-Kassem, J.H., and King, G.R.** (2001). *Basic Applied Reservoir Simulation*. SPE Text Book Series Vol. 7. Richardson, TX, USA, Society of Petroleum Engineers.
- Etherington, J., Pollen T. and Zuccolo L.** (2005). *Comparison of Selected Reserves and Resource Classifications and Associated Definitions*. Oil and Gas Reserves Committee, OGRC, "Mapping" Subcommittee Final Report, SPE.
- Feigl, A.**, (2011). Treatment of Relative Permeabilities for Application in Hydrocarbon Reservoir Simulation Model. *Nafta* 62(7-8) 233-243.
- Hamid, R. Samadi and Mohammad, H. S.** (2013). Static 3D Modeling of Hydrocarbon Reservoir with the Help of RMS Case of Studies: The South East Anticline of Khuzestan Iran. *World Applied Science Journal* 27 (6), 709-713.
- Honarpour, M., Koederitz, L. and Harvey, A. H.** (1987). *Relative Permeability of Petroleum Reservoirs*, Boca Raton, Florida: CRC Press.
- Isaaks, H.E. and Srivastava, R.M.** (1989). *An Introduction to Applied Geostatistics*. London: Oxford University Press..
- Journel, A.G.** (1978). *Mining Geostatistics*. London: Academic Press Inc.
- Kelkar, M. and Perez, G.**, (2002). *Applied Geostatistics for Reservoir Characterization*. SPE. ISBN: 978-1-55563-095-9.
- Larisa, V.B., Sartaj S.G., Stephen L.L. and Xiao H.W.** (2008). Challenges and Technologies in Reservoir Modeling. *Communications in Computational Physics* 6(1), 1-23.
- Lukumon, A., Njoku O., Olawale O., Julius F. and Musa B.** (2014). Static Reservoir Modeling Using Well Log and 3D Seismic Data in a KN Field, Offshore Niger Delta, Nigeria, *International Journal of Geosciences*. 5 (1), 93-106.
- Mattax, C.C. and Dalton, R.L.**, (1990). *Reservoir Simulation*, SPE Monograph Series Vol. 13, Richardson, TX, USA: Society of Petroleum Engineers.
- Newman, G.H.** (1973). Pore Volume Compressibility of Consolidated, Friable, and Unconsolidated Reservoir Rocks under Hydrostatic Loading, *Journal of Petroleum Technology*. 35(3), 139-134.

- Oliver, D.S., Reynolds, A.C., Liu, N.,** (2008). *Inverse Theory for Petroleum Reservoir Characterization and History Matching*. Cambridge, UK, Cambridge University Press.
- Onur, M. and Saddique, A.M.** (1999). Comparison of Derivative Algorithms Used In Pressure Transient Analysis. *The Arabian Journal for Science and Engineering*, 24(1B), 59-78.
- PETREL 2012.3.** (2012). *Schlumberger Geological Modeling Software Reference Manuel*. TX, USA.
- PVTi 2011.1.** (2011). *Schlumberger EoS Modeling Software Reference Manuel*. TX, USA.
- Remy, N., Boucher, A. and Wu J.** (2009). *Applied Geostatistics with SGeMS, A User's Guide*, Cambridge University Press, UK. ISBN 978-0-521-51414-9.
- Rey, J. and Galeotti, S.,** (2008). *Stratigraphy: Terminology and Practice*, Editions OPHRYS. ISBN 9782710809104. Retrieved 28 January 2013.
- Yugi, D., Bolaji, O.B. and Dacun L.** (2004). Literature Review on Methods to Obtain Relative Permeability Data, presented in the 5<sup>th</sup> Conference & Exposition on Petroleum Geophysics. Hyderabad, India.





## **APPENDICES**

### **APPENDIX-A PVTi Fluid Model**

## APPENDIX-A

Components	Mol weight	Crit Pres (psi)	Crit Temp (F)	Omega A	Omega B
H2S	34.076	1296.2	212.81	0.45724	0.077796
CO2	44.01	1071.3	88.79	0.45724	0.077796
N2	28.013	492.31	-232.51	0.45724	0.077796
C1	16.043	667.78	-116.59	0.45724	0.077796
C2	30.07	708.34	90.104	0.45724	0.077796
C3	44.097	615.76	205.97	0.45724	0.077796
IC4	58.124	529.05	274.91	0.45724	0.077796
NC4	58.124	550.66	305.69	0.45724	0.077796
IC5	72.151	491.58	369.05	0.45724	0.077796
NC5	72.151	488.79	385.61	0.45724	0.077796
C6	84	436.62	453.83	0.45724	0.077796
C7	96	426.18	526.73	0.45724	0.077796
C8	107	417.66	575.33	0.45724	0.077796
C9	121	381.51	625.73	0.45724	0.077796
C10	134	350.94	667.13	0.45724	0.077796
C11+	182	285.05	785.13	0.44848	0.077796

Components	Acentric Factor	Parachors	V critic	Z critic	V crit (visc)
H2S	0.1	80	1.5698	0.28195	1.5698
CO2	0.225	78	1.5057	0.27408	1.5057
N2	0.04	41	1.4417	0.29115	1.4417
C1	0.013	77	1.5698	0.28473	1.5698
C2	0.0986	108	2.3707	0.28463	2.3707
C3	0.1524	150.3	3.2037	0.27616	3.2037
IC4	0.1848	181.5	4.2129	0.28274	4.2129
NC4	0.201	189.9	4.0847	0.27386	4.0847
IC5	0.227	225	4.9337	0.27271	4.9337
NC5	0.251	231.5	4.9817	0.26844	4.9817
C6	0.299	271	5.6225	0.25042	5.6225
C7	0.3	312.5	6.2792	0.25281	6.2792
C8	0.312	351.5	6.936	0.26082	6.936
C9	0.348	380	7.7529	0.25394	7.7529
C10	0.385	404.9	8.5539	0.24825	8.5539
C11+	0.59126	475.6	11.472	0.2448	11.472

Components	Z crit (visc)	Boil Temp (F)	Ref Density	Ref Temp (F)
H2S	0.28195	-75.37	61.991	-75.19
CO2	0.27408	-109.21	48.507	67.73
N2	0.29115	-320.35	50.192	-319.09
C1	0.28473	-258.79	26.532	-258.61
C2	0.28463	-127.39	34.211	-130.27

C3	0.27616	-43.69	36.333	-43.87
IC4	0.28274	10.67	34.772	67.73
NC4	0.27386	31.19	36.146	67.73
IC5	0.27271	82.13	38.705	67.73
NC5	0.26844	96.89	39.08	67.73
C6	0.25042	147.02	42.763	60.53
C7	0.25281	197.42	45.073	60.53
C8	0.26082	242.06	46.509	60.53
C9	0.25394	287.96	47.695	60.53
C10	0.24825	330.44	48.569	60.53
C11+	0.2448	461.96	50.95	60

Expt DEW1 : Retrograde Dew Point Pressure Calculation

Peng-Robinson (3-Param) on ZI with PR corr.  
Lohrenz-Bray-Clark Viscosity Correlation

Specified temperature      Deg F      138.0000  
Calculated dew point pressure      PSIA      3855.6426  
Observed dew point pressure      PSIA      3853.0000

-----  
                                 Liquid    Vapour  
Fluid properties      -----  
                                 Calculated    Calculated  
-----

Mole Weight      41.0201    25.6232  
Z-factor      0.8350    0.8274  
Viscosity      0.0753    0.0352  
Density LB/FT3    29.5328    18.6170  
Molar Vol CF/LB-ML    1.3890    1.3763  
-----

-----  
Molar Distributions    Total, Z    Liquid,X    Vapour,Y    K-Values  
Components      -----  
Mnemonic    Number    Measured    Calculated    Calculated    Calculated  
-----

H2S	1	1.4599	1.7299	1.4599	0.8439
CO2	2	2.2198	2.1791	2.2198	1.0187
N2	3	0.2300	0.1550	0.2300	1.4834
C1	4	78.7721	63.8544	78.7721	1.2336
C2	5	5.4795	5.8594	5.4795	0.9352
C3	6	2.9397	3.6982	2.9397	0.7949
IC4	7	0.6899	0.9820	0.6899	0.7026
NC4	8	1.4699	2.2253	1.4699	0.6605
IC5	9	0.6999	1.1805	0.6999	0.5929
NC5	10	0.7499	1.3169	0.7499	0.5694
C6	11	1.3699	2.8541	1.3699	0.4800
C7	12	1.0599	2.5804	1.0599	0.4107
C8	13	0.8799	2.4034	0.8799	0.3661
C9	14	0.5000	1.5555	0.5000	0.3214
C10	15	0.4300	1.5023	0.4300	0.2862
C11+	16	1.0499	5.9251	1.0499	0.1772

Composition Total 100.0000 100.0016 100.0000

-----  
 Expt CVD1 : Constant Volume Depletion

Peng-Robinson (3-Param) on ZI with PR corr.

Lohrenz-Bray-Clark Viscosity Correlation

Density units are LB/FT3

Specific volume units are CF/LB-ML

Viscosity units are CPOISE

Surface Tension units are DYNES/CM

Specified temperature Deg F 138.0000

-----  
 Rel Volume Vap Mole Frn Liq Density Vap Density

Pressure Inserted -----

PSIA Point Calculated Calculated Calculated Calculated

-----  
 3855.642 - Psat 1.0000 29.5328 18.6170  
 3325.000 0.0965 0.9099 31.7683 15.3159  
 2800.000 0.1234 0.8790 33.5306 12.4115  
 2275.000 0.1294 0.8627 35.2396 9.6347  
 1750.000 0.1250 0.8507 37.0670 7.0108  
 1225.000 0.1151 0.8371 39.0655 4.6194  
 700.000 0.1020 0.8161 41.2655 2.5054

-----  
 Liq Z-Fac Vap Z-Fac Surf Tension Liq Sat

Pressure Inserted -----

PSIA Point Calculated Calculated Calculated Calculated

-----  
 3855.642 - Psat 0.8350 0.8274 0.0423  
 3325.000 0.7640 0.7962 0.2534 0.0965  
 2800.000 0.6809 0.7815 0.7902 0.1234  
 2275.000 0.5875 0.7846 1.9177 0.1294  
 1750.000 0.4842 0.8064 3.9649 0.1250  
 1225.000 0.3681 0.8453 7.2237 0.1151  
 700.000 0.2333 0.8987 11.9058 0.1020

-----  
 Liq Visc Vap Visc Moles Extrac

Pressure Inserted -----

PSIA Point Calculated Calculated Calculated

-----  
 3855.642 - Psat 0.0753 0.0352  
 3325.000 0.0909 0.0284 0.1002  
 2800.000 0.1066 0.0233 0.2171  
 2275.000 0.1260 0.0192 0.3508  
 1750.000 0.1530 0.0161 0.4956  
 1225.000 0.1924 0.0140 0.6426  
 700.000 0.2518 0.0127 0.7842

-----  
 2-Ph Z-Fac Liq Mol Vol Vap Mol Vol

Pressure Inserted -----

PSIA Point Observed Calculated Calculated Calculated

3855.642 - Psat		0.8274	1.3890	1.3763
3325.000	0.7880	0.7930	1.4737	1.5359
2800.000	0.7680	0.7675	1.5596	1.7901
2275.000	0.7600	0.7520	1.6563	2.2120
1750.000	0.7640	0.7444	1.7745	2.9554
1225.000	0.7550	0.7356	1.9274	4.4259
700.000	0.7420	0.6961	2.1376	8.2349

Expt CVD2 : Constant Volume Depletion  
 Peng-Robinson (3-Param) on ZI with PR corr.  
 Lohrenz-Bray-Clark Viscosity Correlation  
 Density units are LB/FT3  
 Specific volume units are CF/LB-ML  
 Viscosity units are CPOISE  
 Surface Tension units are DYNES/CM  
 Specified temperature Deg F 138.0000

Pressure	Inserted	Rel Volume	Vap Mole Frn	Liq Density	Vap Density
PSIA	Point	Calculated	Calculated	Calculated	Calculated
3855.642 - Psat		1.0000	29.5328	18.6170	
3325.000	0.0965	0.9099	31.7683	15.3159	
2800.000	0.1234	0.8790	33.5306	12.4115	
2275.000	0.1294	0.8627	35.2396	9.6347	
1750.000	0.1250	0.8507	37.0670	7.0108	
1225.000	0.1151	0.8371	39.0655	4.6194	
700.000	0.1020	0.8161	41.2655	2.5054	

Pressure	Inserted	Liq Z-Fac	Vap Z-Fac	Surf Tension
PSIA	Point	Calculated	Observed	Calculated
3855.642 - Psat		0.8350	0.8274	0.0423
3325.000	0.7640	0.8100	0.7962	0.2534
2800.000	0.6809	0.7950	0.7815	0.7902
2275.000	0.5875	0.8030	0.7846	1.9177
1750.000	0.4842	0.8320	0.8064	3.9649
1225.000	0.3681	0.8780	0.8453	7.2237
700.000	0.2333	0.9360	0.8987	11.9058

Pressure	Inserted	Liq Sat	Liq Visc	Vap Visc	Moles Extrac
PSIA	Point	Calculated	Calculated	Calculated	Calculated
3855.642 - Psat		0.0753	0.0352		
3325.000	0.0965	0.0909	0.0284	0.1002	
2800.000	0.1234	0.1066	0.0233	0.2171	
2275.000	0.1294	0.1260	0.0192	0.3508	
1750.000	0.1250	0.1530	0.0161	0.4956	
1225.000	0.1151	0.1924	0.0140	0.6426	

700.000      0.1020      0.2518      0.0127      0.7842

---



---

2-Ph Z-Fac Liq Mol Vol Vap Mol Vol				
Pressure	Inserted	-----		
PSIA	Point	Calculated	Calculated	Calculated
3855.642	- Psat	0.8274	1.3890	1.3763
3325.000		0.7930	1.4737	1.5359
2800.000		0.7675	1.5596	1.7901
2275.000		0.7520	1.6563	2.2120
1750.000		0.7444	1.7745	2.9554
1225.000		0.7356	1.9274	4.4259
700.000		0.6961	2.1376	8.2349

---

Expt CVD3 : Constant Volume Depletion  
 Peng-Robinson (3-Param) on ZI with PR corr.  
 Lohrenz-Bray-Clark Viscosity Correlation  
 Density units are LB/FT3  
 Specific volume units are CF/LB-ML  
 Viscosity units are CPOISE  
 Surface Tension units are DYNES/CM  
 Specified temperature Deg F 138.0000

---

Rel Volume Vap Mole Frn Liq Density Vap Density					
Pressure	Inserted	-----			
PSIA	Point	Calculated	Calculated	Calculated	Calculated
3855.642	- Psat		1.0000	29.5328	18.6170
3325.000		0.0965	0.9099	31.7683	15.3159
2800.000		0.1234	0.8790	33.5306	12.4115
2275.000		0.1294	0.8627	35.2396	9.6347
1750.000		0.1250	0.8507	37.0670	7.0108
1225.000		0.1151	0.8371	39.0655	4.6194
700.000		0.1020	0.8161	41.2655	2.5054

---



---

Liq Z-Fac Vap Z-Fac Surf Tension Liq Sat					
Pressure	Inserted	-----			
PSIA	Point	Calculated	Calculated	Calculated	Calculated
3855.642	- Psat	0.8350	0.8274	0.0423	
3325.000		0.7640	0.7962	0.2534	0.0965
2800.000		0.6809	0.7815	0.7902	0.1234
2275.000		0.5875	0.7846	1.9177	0.1294
1750.000		0.4842	0.8064	3.9649	0.1250
1225.000		0.3681	0.8453	7.2237	0.1151
700.000		0.2333	0.8987	11.9058	0.1020

---



---

Liq Visc Vap Visc Moles Extrac					
Pressure	Inserted	-----			
PSIA	Point	Calculated	Observed	Calculated	Calculated

Pressure	2-Ph Z-Fac	Liq Mol Vol	Vap Mol Vol	
3855.642 - Psat	0.0753		0.0352	
3325.000	0.0909	0.0279	0.0284	0.1002
2800.000	0.1066	0.0231	0.0233	0.2171
2275.000	0.1260	0.0190	0.0192	0.3508
1750.000	0.1530	0.0162	0.0161	0.4956
1225.000	0.1924	0.0143	0.0140	0.6426
700.000	0.2518	0.0129	0.0127	0.7842

Pressure	2-Ph Z-Fac	Liq Mol Vol	Vap Mol Vol	
3855.642 - Psat	0.8274	1.3890	1.3763	
3325.000	0.7930	1.4737	1.5359	
2800.000	0.7675	1.5596	1.7901	
2275.000	0.7520	1.6563	2.2120	
1750.000	0.7444	1.7745	2.9554	
1225.000	0.7356	1.9274	4.4259	
700.000	0.6961	2.1376	8.2349	

Expt CVD4 : Constant Volume Depletion  
 Peng-Robinson (3-Param) on ZI with PR corr.  
 Lohrenz-Bray-Clark Viscosity Correlation  
 Density units are LB/FT3  
 Specific volume units are CF/LB-ML  
 Viscosity units are CPOISE  
 Surface Tension units are DYNES/CM  
 Specified temperature Deg F 138.0000

Pressure	Rel Volume	Vap Mole Frn	Liq Density	Vap Density
3855.642 - Psat		1.0000	29.5328	18.6170
3700.000	0.0430	0.9581	30.2759	17.5709
3325.000	0.0948	0.9089	31.7703	15.3150
2800.000	0.1219	0.8804	33.5276	12.4124
2275.000	0.1282	0.8639	35.2333	9.6358
1750.000	0.1239	0.8518	37.0594	7.0114
1225.000	0.1141	0.8383	39.0583	4.6196
700.000	0.1012	0.8174	41.2599	2.5053

Pressure	Liq Z-Fac	Vap Z-Fac	Surf Tension
3855.642 - Psat	0.8350	0.8274	0.0423
3700.000	0.8157	0.8166	0.0811
3325.000	0.7640	0.7962	0.2536
2800.000	0.6808	0.7815	0.7898
2275.000	0.5874	0.7846	1.9164

1750.000	0.4841	0.8063	3.9630
1225.000	0.3680	0.8453	7.2220
700.000	0.2332	0.8988	11.9062

Liq Sat		Liq Visc	Vap Visc		
Pressure	Inserted	Observed	Calculated	Calculated	Calculated
PSIA	Point	Observed	Calculated	Calculated	Calculated
3855.642 - Psat			0.0753	0.0352	
3700.000		0.0100	0.0430	0.0800	0.0329
3325.000		0.0550	0.0948	0.0909	0.0284
2800.000		0.1081	0.1219	0.1066	0.0233
2275.000		0.1279	0.1282	0.1260	0.0192
1750.000		0.1298	0.1239	0.1529	0.0161
1225.000		0.1246	0.1141	0.1922	0.0140
700.000		0.1151	0.1012	0.2516	0.0127

Moles Extrac 2-Ph Z-Fac		Liq Mol Vol	Vap Mol Vol		
Pressure	Inserted	Calculated	Calculated	Calculated	Calculated
PSIA	Point	Calculated	Calculated	Calculated	Calculated
3855.642 - Psat			0.8274	1.3890	1.3763
3700.000		0.0276	0.8165	1.4140	1.4155
3325.000		0.1003	0.7931	1.4737	1.5359
2800.000		0.2173	0.7676	1.5595	1.7901
2275.000		0.3510	0.7522	1.6561	2.2119
1750.000		0.4958	0.7449	1.7741	2.9553
1225.000		0.6430	0.7363	1.9270	4.4259
700.000		0.7846	0.6974	2.1371	8.2349

Expt CCE1 : Constant Composition Expansion  
 Peng-Robinson (3-Param) on ZI with PR corr.  
 Lohrenz-Bray-Clark Viscosity Correlation  
 Density units are LB/FT3  
 Specific volume units are CF/LB-ML  
 Viscosity units are CPOISE  
 Surface Tension units are DYNES/CM  
 Specified temperature Deg F 138.0000  
 Liq Sat calc. is Vol oil/Vol Fluid at Sat. Vol

Rel Volume		Vap Mole Frn Liq Density			
Pressure	Inserted	Observed	Calculated	Calculated	Calculated
PSIA	Point	Observed	Calculated	Calculated	Calculated
6500.000		0.8125	0.8058	1.0000	
6008.000		0.8332	0.8282	1.0000	
5506.000		0.8585	0.8553	1.0000	
5004.000		0.8898	0.8882	1.0000	
4504.000		0.9293	0.9289	1.0000	
4403.000		0.9386	0.9384	1.0000	
4304.000		0.9482	0.9482	1.0000	



4204.000	0.9585	0.9587	1.0000	
4057.000	0.9747	0.9751	1.0000	
4003.000	0.9810	0.9815	1.0000	
3988.000	0.9829	0.9833	1.0000	
3979.000	0.9839	0.9844	1.0000	
3968.000	0.9852	0.9857	1.0000	
3959.000	0.9864	0.9868	1.0000	
3949.000	0.9876	0.9881	1.0000	
3940.000	0.9887	0.9892	1.0000	
3928.000	0.9902	0.9907	1.0000	
3917.000	0.9917	0.9921	1.0000	
3908.000	0.9928	0.9932	1.0000	
3897.000	0.9941	0.9946	1.0000	
3855.642 - Psat		1.0000	1.0000	29.5328
3801.000	1.0000	1.0096	0.9827	29.7994
3800.000	1.0084	1.0098	0.9824	29.8043
3701.000	1.0257	1.0282	0.9583	30.2713
3599.000	1.0449	1.0486	0.9401	30.7137
3554.000	1.0540	1.0581	0.9336	30.8988
3416.000	1.0840	1.0894	0.9177	31.4354
3212.000	1.1356	1.1422	0.9022	32.1641
3009.000	1.1979	1.2045	0.8926	32.8387
2800.000	1.2753	1.2814	0.8868	33.5032
2596.000	1.3684	1.3724	0.8839	34.1395
2394.000	1.4830	1.4824	0.8830	34.7706
2192.000	1.6256	1.6183	0.8838	35.4132
1890.000	1.9153	1.8883	0.8876	36.4119
1586.000	2.3502	2.2833	0.8939	37.4804
1294.000	3.0085	2.8604	0.9020	38.5825
996.000	4.1502	3.8289	0.9120	39.8063

Pressure	Vap Density Inserted	Liq Z-Fac Calculated	Vap Z-Fac Calculated	Surf Tension Calculated
6500.000		23.1051	1.1239	
6008.000		22.4791	1.0677	
5506.000		21.7661	1.0106	
5004.000		20.9603	0.9538	
4504.000		20.0410	0.8978	
4403.000		19.8384	0.8867	
4304.000		19.6334	0.8758	
4204.000		19.4198	0.8648	
4057.000		19.0926	0.8489	
4003.000		18.9683	0.8431	
3988.000		18.9334	0.8415	
3979.000		18.9124	0.8405	
3968.000		18.8865	0.8393	
3959.000		18.8653	0.8384	
3949.000		18.8417	0.8373	
3940.000		18.8204	0.8363	
3928.000		18.7918	0.8351	
3917.000		18.7655	0.8339	
3908.000		18.7439	0.8329	

3897.000	18.7175		0.8318	
3855.642 - Psat	18.6170	0.8350	0.8274	0.0423
3801.000	18.2383	0.8283	0.8234	0.0541
3800.000	18.2315	0.8282	0.8234	0.0543
3701.000	17.5773	0.8159	0.8166	0.0808
3599.000	16.9356	0.8025	0.8103	0.1155
3554.000	16.6607	0.7965	0.8077	0.1333
3416.000	15.8410	0.7772	0.8005	0.1994
3212.000	14.6763	0.7470	0.7916	0.3337
3009.000	13.5527	0.7151	0.7853	0.5216
2800.000	12.4193	0.6805	0.7813	0.7866
2596.000	11.3303	0.6451	0.7802	1.1327
2394.000	10.2680	0.6085	0.7818	1.5794
2192.000	9.2240	0.5705	0.7863	2.1492
1890.000	7.7070	0.5108	0.7982	3.2737
1586.000	6.2474	0.4471	0.8163	4.7921
1294.000	4.9224	0.3818	0.8391	6.6713
996.000	3.6561	0.3102	0.8674	9.0717

-----  
-----  
Liq Sat    Liq Visc    Vap Visc    Liq Mole Wt  
Pressure Inserted -----  
PSIA    Point    Calculated    Calculated    Calculated    Calculated

6500.000			0.0488	
6008.000			0.0464	
5506.000			0.0440	
5004.000			0.0415	
4504.000			0.0389	
4403.000			0.0383	
4304.000			0.0378	
4204.000			0.0372	
4057.000			0.0364	
4003.000			0.0361	
3988.000			0.0360	
3979.000			0.0359	
3968.000			0.0359	
3959.000			0.0358	
3949.000			0.0358	
3940.000			0.0357	
3928.000			0.0356	
3917.000			0.0356	
3908.000			0.0355	
3897.000			0.0355	
3855.642 - Psat		0.0753	0.0352	41.0201
3801.000	0.0176	0.0769	0.0344	41.6510
3800.000	0.0179	0.0770	0.0344	41.6627
3701.000	0.0428	0.0800	0.0330	42.7996
3599.000	0.0623	0.0830	0.0316	43.9261
3554.000	0.0694	0.0843	0.0311	44.4119
3416.000	0.0872	0.0883	0.0294	45.8714
3212.000	0.1060	0.0941	0.0272	47.9769
3009.000	0.1189	0.1000	0.0252	50.0555
2800.000	0.1282	0.1063	0.0233	52.2241
2596.000	0.1345	0.1130	0.0216	54.4112

2394.000	0.1386	0.1201	0.0200	56.6868
2192.000	0.1409	0.1281	0.0186	59.1140
1890.000	0.1416	0.1422	0.0168	63.1220
1586.000	0.1393	0.1598	0.0153	67.7693
1294.000	0.1348	0.1813	0.0142	73.0217
996.000	0.1277	0.2097	0.0133	79.5080

Pressure	Inserted	Vap Mole Wt	Liq Mol Vol	Vap Mol Vol
PSIA	Point	Calculated	Calculated	Calculated
6500.000		25.6232		1.1090
6008.000		25.6232		1.1399
5506.000		25.6232		1.1772
5004.000		25.6232		1.2225
4504.000		25.6232		1.2785
4403.000		25.6232		1.2916
4304.000		25.6232		1.3051
4204.000		25.6232		1.3194
4057.000		25.6232		1.3420
4003.000		25.6232		1.3508
3988.000		25.6232		1.3533
3979.000		25.6232		1.3548
3968.000		25.6232		1.3567
3959.000		25.6232		1.3582
3949.000		25.6232		1.3599
3940.000		25.6232		1.3615
3928.000		25.6232		1.3635
3917.000		25.6232		1.3654
3908.000		25.6232		1.3670
3897.000		25.6232		1.3689
3855.642	- Psat	25.6232	1.3890	1.3763
3801.000		25.3411	1.3977	1.3894
3800.000		25.3361	1.3979	1.3897
3701.000		24.8762	1.4139	1.4152
3599.000		24.4567	1.4302	1.4441
3554.000		24.2861	1.4373	1.4577
3416.000		23.8077	1.4592	1.5029
3212.000		23.1999	1.4916	1.5808
3009.000		22.6848	1.5243	1.6738
2800.000		22.2274	1.5588	1.7897
2596.000		21.8403	1.5938	1.9276
2394.000		21.5077	1.6303	2.0946
2192.000		21.2213	1.6693	2.3007
1890.000		20.8749	1.7336	2.7086
1586.000		20.6224	1.8081	3.3010
1294.000		20.4722	1.8926	4.1590
996.000		20.4221	1.9974	5.5857

Expt CCE2 : Constant Composition Expansion  
 Peng-Robinson (3-Param) on ZI with PR corr.  
 Lohrenz-Bray-Clark Viscosity Correlation  
 Density units are LB/FT3

Specific volume units are CF/LB-ML  
 Viscosity units are CPOISE  
 Surface Tension units are DYNES/CM  
 Specified temperature Deg F 138.0000

Liq Sat calc. is Vol oil/Vol Fluid at Sat. Vol

Pressure	Rel Volume	Vap Mole Frn	Liq Density	Vap Density
PSIA	Point	Calculated	Calculated	Calculated
3855.642 - Psat		1.0000	1.0000	29.5328
3801.000		1.0096	0.9827	29.7994
3701.000		1.0282	0.9583	30.2713
3599.000		1.0486	0.9401	30.7137
3554.000		1.0581	0.9336	30.8988
3416.000		1.0894	0.9177	31.4354
3212.000		1.1422	0.9022	32.1641
3009.000		1.2045	0.8926	32.8387
2800.000		1.2814	0.8868	33.5032
2596.000		1.3724	0.8839	34.1395
2394.000		1.4824	0.8830	34.7706
2192.000		1.6183	0.8838	35.4132
1890.000		1.8883	0.8876	36.4119
1586.000		2.2833	0.8939	37.4804
1294.000		2.8604	0.9020	38.5825
996.000		3.8289	0.9120	39.8063

Pressure	Liq Z-Fac	Vap Z-Fac	Surf Tension
PSIA	Point	Calculated	Calculated
3855.642 - Psat		0.8350	0.8274
3801.000		0.8283	0.8234
3701.000		0.8159	0.8166
3599.000		0.8025	0.8103
3554.000		0.7965	0.8077
3416.000		0.7772	0.8005
3212.000		0.7470	0.7916
3009.000		0.7151	0.7853
2800.000		0.6805	0.7813
2596.000		0.6451	0.7802
2394.000		0.6085	0.7818
2192.000		0.5705	0.7863
1890.000		0.5108	0.7982
1586.000		0.4471	0.8163
1294.000		0.3818	0.8391
996.000		0.3102	0.8674

Pressure	Liq Sat	Liq Visc	Vap Visc
PSIA	Point	Observed	Calculated
		Calculated	Calculated

3855.642 - Psat		0.0753	0.0352	
3801.000	0.0008	0.0176	0.0769	0.0344
3701.000	0.0067	0.0428	0.0800	0.0330
3599.000	0.0169	0.0623	0.0830	0.0316
3554.000	0.0223	0.0694	0.0843	0.0311
3416.000	0.0401	0.0872	0.0883	0.0294
3212.000	0.0667	0.1060	0.0941	0.0272
3009.000	0.0898	0.1189	0.1000	0.0252
2800.000	0.1085	0.1282	0.1063	0.0233
2596.000	0.1219	0.1345	0.1130	0.0216
2394.000	0.1310	0.1386	0.1201	0.0200
2192.000	0.1368	0.1409	0.1281	0.0186
1890.000	0.1410	0.1416	0.1422	0.0168
1586.000	0.1412	0.1393	0.1598	0.0153
1294.000	0.1390	0.1348	0.1813	0.0142
996.000	0.1349	0.1277	0.2097	0.0133

Pressure	Inserted	Liq Mole Wt	Vap Mole Wt	Liq Mol Vol	Vap Mol Vol
PSIA	Point	Calculated	Calculated	Calculated	Calculated
3855.642 - Psat		41.0201	25.6232	1.3890	1.3763
3801.000		41.6510	25.3411	1.3977	1.3894
3701.000		42.7996	24.8762	1.4139	1.4152
3599.000		43.9261	24.4567	1.4302	1.4441
3554.000		44.4119	24.2861	1.4373	1.4577
3416.000		45.8714	23.8077	1.4592	1.5029
3212.000		47.9769	23.1999	1.4916	1.5808
3009.000		50.0555	22.6848	1.5243	1.6738
2800.000		52.2241	22.2274	1.5588	1.7897
2596.000		54.4112	21.8403	1.5938	1.9276
2394.000		56.6868	21.5077	1.6303	2.0946
2192.000		59.1140	21.2213	1.6693	2.3007
1890.000		63.1220	20.8749	1.7336	2.7086
1586.000		67.7693	20.6224	1.8081	3.3010
1294.000		73.0217	20.4722	1.8926	4.1590
996.000		79.5080	20.4221	1.9974	5.5857

Expt CCE3 : Constant Composition Expansion  
 Peng-Robinson (3-Param) on ZI with PR corr.  
 Lohrenz-Bray-Clark Viscosity Correlation  
 Density units are LB/FT3  
 Specific volume units are CF/LB-ML  
 Viscosity units are CPOISE  
 Surface Tension units are DYNES/CM  
 Specified temperature Deg F 138.0000  
 Liq Sat calc. is Vol oil/Vol Fluid at Sat. Vol

Pressure	Inserted	Rel Volume	Vap Mole Frn	Liq Density	Vap Density
PSIA	Point	Calculated	Calculated	Calculated	Calculated
6500.000		0.8058	1.0000		23.1051

6008.000	0.8282	1.0000		22.4791
5506.000	0.8553	1.0000		21.7661
5004.000	0.8882	1.0000		20.9603
4504.000	0.9289	1.0000		20.0410
4403.000	0.9384	1.0000		19.8384
4304.000	0.9482	1.0000		19.6334
4204.000	0.9587	1.0000		19.4198
4057.000	0.9751	1.0000		19.0926
4003.000	0.9815	1.0000		18.9683
3988.000	0.9833	1.0000		18.9334
3979.000	0.9844	1.0000		18.9124
3968.000	0.9857	1.0000		18.8865
3959.000	0.9868	1.0000		18.8653
3949.000	0.9881	1.0000		18.8417
3940.000	0.9892	1.0000		18.8204
3928.000	0.9907	1.0000		18.7918
3917.000	0.9921	1.0000		18.7655
3908.000	0.9932	1.0000		18.7439
3897.000	0.9946	1.0000		18.7175
3855.642 - Psat	1.0000	1.0000	29.5328	18.6170

Pressure	Liq Z-Fac	Vap Z-Fac	Surf Tension
PSIA	Point	Calculated	Observed
6500.000		1.1370	1.1239
6008.000		1.0780	1.0677
5506.000		1.0180	1.0106
5004.000		0.9590	0.9538
4504.000		0.9020	0.8978
4403.000		0.8910	0.8867
4304.000		0.8800	0.8758
4204.000		0.8690	0.8648
4057.000		0.8520	0.8489
4003.000		0.8470	0.8431
3988.000		0.8450	0.8415
3979.000		0.8440	0.8405
3968.000		0.8430	0.8393
3959.000		0.8420	0.8384
3949.000		0.8410	0.8373
3940.000		0.8400	0.8363
3928.000		0.8390	0.8351
3917.000		0.8370	0.8339
3908.000		0.8360	0.8329
3897.000		0.8350	0.8318
3855.642 - Psat	0.8350		0.8274
			0.0423

Pressure	Liq Sat	Liq Visc	Vap Visc	Liq Mole Wt
PSIA	Point	Calculated	Calculated	Calculated
6500.000			0.0488	
6008.000			0.0464	

5506.000		0.0440	
5004.000		0.0415	
4504.000		0.0389	
4403.000		0.0383	
4304.000		0.0378	
4204.000		0.0372	
4057.000		0.0364	
4003.000		0.0361	
3988.000		0.0360	
3979.000		0.0359	
3968.000		0.0359	
3959.000		0.0358	
3949.000		0.0358	
3940.000		0.0357	
3928.000		0.0356	
3917.000		0.0356	
3908.000		0.0355	
3897.000		0.0355	
3855.642 - Psat	0.0753	0.0352	41.0201

Pressure	Inserted	Vap Mole Wt	Liq Mol Vol	Vap Mol Vol
PSIA	Point	Calculated	Calculated	Calculated
6500.000		25.6232		1.1090
6008.000		25.6232		1.1399
5506.000		25.6232		1.1772
5004.000		25.6232		1.2225
4504.000		25.6232		1.2785
4403.000		25.6232		1.2916
4304.000		25.6232		1.3051
4204.000		25.6232		1.3194
4057.000		25.6232		1.3420
4003.000		25.6232		1.3508
3988.000		25.6232		1.3533
3979.000		25.6232		1.3548
3968.000		25.6232		1.3567
3959.000		25.6232		1.3582
3949.000		25.6232		1.3599
3940.000		25.6232		1.3615
3928.000		25.6232		1.3635
3917.000		25.6232		1.3654
3908.000		25.6232		1.3670
3897.000		25.6232		1.3689
3855.642 - Psat		25.6232	1.3890	1.3763

Expt FLASH1 : Flash Calculation

Peng-Robinson (3-Param) on ZI with PR corr.

Lohrenz-Bray-Clark Viscosity Correlation

Two phase state

Specified temperature      Deg F      42.0000

Specified pressure      PSIA      610.0000

Mole Percentage in vapour      87.4505

Calculated GOR	MSCF/BBL	8.4926
Observed GOR	MSCF/BBL	8.2290

-----  
 Liquid Vapour  
 Fluid properties -----  
 Calculated Calculated  
 -----

Mole Weight	72.1554	18.9457
Z-factor	0.1981	0.8594
Viscosity	0.2831	0.0113
Density LB/FT3	41.2737	2.4979
Molar Vol CF/LB-ML	1.7482	7.5847

-----

-----  
 Molar Distributions Total, Z Liquid,X Vapour,Y K-Values  
 Components -----  
 Mnemonic Number Measured Calculated Calculated Calculated  
 -----

H2S	1	1.4599	2.2635	1.3445	0.5940
CO2	2	2.2198	1.4966	2.3236	1.5526
N2	3	0.2300	0.0190	0.2603	13.7278
C1	4	78.7721	19.4654	87.2829	4.4840
C2	5	5.4795	6.5159	5.3307	0.8181
C3	6	2.9397	8.4324	2.1515	0.2551
IC4	7	0.6899	3.1688	0.3342	0.1055
NC4	8	1.4699	7.7188	0.5731	0.0742
IC5	9	0.6999	4.5520	0.1471	0.0323
NC5	10	0.7499	5.1038	0.1251	0.0245
C6	11	1.3699	10.3147	0.0862	0.0084
C7	12	1.0599	8.2604	0.0266	0.0032
C8	13	0.8799	6.9356	0.0109	0.0016
C9	14	0.5000	3.9673	0.0024	0.0006
C10	15	0.4300	3.4203	0.0008	0.0002
C11+	16	1.0499	8.3656	5.7715E-05	6.8991E-06

-----  
 Composition Total 100.0000 100.0000 100.0000  
 -----



## CIRRICULUM VITAE



**Name Surname:** Harun KIRMACI  
**Place and Date of Birth:** Erzurum/Türkiye - August 05, 1984  
**Address:** TPAO Genel Müdürlüğü  
Söğütözü/Ankara/Türkiye  
**E-Mail:** hkirmaci@tpao.gov.tr  
**B.Sc.:** 2003 – 2008 – Istanbul Technical University  
Department of Petroleum and Natural Gas Engineering  
**M.Sc.:** 2011 – 2014 – Istanbul Technical University  
Department of Petroleum and Natural Gas Engineering

### Professional Experience and Rewards:

Schlumberger (2008 - 2010), Testing Reservoir Engineer

TPAO – International Projects Department (2010 - 2013), Reservoir Engineer

TPOC Iraq Branch – (2013- ), Subsurface Manager

- Received the Hakan Baylan High Success Award, 2007, ITU
- Received the Mustafa Yelkenci High Success Award, 2008, ITU
- Received the 8<sup>th</sup> SPE Turkey Section Annual Student Paper Contest 1<sup>st</sup> Award, 2008, METU
- Received the ITU Rectorship high success award, 2008, ITU

### List of Publications and Patents:

**Kirmaci H. and Onur M.** “The productivity comparison of horizontal and vertical wells and forecasting performance with the tank type reservoir model for the single/double porosity; isotropic/anisotropic reservoirs”, presented in **IPETGAS, ANKARA, 2011.**